UNIVERSIDAD COMPLUTENSE DE MADRID
FACULTAD DE CIENCIAS QUÍMICAS
Departamento de Química Orgánica

TESIS DOCTORAL

Supramolecular polymerization of π-conjugated systems. Thermodynamic and kinetic control

Polimerización supramolecular de sistemas π-conjugados. Control termodinámico y cinético

MEMORIA PARA OPTAR AL GRADO DE DOCTOR

PRESENTADA POR

Jorge Santos Valera González

Directores

Luis Sánchez Martín
Rafael Gómez Aspe

Madrid
Ed. electrónica 2019

UNIVERSIDAD COMPLUTENSE DE MADRID

FACULTAD DE CIENCIAS QUÍMICAS

DEPARTAMENTO DE QUÍMICA ORGÁNICA

TESIS DOCTORAL

Supramolecular polymerization of π-conjugated systems. Thermodynamic and kinetic control.

Polimerización supramolecular de sistemas π-conjugados. Control termodinámico y cinético.

MEMORIA PARA OPTAR AL GRADO DE DOCTOR
PRESENTADA POR:

Jorge Santos Valera González

Directores: Luis Sánchez Martín y Rafael Gómez Aspe

Madrid, 2018

UNIVERSIDAD COMPLUTENSE DE MADRID

FACULTAD DE CIENCIAS QUÍMICAS

DEPARTAMENTO DE QUÍMICA ORGÁNICA

SUPRAMOLECULAR POLYMERIZATION OF π-CONJUGATED SYSTEMS. THERMODYNAMIC AND KINETIC CONTROL.

POLIMERIZACIÓN SUPRAMOLECULAR DE SISTEMAS π-CONJUGADOS. CONTROL TERMODINÁMICO Y CINÉTICO.

TESIS DOCTORAL

Jorge Santos Valera González

Madrid, 2018

SUPRAMOLECULAR POLYMERIZATION OF π-CONJUGATED SYSTEMS. THERMODYNAMIC AND KINETIC CONTROL.

POLIMERIZACIÓN SUPRAMOLECULAR DE SISTEMAS π-CONJUGADOS. CONTROL TERMODINÁMICO Y CINÉTICO.

Directores:

Luis Sánchez Martín y Rafael Gómez Aspe

Memoria que para optar al grado de

DOCTOR EN CIENCIAS QUÍMICAS

presenta

Jorge Santos Valera González

Madrid

Septiembre, 2018

D. Luis Sánchez Martín, Catedrático de Universidad y D. Rafael Gómez Aspe, Profesor Titular de Universidad, adscritos al Departamento de Química Orgánica de la Universidad Complutense de Madrid,

CERTIFICAN:

Que la presente Memoria, titulada: "**SUPRAMOLECULAR POLYMERIZATION OF π-CONJUGATED SYSTEMS. THERMODYNAMIC AND KINETIC CONTROL**" se ha realizado bajo su dirección en el departamento de Química Orgánica de la Universidad Complutense de Madrid, por el Graduado en Química D. Jorge Santos Valera González, y autorizan su presentación para ser calificada como tesis doctoral.

Y para que conste, firmamos el presente certificado en Madrid, a 14 de septiembre de 2018.

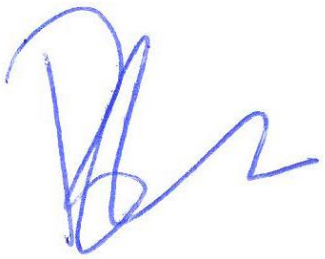

Fdo. Luis Sánchez Martín

Rafael Gómez Aspe

The results presented in the next thesis have been published and listed below:

-J. S. Valera, J. Calbo, R. Gómez, E. Ortí, L. Sánchez; “Blue-emitting pyrene-based aggregates”; *Chem. Commun*. **2015**, *51*, 10142-10145.

-J. S. Valera, R. Sánchez-Naya, F. J. Ramírez, J. L. Zafra, R. Gómez, J. Casado, L. Sánchez; "Solvent-directed helical stereomutation discloses pathway complexity on *N*-heterotriangulene based organogelators"; *Chem. Eur. J*. **2017**, *23*, 11141-11146.

-J. S. Valera, R. Gómez, L. Sánchez; “Tunable energy landscapes to control pathway complexity in self-assembled *N*-heterotriangulenes. Living and seeded supramolecular polymerization”; *Small* **2018**, *14*, 1702437 (1-9). Article selected for the Inside Front Cover Issue.

-J. S. Valera, R. Gómez, L. Sánchez; "Supramolecular polymerization of [5]helicenes. Consequences of self-assembly on configurational stability"; *Org. Lett.* **2018,** *20*, 2020-2023.

-J. S. Valera, R. Gómez, L. Sánchez; “Kinetic traps to activate stereomutation in supramolecular polymers”; ***submitted***.

A mis padres

ACKNOWLEDGMENTS

Esta Tesis Doctoral se ha llevado a cabo en el Departamento de Química Orgánica de la Universidad Complutense de Madrid bajo la dirección de los profesores Luis Sánchez y Rafael Gómez.

En primer lugar querría dar las gracias a mis dos directores:

A Luis, muchísimas gracias por haberme dado la oportunidad de unirme a tu grupo de investigación, así como toda la confianza y ayuda que me has brindado durante estos años. Gracias por hacerme descubrir este tema de investigación, así como por todo lo que me has enseñado y me he divertido contigo en este periodo.

A Rafa, muchísimas gracias por toda tu ayuda durante estos años. Gracias por tus consejos y por tus ánimos, por lo que me he reído contigo, y sobre todo por todo lo que me has enseñado, especialmente en el laboratorio. Te prometí algún compuesto que todavía te debo. Espero dártelo antes de Navidades.

Asimismo, en la realización de este trabajo han participado otros grupos de investigación, a los que querría agradecer su contribución:

Al Prof. Enrique Ortí y al Dr. Joaquín Calbo, de la Universidad de Valencia, por la realización de los cálculos teóricos correspondientes al autoensamblaje de los pirenoimidazoles de la Sección 1, así como por las interesantes discusiones científicas que hemos tenido en los congresos en los que hemos coincidido.

Al Prof. Juan Casado, al Prof. Francisco J. Ramírez y al Dr. José L. Zafra de la Universidad de Málaga, por la realización e interpretación de las medidas de VCD de los geles de *N*-heterotrianguleno de la Sección 3.

I also would like to thank to sensei Shiki Yagai at Chiba University (Japan). Sensei, thank you very much for allowing me to do a three-month internship in your research group. It was an amazing experience, I learn a lot and I spent great moments doing science in your group. Besides, I would like to express my gratitude to my labmates in Japan, especially to Dr. Yuichi Kitamoto, Dr. Deepak Prabhu, Keisuke Aratsu and Hayato Ouchi for their kind help and fruitful discussions. I hope our roads cross in the future. Arigato Gozaimasu!

También querría expresar mi gratitud a aquellas personas cuya ayuda ha resultado indispensable para la realización de muchos de los experimentos que se han incluido en la presente Tesis Doctoral.

Al Prof. Nazario Martín por su generosidad y por posibilitar la separación cuantitativa de los helicenos enantienrriquecidos.

Al Prof. Francisco Ortega y al Prof. Ramón González por hacer posible la realización de las medidas de espectroscopía de fluorescencia.

Al Centro de Microscopía Electrónica, especialmente a Ana Soubrié (AFM) y Alfonso Rodríguez (SEM) por la realización de las imágenes de microscopía.

Al CAI de RMN de la Facultad de Ciencias Químicas de la UCM, con especial mención a Ángel Sánchez, a la Dra. Dolores Molero y a la Dra. Elena Sáez por su gran dedicación en la realización de los experimentos de RMN, así como a su inestimable ayuda para la optimización de los mismos.

A los CAI de Espectrometría de Masas de la Facultad de Ciencias Geológicas y de la Facultad de Ciencias Químicas de la UCM, por la realización de las medidas incluidas en esta Tesis.

A Francisco Javier García y Laura García por la realización de los espectros de FTIR.

A los técnicos de laboratorio Francisco Javier García, Laura García y Javier Cornejo, por su ayuda y disponibilidad en todo momento.

Finalmente, querría mencionar y dar las gracias a todos aquellos que han hecho de estos años algo inolvidable, repletos de buenos momentos y anécdotas divertidas.

A toda la gente de los Nazarios: Javs, Toni, Silvia, Chus, Paul, Alfonso, Javi Sevilla, Marta, y un largo etcétera. A Sonia, a Rosa y a Antonio, con los que he compartido mucha parte del camino. Merecen una mención especial las personas con la que más tiempo he pasado, lecturas de horóscopo incluidas: las madres del Depar, Laura, Marta y Valentina; mis queridas Marina, Sarita y Mikiko y sobre todo a Andrew y a Alisita, con los que he disfrutado tanto fuera (Jäger en mano y tirando de poderosa) como dentro de la Facultad. Tampoco querría olvidar al grupo de Jóvenes Investigadores, especialmente a mi amigo de 45 años, Salvatore.

A toda la gente del Depar y alrededores, con la que me lo he pasado de miedo en las comidas por el mundo, las casas rurales, las pachangas en Montes, los viernes de cañas… y destacando la amistad que me llevo con Helen, Mayka, Dani, Sara y Yago, con los que uno se lo pasa bien en cualquier parte y a (o hasta) cualquier hora.

A mis vecinos de en frente, con los que he compartido muchos años espacio, música a todo volumen, vídeos de APM y alguna que otra cerveza. A Alberto, por ser un tipo abumayé y porque sabes que los jedis son el problema; a Paula, por ser tan buena amiga y porque la fuerza es poderosa en ti; a Alejandro y a Marta. A Sergio, por soportar mis turras y porque hablar y escribir bien es lo que nos distingue de los… ya sabes; y a Matías, por su simpatía. Y como no, gracias a Paloma: por dejarme conocerte entre vídeos de Pantomima, por no dejar de animarme y aguantarme, y porque has conseguido hacer de esta última etapa algo inolvidable.

A todos mis compañeros de laboratorio, empezando por todas aquellas personas que han estado bajo mi tutela estos años y que han participado en este trabajo: Roberto (heterotriangulenos), Manu B. (helicenos), Manu G. y Martin, así como a todos aquellos que han pasado por el grupo y han sufrido mis excentricidades: Sandra, Mercedes, Bea, Álvaro, Alberto, Dani, Julia D., etc. También a Fátima A., por su ayuda en mis comienzos. Finalmente, eternamente agradecido a mi súper compi Julia, por estar siempre dispuesta a echar un cable y a hablar de química; a Yeray, porque empezaste a mi cargo y te has convertido en compañero y amigo; y a Elisa, porque nunca me has negado un intermedio si me hacía falta.

A todos mis grupos de amigos fuera de la Universidad: a mis colegas de Arganda, a los del conser y a los peosos. Gracias por vuestro apoyo y por preguntarme de vez en cuando sobre qué iba mi tesis.

A toda mi familia: a mis tías, a mis primos y a mi abuelo, por su constante cariño y por confiar en mis posibilidades. Y a los que nos dejaron pero siempre estarán.

Y más que nadie a mis padres, porque sin vuestro apoyo y los valores que me habéis transmitido no podría haber superado este reto. Estoy enormemente agradecido por todas las oportunidades que me habéis brindado. Gracias por confiar siempre en mí y darme vuestro cariño incondicional. Esto es tan vuestro como mío.

ABBREVIATIONS AND ACRONYMS

The common abbreviations and acronyms employed in organic chemistry have been used in the present thesis by following the "Guidelines for authors" of *Journal of Organic Chemistry* (2018). These words can be found in the following journal webpage:

https://pubs.acs.org/paragonplus/submission/joceah/joceahauthguide.pdf

Furthermore, the next abbreviations has been also utilized:

AFM	Atomic force microscope
BChl-a	Bacteriochlorophyll a
BINOL	1,1´-bi-2-naphtol
BODIPY	Boron-dipyrromethene
BTA	Benzene 1,3,5-tricarboxamide
CBT	Carbonyl-bridged triarylamine
CGC	Critical gelation concentration
DTA	Dibenzoyl tartaric acid
DLS	Dynamic light scattering
DOSY	Diffusion ordered spectroscopy
ee	Enantiomeric excess
EQ	Equilibrium model
EtOAc	Ethyl acetate
HBC	Hexa-*peri*-hexabenzocoronene
HOPG	Highly oriented pyrolytic graphite
LH I and II	Light harvesting complexes I and II
MCH	Methylcyclohexane
MeOH	Methanol
MEP	Molecular electrostatic potential
MR	Majority rules
NIBT	(5-Hexyl-2,2-bithiophene)-naphthalimide
OFET	Organic field effect transistor

OLED	Organic light emitting diode
OPE-TA	Oligo(phenyleneethynylene) tricarboxamides
OPV	Oligo-*p*-phenylenevinylene
OSC	Organic solar cell
PAH	Polycyclic aromatic hydrocarbons
PBI	Perylene bisimide
PDI	Polydispersity index
ROESY	Rotating-frame Overhäuser effect spectroscopy
SaS	Sergeants and soldiers
SD	Solvent denaturation model
Tol	Toluene
TPA	Triphenylamine

TABLE OF CONTENTS

1. INTRODUCTION **1**

2. BACKGROUND **9**

3. AIM AND SCOPE OF THE THESIS **33**

4. RESULTS AND DISCUSSION **37**

4.1. SUPRAMOLECULAR POLYMERIZATION OF PYRENE DERIVATIVES **39**

4.1.1. Pyrene derivatives 41

4.1.2. Synthesis of pyreneimidazole derivatives **25** and **(*S*)-26** 42

4.1.3. Self-assembly of pyreneimidazoles **25** and **(*S*)-26** in solution 44

4.1.4. Self-assembly of pyreneimidazoles **25** and **(*S*)-26**. Theoretical approach 52

4.2. SUPRAMOLECULAR POLYMERIZATION OF [5]-HELICENES DERIVATIVES **59**

4.2.1. Helicene derivatives 61

4.2.2. Synthesis of [5]-helicenes **35** and **36** 62

4.2.3. Self-assembly of racemic [5]-helicenes **35** and **36** in solution 65

4.2.4. Self-assembly of enantioenriched [5]-helicenes **35** and **36** in solution. Influence of self-assembly on configurational stability 72

4.3. SUPRAMOLECULAR POLYMERIZATION OF *N*-HETEROTRIANGULENES **81**

4.3.1. *N*-heterotriangulenes 83

4.3.2. Synthesis of *N*-heterotriangulenes **48**, **(*S*)-49** and **(*R*)-49** 85

4.3.3. Self-assembly of *N*-heterotriangulenes **48**, **(*S*)-49** and **(*R*)-49** in solution 86

4.3.4. Organogels of *N*-heterotriangulenes **48**, **(*S*)-49** and **(*R*)-49**. Study of the chiroptical features in the gel state 92

4.4. KINETICALLY-CONTROLLED SUPRAMOLECULAR POLYMERIZATION OF *N*-HETEROTRIANGULENES **99**

4.4.1. Kinetically-controlled supramolecular polymerizations 101

4.4.2. Synthesis of *N*-heterotriangulenes **58**, **(*S*)-59** and **(*R*)-59** 102
4.4.3. Self-assembly of *N*-heterotriangulenes **58**, **(*S*)-59** and **(*R*)-59** in solution 105
4.4.4. Kinetic implications in the self-assembly of *N*-heterotriangulenes **58**, **(*S*)-59** and **(*R*)-59** 114
4.4.5. Seeded and living supramolecular polymerizations of *N*-heterotriangulenes **58**, **(*S*)-59** and **(*R*)-59** 117
4.4.6. Out-of-equilibrium transfer and amplification of chirality 123
4.4.7. Co-assembly of *N*-heterotriangulenes **(*S*)-59** and **(*R*)-59**: Majority Rules experiments 124
4.4.8. Co-assembly of *N*-heterotriangulenes **(*S*)-59** and **(*R*)-59** with **58**: Sergeants and Soldiers experiments. 127

5. EXPERIMENTAL SECTION 137

6. CONCLUDING REMARKS 159

7. SUMMARY 165

8. RESUMEN 171

9. REFERENCES 177

1. INTRODUCTION

The term molecular self-assembly makes reference to the spontaneous organization of small building blocks through intermolecular interactions to yield well-defined architectures.[1,2] These resources are ubiquitous in Nature and, therefore, essential to achieve the fascinating complexity exerted by living systems.[3] Hence, the understanding of the mechanisms and principles governing self-assembly is key to comprehend and mimic biological constructions and, additionally, their command results mandatory for their implementation on emerging technological areas.

Supramolecular chemistry is the major field which provides the rules of self-assembly, rendering complex micro and nanostructures directed by the information encoded in the structure of the individual molecules.[4,5] Supramolecular chemistry focuses on reversible non-covalent interactions, including hydrogen-bonding (H-bonding), π-stacking, metal-ligand or van der Waals forces, which are individually weak when compared to covalent bonds.[6] Thus, only the addition or combination of several of these forces affords stable aggregates with prominent morphologies and functions.

Many supramolecular aggregates play a vital role in natural systems. The paradigmatic right-handed triple helix of collagen, one of the most abundant structural proteins in mammals, relies its stability on the intermolecular H-bonds established between the amide groups of left-handed peptide chains (Figure 1). This structure contributes to collagen thermal stability, mechanical strength and capability to interact specifically with other biomolecules.[7,8] This example underlies how the synergy between quite a number of supramolecular interactions can generate robust macromolecules.

[1] G. M. Whitesides, J. P. Mathias, C. T. Seto, *Science* **1991**, *254*, 1312.
[2] G. M. Whitesides, B. Grzybowski, *Science* **2002**, *295*, 2418.
[3] J. M. Lehn, *Proc. Natl. Acad. Sci. U.S.A.* **2002**, *99*, 4763.
[4] J. M. Lehn, *Angew. Chem. Int. Ed.* **1990**, *29*, 1304.
[5] J. M. Lehn, *Science* **1993**, *260*, 1762.
[6] F. Biedermann, H.-J. Schneider, *Chem. Rev.* **2016**, *116*, 5216.
[7] M. D. Shoulders, R. T. Raines, *Annu. Rev. Biochem.* **2009**, *78*, 929.
[8] B. J. G. E. Pieters, M. B. van Eldijk, R. J. M. Nolte, J. Mecinovic, *Chem. Soc. Rev.* **2016**, *45*, 24.

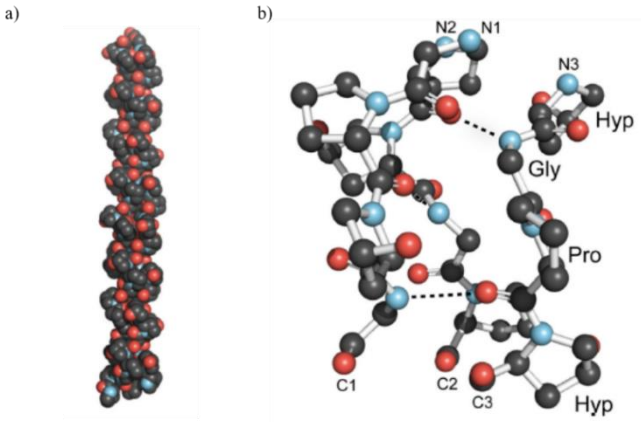

Figure 1. (a) First crystal high-resolution image of collagen right-handed triple helix. (b) Ball and stick model (black, carbon; blue, nitrogen; red, oxygen) of a segment of collagen highlighting the H-bonds between the amides of the different left-handed chains (H atoms are omitted for the sake of simplicity).

Supramolecular polymers are a particular type of supramolecular aggregates comprising one-dimensional structures in which the monomers are held together by means of non-covalent linkages.[9] Although supramolecular polymers exhibit some analogous properties to their covalent counterparts, other features arising from their intrinsic dynamism, such as self-healing and stimuli-responsiveness, can emerge.[10] Eukaryotic cells take advantage of the innate adaptability of these macromolecules in the cytoskeleton. Cytoskeleton controls the shape and deformation of the cell and it is key in essential dynamic cellular functions like division and movement. All these processes stem from the supramolecular polymerization and depolymerization of different proteins to form actin filaments, microtubules and intermediate filaments (Figure 2).[11] In this manner, the reversibility of the non-covalent interactions is responsible for the attainment of functions non-achievable with the only use of covalent bonds.

In an effort to reach the sophistication displayed by Nature, supramolecular polymerization has received increasing attention over the last 30 years[12] and it has

[9] F. Aparicio, F. García, L. Sánchez, in *Encyclopedia of Polymer Science and Technology* Ed. M. Peterca , John Wiley & Sons, Inc., **2012**.
[10] L. Brunsveld, B. J. B. Folmer, E. W. Meijer, R. P. Sijbesma, *Chem. Rev.* **2001**, *101*, 4071.
[11] D. A. Fletcher, R. D. Mullins, *Nature* **2010**, *463*, 485.
[12] C. Fouquey, J. M. Lehn, A. M. Levelut, *Adv. Mater.* **1990**, *2*, 254.

become a topic of growing interest and continuous development.[13] The inherent dynamism of supramolecular polymers furnishes materials which combine good optical, mechanical or electronic properties with the ease of processing.[14] These characteristics make supramolecular polymers appealing and promising alternatives to covalent polymers.

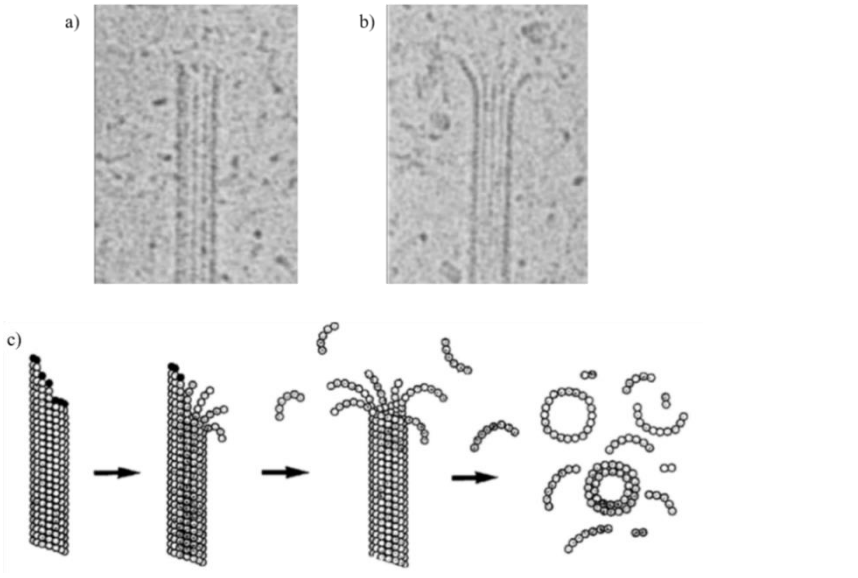

Figure 2. Supramolecular polymerization of α/β tubulin heterodimers gives rise to microtubules. Cryo-TEM images showing the structures of microtubules during (a) elongation and (b) shrinkage. (c) Schematic representation of microtubule depolymerization.

Similarly to their covalent analogues, the mechanism governing the supramolecular polymerization dictates the features and properties of the final macromolecule. Supramolecular polymerization can be considered as the sum of multiple thermodynamic equilibria in each of which a monomer is joined to the polymeric chain.[15,16] If the monomer adds to the growing polymer with the same association constant, regardless of the size of the aggregate, the mechanism is called isodesmic. This mechanism resembles to the step-growth mechanism in covalent

[13] L. Yang, X. Tan, Z. Wang, X. Zhang, *Chem. Rev.* **2015**, *115*, 7196.
[14] T. Aida, E. W. Meijer, S. I. Stupp, *Science* **2012**, *335*, 813.
[15] T. F. A. de Greef, M. M. J. Smulders, M. Wolffs, A. P. H. J. Schenning, R. P. Sijbesma, E. W. Meijer, *Chem. Rev.* **2009**, *109*, 5687.
[16] Z. Chen, A. Lohr, C. R. Saha-Möller, F. Würthner, *Chem. Soc. Rev.* **2009**, *38*, 564.

polymerizations and leads to the obtaining of polydisperse aggregates. On the other hand, if the polymerization demands the formation of a thermodynamically unfavoured nucleus of appropriate size, followed by an elongation process, the mechanism is named nucleation-elongation or cooperative. In analogy to radical covalent polymerization, this mechanism leads to polymers with lower degree of polydispersity. Both mechanisms can be easily assignable if an intrinsic property of the molecule (chemical shift, absorbance, fluorescence, etc.) is plotted against concentration or temperature. While a sigmoidal curve is symptomatic of an isodesmic mechanism, an initial zero slope followed by and hyperbolic loop is ascribable to a cooperative mechanism (Figure 3). There are many mathematical methods in the bibliography that can be employed to obtain a set of relevant thermodynamical parameters (association constants, enthalpy, entropy, etc.) of the supramolecular polymerization process. Some of these methods will be applied in the Results and Discussion section.

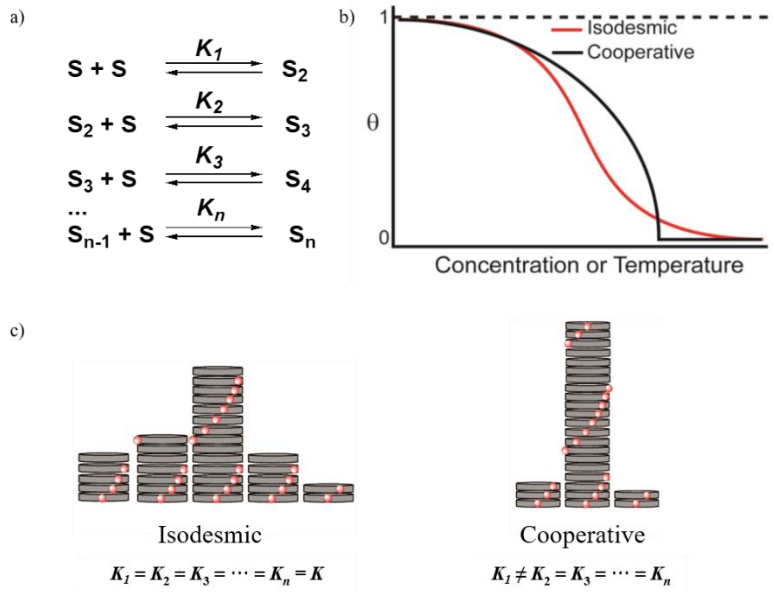

Figure 3. (a) Scheme of the multiple equilibria that compose the supramolecular polymerization process. (b) Variation of an intrinsic property (Θ) against concentration or temperature in isodesmic and cooperative mechanisms. (c) Representation of the degree of polydispersity and the association constants in isodesmic and cooperative mechanisms.

The control achieved over the characteristics and properties of supramolecular polymers have made them to find application in fields ranging from biology to optoelectronics.[14] Especially in the last topic, π-conjugated-based supramolecular polymers have been subjected to intensive studies due to its interesting photophysical features, making them promising candidates as sensors and as main components in different electronic devices.[16]

The control over the spatial arrangement of these scaffolds by means of non-covalent interactions provokes an electronic coupling between monomers that renders aggregates with enhanced properties in comparison to those exhibited by discrete molecules. Therefore, energy harvesting or electron transport, which are highly desirable phenomena for quantum information technologies as well as for efficient solar energy conversion,[17] can be attained by the supramolecular polymerization of π-conjugated compounds.

A remarkable example is depicted in Figure 4, in which molecule **1** is capable of an efficient energy transport at room temperature along single nanofibres due to the self-assembly of carbonyl-bridged triarylamine (CBT) units.[18] Molecule **1** is constituted by a central CBT dye decorated with amides moieties and (5-hexyl-2,2-bithiophene)-naphthalimide (NIBT) chromophores at the periphery. The interaction of **1** through π-stacking between the CBT moieties and H-bonding between the amides generates nanofibres whose further intertwining yields gels in apolar solvents like *o*-dichlorobenzene. The non-covalent forces direct the organization through a cofacial arrangement of the CBTs which diminishes the ability of the system to undergo a radiant decay upon photoexcitation, thus affording a system with a long-lived excited state. The cofacial arrangement of the CBTs into well-ordered domains also precludes the energy transfer to the NIBT moieties, and these features facilitate the separation of charges after photoexcitation, permitting an unprecedented energy transport along macroscopic distances which is only limited by the size of the fibre. Importantly, this energy transport is mainly based in coherent motion thanks to this particular supramolecular organization, although some incoherent motion is also noticed due to the existence of small defects in the nanofibre structure. These outstanding results exemplify the importance of the

[17] S. Ghosh, V. K. Praveen, A. Ajayaghosh, *Annu. Rev. Mater. Res.* **2016**, *46*, 235.
[18] A. T. Haedler, K. Kreger, A. Issac, B. Wittmann, M. Kivala, N. Hammer, J. Köhler, H.-W. Schmidt, R. Hildner, *Nature* **2015**, *523*, 196.

supramolecular polymers based on π-scaffolds and its potential application as electron carriers.

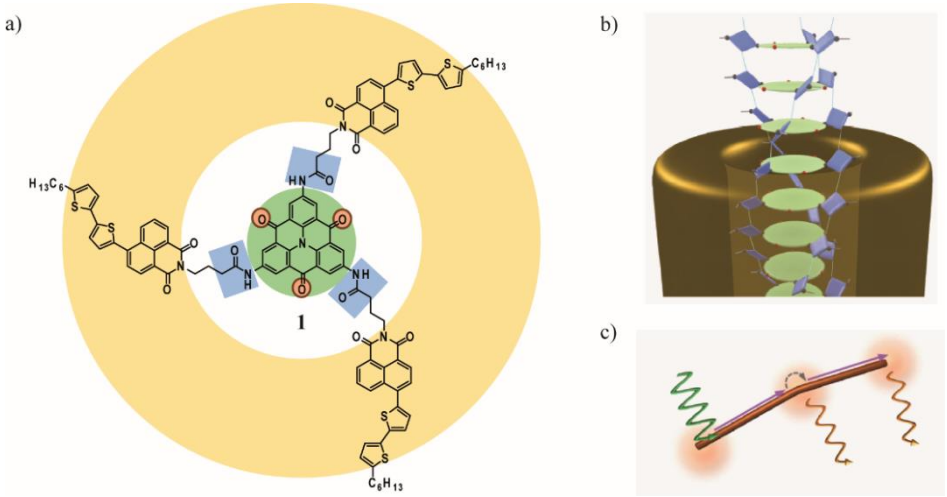

Figure 4. (a) Chemical structure of the CBT **1**, decorated with NIBT at its periphery. (b) Schematic illustration of the cofacial arrangement in the supramolecular polymer formed by **1**. (c) Illustration of the energy transport in molecule **1**. After local illumination at one end (green arrow), coherent energy transport along the ordered nanofibre (violet arrow) takes place. At small defects, like a kink, incoherent energy transfer occurs either to the NIBT periphery, with subsequent photoluminescence (orange arrow), or to the next ordered domain of the core (black dashed arrow), where after coherent transport along the fibre, photoluminescence takes place at the nanofibre's end.

Nowadays, the versatility of organic chemistry makes possible to synthesize almost any monomer, opening the way to the obtaining of supramolecular polymers with an ample range of physicochemical properties. Recently, applications to other fields like biomedical chemistry,[19,20] and the fine tuning exerted in kinetically-controlled and fuel-driven supramolecular polymerizations[21,22] have widen the scope of these dynamic assemblies, making of supramolecular polymerization an emerging and evolving area.

[19] A. Vidyasagar, K. Handore, K. M. Sureshan, *Angew. Chem. Int. Ed.* **2011**, *50*, 8021.
[20] F. Aparicio, E. Matesanz, L. Sánchez, *Chem. Commun.* **2012**, *48*, 5757.
[21] E. Mattia, S. Otto, *Nat. Nanotech.* **2015**, *10*, 111.
[22] S. Dhiman, A. Sarkar, S. J. George, *RSC Advances* **2018**, *8*, 18913.

2. BACKGROUND

π-Conjugated systems display intrinsic properties like luminescence, charge transport and electronic conductivity due to its delocalized π-cloud.[23] These features make π-conjugated compounds appealing candidates in the field of organic electronics and they have already found application in electronic devices like organic field-effect transistors (OFETs),[24] solar cells (OSCs)[25] and light emitting diodes (OLEDs).[26] However, the performance of these devices is often limited by the lack of order of the interacting molecules or polymers due, in some cases, to the presence of ill-defined aggregates, especially when π-conjugated polymers are employed.[27,28] In this regard, a bottom-up approach was envisaged as a promising solution, making supramolecular polymerization of organic semiconductor molecules a topic in continuous motion.[16] Additionally, the electronic coupling between π-conjugated molecules gives rise to functionalities and properties non-exhibited by single building blocks. In this way, control over the morphology of the final supramolecular polymers and tuning the different hierarchical order levels are essential aspects for the attainment of optimal devices based on π-conjugated systems.[29]

The appropriate arrangement of molecules with semiconductor properties is also indispensable in natural chemical processes like photosynthesis. Chlorophyll aggregates are light-harvesting natural systems essential in photosynthetic organisms. These photosynthetic apparatus are mainly constituted by chlorine or bacteriochlorine skeletons, which are derivatives of the porphyrin scaffold.[30] The self-assembly of these molecules in a cyclic arrangement through π-stacking and the assistance of proteins in purple bacteria generates slipped face-to-face aggregates capable of generating and efficiently transporting the exciton after photoexcitation (Figure 5).[31] This example brings to light the importance of the proper supramolecular organization of π-systems and the obtaining of complex functionalities non-attainable by discrete molecules.

[23] M. Pope, C. E. Swenberg in *Electronic Processes in Organic Crystals and Polymers,* 2nd ed.; Oxford University Press, **1999**.
[24] M. Muccini, *Nat. Mater.* **2006**, *5*, 605.
[25] A. W. Hains, Z. Liang, M. A. Woodhouse, B. A. Gregg, *Chem. Rev.* **2010**, *110*, 6689.
[26] K. Müllen, U. Scherf, in *Organic Light Emitting Devices*, VCH: Weinheim, Germany **2006**.
[27] M. Gsänger, D. Bialas, L. Huang, M. Stolte, F. Würthner, *Adv. Mater.* **2016**, *28*, 3615.
[28] M. Mas-Torrent, C. Rovira, *Chem. Rev.* **2011**, *111*, 4833.
[29] O. Ostroverkhova, *Chem. Rev.* **2016**, *116*, 13279.
[30] X. Hu, A. Damjanović, T. Ritz, K. Schulten, *Proc. Natl. Acad. Sci. U.S.A.* **1998**, *95*, 5935.
[31] F. Würthner, T. E. Kaiser, C. R. Saha-Möller, *Angew. Chem. Int. Ed.* **2011**, *50*, 3376.

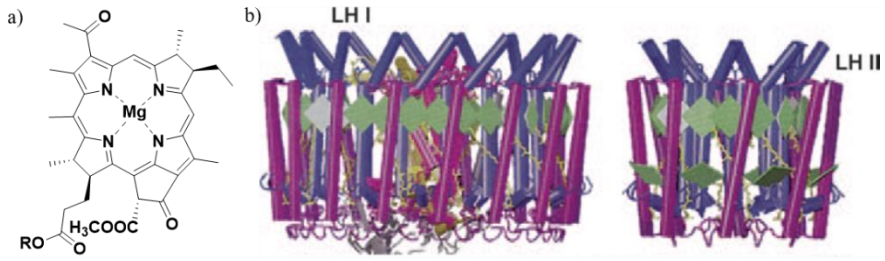

Figure 5. (a) General chemical structure of bacteriochlorophyll-a (BChl-a). (b) Light harvesting complexes I (LH I) and II (LH II) of purple bacteria. The circular arrangement of BChl-a (green squares) in a protein scaffold through π-stacking allows the efficient exciton transport in photosynthetic systems.

Inspired by its pivotal relevance in natural processes, the initial strategy to generate functional supramolecular polymers based on π-conjugated molecules involved the endowing of aromatic substrates like hexa-*peri*-hexabenzocoronenes (HBCs),[32,33] or perylene bisimides (PBIs)[34] with alkyl chains that enhance the solubility of these scaffolds in organic solvents. This design implies the self-organization of these moieties by π-stacking and solvophobic effects, and it also favours liquid-crystal behaviour. The supramolecular polymerization of these molecules has been described to proceed in an isodesmic way and therefore, the polydispersity index (PDI) of the obtained polymers should be high.[15] This strategy shows some limitations due to the lack of directionality of π-stacking, which affords other undesired morphologies that undermine the features of the resulting supramolecular polymer.[35]

[32] M. Kastler, W. Pisula, D. Wasserfallen, T. Pakula, K. Müllen, *J. Am. Chem. Soc.* **2005**, *127*, 4286.
[33] X. Feng, W. Pisula, M. Takase, X. Dou, V. Enkelmann, M. Wagner, N. Ding, K. Müllen, *Chem. Mater.* **2008**, *20*, 2872.
[34] Z. Chen, V. Stepanenko, V. Dehm, P. Prins, L. D. A. Siebbeles, J. Seibt, P. Marquetand, V. Engel, F. Würthner, *Chem. Eur. J.* **2007**, *13*, 436.
[35] C. R. Martinez, B. L. Iverson, *Chem. Sci.* **2012**, *3*, 2191.

To circumvent this problem, the combination of highly directional non-covalent forces like intermolecular H-bonding and π-stacking has been unveiled as a straightforward alternative.[36,37] The high selectivity and directionality of H-bonds supplement π-stacking, giving access to systems with a broader range of morphologies and properties, as well as high internal order derived from the cooperative mechanism emerging from the joining of both forces.[38]

The relevance of this strategy is emphasized in the self-assembly in apolar solvents of chiral oligo-*p*-phenylenevinylene (OPVs) moieties **2-4** decorated with an ureidotriazine moiety at one of the ends and a trialcoxy chain at the opposite part of the molecule.[39] The high complementarity between the donor and acceptor groups in the ureidotriazine moiety leads to a quadruple H-bond array affording dimers that serve as the main scaffold for further growing of the polymer through π-stacking (Figure 6).

The transfer of chirality from the chiral centres to the supramolecule provokes the formation of fibres with a preferred helicity (*M*-type helices) making circular dichroism (CD) studies accessible. Thus, variable temperature (VT) experiments, performed at slow rates to avoid kinetic effects, in UV-Vis, CD and photoluminescence spectroscopies showcase two clear regimes which can be assigned to nucleation and elongation processes, respectively. The authors also applied for the first time a cooperative mathematical model for protein folding to the investigation of supramolecular polymerizations, giving access to a set of thermodynamic data of the supramolecular polymerization process. Additional studies regarding the variation of the longitude of the alkyl chain in the solvent give insight to the importance of the solvent features in the transition temperature from the nucleation regime to the elongation one, which is termed elongation temperature or T_e. This is a remarkable example of a cooperative system in which hierarchical order is achieved by a synergy between H-bonds and π-stacking.

[36] D. González-Rodríguez, A. P. H. J. Schenning, *Chem. Mater.* **2011**, *23*, 310.
[37] E. D. Glowacki, M. Irimia-Vladu, S. Bauer, N. S. Sariciftci, *J. Mater. Chem. B* **2013**, *1*, 3742.
[38] C. Rest, R. Kandanelli, G. Fernández, *Chem. Soc. Rev.* **2015**, *44*, 2543.
[39] P. Jonkheijm, P. van der Schoot, A. P. H. J. Schenning, E. W. Meijer, *Science* **2006**, *313*, 80.

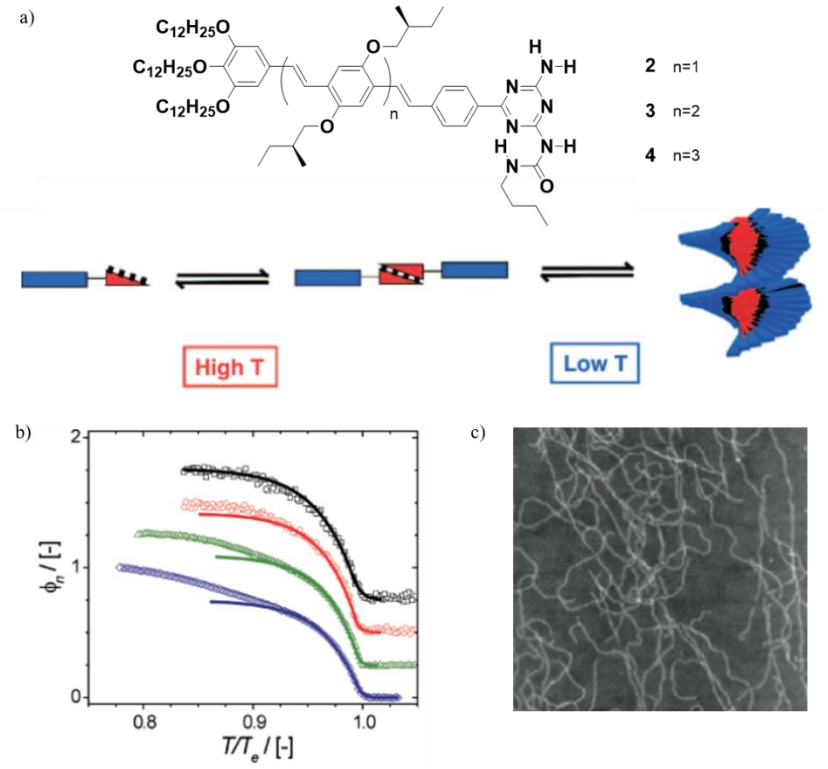

Figure 6. (a) Chemical structure of OPVs derivatives **2-4** and schematic representation of the self-assembly process of these compounds in apolar solvents after cooling. (b) Normalized CD curves of **3** in dodecane (λ = 466 nm, cooling rate 0.5 K min^{-1}) at different concentrations (black c_T = 5.4 μM, red c_T = 11 μM, green c_T = 48 μM, blue c_T = 240 μM). (c) Atomic force microscope (AFM) images of **3** revealing fibrillar structures (drop casting, c_T =130 μM, HOPG).

The coupling between the dipole moments of the monomers in the formation of π-conjugated aggregates can give room to excitonic states rendering supramolecular polymers with characteristic optoelectronic signatures which can be described by the exciton model of Kasha.[40] The situation can be simplified considering the formation of a benzene dimer as depicted in Figure 7. The monomers can be arranged in a face-to-face manner (angle between transition dipole moments Θ = 90º) what makes only possible the transition to the highest level of the excited state, being featured by a hypsochromic shift in the UV-Vis spectrum. These aggregates,

[40] M. Kasha, H. R. Rawls, M. A. E. Bayoumi, *Pure Appl. Chem.* **1965**, *11*, 371.

which have been termed H-aggregates, exhibit also a quenching in fluorescence emission. On the other hand, the slipped face arrangement (Θ = 0º) affords J-aggregates, whose benchmark is the bathochromic effect in UV-Vis spectrum and, especially, the slight Stokes shift in fluorescence spectroscopy accompanied by high quantum yields,[31] due to the fact that only the lowest energy level of the excited state is available. Intermediate situations can arise depending on the angle between the transition dipole moments.

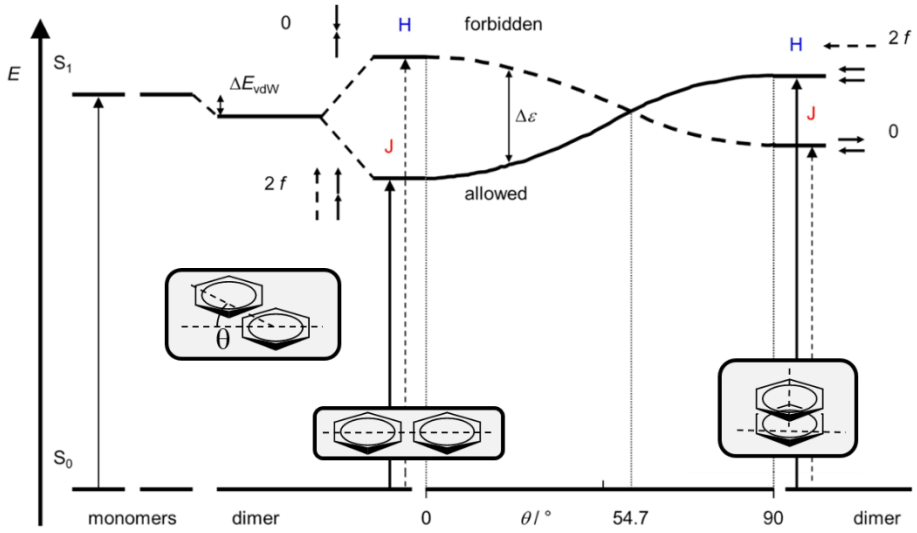

Figure 7. Schematic illustration of the energy levels in the excitonic coupling of benzene dimers. Central box corresponds to the ideal J-aggregate, whereas right box corresponds to the ideal H-aggregate. The left box makes reference to intermediate situations.

The inclusion of amides capable of forming H-bonding in different PBI derivatives has been extensively studied by Prof. Würthner´s group in order to get well-defined H- and, primarily, J-aggregates. PBIs are n-type acceptor molecules with intense photoluminescence[41] which can self-assemble by means of π-stacking. To generate cooperative supramolecular polymerizations, imide-imide H-bonding[42] or side chain amide-amide H-bonding,[43,44] among other strategies, have been combined

[41] F. Würthner, C. R. Saha-Möller, B. Fimmel, S. Ogi, P. Leowanawat, D. Schmidt, *Chem. Rev.* **2016**, *116*, 962.
[42] T. E. Kaiser, V. Stepanenko, F. Würthner, *J. Am. Chem. Soc.* **2009**, *131*, 6719.
[43] S. Ghosh, X.-Q. Li, V. Stepanenko, F. Würthner, *Chem. Eur. J.* **2008**, *14*, 11343.
[44] V. Stepanenko, X.-Q. Li, J. Gershberg, F. Würthner, *Chem. Eur. J.* **2013**, *19*, 4176.

with their strong π-π interactions. Usually, the first approach yields J-aggregates, while in the second one different types of aggregates can be generated, having the substitution pattern of the PBI core and the peripheral alkyl chains a huge impact on the optoelectronic properties of the resulting aggregates. An illustrative example is that of molecules **5-11** (Figure 8). The insertion of linear or branched alkyl chains at the periphery of these PBI derivatives results in totally different modes of aggregation. In the case of **5**, decorated with linear alkyl chains, solvent-dependent UV-Vis spectra in methylcyclohexane/chloroform (MCH/$CHCl_3$) mixtures reveal the emergence of a hypsochromically shifted band, symptomatic of face to face H-type aggregates. On the other hand, the analogous study in the same conditions for **7**, endowed with branched and chiral chains, displays a bathochromically shifted band characteristic of slipped-face J-type aggregates. Owing to the structural similarity between **6** and **10** with **5**, the molecules also generate H-aggregates, while molecule **8**, with predominance of branched chains, affords J-aggregates. In the case of **11**, as a result of the combination of linear and branched chains, the presence of both types of aggregates is unveiled. **9** does not self-assemble in these conditions because of the steric hindrance imparted by its long substituents. The strong tendency of these compounds to aggregate is also proved by their ability to form organogels in different solvents. The different way of packing makes **5-11** to form gels with dissimilar stabilities in a range of organic solvents, being compounds **7** and **8** stronger gelators than the rest of compounds.

To justify these findings, the authors propose that the presence in the γ position of the alkyl chain of a methyl group in **7** and **8** inhibits the dense packing required for the formation of H-aggregates, thus furnishing J-aggregates. This work pinpoints the importance of the steric hindrance imparted by the alkyl chains in the supramolecular polymerization of planar dye aggregates. Further revisiting of these systems discloses the existence of a cooperative mechanism in the self-assembly of **5**,[19] as usually shown when the combination of π-stacking and H-bonding takes place, as well as kinetic effects which will be discussed in the following paragraphs.

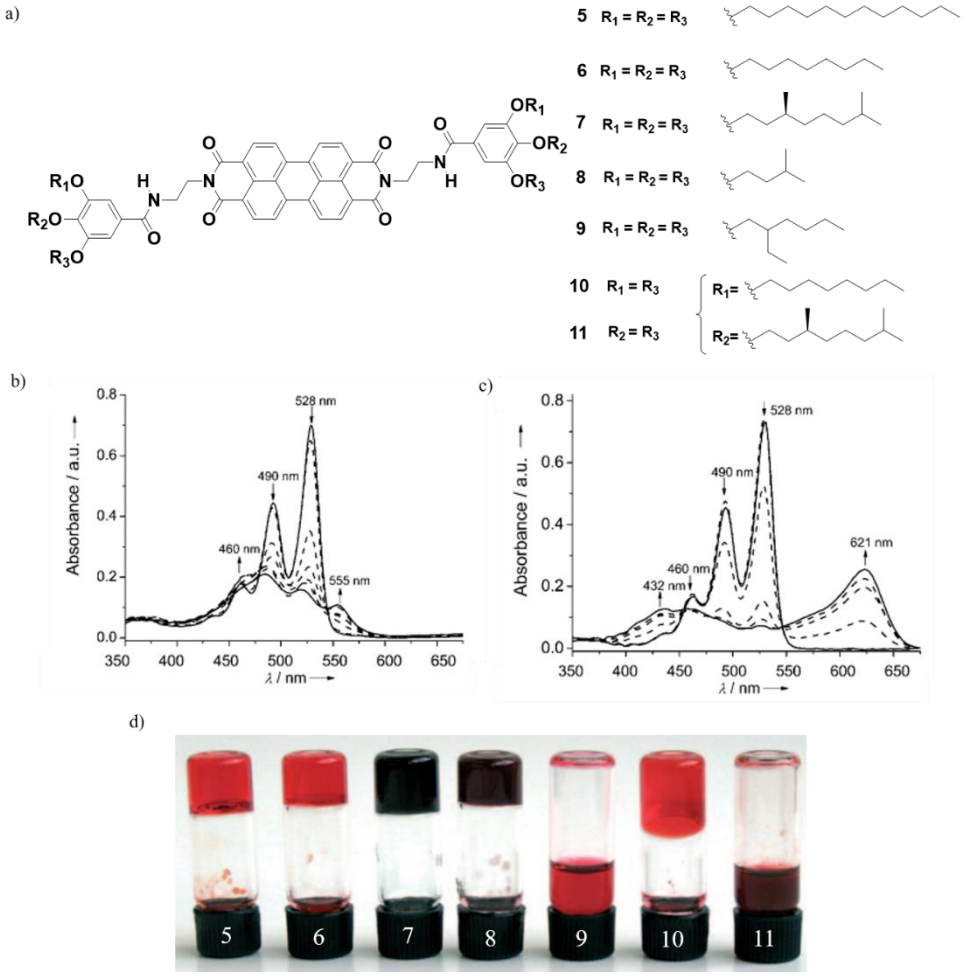

Figure 8. (a) Chemical structure of PBI derivatives **5**-**11**. Solvent-dependent UV-Vis studies (c_T = 10 μM) in MCH/$CHCl_3$ mixtures of **5** (b) and **8** (c) at 25 ºC. (d). Organogels of compounds **5**-**11** in toluene.

As it has been aforementioned, another important feature resulting from the supramolecular polymerization of π-conjugated molecules in organic solvents is the formation of organogels, also called π-gels.[45,46] In gels, the entanglement of 1D fibres can immobilize the solvent molecules producing soft materials whose

[45] A. Ajayaghosh, V. K. Praveen, *Acc. Chem. Res.* **2007**, *40*, 644.
[46] S. S. Babu, V. K. Praveen, A. Ajayaghosh, *Chem. Rev.* **2014**, *114*, 1973.

formation facilitates the transfer of the molecular and supramolecular information to the macroscopic level. In this way, the modulation of the optoelectronic properties through self-assembly can be translated to useful materials. Generally, the combination of π-π interactions, H-bonding and long alkyl chains gives rise to the formation of gels in organic solvents. Our research group in collaboration with Prof. Ajayaghosh has described a noteworthy example of this process derived from the study of the self-assembly of an *N*-annulated perylenedicarboxamide in different organic solvents.[47] *N*-annulated perylene derivatives are p-type donor molecules whose self-assembly permits to attain materials with interesting anisotropic properties. Cooling curves of **12** in MCH depict a non-sigmoidal shape diagnostic of a cooperative mechanism. The packing of the resulting fibres can trap at high concentrations organic solvents like toluene (Tol), yielding organogels (Figure 9).

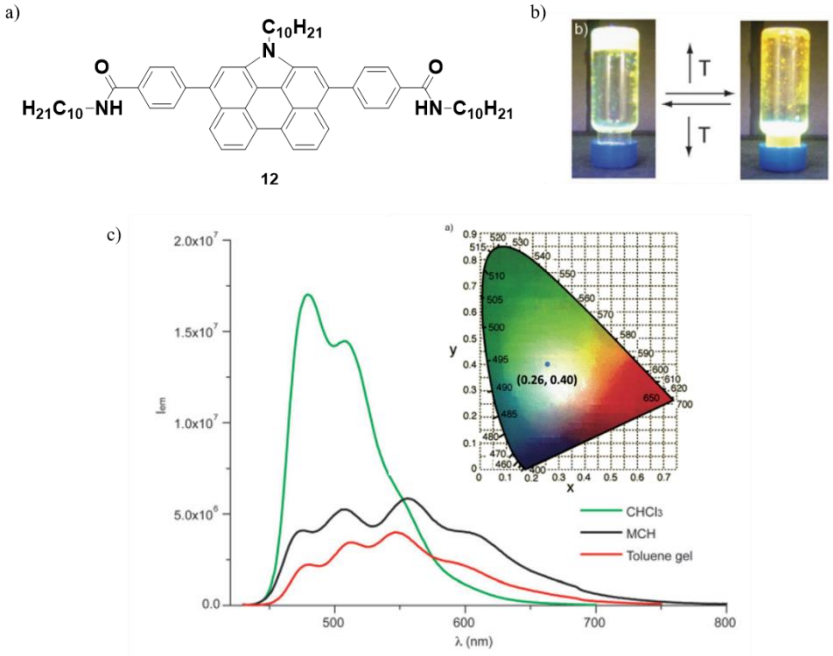

Figure 9. (a) *N*-Annulated perylenedicarboxamide **12**. (b) Gel to sol transition in Tol of **12** under illumination at λ = 360 nm. (c) Emission spectra of **12** (λ = 420 nm) under different conditions (green: $CHCl_3$ c_T = 1 μM, black: MCH c_T = 10 μM, red: Tol gel). The inset shows the chromaticity diagram CIE of **12** gel in Tol, which is in the white light zone.

[47] F. García, J. Buendía, S. Ghosh, A. Ajayaghosh, L. Sánchez, *Chem. Commun.* **2013**, *49*, 9278.

The studies of the fluorescence emission and time decay in both aggregate and gel state show an aggregation quenching effect compared to the monomer and, interestingly, a light emission range whose resulting chromaticity is close to the white light region. The electrical conductivity of the gel fibres obtained in Tol exhibits values which are in the same range than those reported for conductive materials like tetrathiafulvalene or oligothiophenes. This work demonstrates the huge impact that self-assembly through π-π interactions and H-bonding imparts to the optoelectronic features of the constituting building blocks and enhances the importance of the gels as a means to transmit the supramolecular information to the macroscopic features.

These examples underline the relevance of the supramolecular polymerization of π-conjugated molecules through π-π interactions and H-bonding as a fine strategy to supply a series of versatile macromolecules. The reversibility of the non-covalent interactions permits the tuning of the optoelectronic properties by changing the temperature, the concentration or the solvent composition. Nevertheless, the inherent dynamism of supramolecular polymers also constitutes a handicap given that this thermodynamic approach only provides access to a scarce number of morphologies with relatively high distribution of sizes, even when the polymerization proceeds under a cooperative mechanism. The different mathematical methods describing isodesmic or nucleation-elongation mechanisms do not include kinetic considerations, although it is recognized the intrinsic lag phase associated to the formation of the nucleus in cooperative mechanisms. Additionally, kinetic effects have arisen in many systems yielding undesired structures which have prompted the development of a series of protocols to avoid the presence of non-equilibrium structures in order to obtain the desired morphology.[48] Recent investigations in the supramolecular polymerization field have given the path to the study of the kinetic implications, resulting in many cases for the competition among strong non-covalent interactions. Remarkably, the exploitation of kinetically-controlled aggregates could open new venues in the self-assembly of π-conjugated compounds. Thus, self-assembly of extended aromatic molecules endowed with functional groups capable of forming H-bonds is probably the new paradigm to study far-from-equilibrium supramolecular polymerizations,

[48] P. A. Korevaar, T. F. A. de Greef, E. W. Meijer, *Chem. Mater.* **2014**, *26*, 576.

in which the control over the different aggregation pathways and control over the lag phases affords new and unprecedented properties and functions.[49,50,51]

In their seminal work of 2012,[52] Prof. Meijer et al. revisited the self-assembly of the OPV derivative **3**, which had been shown to form *M*-type helices in apolar solvents when the supramolecular polymerization proceeds under thermodynamic control (slow cooling rates, *i.e.*, 0.5 K min^{-1}). Remarkably, cooling down a hot solution of **3** in MCH in an ice bath affords kinetically-trapped *P*-type helices (***P*-3**) that evolve with time to more stable *M*-type helices (***M*-3**). The competition of multiple aggregation pathways for the building blocks is widespread in protein folding and this phenomenon has been termed pathway complexity. In this case, the off-pathway or metastable intermediate *P*-type aggregate sequesters the monomer and avoids the formation of the on-pathway *M*-type polymer (Figure 10a). Further stopped-flow experiments, in which a solution of monomeric **3** in $CHCl_3$ is injected into a MCH reservoir in order to force self-assembly under out-of-equilibrium conditions, enables the quantification of the kinetic effects. Experiments performed at 298 K disclose the formation of the off-pathway product only at high concentrations, and t-50 (the time at which the 50% of the aggregation has occurred) increases with concentration. The authors include a theoretical model to describe the system covering different kinetic aspects and considering, after examination of the experimental data, that the transition from the off-pathway to the on-pathway aggregate involves depolymerization and repolymerization. The resulting model predicts that nucleation events are more energetically favoured in the formation of the *P*-helix, while the elongation process is more feasible in the growing of *M*-helix, what explains the initial appearance of ***P*-3**.

Encouraged by the good agreement between theoretical and experimental results, the authors directed the formation of the kinetic aggregate by the addition of *(S)*-chiral dibenzoyl tartaric acid (DTA) as proper chiral auxiliary. The addition of this compound yields only *P*-type helices (***P*-DTA-3**) that, after removal of the chiral auxiliary by aqueous extraction, remains stable at 273 K, producing ***P*-3** aggregates. Subsequent annealing at 298 K provokes the stereomutation from ***P*-3** to ***M*-3**

[49] F. Würthner, *Nat. Chem.* **2014**, *6*, 171.
[50] R. D. Mukhopadhyay, A. Ajayaghosh, *Science* **2015**, *349*, 241.
[51] D. van der Zwaag, T. F. A. de Greef, E. W. Meijer, *Angew. Chem. Int. Ed.* **2015**, *54*, 8334.
[52] P. A. Korevaar, S. J. George, A. J. Markvoort, M. M. J. Smulders, P. A. J. Hilbers, A. P. H. J. Schenning, T. F. A. de Greef, E. W. Meijer, *Nature* **2012**, *481*, 492.

(Figure 10b). In this way, kinetic studies enrich the understanding of complex supramolecular mechanisms and show the potential of pathway complexity to generate new and complex functionalities in supramolecular polymerizations, as well as the importance of the preparation methodologies in order to avoid spurious competing aggregates.

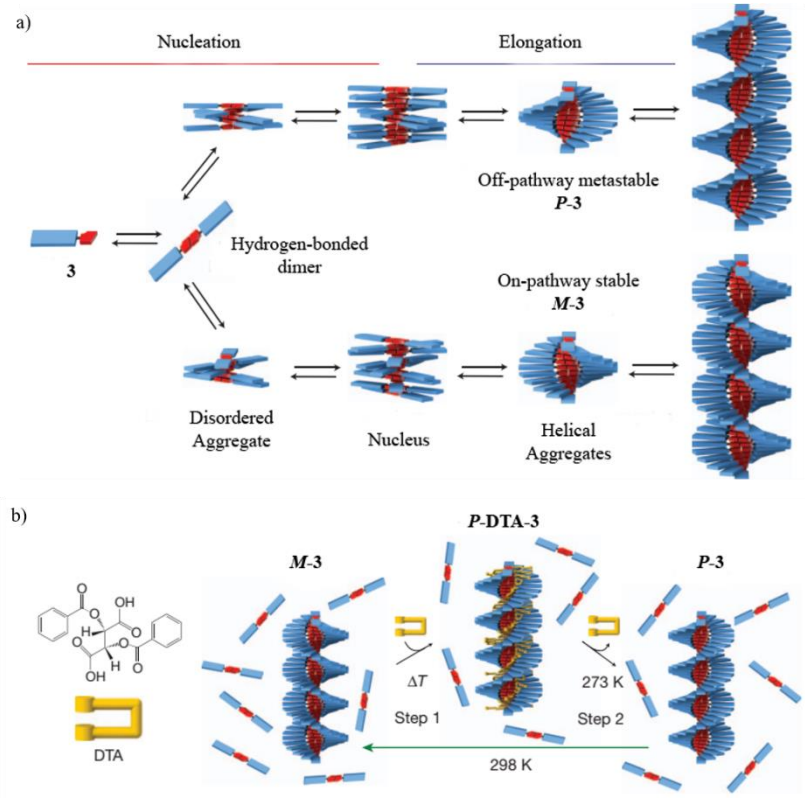

Figure 10. (a) Pathway complexity in **3**, affording off-pathway *P*-type helices (***P*-3**) and on-pathway *M*-type helices (***M*-3**). (b) Schematic representation of the chiral auxiliary strategy to form ***P*-DTA-3**. Subsequent removal of the chiral auxiliary generates ***P*-3** that, after annealing at 298 K, yields ***M*-3**.

Living covalent polymerization is a kinetically-controlled process which renders polymers with defined size and properties and it implies the control over initiation and propagation processes in chain-growth mechanisms.[53] The equivalent living

[53] M. Szwarc, *Nature* **1956**, *178*, 1168.

supramolecular polymerization was an elusive milestone out of reach by means of thermodynamically controlled polymerizations. The command over nucleation and elongation in cooperative mechanisms can be seen as the supramolecular counterpart of initiation and propagation. Unfortunately, even though nucleation involves an energy uphill, this activation barrier is not sufficiently high to avoid elongation, making in this way living supramolecular polymerization unachievable in equilibrium conditions.[54]

Thus, the prevention of spontaneous nucleation is imperative in order to attain living supramolecular polymerizations. Among different strategies, pathway complexity has been envisioned as a useful tool to fulfil this goal. The presence of an off-pathway aggregate which act as a monomer reservoir slows down the nucleation of the on-pathway aggregate. The addition of nucleus or seeds to the on-pathway polymer forces the growing of the thermodynamic polymer in a living manner and, therefore, the attainment of programmable supramolecular polymerizations.[55]

This strategy was elegantly developed by Dr. Sugiyasu, Prof. Takeuchi et al. in the self-assembly of the porphyrin-based molecule **13** (Figure 11a).[56] Cooling a solution of **13** in MCH at 1 K min^{-1} provokes the emergence of a new red-shifted band characteristic of the formation of a J-aggregate. This pattern changes after three days giving rise to an H-aggregate. AFM shows that these two aggregates have different morphologies since the J-aggregates are organized into nanoparticles while the H-aggregates possess a nanofibrillar structure (Figure 11b). Kinetic studies unveil that the transformation from the J- to the H-aggregate have a sigmoidal shape ascribable to an autocatalytic process. The transition is also favoured by lower concentrations, higher temperatures and stirring, implying that H-aggregate recruits from the monomer, not from the J-aggregate. Mechanistic studies reveal that the formation of the J-aggregate proceeds through an isodesmic mechanism, and, on the other hand, the supramolecular polymerization of the H-aggregate is governed by a nucleation-elongation mechanism. All this data demonstrate that the J-aggregate is an off-pathway aggregate which retards the formation of the on-pathway H-aggregate, in analogy to the aforementioned OPV **3**. The kinetically-trapped aggregate sequesters the monomer and avoids the formation of the thermodynamic

[54] D. Zhao, J. S. Moore, *Org. Biomol. Chem.* **2003**, *1*, 3471.
[55] S. Dhiman, S. J. George, *Bull. Chem. Soc. Jap.* **2018**, *91*, 687.
[56] S. Ogi, K. Sugiyasu, S. Manna, S. Samitsu, M. Takeuchi, *Nat. Chem.* **2014**, *6*, 188.

polymer, whose nucleation acts as a "seed" that unchains the elongation. Thus, the addition of an external seed of the H-aggregate to a solution of the J-aggregate triggers and speeds up the transformation from the J-aggregate to the H-aggregate.

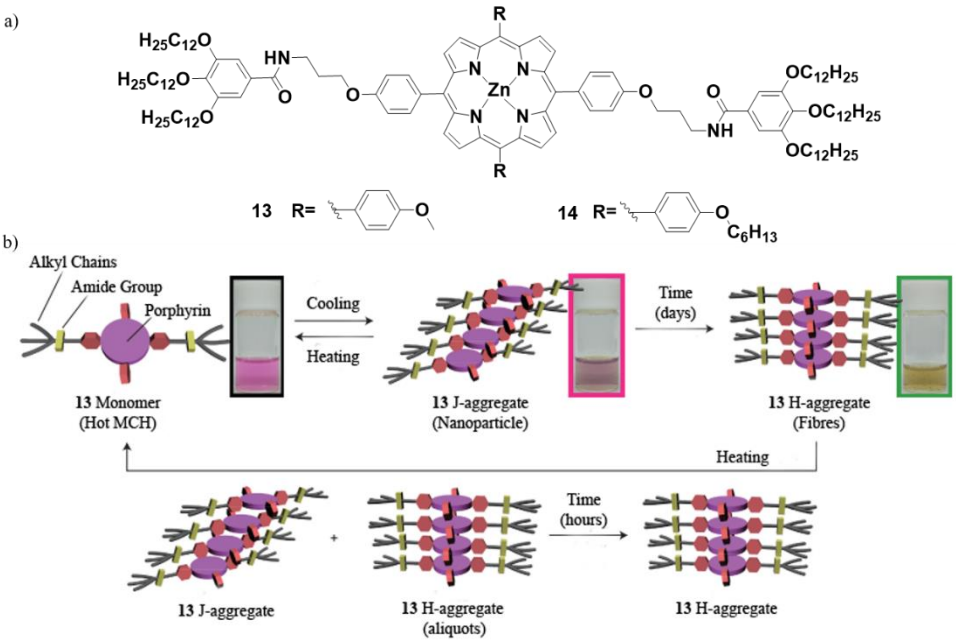

Figure 11. (a) Chemical structure of porphyrins **13** and **14**. (b) Schematic representation of the self-assembly of **13** in MCH. The initial formation of J-aggregates renders nanoparticles that evolve with time to H-aggregate nanofibres. The addition of H-aggregate seeds to a J-aggregate stock speeds up the transition and permits the tuning of the size of the final supramolecular polymer.

This strategy had been previously reported for the self-assembly of covalent block copolymers[57,58] and also a similar approach has been developed to obtain p-n heterojunctions based on π-conjugated supramolecular polymers.[59] In this way, the addition of a J-aggregate solution to an H-aggregate seed solution in a 1:1 ratio permits the formation of H-aggregates in only ten minutes. The subsequent addition of an aliquot from a monomer reservoir enables the growing of the polymer in a controlled manner, achieving low polydispersities (PDI:1.1) and defined sizes

[57] X. Wang, G. Guerin, H. Wang, Y. Wang, I. Manners, M. A. Winnik, *Science* **2007**, *317*, 644.
[58] P. A. Rupar, L. Chabanne, M. A. Winnik, I. Manners, *Science* **2012**, *337*, 559.
[59] W. Zhang, W. Jin, T. Fukushima, A. Saeki, S. Seki, T. Aida, *Science* **2011**, *334*, 340.

which are directly depending on the number of cycles, in analogy to living polymerizations (Figure 12). This process has been termed seeded approach.

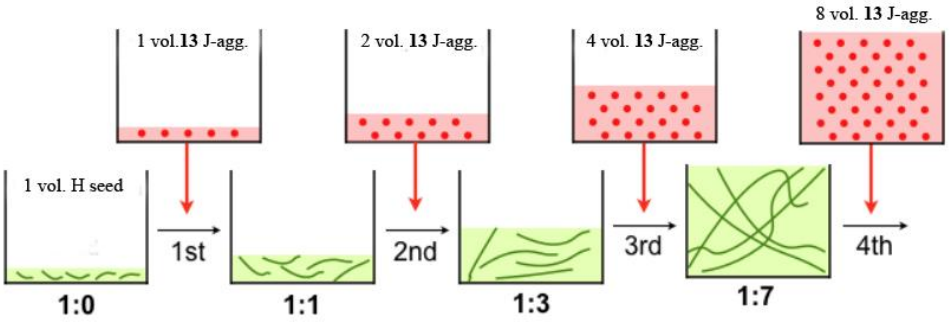

Figure 12. Scheme of the living supramolecular polymerization of **13** through the seeded approach. The addition of subsequent amounts of metastable aggregate to a seed solution of the thermodynamic aggregate supplies polymers with low polydispersities and increasing sizes depending on the number of cycles.

Interestingly, the authors also explored how the structural modifications in the *meso* positions of the porphyrin core affect to the pathway complexity of these scaffolds.[60,61] The resulting energy landscapes for different porphyrin-based systems enhance the importance of steric hindrance in the central core in order to obtain different types of aggregates. The more impressive results are observed in the self-assembly process of compound **14** (Figures 11a and 13). Similarly to **13**, the supramolecular polymerization of **14** in apolar solvents also renders metastable J-aggregates that change over time to form H-aggregates. Surprisingly, these kinetically-trapped monomers can also transform to 2D nanosheets, acting as an on-pathway intermediate in this pathway, *i.e.*, intermediates that do not depolymerize to produce the thermodynamic aggregate. The authors attribute this ability to the efficient interdigitation among alkyl chains in the *meso* positions through van der Waals forces. Tuning the kinetic transitions permits both 1D and 2D living supramolecular polymerizations. These results emphasize the relevance of pathway complexity as a tool to achieve both monodisperse polymers as well as hierarchically ordered structures.

[60] S. Ogi, T. Fukui, M. L. Jue, M. Takeuchi, K. Sugiyasu, *Angew. Chem. Int. Ed.* **2014**, *53*, 14363.
[61] T. Fukui, S. Kawai, S. Fujinuma, Y. Matsushita, T. Yasuda, T. Sakurai, S. Seki, M. Takeuchi, K. Sugiyasu, *Nat. Chem.* **2017**, *9*, 493.

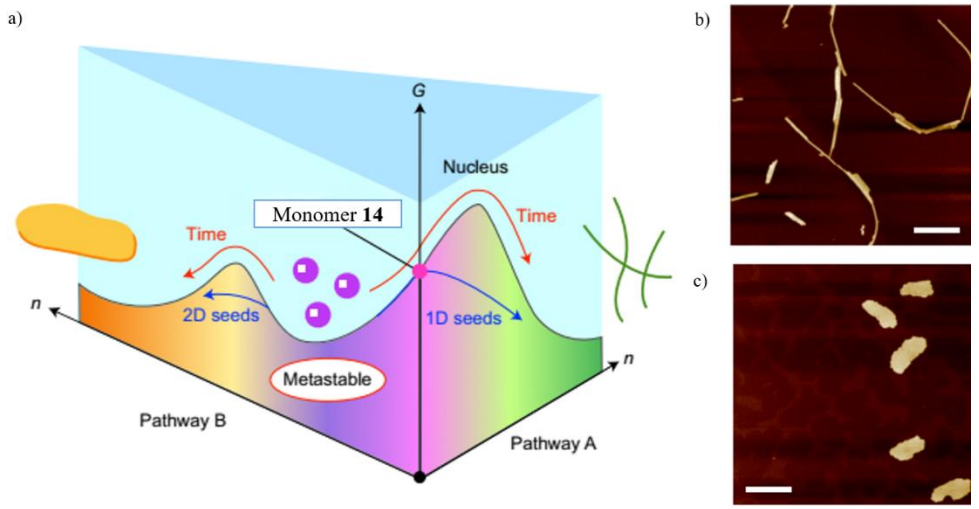

Figure 13. (a) Energy landscapes in the supramolecular polymerization of compound **14**. Metastable nanoparticles can evolve to form 1D nanofibres or 2D nanosheets, permitting living supramolecular polymerizations in both pathways. AFM images of (b) the 1D nanofibres obtained after sonication of metastable nanoparticles and (c) 2D nanosheets obtained by the seeded approach in a living manner.

Another way to develop programmable supramolecular polymerization involves the design of a dormant monomer which prevents the unleashing of nucleation. Thus, the addition of a properly designed initiator can "wake up" or activate the monomer and launch the growing of the polymer in a similar way than radical polymerizations. This way was cleverly disclosed by Prof. Aida and co-workers in the realization of chain-growth supramolecular polymerization of a C_5-symmetric corannulene derivative,[62] a bowl-shaped π-conjugated molecule whose structure resembles partially to fullerene C_{60}. **15** is unable to polymerize at room temperature in organic solvents due to the establishment of an array of intramolecular H-bonds between the amides.[63] However if compound **16**, which is the *N*-methylated counterpart of **15**, is added to a solution of **15**, it acts as initiator of the polymerization because of the presence of a free carbonyl group which behaves as a proton acceptor of H-bonding interactions with **15** (Figure 14). Dynamic light scattering (DLS) experiments, size exclusion chromatography and AFM

[62] J. Kang, D. Miyajima, T. Mori, Y. Inoue, Y. Itoh, T. Aida, *Science* **2015**, *347*, 646.
[63] J. Kang, D. Miyajima, Y. Itoh, T. Mori, H. Tanaka, M. Yamauchi, Y. Inoue, S. Harada, T. Aida, *J. Am. Chem. Soc.* **2014**, *136*, 10640.

experiments prove, not only the growing of the polymers with increasing amounts of **15**, but also the preservation of a low polydispersity index (PDI:1.2) in all the cycles. Interestingly, the chiral counterparts of **15**, **(*S*)-15** and **(*R*)-15**, can yield a stereoselective polymerization when using as initiators **(*S*)-16** and **(*R*)-16**, respectively. Remarkably, utilizing the non-matching chiral centres among initiator and monomer does not unchain the polymerization. This technique can be applied to resolve a racemic mixture of **(*S*)-15** and **(*R*)-15** when using the proper initiator and also to induce a strong chiral amplification if **(*S*)-16** or **(*R*)-16** initiate the polymerization of **15**. In this way, the authors apply the principles of living supramolecular polymerization to achieve homochiral polymers.

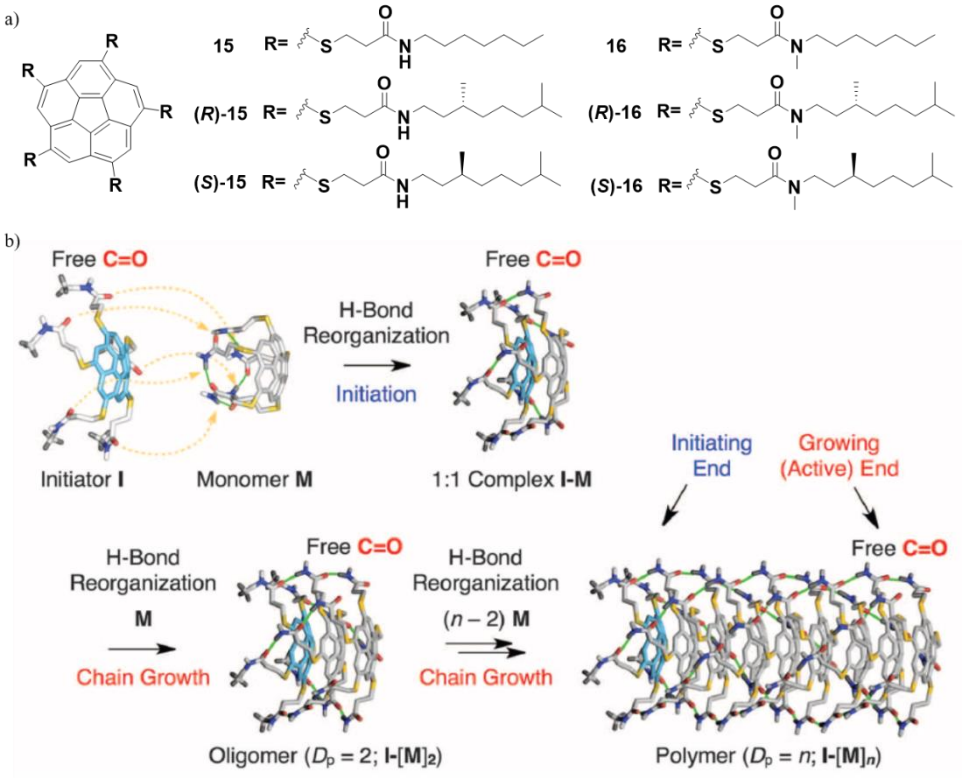

Figure 14. (a) Chemical structure of monomers **15**, **(*S*)-15** and **(*R*)-15** and initiators **16**, **(*S*)-16** and **(*R*)-16**. (b) Concept of the chain-growth living supramolecular polymerization. The properly designed initiator breaks the intramolecular H-bonding array of the dormant monomer and triggers the supramolecular polymerization in a living way.

Prof. Würthner and co-workers have also exploited the existence of intramolecular H-bonding in the aforementioned PBI **5** to delay spontaneous nucleation and perform living supramolecular polymerizations through the seeded approach (Figure 15).[64] The hysteresis revealed after performing heating and cooling curves, and the different T_e observed in the cooling curves in MCH/Tol (2/1) when different rates are applied, imply the inability of the monomer to rapidly undergo supramolecular polymerization due to kinetic reasons. The existence of an intramolecular H-bonding in **5**, which is stabilized by the formation of a 7-membered ring pseudo-cycle and demonstrated by VT-NMR as well as FTIR experiments in solution, prevents the nucleation. The authors also explored the influence of the solvent in the nucleation kinetics, being the hysteresis gap higher with increasing polarity of the solvent. Kinetics studies disclose a sigmoidal shape in the transition from the trapped monomer to the supramolecular polymer which is assignable to an autocatalytic process. Higher concentrations and lower temperatures speed up this transformation, which is the opposite trend to that observed when an off-pathway aggregate is involved. With all this data in hand the authors performed the seeded supramolecular polymerization approach.

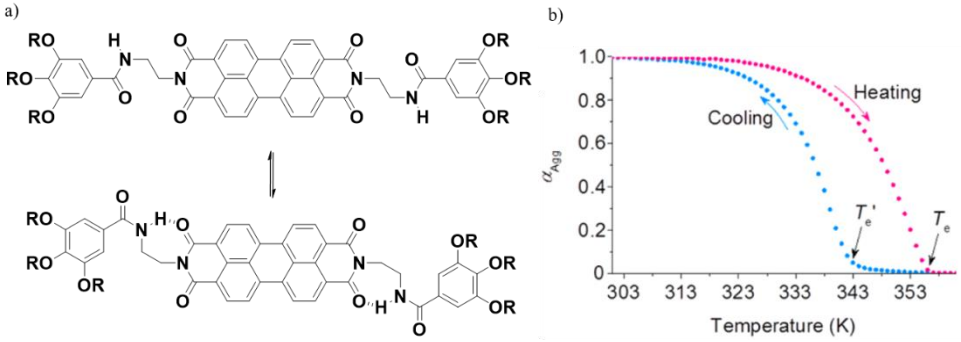

Figure 15. (a) Equilibrium between the open and closed monomer structures of **5**. (b) Cooling and heating curves of **5** disclosing a gap between T_e characteristic of kinetic effects in the supramolecular polymerization.

These authors also explored some structural modifications in order to gain insight in the chemical requirements that are necessary to attain programmable supramolecular polymerizations.[65] The substitution of the ethylene bridge in **5** by

[64] S. Ogi, V. Stepanenko, K. Sugiyasu, M. Takeuchi, F. Würthner, *J. Am. Chem. Soc.* **2015**, *137*, 3300.
[65] S. Ogi, V. Stepanenko, J. Thein, F. Würthner, *J. Am. Chem. Soc.* **2016**, *138*, 670.

longer alkyl chains (from propylene to pentylene) affects the stability of the intramolecular H-bond, which directly impacts the kinetics of the supramolecular polymerization process. FTIR in solution and fluorescence spectroscopy unravel the decreasing tendency of forming H-bonding with increasing alkyl chain length, due to the destabilization of the pseudo-cycle. Surprisingly, whereas the self-assembly of **17** and **19** follows a similar route than **5**, the intramolecular H-bonded state in **18** permits the formation of an off-pathway state that changes through time to the on-pathway aggregate (Figure 16). This system possesses features which are close to those of the porphyrin-based system described by Dr. Sugiyasu, Prof. Takeuchi et al. and can be subjected to the seeded approach, which is also employed in the gel state.

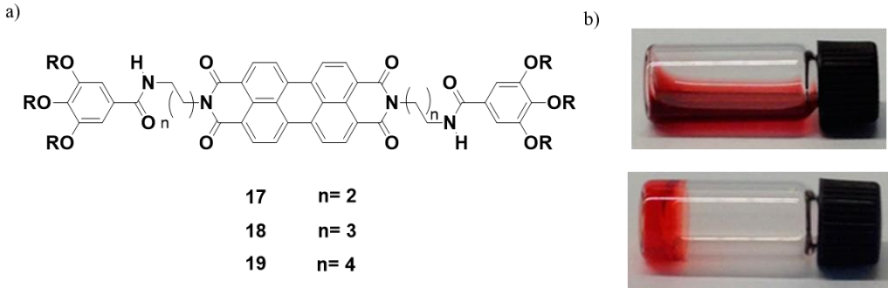

Figure 16. (a) Chemical structure of compounds **17**-**19**. (b) The off-pathway aggregate displayed by **18** is not able to form gels (upper image). The addition of a seed of the on-pathway aggregate triggers the transition and permits the obtaining of gels (lower image).

Finally, further substitution patterns are investigated, like the substitution at the 1 and 7 position in the central core, rendering molecule **20**. Self-assembly experiments of **20** show the formation of an H-aggregate under kinetic conditions (cooling curve 5 K min^{-1}) through an isodesmic mechanism. This metastable aggregate transforms into J-type aggregates with time, which can also be generated when applying slow cooling rates, and unveils a cooperative mechanism for this pathway (Figure 17).[66] The exploitation of this transition permits the fulfilment of living supramolecular polymerization in a multicycle way. Hence, the kinetic stability of the trapped monomer and the off-pathway intermediate constitutes the essential tool for the realization of one or more cycles in living supramolecular polymerization, what affects to the size of the final aggregate.

[66] W. Wagner, M. Wehner, V. Stepanenko, S. Ogi, F. Würthner, *Angew. Chem. Int. Ed.* **2017**, *56*, 16008.

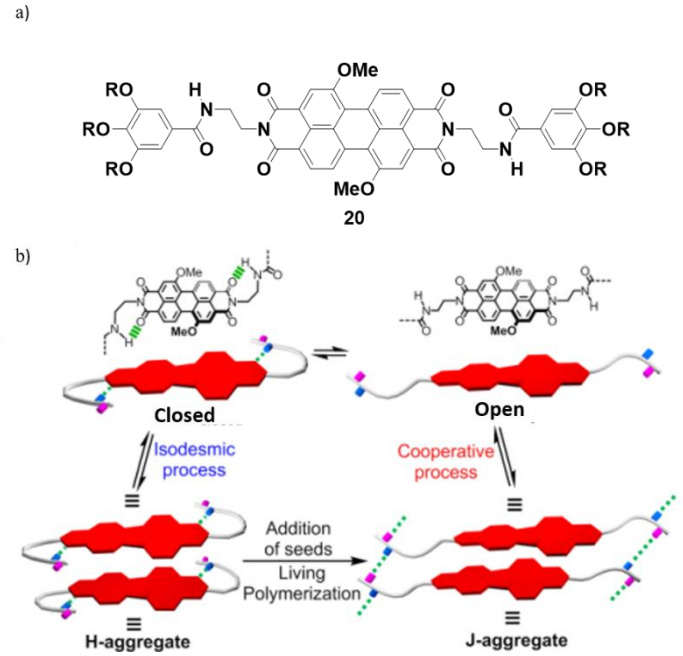

Figure 17. (a) Chemical structure of 1,7-dimethoxy substituted PBI **20**. (b) Schematic representation of the pathway complexity depicted by **20**. The closed conformation can polymerize to afford a metastable H-aggregate though π-stacking, whereas the open conformation can yield J-aggregates by means of H-bonding and π-stacking.

The chemical substitution pattern in the formation of the intramolecular H-bond can also have a decisive role in the order generated in the different hierarchical levels. A noticeable example has been provided by our research group when studying the self-assembly of *N*-annulated perylene derivatives **21**-**24**.[67,68] The supramolecular polymerization of the perylenetetracarboxamide **21** in organic solvents provokes a three-domain self-assembly involving pathway complexity and hierarchical order through bundling of the 1D obtained fibres. The lack of amides in **24** makes this compound unable to polymerize in organic solvents by the sole operation of π-stacking. Especially captivating are the differences encountered when studying the self-assembly of the perylenedicarboxamides **22** and **23**, which only differ in the different connectivity of the amide to the perylene core. The presence of an ester group close to the amide can afford in both cases an intramolecular H-bonding in

[67] E. E. Greciano, L. Sánchez, *Chem. Eur. J.* **2016**, *22*, 13724.
[68] E. E. Greciano, B. Matarranz, L. Sánchez, *Angew. Chem. Int. Ed.* **2018**, *57*, 4697.

analogy to the systems showcased in the previous paragraphs, as has been demonstrated by NMR experiments. UV-Vis studies of **22** unveil the presence of a metastable aggregate that evolves to a more stable aggregate though time. The kinetic effects observed are characteristic of an on-pathway intermediate which directly rearranges into the thermodynamic product with no need to depolymerize, which is opposite to the behaviour of the previously mentioned systems. This transition can be speeded up with the addition of seeds in different ratios. On the other hand UV-Vis studies of **23** only disclose the presence of one type of aggregate. However, the cooling curves have two transitions which are symptomatic of a hierarchical process, probably due to the efficient interdigitation between the 1D supramolecular polymers. AFM images unravel the presence of single entities of compound **22** and an entangled network of fibres for compound **23**, which is in agreement with the spectroscopical data (Figure 18).

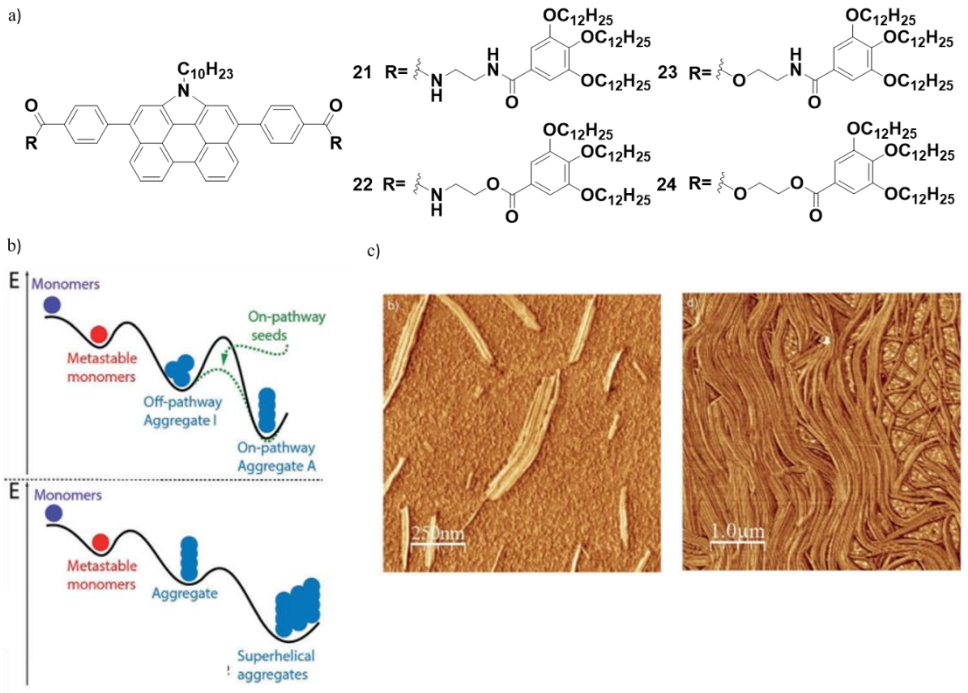

Figure 18. (a) Chemical structure of *N*-annulated perylene derivatives **21**-**24**. (b) Energy landscapes in the supramolecular polymerization of compounds **22** (upper image) and **23** (lower image). (c) AFM phase images of **22** showing 1D aggregates (left image) and **23** revealing a bundle of fibres (right image).

To justify these findings, the authors postulate that in the case of **22**, the amide is very close to the aromatic core and the aromatic wedges present higher degree of conformational freedom, which provokes a less efficient π-stacking in the central moiety yielding, in this way a metastable aggregate. Opposite to **22**, in **23** the outer amide diminishes the degree of freedom of the peripheral chain, restricting the π-stacking of the central core and allowing a proper disposition of the alkyl chains to interdigitate.

All these examples bring out how subtle molecular modifications have huge impact not only on the morphology of the final macromolecule but also on the pathways and kinetic effects involved in the supramolecular polymerization process. Besides the requirement of a cooperative mechanism, the ability to form intramolecular H-bonding coupled with strong aromatic interactions has been shown to be a proper strategy to achieve kinetically-controlled complex supramolecular systems.[21] Additionally, the kinetic studies have also revealed the strong dependence between the position of the different functional groups and the stability of the dissimilar entities involved in the supramolecular polymerization process, what constitutes a key fact for the attainment of living and seeded supramolecular polymerizations by means of non-equilibrium supramolecular polymerizations.[69] These insights expose the potential applications of well-defined supramolecular polymers based-on π-conjugated molecules and the emergence of incoming morphologies like block supramolecular copolymerization[70] or surface-grafted supramolecular polymerizations,[71] which are essential for the realization of important electronic processes. Thus, the capability to control the transition between kinetic and thermodynamic polymers open venues to a new generation of chemical systems with outstanding properties and sophisticated functions.[72]

[69] A. Sorrenti, J. Leira-Iglesias, A. J. Markvoort, T. F. A. de Greef, T. M. Hermans, *Chem. Soc. Rev.* **2017**, *46*, 5476.
[70] S. H. Jung, D. Bochicchio, G. M. Pavan, M. Takeuchi, K. Sugiyasu, *J. Am. Chem. Soc.* **2018**, *140*, 10570.
[71] H. Frisch, E.-C. Fritz, F. Stricker, L. Schmüser, D. Spitzer, T. Weidner, B. J. Ravoo, P. Besenius, *Angew. Chem. Int. Ed.* **2016**, *55*, 7242.
[72] G. Ashkenasy, T. M. Hermans, S. Otto, A. F. Taylor, *Chem. Soc. Rev.* **2017**, *46*, 2543.

3. AIM AND SCOPE OF THE THESIS

The relevance of self-assembling π-conjugated compounds, as shown in the Background section, makes imperative further understanding of the structural and mechanistic rules which govern the formation of supramolecular aggregates based on π-scaffolds. The main aim of the present thesis consists in the study of the supramolecular polymerization process of different π-compounds (namely pyrenes, helicenes and *N*-heterotriangulenes) to yield highly organized nanostructures in organic solvents. The general strategy involves the decoration of these moieties with amide groups capable of forming H-bonding that, in combination with the π-stacking among the aromatic units, should render supramolecular polymers through a cooperative mechanism. Additionally, long alkyl chains are also included in the periphery of the π-scaffolds to enhance the solubility of these compounds in apolar media and direct the formation of organogels. The synergy between spectroscopic and microscopic techniques permits the extraction of the thermodynamic parameters governing the process and the visualization of the morphology of the resulting aggregates. Other objectives comprise the study of kinetically-controlled supramolecular polymerizations through an adequate molecular design and the study of the transfer and amplification of chirality phenomena in equilibrium and out-of-equilibrium conditions by means of the inclusion of distinct asymmetry centres.

To gain insight in the properties of pyrene aggregates, an achiral and a chiral pyreneimidazole derivatives, decorated with an amide group, have been synthesized and investigated in Section 1. The endowing of the pyrene core with bulky substituents should diminish its strong tendency to interact through π-stacking, thus enhancing the solubility of the aggregate. The combination of the π-interactions with the H-bonds established by the imidazole ring and the amide moiety should render supramolecular polymers in organic solvents. The presence of additional alkyl chains in the periphery aids to increase the solubility of these aggregates in organic solvents, and should also direct the formation of organogels.

To investigate the configurational stability of [5]-helicenes unsubstituted at the fjord positions, as well as their self-assembling capability, the supramolecular polymerization of two 5,7,8,10-tetrasubstituted [5]-helicene derivatives, endowed with two and four amides, has been studied in Section 2. These molecules should form supramolecular polymers in solution through π-stacking and H-bonding. Additionally, the chiral resolution of the atropisomers of these helicenes could make also feasible the study of the different supramolecular polymerization of the

enantiomers in solution, thus shedding light in the relevance of atropisomerism in supramolecular polymerizations and *vice versa*.

Considering previous studies in the supramolecular polymerization of C_3-symmetric molecules and the emerging importance of the *N*-heterotriangulene scaffold in organic electronics, the last two Sections are devoted to this moiety. Thus, in Section 3 the evaluation of the self-assembly features of *N*-heterotriangulene-ethynylene-extended tricarboxamides is carried out. The presence of the aromatic core and the amide moieties should favour the self-assembly through π-stacking and H-bonding. Besides, the inclusion of ethynylene groups has been described to yield more soluble *N*-heterotriangulene derivatives and, at the same time, extends the π-core and enables it to interact through stronger non-covalent interactions. Importantly, the inclusion of long alkyl chains should facilitate the formation of organogels.

On the quest of kinetically-controlled supramolecular polymerizations, in Section 4 a new family of *N*-heterotriangulenes, in which the introduction of an inner ester and an ethylene bridge between this group and the amide functionality should provide a perfect substitution pattern for the formation of an intramolecular H-bond stabilized by a 7-membered pseudocycle, is investigated. This intramolecular interaction should slow down the polymerization and could generate metastable species. The control over out-of-equilibrium entities could allow the attainment of seeded supramolecular polymerizations, thus furnishing aggregates with low polydispersity. Additionally, the introduction of lineal and branched alkyl chains increases the solubility of the supramolecular polymers and, in the latter case, permits studying the influence of the chiral chain in kinetically-controlled supramolecular polymerizations and in the seeded approach.

Finally, the presence of chiral centres and the kinetic effects experienced by these *N*-heterotriangulene family allows to study transfer and amplification of chirality phenomena in out-of-equilibrium conditions. Thus, the chiral centres at the peripheral chains, as well as their ability to generate kinetically-trapped monomers *M** and metastable aggregates, should permit the investigation of the chiroptical features of pristine solutions of these compounds and also their co-assembly characteristics by means of *MR* and *SaS* experiments. The tuning of temperature and time could disclose novel phenomena concerning kinetically-controlled amplification of chirality in dynamic systems as well as new emerging scenarios.

4. RESULTS AND DISCUSSION

4.1. Supramolecular polymerization of pyrene derivatives

4.1.1. Pyrene derivatives

Among polycyclic aromatic hydrocarbons (PAHs), pyrene (Figure 19) is probably the most employed as fluorescent probe due to its capability to form excimers, its long lived excitation states, high quantum yield and easy distinction between the monomer and the excimer emission pattern.[73] Furthermore, its well-known photophysical and electronic properties have made pyrene a good candidate for its application in organic electronic dispositives.[74] The optical and electronic properties of pyrene can be easily tuned by modifying the substitution patterns and also by its bestowing with donor or acceptor groups, giving rise to pyrene derivatives with outstanding functions.[75] However, pyrene possesses a high tendency to interact by π-π stacking in the solid state, what supresses its emissive properties.[76] On the other hand, in order to generate pyrene-based electronic devices, the supramolecular organization of this scaffold results mandatory. Thus, to obtain pyrene derivatives with possible technological applications, a fine balance among the different non-covalent interactions should be considered, in such a way that the essential supramolecular organization do not counteract with its outstanding electric and emissive properties.

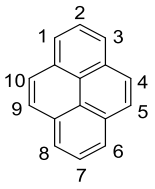

Figure 19. Chemical structure of pyrene. The numbers depict the substitution positions.

To attain this goal, the two pyreneimidazole derivatives **25** and **(*S*)-26** have been designed (Figure 20). The endowing of the pyrene core with bulky substituents at the positions 2 and 7 diminishes its strong tendency to interact by means of π-π interactions, while the presence of an imidazole ring fused to the 4 and 5 positions and an amide moiety in the periphery permits the formation of H-bonds which

[73] T. M. Figueira-Duarte, K. Müllen, *Chem. Rev.* **2011**, *111*, 7260.
[74] C. Wang, H. Dong, W. Hu, Y. Liu, D. Zhu, *Chem. Rev.* **2012**, *112*, 2208.
[75] M. Stępień, E. Gońka, M. Żyła, N. Sprutta, *Chem. Rev.* **2017**, *117*, 3479.
[76] F. Liu, C. Tang, Q.-Q. Chen, F.-F. Shi, H.-B. Wu, L.-H. Xie, B. Peng, W. Wei, Y. Cao, W. Huang, *J. Phys. Chem. C* **2009**, *113*, 4641.

should render supramolecular polymers in apolar solvents. The presence of alkyl chains also aids to further increase the solubility of these aggregates in organic solvents, what is an important issue for its processability, and should also direct the formation of organogels.

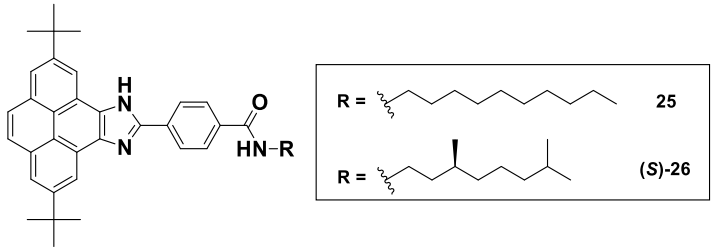

Figure 20. Chemical structure of the pyreneimidazole derivatives **25** and **(*S*)-26**.

4.1.2. Synthesis of pyreneimidazole derivatives 25 and (S)-26

The synthesis of pyreneimidazole derivatives **25** and **(*S*)-26** involves a series of chemical reactions which are summarized in Scheme 1. First, the synthesis of the peripheral chains has been carried out. The catalytic hydrogenation of the double bond of (*S*)-citronellol generates the branched alcohol **(*S*)-27**.[77] A Mitsunobu reaction between phtalimide and **(*S*)-27**, using diisopropyl azodicarboxylate (DIAD) and PPh_3 as coupling agents, affords compound **(*S*)-28**.[78] Subsequent reaction of **(*S*)-28** with hydrazine yields the chiral amine **(*S*)-29** in good yields.[79] Further amidation of 4-formilbenzoic acid with commercial 1-decilamine (**30**) and with **(*S*)-29**, using 1-ethyl-3-(3-dimethylaminopropyl)carbodiimide hydrochloride (EDC) as coupling agent and 4-dimethylaminopyridine (DMAP) as base, enables the obtaining of the 4-formilbenzamides **31** and **(*S*)-32**, respectively.

The aromatic central core has been prepared following a multistep approach previously described in the literature. Prior studies have revealed the importance of including alkyl chains in the central core in order to avoid solubility problems. To attain this goal, two bulky *tert*-butyl groups have been included selectively at the 2

[77] M. Nieuwenhuizen, M. L, T. F. A. de Greef, R. L. J. van der Bruggen, J. M. J. Paulusse, W. P. J. Appel, M. M. J. Smulders, R. P. Sijbesma, E. W. Meijer, *Chem. Eur. J.* **2010**, *16*, 1601.
[78] T. Terashima, T. Mes, T. F. A. de Greef, M. A. J. Gillissen, P. Besenius, A. R. A. Palmans, E. W. Meijer, *J. Am. Chem. Soc.* **2011**, *133*, 4742.
[79] G. Koeckelberghs, L. De Cremer, W. Vanormelingen, W. Dehaen, T. Verbiest, A. Persoons, C. Samyn, *Tetrahedron* **2005**, *61*, 687.

and 7 positions through a Friedel-Crafts alkylation, utilizing *tert*-butyl chloride as reagent and $AlCl_3$ as catalyst, giving rise to compound **33**.[80] The oxidation at the 4 and 5 positions, using $RuCl_3$ in the presence of $NaIO_4$ as oxidative catalytic system, provides the pyrenodione **34**.[81] In this reaction the stoichiometric control results indispensable to obtain 4,5-pyrenedione **34** over 4,5,9,10-pyrenetetraone. Finally, the condensation of **34** with the formilbenzamides **31** and **(*S*)-32** in an ammonium acetate/acetic acid medium at reflux,[82] generates the imidazole ring thus furnishing compounds **25** and **(*S*)-26** in moderate yields.

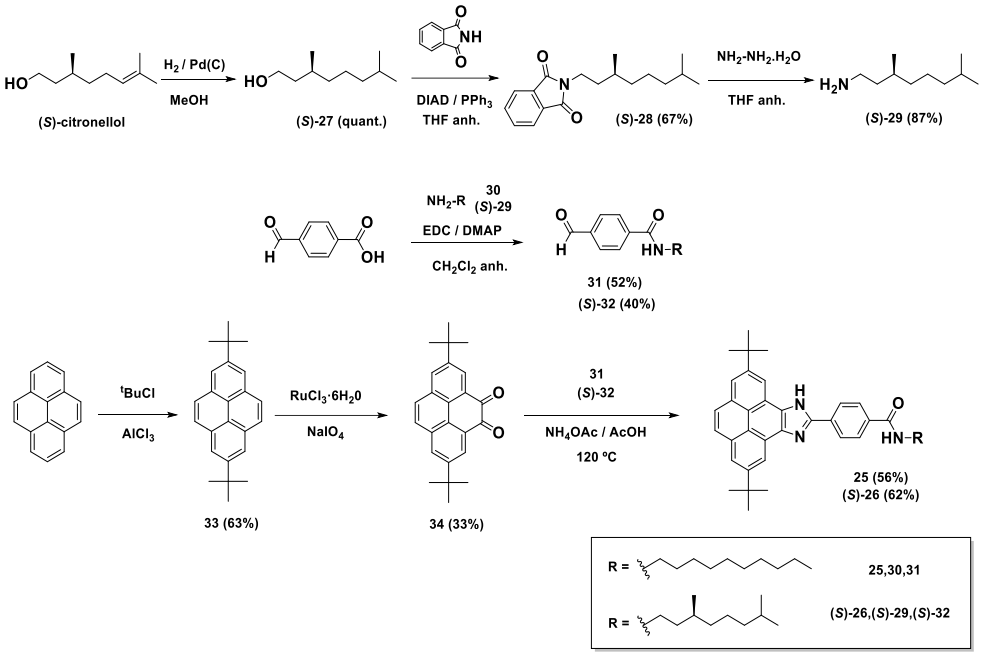

Scheme 1. Synthesis of pyreneimidazole derivatives **25** and **(*S*)-26**.

The chemical structure of all the new synthesized compounds has been determined by means of the usual spectroscopic techniques (the complete characterization can be consulted in the Experimental Part Section).

[80] T. Yamato, A. Miyazawa, M. Tashiro, *Chem. Ber.* **1993**, *126*, 2505.
[81] J. Hu, D. Zhang, F. W. Harris, *J. Org. Chem.* **2005**, *70*, 707.
[82] D. Kumar, K. R. J. Thomas, C.-C. Lin, J.-H. Jou, *Chem. Asian J.* **2013**, *8*, 2111.

4.1.3. Self-assembly of pyreneimidazoles 25 and (S)-26 in solution

The first hint of the capability of compounds **25** and **(*S*)-26** to self-assemble is disclosed by FTIR studies (Figure 21). The low values of the N-H stretching bands ($\tilde{\upsilon}$ ~ 3200 cm^{-1}), when compared to the referenced value of $\tilde{\upsilon}$ = 3450 cm^{-1}, are a first symptom of the presence of H-bonds in the aggregate. Additionally, the values of the Amide I ($\tilde{\upsilon}$ = 1650 cm^{-1}) and Amide II ($\tilde{\upsilon}$ = 1560 cm^{-1}) deformations are a neat diagnostic of the formation of H-bonding between amides.[83,84] Besides, these last two frequencies have two additional shoulders which could be assignable to the C=N stretching and the C-N bending of the imidazole ring, what would imply the participation of this ring in the H-bonding array.

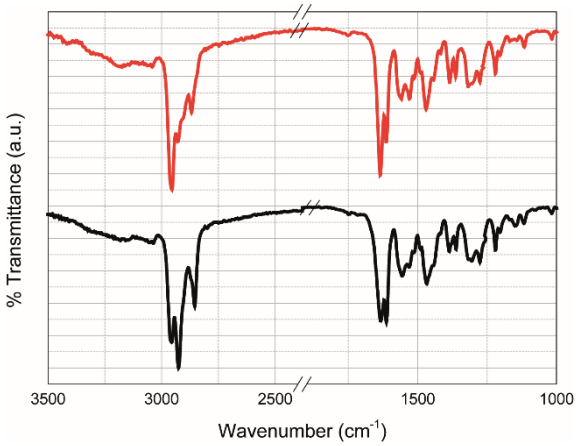

Figure 21. Partial FTIR spectra of **25** (black line) and **(*S*)-26** (red line) at room temperature.

A conclusive evidence of the ability of **25** and **(*S*)-26** to form organized supramolecular entities arises from variable concentration ^{1}H NMR studies (Figure 22). The downfield shift experienced by the imidazole protons (δ ~ 13 ppm, white dot) and the triplet of the amide proton (δ ~ 6.5 ppm, orange dot) with increasing concentration constitutes an indication of the involvement of these groups in H-bonding. The shielding of the methylene group in α to the amide (δ ~ 3.3 ppm, green dot) is also related to this non-covalent interaction. On the other hand, the aromatic protons show an opposite pattern. Whilst one of the protons ascribable to the pyrene

[83] E. Pretsch, P. Bülhman, M. Badertscher, in *IR Spectroscopy in Structure Determination of Organic Compounds*, Springer, **2009**.
[84] F. García, L. Sánchez, *J. Am. Chem. Soc.* **2012**, *134*, 734.

moiety (δ ~ 9 ppm, black dot) suffers a deshielding effect with increasing concentrations, the protons referable to the aromatic system (δ ~ 8.2 ppm, blue dot and δ ~ 7.5 ppm, red dot) shift to high fields upon the same conditions, what evidences the involvement of these protons in C-H···π interactions and π-π stacking, respectively.

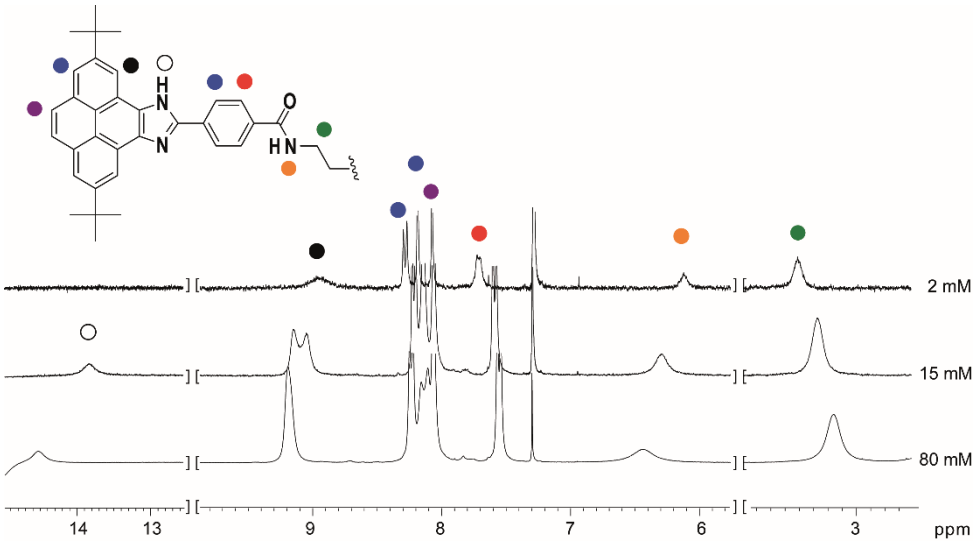

Figure 22. Partial ^{1}H NMR spectra of **25** at different concentrations ($CDCl_3$, 300 MHz, 298 K).

To gain insight into the supramolecular polymerization mechanism and to extract the thermodynamic data of the process, VT-UV-Vis studies have been performed at different concentrations using MCH as solvent (Figure 23a). The bands observed at around λ = 355 and λ = 400 nm in the UV-Vis spectra of both **25** and **(*S*)-26** experience a slight bathochromic shift and a broadening after decreasing the temperature, denoting an aggregation process. The presence of crossing points between the different spectra is diagnostic of the existence of different stoichiometric species. Plotting the variation of the absorbance at λ = 404 nm against temperature results in cooling curves with an apparent sigmoidal shape, characteristic of an isodesmic supramolecular polymerization mechanism (Figure 23b).

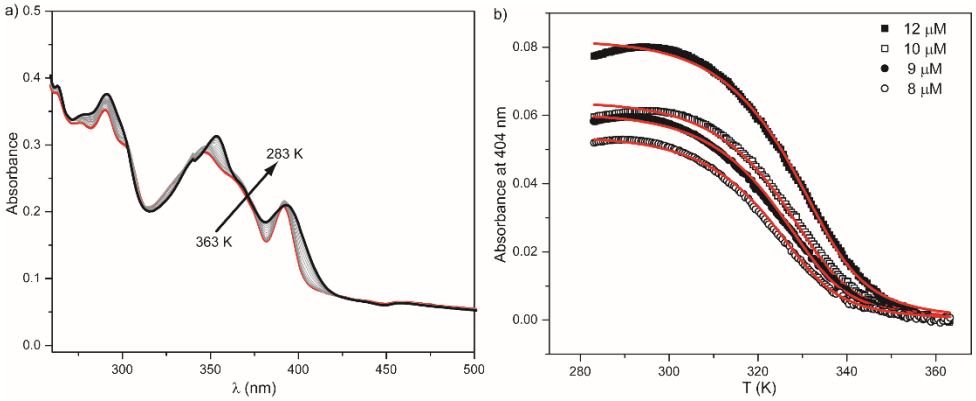

Figure 23. (a) VT-UV-Vis spectra of **25** in MCH (c_T = 8 μM). (b) Cooling curves of **25** at different concentrations (λ = 404 nm, 1 K min^{-1}). The red lines correspond to the fitting by the equilibrium (EQ) model.

The set of thermodynamic data derived of the supramolecular polymerization have been calculated by employing the equilibrium (EQ) model developed by ten Eikelder, Meijer et al. for the self-assembly of 1,3,5-benzene tricarboxamides (BTAs).[85,86] In this approach, the formation of the supramolecular polymer through a cooperative mechanism is simplified in a two-step model describing nucleation and elongation, which are defined by K_n and K_e, respectively. The σ parameter measures the relationship between these two constants ($\sigma = K_n / K_e$) and reflects the degree of cooperativity of the supramolecular polymerization, being $\sigma = 1$ for isodesmic mechanisms and $\sigma < 1$, for cooperative mechanisms. By using the Arrhenius equation it is possible to relate both equilibrium constants with the elongation enthalpy (ΔH_e), the entropy (ΔS), the nucleation enthalpy (ΔH_n) and the mismatch penalization enthalpy (ΔH_{mm}). This model considers the entropy independent of the supramolecular process. Contrary, the value of (ΔH_e), is affected by (ΔH_n) and/or (ΔH_{mm}). The nucleation enthalpy is independent of the chirality of the aggregate and makes reference to the energetic cost required to generate the active nucleus, while mismatch penalty energy takes into consideration the incompatibility when adding a chiral monomer into an aggregate of opposite helicity. The next three equations depict all these processes as following:

[85] A. J. Markvoort, H. M. M. ten Eikelder, P. A. J. Hilbers, T. F. A. de Greef, E. W. Meijer, *Nat. Comm.* **2011**, *2*, 509.
[86] H. M. M. ten Eikelder, A. J. Markvoort, T. F. A. de Greef, P. A. J. Hilbers, *J. Phys. Chem. B* **2012**, *116*, 5291.

$$K_n = e^{-\left(\Delta H_e^0 - T\Delta S^0\right)/(RT)} \quad \textbf{Eq. 1}$$

$$K_e = K_n e^{\Delta H_{mm}^0/(RT)} \quad \textbf{Eq. 2}$$

$$\sigma = e^{\Delta H_n^0/(RT)} \quad \textbf{Eq. 3}$$

The thermodynamic data obtained for the supramolecular polymerization of **25** and **(*S*)-26** are summarized in Table 1. Both compounds show dissimilar thermodynamic values except for the total free energy Δ*G*, which is comparable for both **25** and **(*S*)-26**. These differences can be attributed to the different nature of the alkyl chains and demonstrate the high impact of the different variations in the peripheral moieties in the supramolecular polymerization. Additionally, the cooperativity factor of both pyreneimidazole derivatives is below 1, what indicates a certain degree of cooperativity in the supramolecular polymerization despite the sigmoidal shape of the cooling curves. Notably, the value is smaller in the case of chiral **(*S*)-26** than for achiral **25**. This result can been explained due to the higher order required to generate the nucleus in molecules with the branched chains because of steric hindrance.[87]

Table 1. Thermodynamic parameters for **25** and **(*S*)-26** in MCH.

	25	**(*S*)-26**
ΔH_e [kJ mol^{-1}]	-72 ± 1	-52 ± 1
ΔS [J K^{-1}mol^{-1}]	-122 ± 3	-58 ± 2
ΔH_n [kJ mol^{-1}]^a	-7.1 ± 0.2	-11.5 ± 0.2
ΔG [kJ mol^{-1}]^a	-35.9	-34.7
σ [-]^b	5.5×10^{-2}	9.3×10^{-3}
K_e [L mol^{-1}]^b	2.0×10^6	1.5×10^6
K_n [L mol^{-1}]^b	1.1×10^5	1.2×10^4

[a] The nucleation penalty ΔH_n is negative, which implies that the enthalpy gain is smaller for nucleation compared to elongation. [b] The equilibrium constants for elongation (K_e) and dimerization (K_n) and the cooperativity factor (σ) are calculated at 298 K.

[87] C. Kulkarni, E. W. Meijer, A. R. A. Palmans, *Acc. Chem. Res.* **2017**, *50*, 1928.

Taking into account the well-known fluorescence features of pyrene, the emission properties of **25** and **(*S*)-26** have been investigated in $CHCl_3$ and MCH. Unexpectedly, the emission spectra in MCH at c_T = 10 μM, conditions under which **25** and **(*S*)-26** are aggregated, disclose the typical pattern of monomeric pyrene with maxima at λ = 400, 423 and 447 nm (Figure 24a, black line). In contrast, the emission spectra in $CHCl_3$ at c_T = 10 μM, a good solvent that facilitates the solvation of isolated molecules, feature broad, structureless and bathochromically shifted bands respect to the monomeric pattern centred at λ = 448 nm, evidencing the formation of pyrene excimers (Figure 24a, red line). It is worthy to indicate that an excimer is constituted by two molecules which are weakly interacting in the ground state and after the absorption of light as monomers experience a rearrangement in the excited state and generate the emission pattern of a dimer.[88] The strong tendency of pyrene to form excimers through π-stacking both in solution and in the solid state is widely known and the monomeric pattern of **25** in $CHCl_3$ can only be observed at highly diluted concentration (7 nM) and after degassing (Figure 24b).

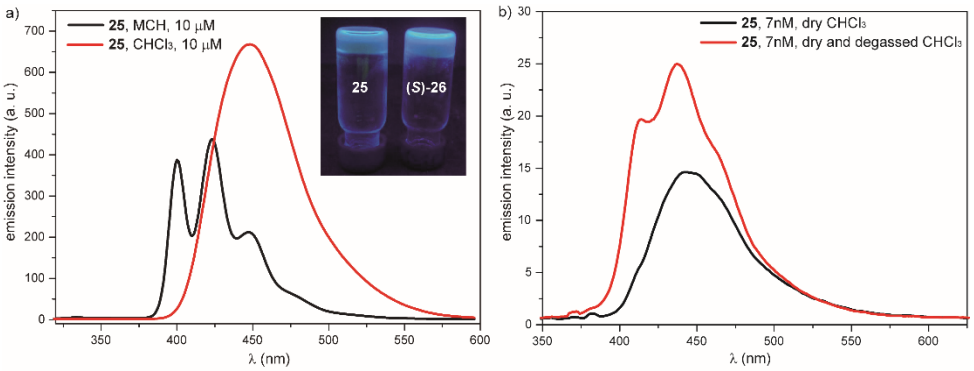

Figure 24. (a) Emission spectra of **25** (298 K, c_T = 10 μM, λ_{exc} = 334 nm) in MCH (black line) and $CHCl_3$ (red line). The inset shows a picture of the cyclohexane gels obtained from compounds **25** and **(*S*)-26** with illumination at 364 nm. (b) Emission spectra of **25** (298 K, c_T = 7 nM, λ_{exc} = 334 nm) in $CHCl_3$ before (black line) and after (red line) degassing the solution.

[88] F. M. Winnik, *Chem. Rev.* **1993**, *93*, 587.

The formation of excimers quenches the fluorescence of pyrene and it is a typical feature of self-assembling pyrene units. Contrary to most of the pyrene based-aggregates, compounds **25** and **(*S*)-26** show a remarkable value of the fluorescence quantum yield ($\phi_f = 0.43$) in the aggregated state (MCH, $c_T = 10$ μM). As expected, lower ϕ_f values are measured for the excimer formed in $CHCl_3$ (0.38 and 0.22 for **25** and **(*S*)-26**, respectively). This unusual emissive behaviour has only been described for a pyrene derivative endowed with a chiral oligo(glutamic acid) side chain,[89] and it was ascribed to a helical supramolecular organization. Additionally, both **25** and **(*S*)-26** readily form gels in cyclohexane at a concentration of *ca.* 1 wt %. Remarkably, the organogels exhibit blue emission upon irradiation at 364 nm (Figure 24a, inset).

The transfer of chirality from the molecular level to supramolecular structures has been known since the pioneering studies on covalent polyisocyanates by Prof. Green.[90] Thus, the presence of a chiral centre can direct the self-assembly to obtain supramolecular helices with preferred handedness. **(*S*)-26** has been endowed with a stereogenic centre in its periphery, what can be used to analyse the helical arrangement of the aggregate. Notably, it also permits the accomplishment of amplification of chirality experiments, which mainly consist on two types of methods. The first one, named sergeants and soldiers experiment (*SaS*), makes reference to the process by which little amounts of chiral compounds (sergeants) condition the self-assembly of achiral molecules (soldiers) to yield helices of a preferred handedness.[91] The other process, termed majority rules (*MR*), describes enantiomer mixtures in which a little excess of one of the enantiomers conditions the helicity of the whole mixture.[92]

Therefore, in an initial attempt to justify the observed emission properties, the inherent chirality of **(*S*)-26** has been utilized to put in evidence the possible helical organization of the aggregates formed by **25** and **(*S*)-26**. **(*S*)-26** aggregates exhibit a weak dichroic response with a poorly defined bisignated Cotton effect centred at

[89] Y. Kamikawa, T. Kato, *Langmuir* **2007**, *23*, 274.
[90] M. M. Green, J.-W. Park, T. Sato, A. Teramoto, S. Lifson, R. L. B. Selinger, J. V. Selinger, *Angew. Chem. Int. Ed.* **1999**, *38*, 3138.
[91] M. M. J. Smulders, I. A. W. Filot, J. M. A. Leenders, P. van der Schoot, A. R. A. Palmans, A. P. H. J. Schenning, E. W. Meijer, *J. Am. Chem. Soc.* **2010**, *132*, 611.
[92] M. M. J. Smulders, P. J. M. Stals, T. Mes, T. F. E. Paffen, A. P. H. J. Schenning, A. R. A. Palmans, E. W. Meijer, *J. Am. Chem. Soc.* **2010**, *132*, 620.

around λ = 253 nm (Figure 25a). In addition, *SaS* experiments have been performed by mixing achiral **25** and chiral **(*S*)-26** to investigate amplification of chirality phenomena. The *SaS* experiment reveals a linear increase of the dichroic response upon the addition of chiral sergeant (Figure 25b). The weak dichroic signals and the lack of amplification of chirality are symptomatic of the inability of **25** and **(*S*)-26** to furnish helical structures, and, contrary to the aforementioned pyrene derivative, this supramolecular organization cannot be invoked to explain the observed emission features.

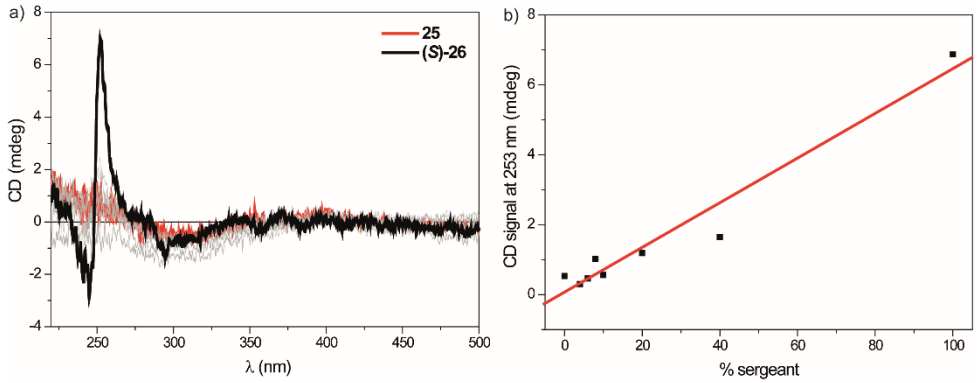

Figure 25. Sergeants-and-soldiers (*SaS*) experiments resulting of the mixing of achiral **25** with chiral **(*S*)-26** (298 K, MCH, c_T = 10 μM). Panel (a) depicts the CD spectra of **25** (red line) and **(*S*)-26** (black line) and panel (b) represents the linear variation of the CD response at λ = 253 nm when increasing the amount of the chiral sergeant **(*S*)-26**.

A rotating-frame Overhäuser effect spectroscopy (ROESY) ^{1}H NMR experiment has been performed in order to clarify the molecular arrangement of the supramolecular polymers formed by **25** and **(*S*)-26** (Figure 26). This experiment has been carried out at a concentration (45 mM) at which the molecule had been previously checked to be aggregated by means of diffusion-ordered spectroscopy (DOSY) NMR.[93] ROESY spectrum of **25** shows a number of intramolecular through-space signals between the protons spatially close within the molecule (dotted blue circles in Figure 26). More interestingly, ROESY experiments also show spatial contacts that can only be explained invoking intermolecular order (dotted green lines in Figure 7). The most remarkable contacts are those observed between the methylene units of the alkyl side chain and most of the aromatic protons of the pyrene moiety. These contacts can be an indication of an alternated

[93] A. Wong, R. Ida, L. Spindler, G. Wu, *J. Am. Chem. Soc.* **2005**, *127*, 6990.

distribution of the pyrene units in the aggregated state that would be in agreement with the monomeric emission properties.

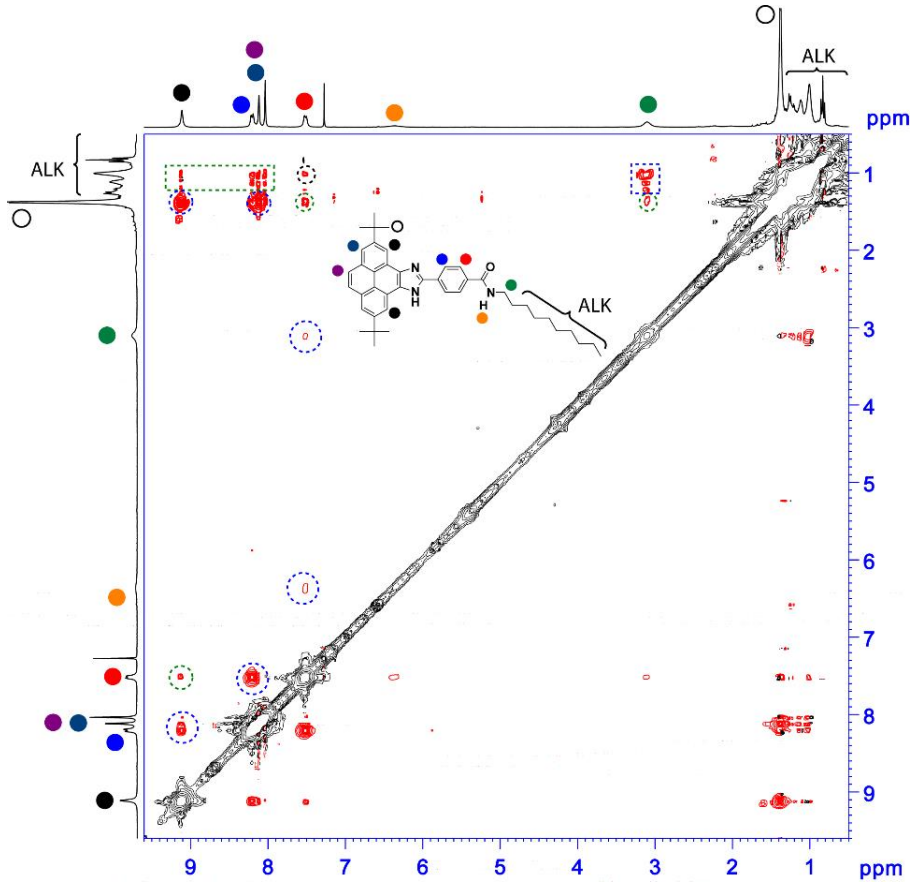

Figure 26. ROESY ^{1}H NMR spectrum of **25** ($CDCl_3$, 300 MHz, 45 mM, 298 K). The dotted blue, green and black lines highlight intra-, intermolecular or both through-space coupling signals, respectively. The inset shows the chemical structure of **25** displaying the anisochronous protons by coloured circles.

4.1.4. Self-assembly of pyreneimidazoles 25 and (S)-26. Theoretical approach

Even though the presence of H-bonds and some aromatic interactions are evident, as well as the monomeric emission and the lack of supramolecular helices, the molecular arrangement within the aggregate is still elusive. To give insight into this pattern, the group of Prof. Ortí has made an extensive computational study of the pyreneimidazole derivatives **25**. Thus, theoretical calculations have been carried out for **25** within the density functional theory (DFT) framework to shed light on the structural and energetic aspects of the pyreneimidazole system upon aggregation (see Experimental Section Part for computational details). The discrete molecule showcases a minimum-energy planar structure in which the amide group exposes an out-of-plane disposition, making H-bonding interactions between neighbouring molecules easier (Figure 27).

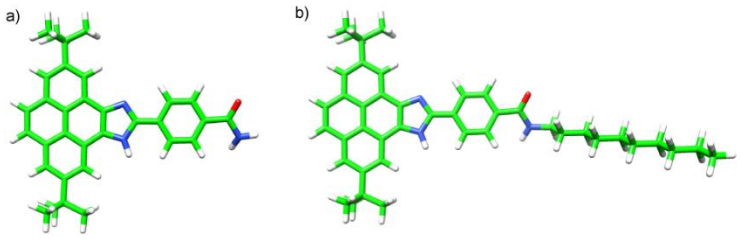

Figure 27. (a) Pyreneimidazole system **25** simplified by the elimination of the aliphatic chain. (b) B97D/6-31G** minimum-energy geometry calculated for compound **25**. The replacement of the aliphatic decyl chain by a H atom reduces the computational cost.

The calculation and analysis of the molecular electrostatic potential (MEP) can bring to light the specific contributions of the different parts of the molecule in the non-covalent interactions involved in the supramolecular polymerization of pyrene derivatives **25** and **(*S*)-26** (Figure 28). The MEP surface of **25** unravels that the highest potential energy points are located at the amide and the imidazole groups. The negative potential energies of -55.7 and -54.6 kcal mol^{-1} calculated in the oxygen and nitrogen vicinity, respectively, and the positive potentials of +101.2 and +121.0 kcal mol^{-1}, which are displayed in the N-H region of the amide and the imidazole, respectively, make feasible the strong electrostatic interactions between monomers by means of H-bonding interactions involving the participation of the amide group and the imidazole ring. Additional to this main force, weak π–π and/or

C–H···π dispersion interactions between the aromatic units and the aliphatic chains can also be expected.

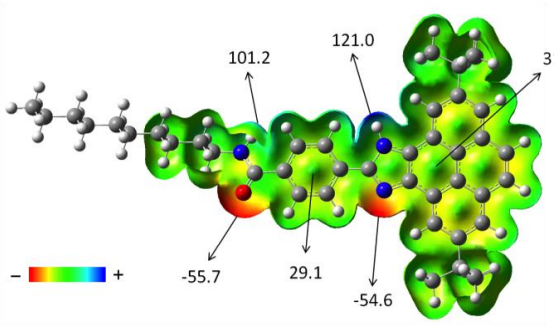

Figure 28. B3LYP/6-31G** molecular electrostatic potential surface of **25** mapped onto the electron density isosurface with isovalue = 0.01 a.u. The surface has been cut parallel to the viewing plane. Potential energies (in kcal mol^{-1}) are indicated for relevant points on the surface.

A set of dimers of **25**, as the minimal supramolecular units, have been modelled considering the different interacting moieties that could be involved in its supramolecular organization: the aromatic structure (π-stacking), the polar amide and imidazole groups (H-bonds) and the nonpolar long aliphatic chain (C-H···π and C-H···C-H interactions). In the first group of dimers (dimers A-C, Figure 29) the supramolecular organization is mainly due to π-stacking. Two monomers of **25** may arrange either in a parallel or antiparallel disposition by the π-stacking of the pyreneimidazole cores (dimer A) or with the benzamide group (dimer B). In dimer A, the rotation of ~ 30º of the upper monomer around the perpendicular axis also permits the establishment of an amide-amide H-bond. This structure would grow generating helical structures, what would not be in agreement with the results obtained by CD spectroscopy. In dimer B, an additional weak H-bonding N–H···N interaction among imidazole ring is also present. Similarly to A, dimer C is disposed in a parallel mode but in this case the amide groups are pointing in opposite directions forming in this way a non-linear H-bond. In addition to the π-stacking, the polar imidazole and amide groups constitute high potential energy regions for the supramolecular stabilization of the dimer as unveiled by MEP studies. Like this, dimers D-F, in which the formation of highly directional H-bonds is the main drive force, have been also simulated (Figure 29). Whilst dimers D and E are only stabilized by the H-bond formation between amides and imidazole rings, respectively, dimer F is capable of stablishing two H-bonds implying the

participation of amide and imidazole rings in an alternated way which also renders an additional CH···π stabilization due to the interaction between the aliphatic chains and the pyreneimidazole ring. Table 2 summarizes the interaction energy (E_{int}) and the main intermolecular forces governing the self-assembly of dimers A–F calculated at the B97D3/6-31G** level.

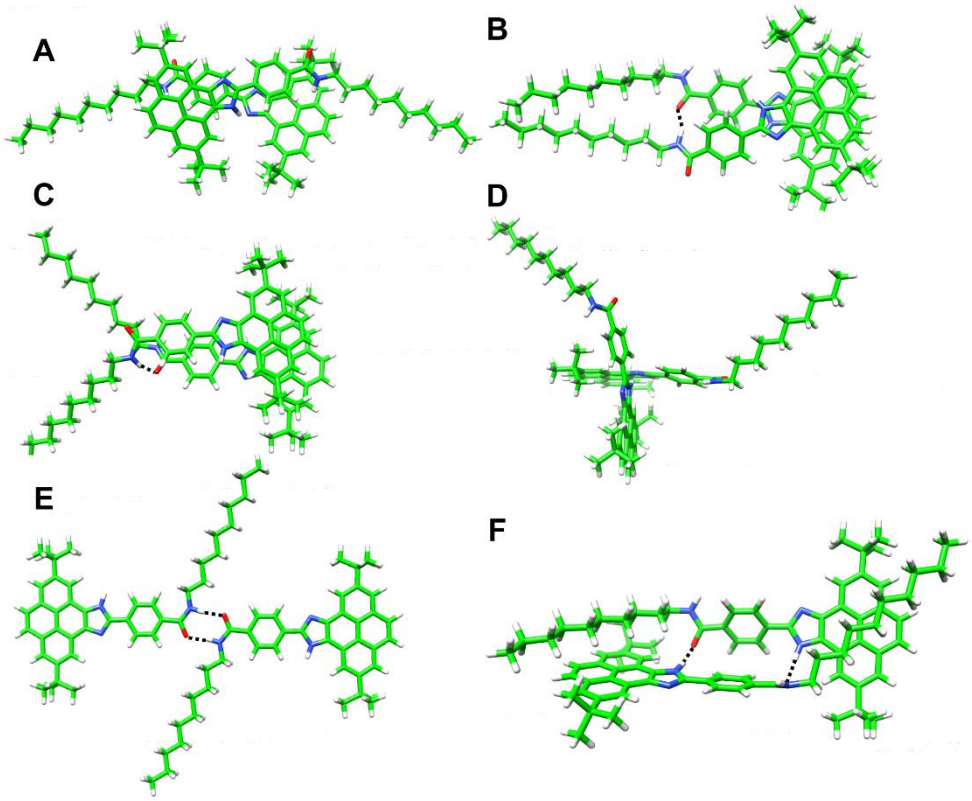

Figure 29. Minimum-energy geometries calculated for the different dimers postulated for **25** at the B97D3/6-31G** level of theory.

Table 2. Interaction energy (E_{int}), number of H-bond contacts (n_{HB}), length of the closest H-bond contact (d_{HB}) and dominant dispersion interactions π-π, CH···π and CH···CH that characterize dimers A–F.

	E_{int} [kcal mol^{-1}]	n_{HB}	d_{HB} [Å]	π-π	CH···π	CH···CH
A	-54.6	1	1.918	✓	–	✓
B	-51.0	1	2.064	✓	–	–
C	-53.7	1	2.051	✓	–	–
D	-32.0	1	1.826	–	✓	–
E	-7.7	2	1.822	–	–	–
F	-61.7	2	1.839	–	✓	–

A topological analysis of the electron density has been also carried out by means of the NCIPLOT software to obtain the non-covalent interaction surfaces, which affords additional information on the origin of the supramolecular aggregation (Figure 30). Considering that they are stabilized by similar non-molecular interactions, dimers A, B and C display interaction energies with close values. In the case of dimer A, its slightly higher stability is due to the stabilizing C-H···C-H interactions among the aliphatic chains. Dimers B and C also showcase the typical green surface indicative of dispersion interactions along the π–π skeleton between monomers. In these three dimers, weak H-bonds can also be formed as unveiled by the closest NH···N/O contacts in the range of 1.92-2.06 Å (Table 2). This fact is totally different from dimers D-F. Dimer D generates a cross-shape pattern which enables the formation of strong H-bonds between the imidazole rings (N-H···N distance of 1.83 Å) and also the stabilization by means of C-H···π interactions involving the tert-butyl groups of one monomer and the pyrene group of the adjacent monomer. Nevertheless, the high interaction energy (-32.0 kcal mol^{-1}) discards this possible arrangement when compared to π-stabilized dimers A-C (Table 2). Dimer E is stabilized by two H-bonding interactions between the two amides in a *cis* disposition, making the occurrence of dimer E very unlikely because of the high barrier (15 kcal mol^{-1}) that has to be overcome to convert a *trans* amide into a *cis* amide. Additionally, the small interaction energy (-7.7 kcal mol^{-1}) resulting from the lower stability of the *cis* conformation, rules out this dimer. Finally, dimer F combines H-bonding interactions between the imidazole and amide groups and C–H···π stabilizing interactions between the alkyl chains and the pyrene cores (Figure 29 and Figure 30).

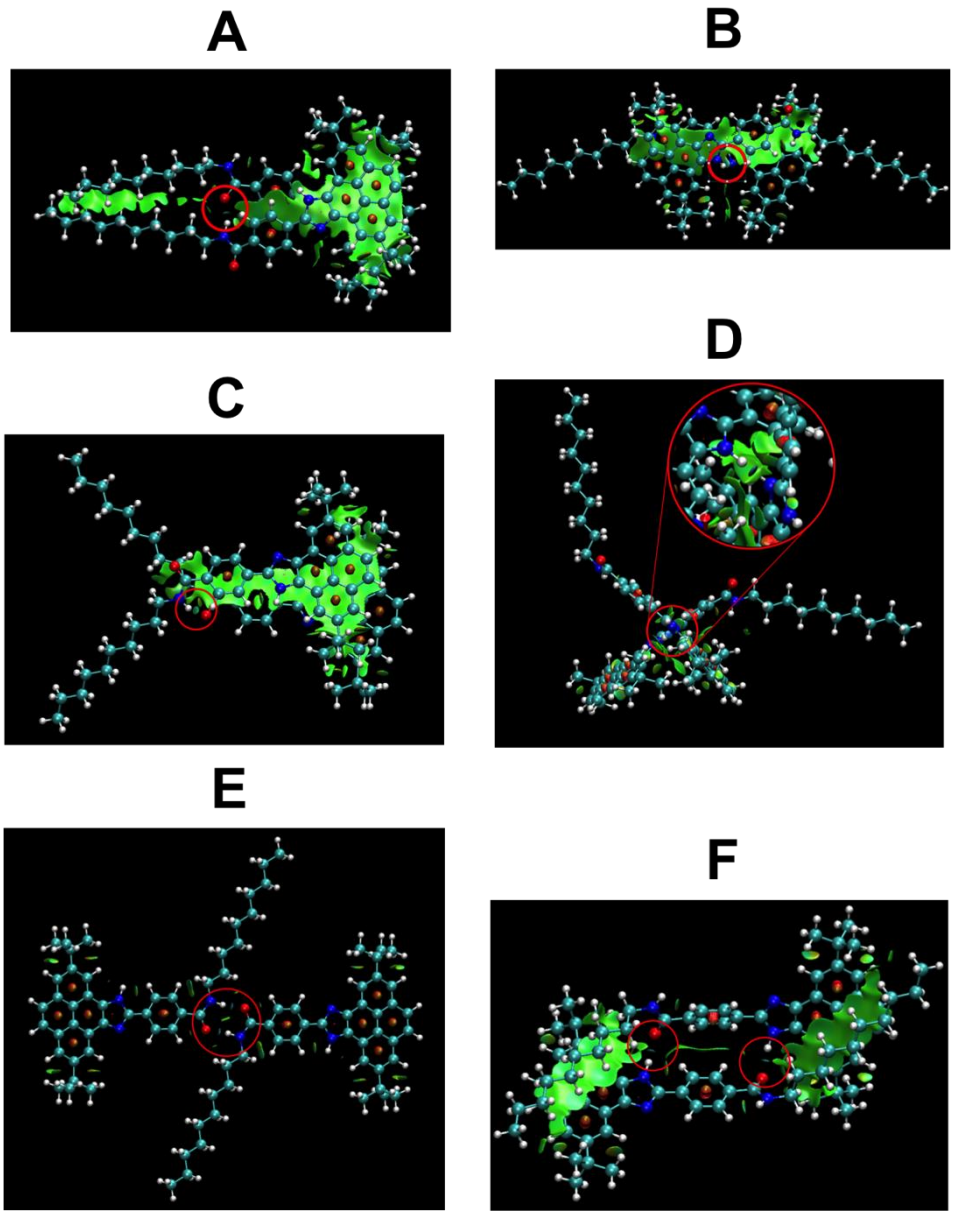

Figure 30. Non-covalent interaction surfaces representing H-bonds (in blue and surrounded by red circles) and dispersion forces (in green) for dimers A−F of compound **25**. Intramolecular ring-centroid repulsions are drawn in dark red.

The additive effect of these interactions in dimer F leads to the highest stability (E_{int} = -61.7 kcal mol^{-1}) among all the computed dimers. Importantly, this dimer also allows us to identify all the ROESY signals observed experimentally and, in particular, the short contacts between the alkyl chains and the pyrene cores (Figure 31).

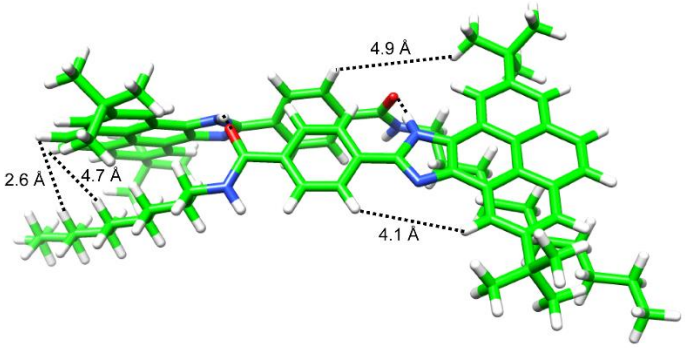

Figure 31. Minimum-energy geometry calculated for dimer F. The dotted lines show the distances between aromatic pyrene protons and alkyl chains and are in agreement with the selected contacts observed in the ROESY experiment.

The absence of π-stacking between the pyrene cores in dimer F also concurs with the monomeric emission revealed by fluorescence spectroscopy. This synergy among experiments and theory make of dimer F the most plausible arrangement for compounds **25** and **(*S*)-26**. In order to rationalize the growing of dimer F from the nonplanar and distorted disposition of the monomers, the tetramer shown in Figure 32 has been built up through an imidazole-amide-imidazole H-bond sequence. The minimum-energy geometry computed for the tetramer reveals that the H-bonding motifs are preserved along the monomeric pairs. The average NH (amide) - N (imidazole) contact has been shown to be 2.18 Å, whereas the CO (amide) - HN (imidazole) interaction is 1.82 Å. The total interaction energy in the tetramer reaches -182.1 kcal mol^{-1}, which corresponds with an E_{int} = -60.7 kcal mol^{-1} dimer pairs. This value is very close to the E_{int} computed for dimer F (-61.7 kcal mol^{-1}), involving in this way that the oligomer can easily grow keeping the strong H-bond pattern and the stabilizing C-H···π forces. Finally, these low values also explain the small degree of cooperativity in the supramolecular polymerization of this pyreneimidazole-based aggregates.[94]

[94] C. Kulkarni, S. Balasubramanian, S. J. George, *ChemPhysChem* **2013**, *14*, 661.

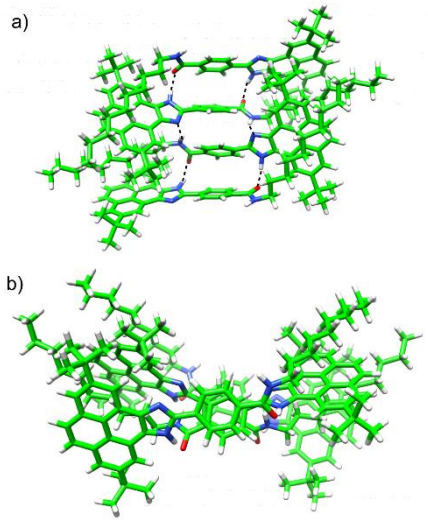

Figure 32. Side (a) and top (b) views of the B97D3/6-31G**-optimized geometry calculated for the tetramer of **25**. Dotted lines emphasise the H-bonding array established between the imidazole and amide units. Only the H atoms involved in H-bonding interactions are shown.

These results demonstrate the tremendous influence that the inclusion of bulky groups and the imidazole ring imparts in the supramolecular polymerization of pyreneimidazole derivatives. The incorporation of the *tert*-butyl groups is a must in order to enhance the solubility of the aggregate. However, they strongly diminish the capability of the **25** and **(*S*)-26** to experience efficient π-stacking, which not only affects to the supramolecular polymerization mechanism, but also to the emission pattern observed for these pyreneimidazole aggregates. The imidazole ring turns to be an important moiety to drive the organization of pyrene derivatives in combination with the amide functionality. Moreover, the combination between experimental and theoretical data prove the importance of the synergy between H-bonding and notably, CH···π interactions, to direct the formation of supramolecular polymers. Even though this strategy is not probably the most adequate to generate highly ordered supramolecular polymers, since its formation proceeds though a weakly cooperative mechanism, it permits to obtain macromolecules which keep some of the properties of the non-aggregated molecules.

4.2. Supramolecular polymerization of [5]-helicenes derivatives

4.2.1. Helicene derivatives

[n]-Helicenes are a unique type of PAH constituted by *ortho*-fused aromatic rings in which n ≥ 4.[95] The steric hindrance between the protons of the terminal rings confers to these carbon-rich compounds their genuine twisted geometry, making them useful scaffolds for enantioselective catalysis, sensing, and to build up distorted nanographenes or nanoribbons.[96] Their helical disposal confers to helicenes inherent chirality, yielding two different types of enantiomers (*M* or *P*) despite the absence of stereogenic centres. The stability of these atropisomers against racemization is strongly dependent on the number of aromatic rings and on the substituents introduced on the fjord region, *i.e.*, the inner part at the helicene core.[97] Hence, [4]-helicenes possess strong tendency to racemize in solution in short times, being only stable when substituted at the inner 1 and 12 positions. Contrastingly, enantiomeric [n]-helicenes with n ≥ 6 are configurationally stable despite having an unsubstituted pattern in the 1 and 16 positions.[98] [5]-Helicenes are appealing molecules since they are at the intermediate point of this trend. They possess partial configurational stability which can be increased with the substitution on one or both of the 1 and 14 positions, showing an ample range of racemization energies $\Delta G^{\ddagger}(T)$, directly depending on the torsional angle (Θ) between peripheral rings[99] (Figure 33).

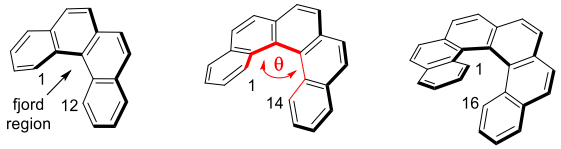

Figure 33. Chemical structure of *P*-[4]-helicene, [5]-helicene and [6]-helicene.

Self-assembly of [n]-helicenes has been widely studied in surfaces[100] but barely in solution.[101] The organization of these scaffolds through non-covalent interactions

[95] Y. Shen, C.-F. Chen, *Chem. Rev.* **2012**, *112*, 1463.
[96] M. Gingras, *Chem. Soc. Rev.* **2013**, *42*, 1051.
[97] M. Shigeno, Y. Kushida, M. Yamaguchi, *Chem. Commun.* **2016**, *52*, 4955.
[98] R. H. Janke, G. Haufe, E.-U. Würthwein, J. H. Borkent, *J. Am. Chem. Soc.* **1996**, *118*, 6031.
[99] P. Ravat, R. Hinkelmann, D. Steinebrunner, A. Prescimone, I. Bodoky, M. Juríček, *Org. Lett.* **2017**, *19*, 3707.
[100] K.-H. Ernst, *Acc. Chem. Res.* **2016**, *49*, 1182.
[101] C. Nuckolls, T. J. Katz, L. Castellanos, *J. Am. Chem. Soc.* **1996**, *118*, 3767.

enhances their chiroptical properties, depicting new scenarios for applications. Even though π-stacking has been considered as the main driving force in the supramolecular polymerization of helicene derivatives, their distorted arrangement could weaken the supramolecular interactions and the introduction of functional groups capable of establishing other intermolecular forces is therefore a must. Besides, these moieties are perfect scaffolds to explore the influence of axial chirality in supramolecular polymerization processes, whose importance has been demonstrated by our research group in referable systems.[102,103]

To investigate the configurational stability of [5]-helicenes unsubstituted at the fjord positions, 5,7,8,10-tetrasubstituted [5]-helicenes **35** and **36**, endowed with two and four amides, respectively, have been synthesized. These compounds can experience self-assembly in solution through π-stacking and H-bonding (Figure 34). Additionally, the resolution of the atropisomers of **35** and **36** could make also feasible the study of the supramolecular polymerization of the enantiomers themselves in solution, thus shedding light in the relevance of atropisomerism in supramolecular polymerizations and *vice versa*.

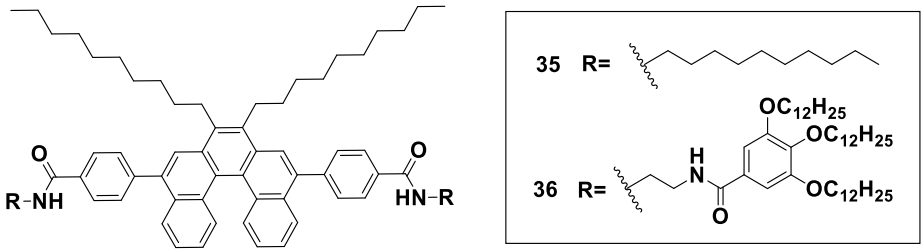

Figure 34. Chemical structure of [5]-helicene derivatives **35** and **36**.

4.2.2. Synthesis of [5]-helicenes 35 and 36

The synthesis of the [5]-helicene derivatives **35** and **36** involves a multistep approach requiring the preparation of the peripheral chains and the subsequent generation of the aromatic core, which are finally joined by a Suzuki-type coupling. The obtaining of the external chains is achieved by following the method depicted in Scheme 2.[104] First, a triple Williamson etherification of the commercial

[102] F. Aparicio, B. Nieto-Ortega, F. Nájera, F. J. Ramírez, J. T. López Navarrete, J. Casado, L. Sánchez, *Angew. Chem. Int. Ed.* **2014**, *53*, 1373.
[103] J. Buendía, E. E. Greciano, L. Sánchez, *J. Org. Chem.* **2015**, *80*, 12444.
[104] A. Dawn, N. Fujita, S. Haraguchi, K. Sada, S. Shinkai, *Chem. Commun.* **2009**, 2100.

compound methyl-3,4,5-trihydroxybenzoate with 1-bromododecane yields **37** quantitatively. Subsequent hydrolysis of the ester group of **37** in basic media affords the carboxylic acid **38**. Further monoamidation of **38** with ethylendiamine in excess, using HBTU as activating agent, permits to accomplish the synthesis of amine **39**. The final amidation reaction between 4-carboxyphenylboronic acid and 1-decilamine (**30**) or amine **39**, using EDC as activating agent and DMAP as base, permits the obtaining in moderate yields of the boronic acids **40**[47] and **41**,[67] respectively.

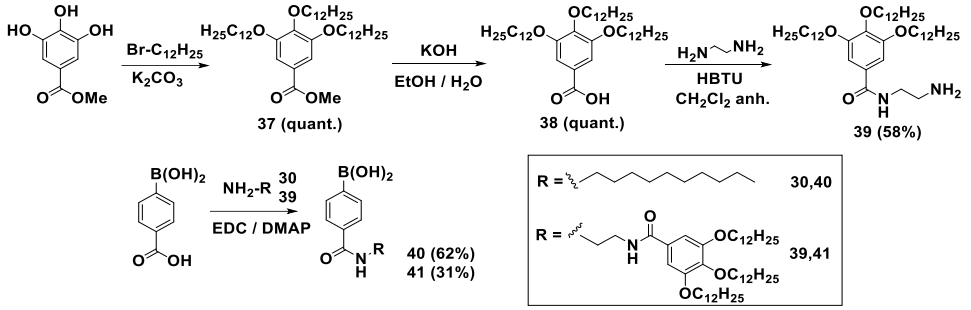

Scheme 2. Synthesis of boronic acids **40** and **41**.

Usually, synthetic approaches for the obtaining of helicene cores involve photochemical methods.[105] However, [5]-helicenes themselves are photoreactive and tend to give further overannulation when exposed to light. To circumvent this problem, the introduction of suitable substituents at proper positions[106] and chemical approaches usually based-on coupling reactions[107] or radical cyclizations[108] have been demonstrated to be the most useful alternatives. In this synthesis, a previously described path which involves a series of modifications with racemic 1,1´-bi-2-naphtol (BINOL) as starting material has been partially followed.[109,110] Initially, reaction of BINOL with triflic anhydride and following Kumada-type coupling between the resulting triflate derivative and methylmagnesium iodide, using $NiCl_2$(dppp) as catalyst, generates the dimethylated binaphtyl **42**. A radical bromination in the methyl groups of **42** utilizing NBS as bromine source and

[105] M. Gingras, *Chem. Soc. Rev.* **2013**, *42*, 968.
[106] N. Ito, T. Hirose, K. Matsuda, *Org. Lett.* **2014**, *16*, 2502.
[107] S. K. Collins, A. Grandbois, M. P. Vachon, J. Côté, *Angew. Chem. Int. Ed.* **2006**, *45*, 2923.
[108] D. C. Harrowven, I. L. Guy, L. Nanson, *Angew. Chem. Int. Ed.* **2006**, *45*, 2242.
[109] T. Ooi, M. Kameda, K. Maruoka, *J. Am. Chem. Soc.* **2003**, *125*, 5139.
[110] S. Goretta, C. Tasciotti, S. Mathieu, M. Smet, W. Maes, Y. M. Chabre, W. Dehaen, R. Giasson, J.-M. Raimundo, C. R. Henry, C. Barth, M. Gingras, *Org. Lett.* **2009**, *11*, 3846.

benzoyl peroxide as initiator provides the tetrabrominated compound **43** in good yield. Subsequent basic removal of the acidic proton in α to the aromatic core provokes the elimination of one bromine atom and a cyclization reaction to generate 7,8-dibromo-[5]-helicene (**44**). A Sonogashira-type coupling of **44** with 1-decynyl generates compound **45**, which is subjected to catalytic hydrogenation to obtain **46**. In this reaction, the absence of light is necessary in order to avoid undesired ene-diene adducts. Helicene **46** is afterwards subjected to a selective bromination in the 5- and 10- positions[111] getting in this way compound **47**. Finally, the Suzuki-type coupling between **47** and the previously synthesized **40** or **41**, using $Pd(PPh_3)_4$ as catalyst allows the attainment in good yields of the racemic mixtures of compounds **35** and **36**, respectively.

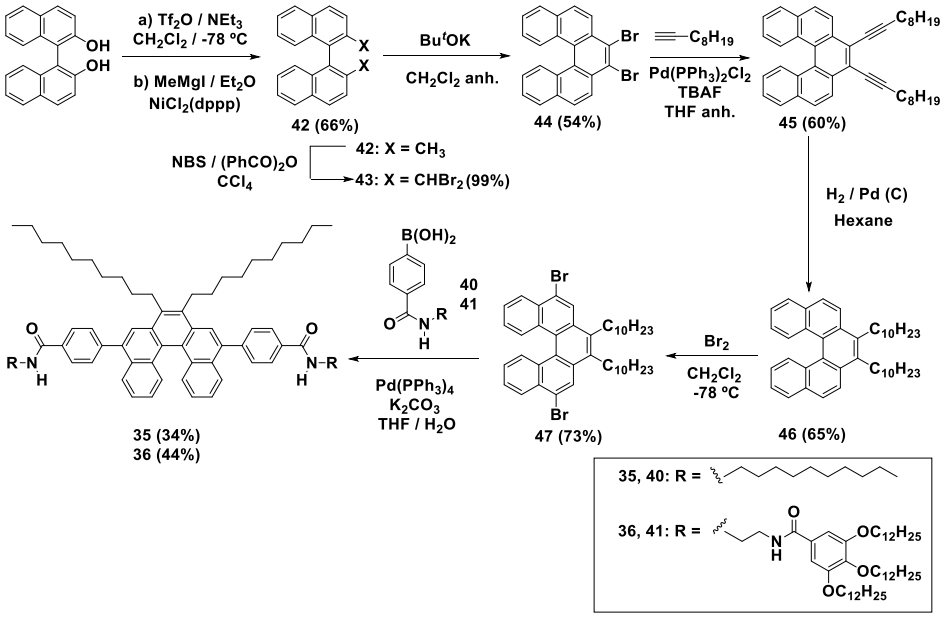

Scheme 3. Synthesis of the [5]-helicene core and target compounds **35** and **36**.

The chemical structure of all the new synthesized compounds has been determined by means of the usual spectroscopic techniques (the complete characterization can be consulted in the Experimental Part Section).

[111] P. Ravat, T. Šolomek, M. Rickhaus, D. Häussinger, M. Neuburger, M. Baumgarten, M. Juríček, *Angew. Chem. Int. Ed.* **2016**, *55*, 1183.

4.2.3. Self-assembly of racemic [5]-helicenes 35 and 36 in solution

The presence of two amide groups in **35** and four in **36** should provide these two molecules different capability to form supramolecular polymers. Thus, FTIR studies indicate a first hint of this dissimilarity (Figure 35). The low values of the N-H stretching band in **35** and **36** ($\tilde{\upsilon}$ ~ 3330 and 3300 cm^{-1}, respectively), upon comparison to the referenced value of free N-H at $\tilde{\upsilon}$ = 3450 cm^{-1}, are a first evidence of the presence of H-bonds in both aggregates. However, the slight higher value of this band for **35** is diagnostic of its lower tendency to self-assemble in comparison with **36**. Besides, the values of the amide I stretching ($\tilde{\upsilon}$ ~ 1630 cm^{-1}) and amide II deformation ($\tilde{\upsilon}$ ~ 1545 cm^{-1}) for both compounds are also diagnostic of the formation of H-bonding between the amides for the two molecules.[83,84]

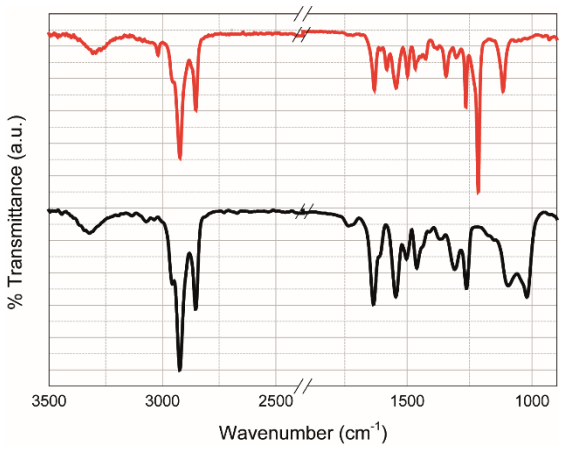

Figure 35. Partial FTIR spectra of **35** (black line) and **36** (red line) at room temperature.

Variable concentration ^{1}H NMR studies of **35** disclose a first hint of the small ability of this compound to form supramolecular entities in solution (Figure 36). Thus, no shifts are visible in the protons corresponding to the aromatic protons when the concentration is increased, which evidences the lack of π-stacking. The subtle movement to low fields of the triplet corresponding to the amide proton (δ ~ 6.3 ppm, red dot) upon increasing concentration can be symptomatic of the participation of this proton in H-bonding. However, this slight deshielding is not accompanied by other shifts. These results can be attributed to the incapacity of **35** to self-assemble in solution.

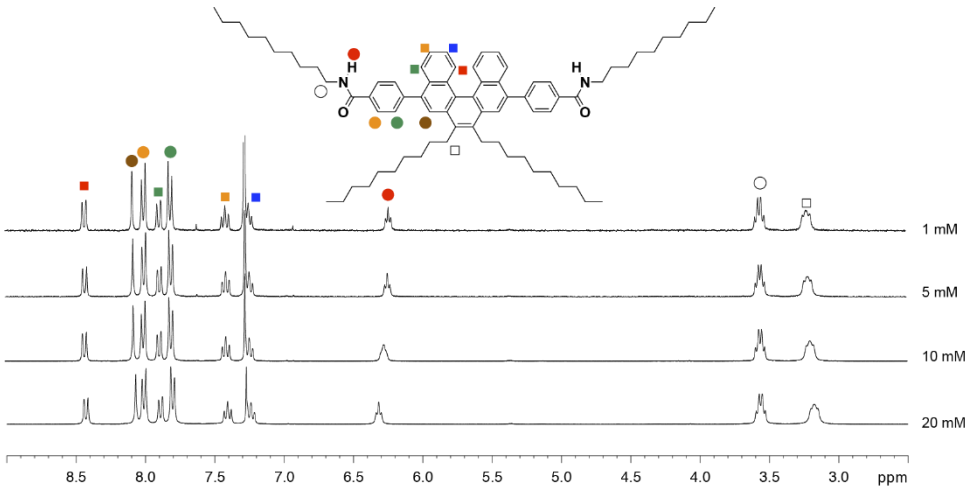

Figure 36. Partial ^{1}H NMR spectra of **35** at different concentrations ($CDCl_3$, 300 MHz, 298 K).

The definitive proof of the inability of **35** to form supramolecular polymers has been uncovered by variable temperature UV-Vis spectroscopy (Figure 37). The UV-Vis spectra of **35** at 20 ºC and at 90 ºC is the same and show no crossing points even at high concentrations, thus discarding the existence of intermolecular interactions. The synergy between π-stacking and two amides has been demonstrated to yield supramolecular polymers in referable planar aromatic surfaces.[47] However, the curved geometry of helicenes precludes, or at least diminishes, the π-π interactions of these scaffolds and, therefore, **35**, only endowed with two amides, does not self-assemble in solution.

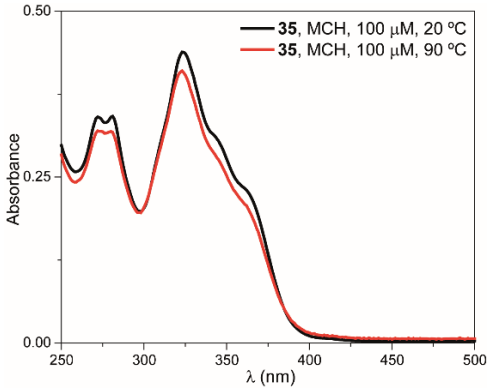

Figure 37. UV-Vis spectra of **35** at 20ºC (black line) and 90ºC (red line) in MCH (c_T = 100 μM).

The situation changes drastically for compound **36**, decorated with four amides. The inclusion of two additional carboxamides with respect to **35** reinforces the H-bonding array and clearly enhances the tendency to aggregate in solution. Variable concentration ^{1}H NMR studies of **36** in $CDCl_3$ disclose a much richer scenario than the analogous experiment realized for **35** (Figure 38). The triplets corresponding to the two amide protons (δ ~ 7.5 ppm, blue and red dots) experience a clear deshielding upon increasing concentrations which can be ascribed to their participation in H-bonding. Nevertheless, the aromatic protons do not exhibit a defined behaviour attributable to their involvement in π-stacking. The protons corresponding to the peripheral rings and the *para*-substituted benzene ring show only a slight shielding upon increasing concentration. Notably, there is a clear movement to high fields of the proton closer to the alkyl chain in the helicene core (δ ~ 8.0 ppm, brown dot) which, together with the shielding of the proton ascribable to the methylene group in α to the helicene group (δ ~ 3.0 ppm, white square), can be assignable to an aromatic interaction in this part of the molecule.

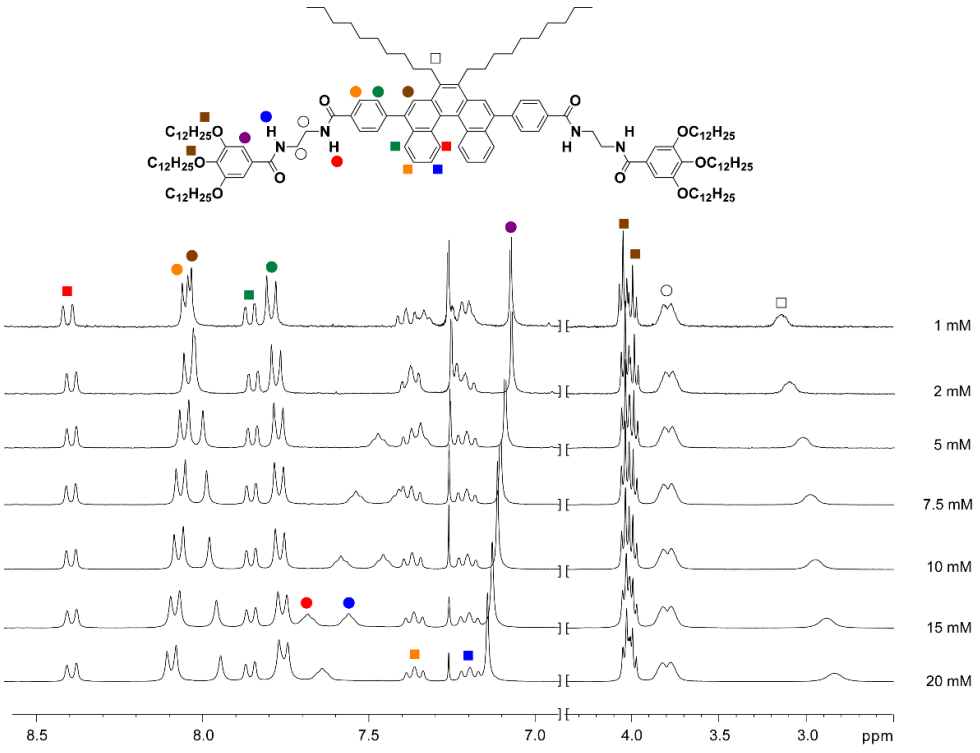

Figure 38. Partial ^{1}H NMR spectra of **36** at different concentrations ($CDCl_3$, 300 MHz, 298 K).

To further corroborate the ability of **36** to self-assemble in solution, DOSY ^{1}H NMR experiments have been carried out at different concentrations (Figure 39).[93] The different values of hydrodynamic radii at high (c_T = 20 mM) and low (c_T = 1 mM) concentrations exhibited by compound **36** confirm its capability to form ordered aggregates in solution since the diffusion of the sample is slower in the concentrated solution than in the diluted one. The combination of these two experiments suggests the existence of an efficient H-bonding array between amides that, however, is not accompanied by any remarkable π-stacking interaction between the aromatic moieties.

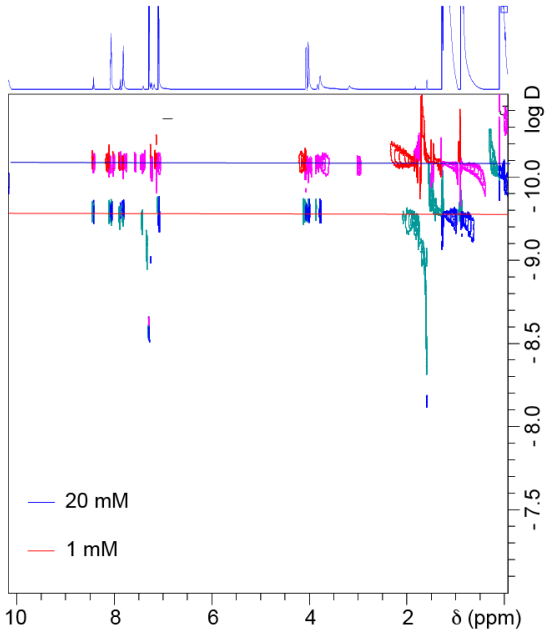

Figure 39. Partial DOSY ^{1}H NMR (Δ = 160 ms, t = 3 ms) spectra of **36** at different concentrations ($CDCl_3$, 298 K, 300 MHz).

ROESY ^{1}H NMR is a useful technique to demonstrate the molecular arrangement within supramolecular aggregates. However, the through-space coupling contacts found for **36** are only assignable to intramolecular interactions as summarized in Figure 40a. The lack of intermolecular interactions, can be justified considering the absence of π-stacking and the predominance of H-bonding as the main driving force in the self-assembly of racemic **36**. Another explanation could be that the functional groups involved in the non-covalent forces are also close within the aggregate (Figure 40b).

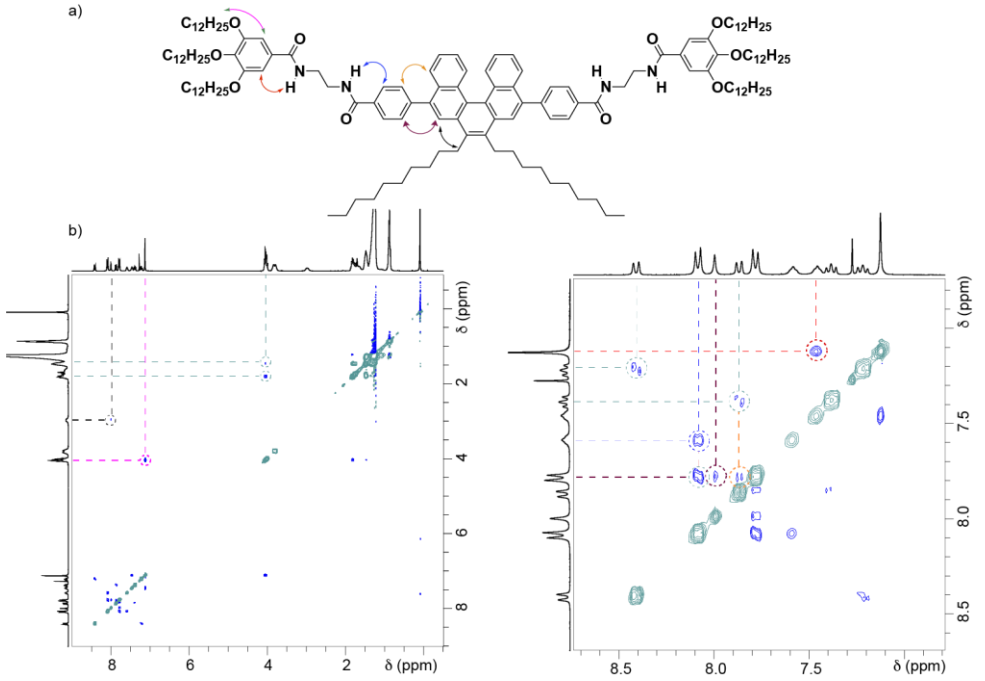

Figure 40. (a) The curved arrows in the structure of [5]-helicene **36** depict the intramolecular through-space coupling signals. (b) ROESY ^{1}H NMR spectra ($CDCl_3$, 300 MHz, c_T = 20 mM, 293 K) of **36**. The dotted colored lines highlight the intramolecular through-space coupling signals.

To disentangle the mechanism of the supramolecular polymerization of **36**, VT-UV-Vis experiments have been performed at different concentrations using MCH as solvent (Figure 41a). The spectrum at 10 ºC exhibits two maxima at λ = 270 and λ = 324 nm as well as an additional shoulder at λ = 374 nm. Heating the solution to 90 ºC provokes a bathochromic shift in the band at λ = 324 nm by only 2 nm and also reveals the appearance of an isosbestic point at λ = 320 nm. The slight modification upon temperature change in this absorbance region seems to be in agreement with the lack of efficient π-π interactions in the self-assembly of **36**. Plotting the absorbance variation at λ = 339 nm against temperature furnishes a curve that cannot be accurately fitted by the EQ model, previously used for the obtaining of the thermodynamic data in the supramolecular polymerization of pyreneimidazole derivatives in Section 1 (Figure 41b). A plausible explanation to this deviation can be that the enantiomerization of the helicene core takes place simultaneously to disassembly.

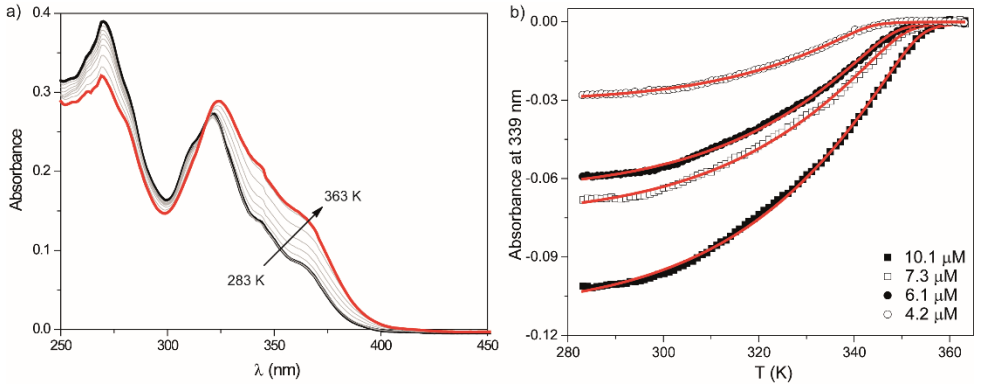

Figure 41. (a) VT-UV Vis spectra of **36** in MCH (c_T = 7.3 μM). (b) UV-Vis cooling curves of **36** in MCH (λ = 339 nm, 1 K min^{-1}) at different concentrations. The red lines show the fitting by the EQ model.

To avoid this problem, the solvent denaturation model (SD)[112] has been applied in order to get all the thermodynamic data of the supramolecular polymerization of **36**. This model considers the supramolecular polymerization as a balance between the effect of mixing a "good" solvent, in which the monomer is dissociated, and a "bad" solvent, in which the aggregation process is favoured. The self-assembly process is considered as a sequence consisting in the addition of a monomer to the polymer chain which is defined by the thermodynamic constant K_e. As it has been previously mentioned, in the case of a cooperative mechanism, the nucleation is governed by K_n and both constants are related by the cooperativity degree σ ($\sigma = K_n / K_e$), being $\sigma < 1$ in nucleation-elongation processes, and $\sigma = 1$ for isodesmic systems. K_e relates to the free energy of Gibbs associated to the addition of the monomer to the chain ($\Delta G^{0'}$) as described by the following equation:

$$K_n = e^{\Delta G^{0'}/(RT)} \qquad \textbf{Eq. 4}$$

This model also considers that the free energy $\Delta G^{0'}$ is linearly dependant of the molar fraction of good solvent f as depicted in Equation 5, where ΔG^0 is the free energy regarding the addition of the monomer to the pure bad solvent and the m parameter measures the capacity of the good solvent to associate with the monomer, destabilizing in this way the supramolecular polymer.

$$\Delta G^{0'} = \Delta G^0 + mf \qquad \textbf{Eq. 5}$$

[112] P. A. Korevaar, C. Schaefer, T. F. A. de Greef, E. W. Meijer, *J. Am. Chem. Soc.* **2012**, *134*, 13482.

To realize this study, solutions of **36** in MCH (bad solvent) and in $CHCl_3$ (good solvent) have been mixed keeping constant c_T (Figure 42). In these experiments, heating the samples is not a requirement, thus avoiding the effect of the [5]-helicene racemization. The curve resulting after plotting the variation of the degree of aggregation (α) *versus* the molar fraction of the good solvent can be fitted to the SD model to attain the corresponding thermodynamic parameters. The sigmoidal curve and the very low derived value for the degree of cooperativity σ (0.35) indicates that the self-assembly of the racemic mixture of **36** is governed by an isodesmic mechanism (Figure 42b and Table 3).

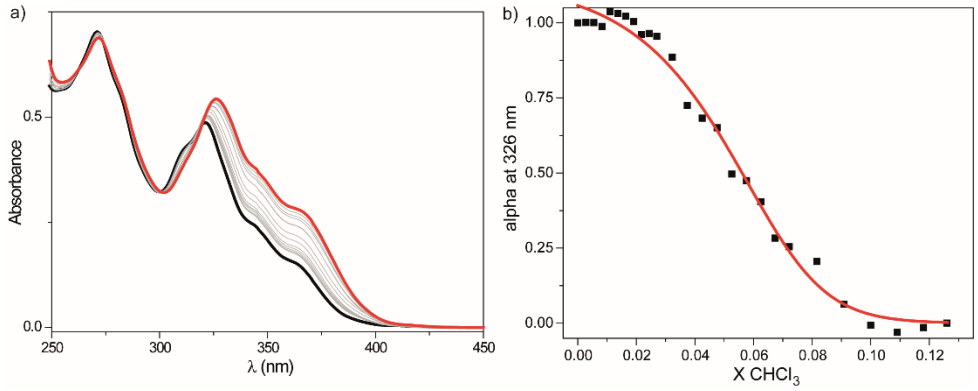

Figure 42. (a) UV-Vis spectra of **36** in MCH/$CHCl_3$ mixtures (c_T = 10 µM, 293 K). The black and red lines depict the UV-Vis spectra of **36** in MCH and $CHCl_3$, respectively. (b) Plot of the degree of aggregation (α) *versus* the molar fraction of the good solvent ($CHCl_3$). The red line shows the fitting to the SD model (λ = 326 nm).

Table 3. Thermodynamic data for the supramolecular polymerization of **36** and **(*M*)-36** derived by the SD Model.

	36	**(*M*)-36**
ΔG^0 [kJ mol^{-1}]	-36.1	-38.5
σ [-]	0.35	0.001
K_e [M^{-1}]	2.1×10^6	5.6×10^6
K_n [M^{-1}]	0.7×10^6	6.1×10^3

Finally, to get insight on the morphology of the supramolecular polymers of **36**, AFM images have been obtained by drop-casting a 10 μM solution of **36** in MCH onto mica. The images clearly show the existence of ill-defined agglomerates (Figure 43). This morphology is typical of supramolecular polymers whose aggregation proceeds under an isodesmic mechanism.

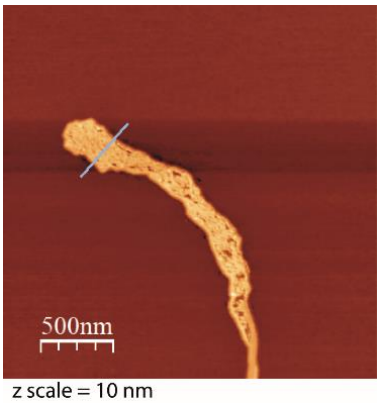

Figure 43. AFM image obtained after drop-casting a MCH solution of the racemic mixture of **36** (c_T = 10 μM, 298 K, mica, z scale = 10 nm).

4.2.4. Self-assembly of enantioenriched [5]-helicenes 35 and 36 in solution. Influence of self-assembly on configurational stability

The presence of an axial axis in [n]-helicenes yields *P* and *M* enantiomers that have been obtained in equal amounts, thus generating a racemic mixture, considering the non-stereoespecific synthetic route employed in their obtaining. However, these atropisomers can be resolved by chiral HPLC. In this way, the corresponding *P* and *M* enantiomers of compounds **35** (***P*-35** and ***M*-35**) and **36** (***P*-36** and ***M*-36**) have been isolated after performing HPLC separations in order to study the self-assembly process of the enantioenriched helicenes in solution. To attain this goal, a (R,R)-Whelk 01 chiral column has been employed with a mixture toluene/2-propanol 97:3 as eluent for **35** and a mixture hexane/2-propanol 80:20 as eluent for **36** (Figure 44).

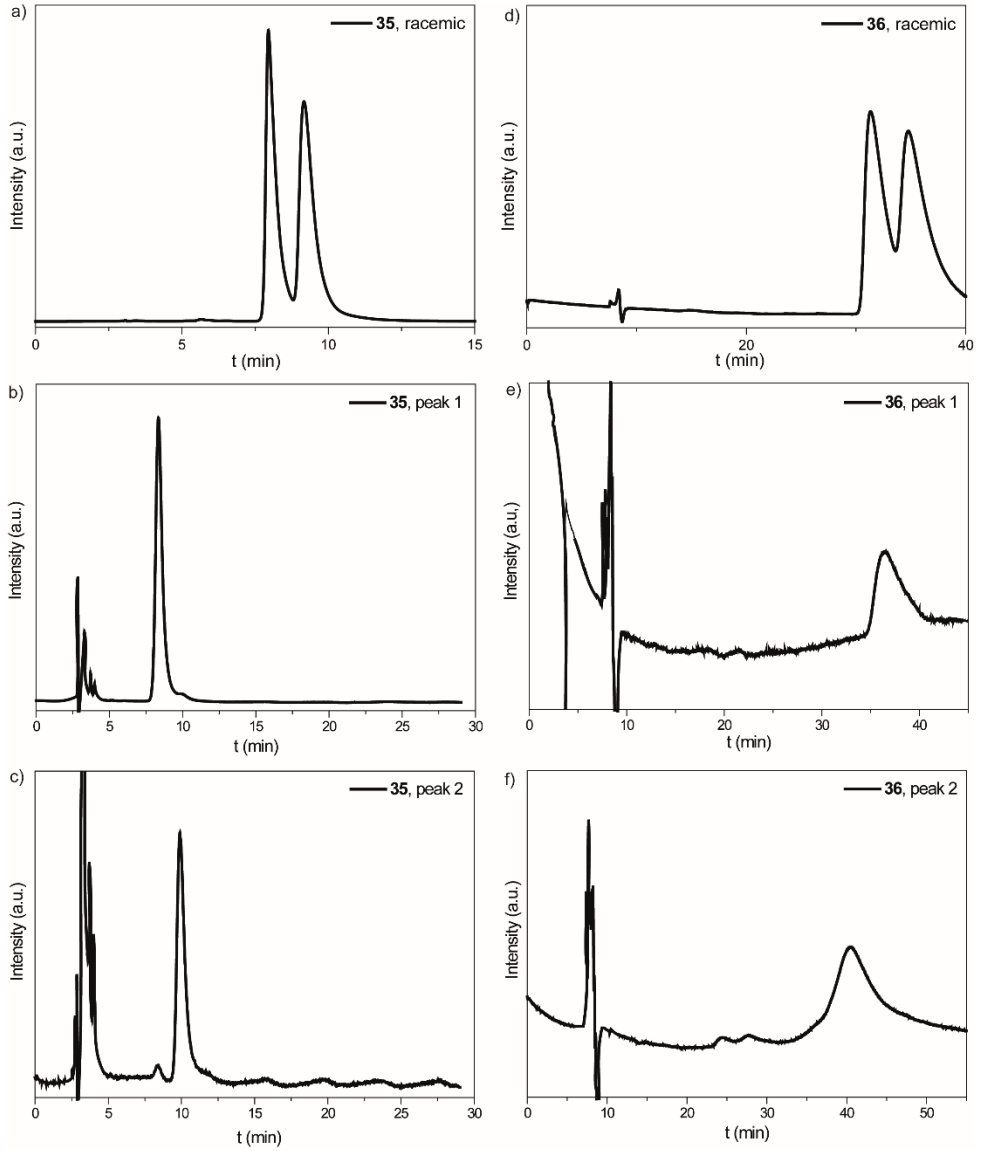

Figure 44. HPLC traces of helicenes **35** (a) and **36** (d) on a (*R*,*R*)-Whelk 01 chiral column. Chromatograms of the pure first (b) and second (c) isolated peaks of **35**, and of peaks 1 (e) and 2 (f) of **36.**

After the chiral separation, CD studies have been employed to unravel the absolute configuration of each one of the enantiomers obtained. The first eluted peak of **35** shows a positive sign centered at λ = 333 nm and a negative value of the concomitant band centered at λ = 313 nm (Figure 45). This positive Cotton effect has been ascribed to *P*-type helicenes.[113,114] Therefore, peak 1 in the mixture of enantiomers **35** has been designated as ***P*-35** whereas peak 2 is assignable to ***M*-35**.

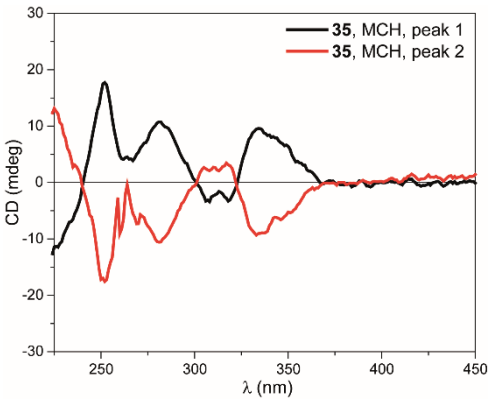

Figure 45. CD spectra of peak 1 (black line) and peak 2 (red line) of helicene **35** in $CHCl_3$ (c_T = 10 μM, 293 K).

On the other hand, the first peak isolated for **36** discloses a negative value at λ = 374 nm and a positive value of the adjacent band centered at λ = 342 nm (Figure 46a). Therefore, differently from **35**, peak 1 in **36** corresponds to ***M*-36** whereas peak 2 is assignable to ***P*-36**. Importantly, and also in a dissimilar fashion to ***P*-35** and ***M*-35**, the enantioenriched solutions of **36** in a bad solvent like MCH unravel a CD pattern which is different from that obtained in $CHCl_3$, denoting the capability of ***M*-36** and ***P*-36** to self-assemble in solution (Figure 46b).

[113] N. Harada, K. Nakanishi, *J. Am. Chem. Soc.* **1969**, *91*, 3989.
[114] T. Taniguchi, T. Usuki, *Circular Dichroism Spectroscopy*, John Wiley & Sons, Inc. **2012**.

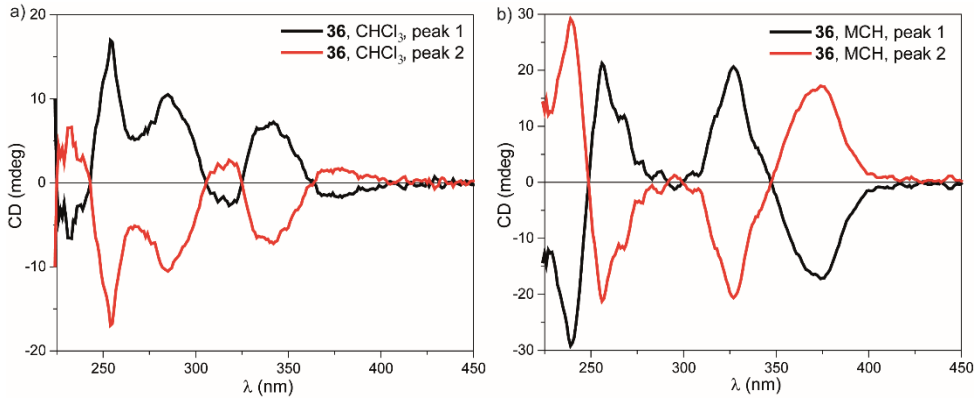

Figure 46. (a) CD spectra of peak 1 (black line) and peak 2 (red line) of **36** in $CHCl_3$ (c_T = 10 μM, 293 K). (b) CD spectra of peak 1 (black line) and peak 2 (red line) of **36** in MCH (c_T = 10 μM, 293 K).

These changes make feasible the applicability of the SD model after denaturation of the ***M*-36** aggregate in MCH upon adding $CHCl_3$ (Figure 47). Remarkably, the supramolecular polymerization of ***M*-36** proceeds in a cooperative way as reflected by the low value of σ, depicting a completely different scenario for the self-assembly of the enantioenriched compounds when compared to racemic **36** (Table 3). Similar results had been unveiled for referable atropisomers in PBI aggregates.[115]

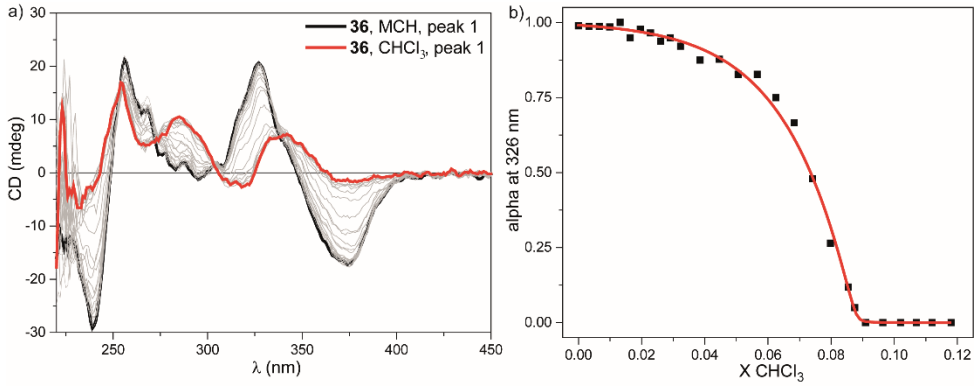

Figure 47. CD spectra (a) and denaturation curve (b) of ***M*-36** in MCH/$CHCl_3$ mixtures (c_T = 10 μM, 293 K). The red line in (b) describes the fitting to the SD model (λ = 326 nm).

[115] Z. Xie, V. Stepanenko, K. Radacki, F. Würthner, *Chem. Eur. J.* **2012**, *18*, 7060.

The mechanistic dissimilarities in the supramolecular polymerization of **36** and ***M*-36** have also consequences in the morphology of the final aggregates, as it has been shown by AFM measurements. The AFM images of ***M*-36**, obtained after drop-casting of a 10 μM solution in MCH, exhibit rod-like structures of around 3.5 nm height (Figure 48), which differ from the ill-defined structures shown in Figure 43.

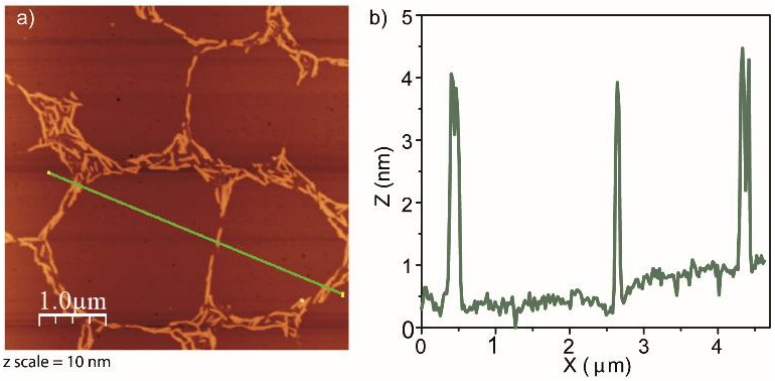

Figure 48. (a) AFM image obtained after drop-casting and MCH solution of ***M*-36** (c_T = 10 μM, 298 K, mica, z scale = 10 nm). (b) Height profile (green line in panel (a)) of the rod-like structures formed by the self-assembly of ***M*-36**.

During the investigation of the self-assembly of enantioenriched solutions, it has been noticed that the ***M*-36** aggregates resist against racemization during longer times than expected considering the 1,14-unsubstituted pattern exhibited by the molecule. As it has been pointed out at the beginning of this Section, the stability of [5]-helicenes is highly dependent on the torsional angle Θ, which, in turn, is related to the size and nature of the substituents located at the 1 and 14 positions (Figure 33). The studies performed by ^{1}H NMR spectroscopy demonstrate that the self-assembly of these helicenes only occurs by means of H-bonding, thereby maintaining the torsional angle. Thus, the configurational stability, which is determined by the value of the free energy of racemization $\Delta G^{\neq}(T)$, of both ***M*-36** and ***P*-36** is expected to be the same in the aggregated or in the molecular dissolved state. The monitoring of the changes of an intrinsic molecular property like CD intensity with time, permits the obtaining of the racemization constant (k_{rac}), and the subsequent calculation of the $\Delta G^{\neq}(328)$ by including this value in the Eyring equation (see the Experimental Part Section for further details). The derived $\Delta G^{\neq}(328)$ value of the molecularly dissolved solution of ***M*-36** in $CHCl_3$ has been calculated to be 23 ± 2 kcal mol^{-1}, which is the range of the previously described values of [5]-unsubstituted helicenes at this temperature.[99] Interestingly, heating a

solution of ***M*-36** in MCH to 328 K (conditions in which ***M*-36** is mainly aggregated) shows no changes with time, what reflects the configurational stability attained by self-assembly (Figure 49).

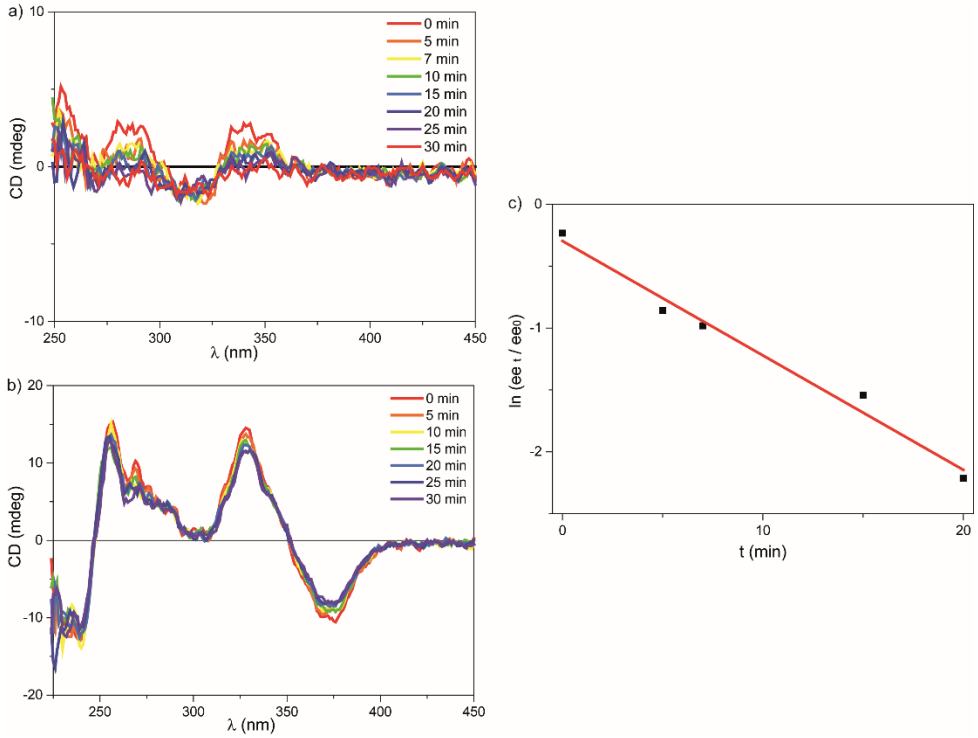

Figure 49. CD spectra of ***M*-36** in $CHCl_3$ (a) and MCH (b) (c_T = 10 μM, 328 K). (c) Plot of the natural logarithm of the variation of enantiomeric excess of ***M*-36** *versus* time in $CHCl_3$ to derive the racemization constant k_{rac}.

To further prove the influence of the supramolecular polymerization in the increasing stability against racemization described for ***M*-36**, the racemization barrier of ***P*-35** has also been investigated in MCH, conditions in which this molecule does not experience supramolecular polymerization (Figure 50). The resulting $\Delta G^{\neq}(328)$ value for this enantiomer racemization is 24 ± 1 kcal mol^{-1}, in good agreement with the values obtained for molecularly dissolved ***M*-36**.

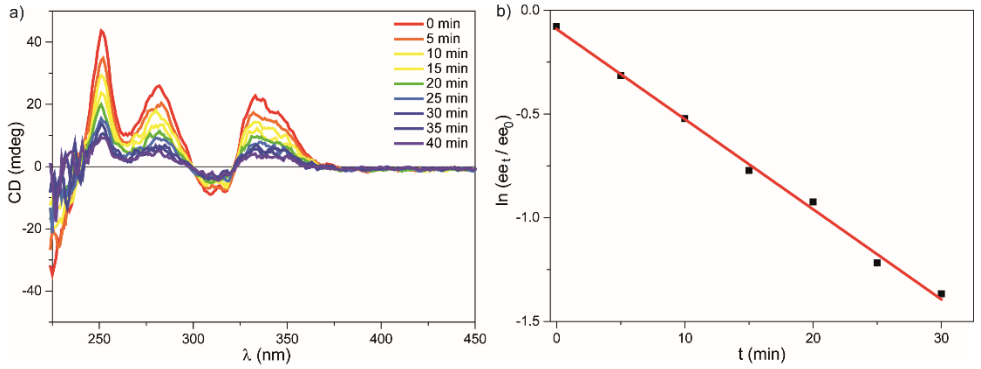

Figure 50. CD spectra of ***P*-35** in MCH (a) (c_T = 10 μM, 328 K). (b) Plot of the natural logarithm of the variation of enantiomeric excess of ***P*-35** *versus* time in MCH to derive the racemization constant k_{rac}.

Finally, to discard a solvent effect, the CD spectra of a solution 10 μM of ***M*-36** in MCH at different temperatures have been registered (Figure 51). The non-sigmoidal curve obtained after representation of the changes of the dichroic signal with the temperature are symptomatic of a nucleation-elongation mechanism. Importantly, the dichroic signal only cancels after T_e, which implies that the racemization takes place just after depolymerization, demonstrating the contribution of self-assembly to maintain the configurational stability of [5]-helicenes ***M*-36** and ***P*-36**.

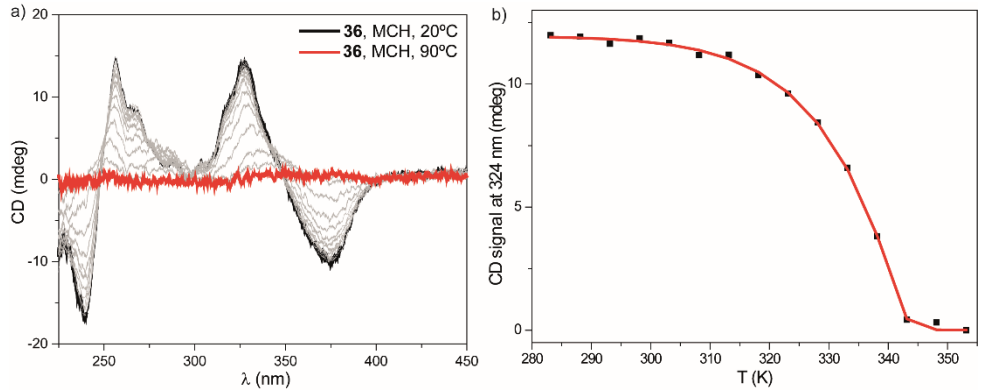

Figure 51. (a) VT-CD spectra of ***M*-36** in MCH (c_T = 10 μM). (b) Variation of the dichroic response of ***M*-36** in MCH against temperature (λ = 324 nm, 1 K min^{-1}). The red line in the inset corresponds to the fitting to the EQ model.

To conclude, these studies demonstrate the huge importance of the number of amides groups to generate supramolecular polymers based on [5]-helicenes. This is the result of the need to compensate the lack of efficient π-stacking derived from the twisted geometry of the helicene core, which also affects to the supramolecular polymerization mechanisms, making H-bonding a requirement *sine qua non* to afford self-assembling helicenes. Notably, the resolution of the racemic mixtures of **36** and the study of the supramolecular polymerization process of the enantioenriched mixtures prove the importance of the enantiopurity of the sample in the supramolecular polymerization mechanism and, unexpectedly, the capability of self-assembling 1,14-unsubstituted [5]-helicenes to avoid racemization, thus showing the importance of self-assembly as a new tool to stabilize the configuration of unstable enantiopure helicenes.

4.3. Supramolecular polymerization of *N*-heterotriangulenes

4.3.1. N-heterotriangulenes

Triangulenes are a special class of PAH comprised by six fused benzene rings, whose intrinsic birradical character imparted by their non-Kekulé structure makes them appealing candidates for optoelectronic devices.[116] The inclusion of heteroatoms in the central and bridging positions generates further applications, affording a series of compounds which have been termed heterotriangulenes.[117] The nitrogen-centred members of this family, *i.e*. *N*-heterotriangulenes, are a very versatile scaffold in which the substituent of the tether position conditions a p- or n-type semiconducting behaviour and also determines the shape of the molecule[118] (Figure 52). Thus, the presence of carbonyl groups in the bridging positions gives rise to planar carbonyl-bridged triarylamines CBTs with hole injection ability, whose self-assembly process has been demonstrated to generate thermotropic liquid crystallinity[119] and unprecedented coherent energy transport.[18] Additionally, the versatility of the carbonyl group makes accessible a series of modifications, permitting the tuning of the electronic properties.[120,121]

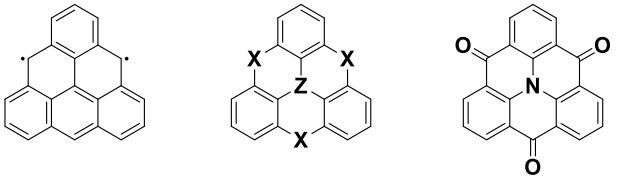

Figure 52. From left to right, chemical structure of triangulene, heterotriangulene and CBT.

Furthermore, their C_3 symmetry imparts to CBTs the perfect shape to study supramolecular polymerization processes. As it has been demonstrated in the self-assembly in solution of other C_3-symmetric molecules like 1,3,5-benzene-

[116] N. Pavliček, A. Mistry, Z. Majzik, N. Moll, G. Meyer, D. J. Fox, L. Gross, *Nat. Nanotech.* **2017**, *12*, 308.
[117] J. E. Field, D. Venkataraman, *Chem. Mater.* **2002**, *14*, 962.
[118] N. Hammer, T. A. Schaub, U. Meinhardt, M. Kivala, *Chem. Rec.* **2015**, *15*, 1119.
[119] M. Kivala, W. Pisula, S. Wang, A. Mavrinskiy, J.-P. Gisselbrecht, X. Feng, K. Müllen, *Chem. Eur. J.* **2013**, *19*, 8117.
[120] C.-M. Chou, S. Saito, S. Yamaguchi, *Org. Lett.* **2014**, *16*, 2868.
[121] N. Hammer, T. E. Shubina, J.-P. Gisselbrecht, F. Hampel, M. Kivala, *J. Org. Chem.* **2015**, *80*, 2418.

tricarboxamides BTAs[87] or triphenylamines (TPAs),[122] this geometry constitutes the paradigm to generate supramolecular helices, thus making possible studies of transfer and amplification of chirality. Our research group has also extensively investigated the supramolecular polymerization process in oligo (phenylene-ethynylene) tricarboxamides (OPE-TAs)[123] derivatives, showing the relevance of the extended π-conjugation in the self-assembly process compared to BTAs.

To gain insight into the self-assembly features of *N*-heterotriangulenes, the achiral CBT **48** and their chiral counterparts **(*S*)-49** and **(*R*)-49** (Figure 53) have been synthesized. The presence of the aromatic core and the amide moieties should direct the self-assembly through π-stacking and H-bonding. Besides, the inclusion of ethynylene groups has been described to yield more soluble *N*-heterotriangulene derivatives and, at the same time, extends the π-core and enables it to interact through stronger non-covalent interactions.

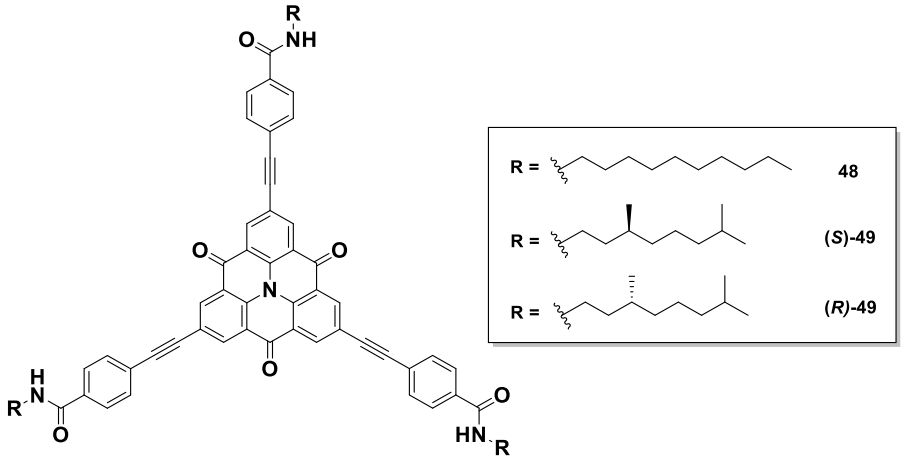

Figure 53. Chemical structure of *N*-heterotriangulenes **48**, **(*S*)-49** and **(*R*)-49**.

[122] T. Kim, T. Mori, T. Aida, D. Miyajima, *Chem. Sci.* **2016**, *7*, 6689.
[123] F. García, P. M. Viruela, E. Matesanz, E. Ortí, L. Sánchez, *Chem. Eur. J.* **2011**, *17*, 7755.

4.3.2. Synthesis of N-heterotriangulenes 48, (S)-49 and (R)-49

The synthesis of CBTs **48**, **(*S*)-49** and **(*R*)-49** is initiated with the generation of the peripheral side chains.[84] First, the amidation of 4-iodobenzoic acid with the commercial amine **30**, **(*S*)-29** and **(*R*)-29** (whose synthesis has been carried out analogously to that of **(*S*)-29**, as described in Scheme 1) using EDC as activating agent and DMAP as base, yields the 4-iodobenzamides **50** and **51** (Scheme 4). Subsequent Sonogashira-type coupling between trimethylsilyl acetylene and the corresponding iodobenzamides permits the generation of **52**, **(*S*)-53** and **(*R*)-53**. The removal of the silyl protecting group in basic media affords the final alkynes **54**, **(*S*)-55** and **(*R*)-55** in good yields. These alkynes are good candidates for further Sonogashira couplings with halogenated aromatic derivatives.

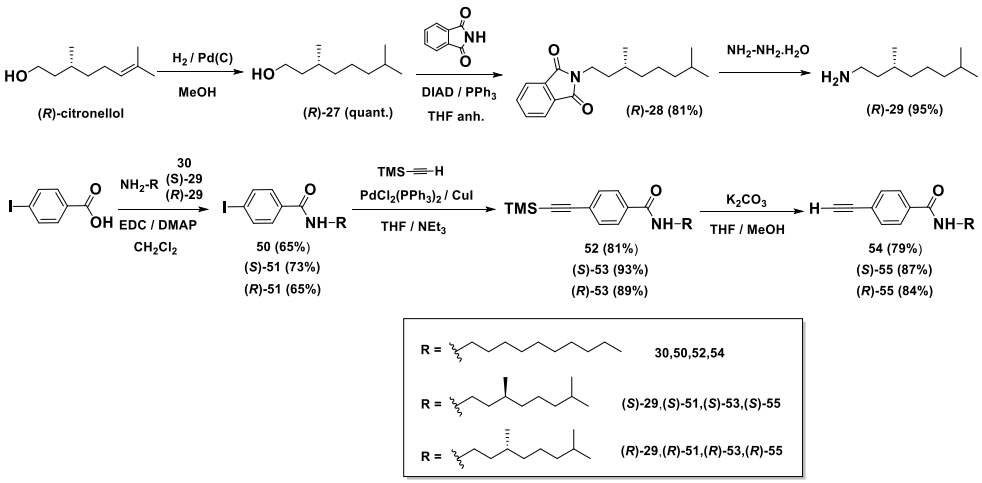

Scheme 4. Synthesis of the alkynes **54**, **(*S*)-55** and **(*R*)-55**.

The synthesis of the iodinated *N*-heterotriangulene core **57** has been reported by Prof. Chen *et al.* in a multistep approach.[124] The initial Ullmann-type coupling between 2-methyl anthranilate and 2-methyl iodobenzoate, using a Cu/CuI pair as activating system, renders a triarylamine which is further subjected to iodination to attain **56**. The basic hydrolysis of **56** and the following formation of an acyl chloride renders a molecule which, in presence of a Lewis acid as $SnCl_4$, experiences a Friedl-Crafts acylation, affording the carbonyl-tethered triphenyl **57**. The presence of the iodine atoms makes this scaffold a versatile substrate for C-C couplings. Thus,

[124] H. Zhang, S. Wang, Y. Li, B. Zhang, C. Du, X. Wan, Y. Chen, *Tetrahedron* **2009**, *65*, 4455.

a final Sonogashira-type triple coupling between the iodinated **57** and the alkynes **54** and **55** yields the target CBTs **48**, **(*S*)-49** and **(*R*)-49**.

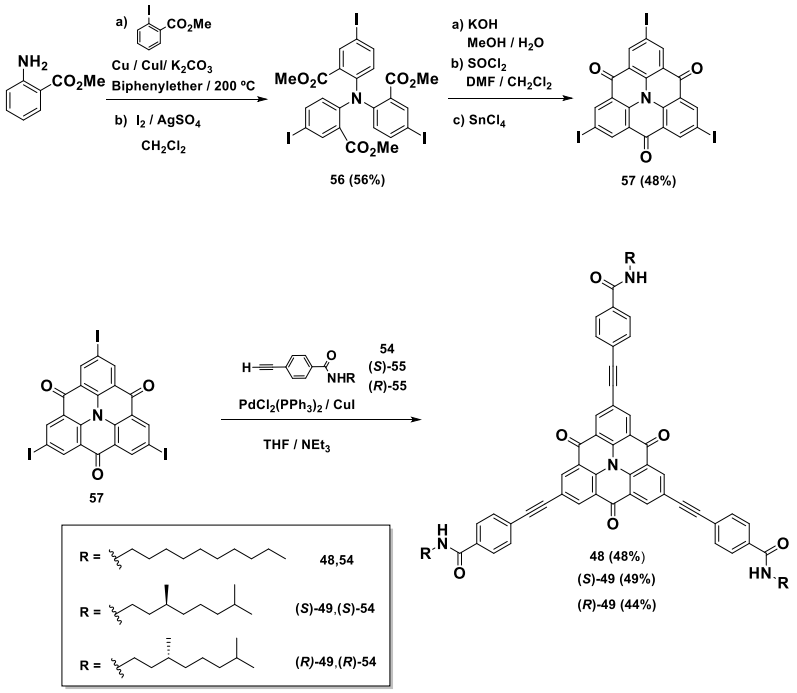

Scheme 5. Synthesis of the *N*-heterotriangulenes **48**, **(*S*)-49** and **(*R*)-49**.

The chemical structure of all the new synthesized compounds has been determined by means of the usual spectroscopic techniques (the complete characterization can be consulted in the Experimental Section Part).

4.3.3. Self-assembly of N-heterotriangulenes 48, (S)-49 and (R)-49 in solution

The strong tendency of CBTs **48**, **(*S*)-49** and **(*R*)-49** to aggregate in solution has been firstly disclosed by the ^{1}H NMR spectra in $CDCl_3$. The broad signals unravelled even at concentrations as low as 1 mM are a clear diagnostic of the very high capability of these derivatives to self-assemble in solution (Figure 54).

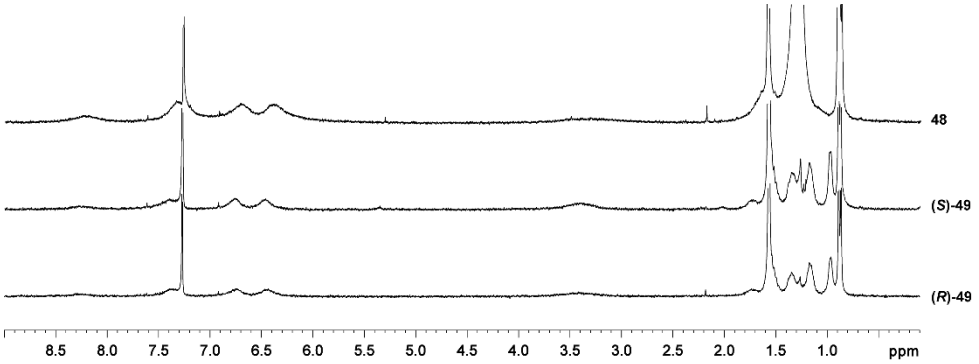

Figure 54. ^{1}H NMR spectra of **48**, **(*S*)-49** and **(*R*)-49** in $CDCl_3$ at c_T = 1 mM (300 MHz, 293 K).

FTIR spectroscopy also indicates the ability of CBTs to interact by non-covalent interactions (Figure 55). The values of the N-H and Amide I stretching bands at $\tilde{\upsilon}$ ~ 3300 cm^{-1} and $\tilde{\upsilon}$ ~ 1635 cm^{-1}, respectively, as well as the low value of the Amide II deformation band ($\tilde{\upsilon}$ ~ 1545 cm^{-1}) are typical of an α-helix arrangement through the formation of H-bonding between amides.[125]

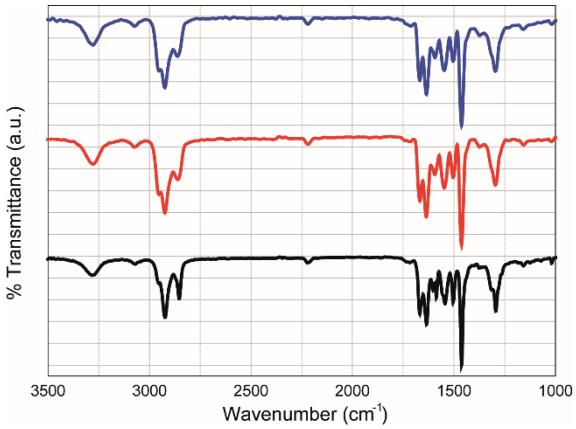

Figure 55. Partial FTIR spectra of **48** (black line), **(*S*)-49** (red line) and **(*R*)-49** (blue line) at room temperature.

[125] J. Puigmartí-Luis, V. Laukhin, Á. Pérez del Pino, J. Vidal-Gancedo, C. Rovira, E. Laukhina, D. B. Amabilino, *Angew. Chem. Int. Ed.* **2007**, *46*, 238.

The evaluation of the spectroscopic features of the aggregates has been carried out by UV-Vis experiments. The solubility of **48**, **(*S*)-49** and **(*R*)-49** in apolar solvents like MCH is scarce, making necessary the addition of a good cosolvent like Tol to enable the study of the supramolecular polymerization process in solution. The spectrum of **48** in a MCH/Tol mixture (3/7) in the disaggregated state (90 ºC) exhibits a main band centred at λ = 443 nm with an adjacent shoulder at λ = 416 nm, which is accompanied by a π-π* transition band at λ = 349 nm with a concomitant shoulder at λ = 333 nm. Importantly, these UV-Vis signatures are also observed at room temperature in good solvents like $CHCl_3$, identifying the features of the monomeric state. After cooling down the MCH/Tol solution, a broadening effect and the loss of the vibronic fine structure are noticed, standing out the emergence of a band at λ = 465 nm (Figure 56a). These spectroscopic signatures have been ascribed to the formation of face-to-face H-aggregates with a rotated geometry in analogy to dyes like boron-dipyrromethene (BODIPY)[126] and PBI[127].

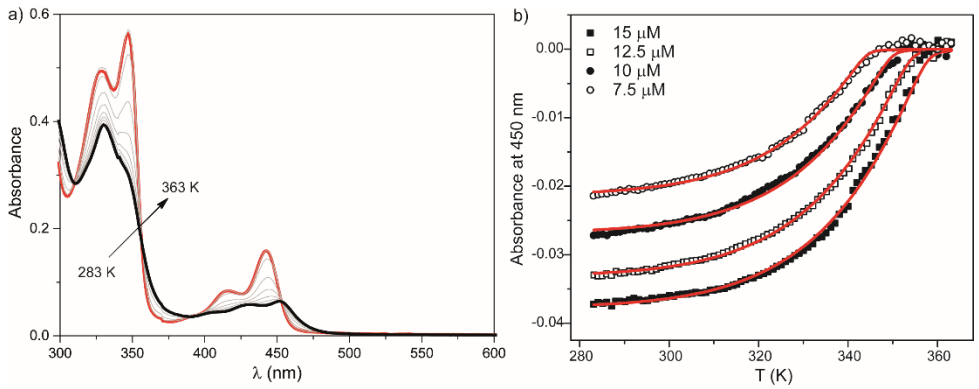

Figure 56. (a) VT-UV-Vis spectra of **48** in a MCH/Tol (3/7) mixture (c_T = 10 μM). (b) Cooling curves of **48** in a MCH/Tol 3/7 mixture (λ = 450 nm, 1 K min^{-1}). The red lines illustrate the fitting with to the EQ model.

The fitting of the cooling curves to the previously mentioned EQ model affords the complete set of thermodynamic parameters governing the supramolecular polymerization (Figure 56b and Table 4). The data obtained for the supramolecular

[126] A. Rödle, B. Ritschel, C. Mück-Lichtenfeld, V. Stepanenko, G. Fernández, *Chem. Eur. J.* **2016**, *22*, 15772.
[127] X.-Q. Li, V. Stepanenko, Z. Chen, P. Prins, L. D. A. Siebbeles, F. Würthner, *Chem. Commun.* **2006**, 3871.

polymerization of compounds **48**, **(*S*)-49** and **(*R*)-49** unravel an enthalpically-driven process which proceeds through a cooperative mechanism. The values obtained for the three compounds in the MCH/Tol mixture are very close for the parameters evaluated. The values of σ are higher than those obtained for other C_3-symmetric molecules.[128] However, this comparison is not very accurate since the parameters obtained for BTAs and OPE-TAs have been measured in pure MCH. Furthermore, the evaluation of the self-assembly capability of **48** has been also studied in other solvents like Tol and CCl_4. The disruption of the π-π interactions diminishes the strong tendency of *N*-heterotriangulenes to aggregate in Tol, what is reflected in a lower value of the T_e and the higher σ in comparison with the value obtained in the MCH/Tol mixture (Figure 57). On the other hand, the supramolecular polymers obtained in the apolar CCl_4 remain stable even at high temperatures, preventing in this way the study of the self-assembly process in this solvent. The data obtained for these compounds in different conditions and solvents are summarized in Table 4.

Table 4. Thermodynamic parameters of compounds **48**, **(*S*)-49** and **(*R*)-49**.

	(*S*)-49[a]	**(*R*)-49**[a]	**48**[a]	**48**[b]
ΔH_e [kJ mol^{-1}][c]	-49.6 ± 0.3	-54.9 ± 0.7	-51.6 ± 0.3	-51.8 ± 0.5
ΔS [J K^{-1}mol^{-1}][c]	-48 ± 1	-61 ± 2	-52 ± 1	-63 ± 1
ΔH_n [kJ mol^{-1}][c]	-21.4 ± 0.5	-26.2 ± 1.6	-20.8 ± 0.4	-17.8 ± 0.3
σ [-][d]	1.7 x 10^{-4}	2.4 x 10^{-4}	2.2 x 10^{-4}	7.5 x 10^{-4}
K_e [L mol^{-1}][d]	1.5 x 10^{6}	2.7 x 10^{6}	2.1 x 10^{6}	6.1 x 10^{5}
K_n [L mol^{-1}][d]	2.7 x 10^{2}	0.7 x 10^{2}	4.8 x 10^{2}	4.6 x 10^{2}

[a] In a mixture of MCH/Tol 3/7 as solvent. [b] In toluene as solvent. [c] ΔH_e=enthalpy of elongation; ΔH_n=enthalpy of nucleation. [d] The equilibrium constants for elongation and dimerization, K_e and K_n, and the cooperativity factor σ are calculated at 298 K.

[128] F. García, P. A. Korevaar, A. Verlee, E. W. Meijer, A. R. A. Palmans, L. Sánchez, *Chem. Commun.* **2013**, *49*, 8674.

Self-assembly of referable *N*-heterotriangulene derivatives has been described to yield kinetically stable aggregates, disclosing the presence of pathway complexity.[129] To evaluate this scenario the presence of hysteresis has been checked by registering heating and cooling curves. The existence of competing metastable species makes that opposite reactions cannot equilibrate, showing a hysteresis cycle.[69] The cooling and heating curves of **48** in Tol possess the same T_e values, making the possibility of kinetic effects in the self-assembly of this family of CBTs unlikely (Figure 57b).

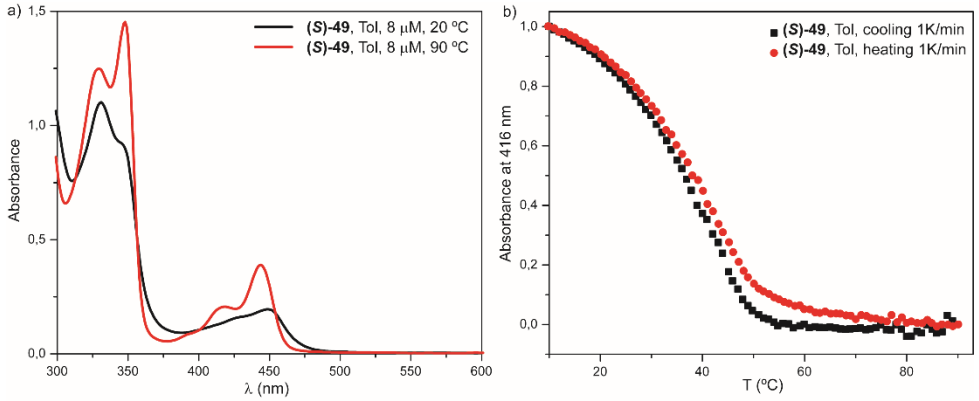

Figure 57. (a) UV-Vis spectra of **(*S*)-49** (c_T = 8 μM) in Tol at 20 ºC (black line) and 90 ºC (red line). (b) Heating (red points) and cooling (black points) of **(*S*)-49** in Tol (c_T = 8 μM, 1 K min^{-1}).

The intrinsic chirality of **(*S*)-49** and **(*R*)-49** paves the way for CD spectroscopy studies. The CD spectrum of **(*S*)-49** in a MCH/Tol (3/7) mixture renders a clear bisignated Cotton effect with a positive band at λ = 346 nm and a negative band centred at λ = 324 nm. This dichroic pattern is also observed in other solvents like Tol and CCl_4. This signature is typical of *P*-type helices and is in agreement with the α-helix arrangement unveiled by FTIR values. In contrast, **(*R*)-49** discloses a mirror-like spectrum in the same conditions, yielding *M*-type helices as shown by its negative bisignated Cotton effect. Remarkably, these spectrum signatures are maintained in other solvents like toluene and CCl_4 (Figure 58). Importantly, lineal

[129] A. T. Haedler, S. C. J. Meskers, R. H. Zha, M. Kivala, H.-W. Schmidt, E. W. Meijer, *J. Am. Chem. Soc.* **2016**, *138*, 10539.

dichroism contamination arising from the macroscopic alignment of the fibres in solution has been discarded in all the conditions evaluated.[130]

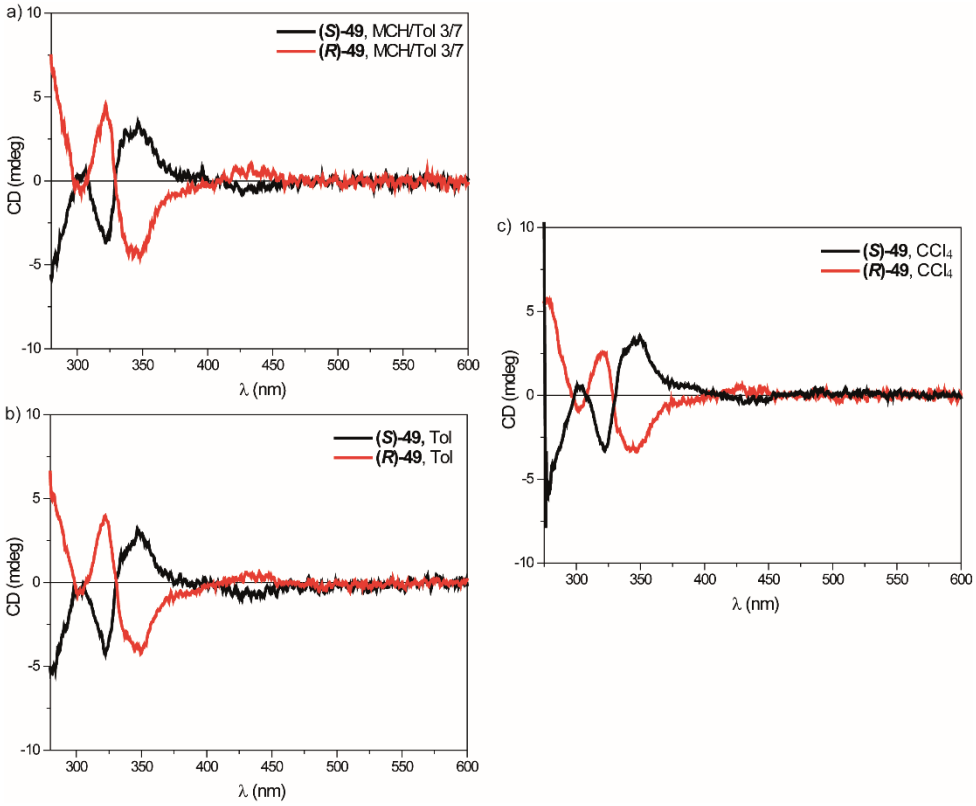

Figure 58. CD spectra of **(*S*)-49** (black line) and **(*R*)-49** (red line) in different solvents (c_T = 100 μM, 293 K).

To identify the morphology of the supramolecular polymers formed by CBT derivatives, AFM images of **(*S*)-49** and **(*R*)-49** have been obtained by drop-casting a 7 μM Tol solution obtained by dilution of the gel onto mica. These images depict a bundle of fibres of 4 nm height, thus fitting with the rough size of *N*-heterotriangulene.[117,119] This morphology is also in agreement with the combination of π-stacking and H-bonding that yields 1D helices (Figure 59). Unfortunately, AFM images of the aggregates in more apolar solvents like MCH or CCl_4 unveil

[130] J. Buendía, J. Calbo, E. Ortí, L. Sánchez, *Small* **2017**, *13*, 1603880.

amorphous aggregates due to higher tendency of **48**, **(*S*)-49** and **(*R*)-49** to self-assemble in these solvents.

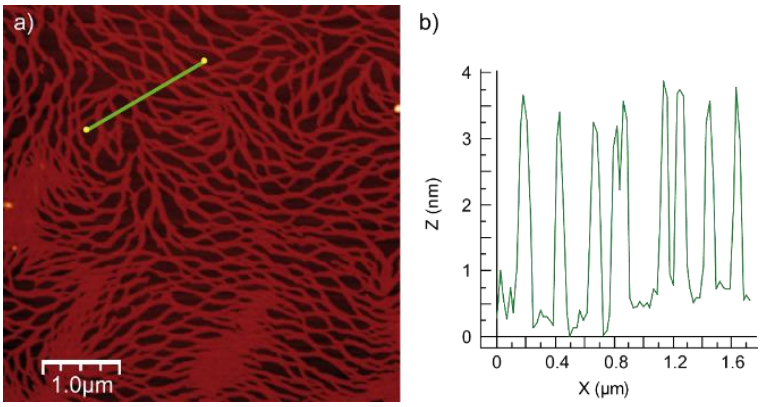

Figure 59. (a) Height AFM image and (b) height profile along the green line of a drop-casted solution of a diluted gel of **(*S*)-49** in Tol onto mica at c_T = 7 μM. The z scale is 25 nm.

4.3.4. Organogels of N-heterotriangulenes 48, (S)-49 and (R)-49. Study of the chiroptical features in the gel state

The high capability of compounds **48**, **(*S*)-49** and **(*R*)-49** to self-assemble in organic solvents can also lead to the formation of organogels.[45,46] *N*-heterotriangulenes **48** and **49** have been demonstrated to form gels in apolar solvents like Tol and CCl_4 (Figure 60), although the critical gelation concentration (CGC) and the visual appearance of the gels in both solvents are very different. Thus, the CGC in CCl_4 is 9 mM, whereas in Tol is around 33 mM. Interestingly, the Tol gels are more opaque, especially in the case of compound **48**. These findings can be explained considering the different polarities of the solvents ($E_{T\,(30)\,Tol}$=33.9 kcal mol^{-1} and $E_{T\,(30)\,CCl4}$=32.4 kcal mol^{-1}) as well as the branched nature of the alkyl chains in compounds **(*S*)-49** and **(*R*)-49**, which can difficult the intertwining of the 1D fibres, leading to the formation of less stable gels.

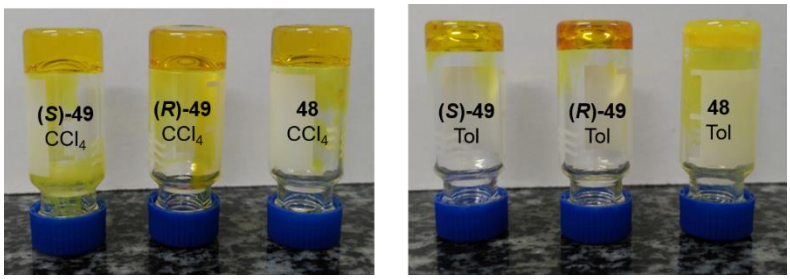

Figure 60. Organogels of **48**, **(*S*)-49** and **(*R*)-49** in CCl_4 (left image) and in Tol (right image).

As it has been confirmed by spectroscopic data, the self-assembly of *N*-heterotriangulenes is likely to proceed through the establishment of a triple array of H-bonds between the amide groups and the π-stacking of the CBT cores, yielding supramolecular helices. Further bundling of the peripheral chains at high concentrations could generate hierarchical superhelices whose interaction would afford the gel grid. To shed light in the formation of the gels, the vibrational circular dichroism (VCD) spectra have been registered for the gels of CBTs **(*S*)-49** and **(*R*)-49** in Tol and in CCl_4 by the group of Prof. Juan Casado (Figure 61).

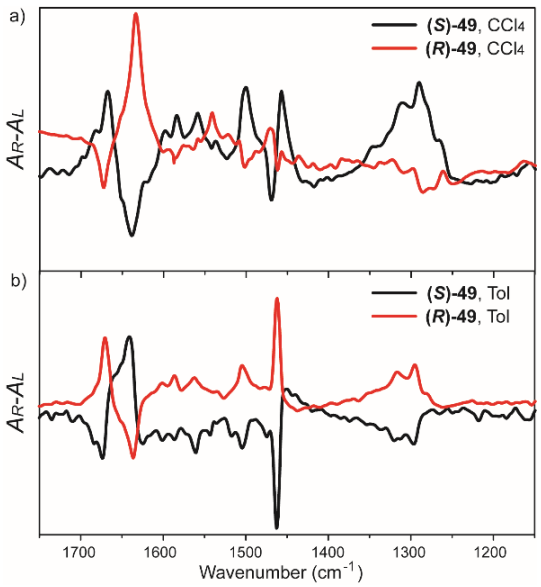

Figure 61. VCD spectra of the gels (20000 scans each) of **(*S*)-49** and **(*R*)-49** in CCl_4 (a) and Tol (b) at 25 ºC. c_T = 20 mg mL^{-1} in Tol and c_T = 5 mg mL^{-1} in CCl_4.

VCD spectra unveil a mirror-like pattern for both compounds. The most noticeable bands are the bisignated carbonyl stretching band at $\tilde{\upsilon}$ = 1650 cm^{-1}, which arise from the combination of the aforementioned internal carbonyl group of the *N*-heterotriangulene core ($\tilde{\upsilon}$ = 1660 cm^{-1}) and the outer amide ($\tilde{\upsilon}$ = 1620 cm^{-1}). The low values of the amide band are due to their participation in the H-bond array. It should be pointed out that the resulting bisignated pattern can also stem from the monosignated signature of the inner carbonyl and the bisignated pattern of the amide vibration. The other intense band at $\tilde{\upsilon}$ = 1440 cm^{-1} is probably due to the scissoring deformation vibration of the methylene group δ (CH_2) that exposes a monosignated pattern.

The most prominent aspect of the VCD spectra of **(*S*)-49** and **(*R*)-49** is that the same enantiomer exhibits an inversion in the carbonyl stretching band by changing the solvent. Thus, a different chiral response can be generated with an achiral agent, making of these gels a solvent-dependent chiroresponsive system. This behaviour has not been described previously for supramolecular polymers, and a plausible explanation could be the presence of a metastable aggregation pathway in the supramolecular polymerization of compounds **(*S*)-49** and **(*R*)-49**, rendering helices with opposite handedness whose further interaction generates gels with different chiroptical properties. This hypothesis has been discarded after examining the CD measurements reflected in Figure 58, denoting the same CD pattern for a given enantiomer in Tol and in CCl_4. However, the different interaction among these 1D helices and the solvent can give rise to a metastable pathway in the gel formation that finally evolves to the thermodynamic stable gel. VCD has also been utilized to elucidate the presence of kinetic species in supramolecular polymerizations.[102] Therefore, the VCD spectra of both compounds in Tol and in CCl_4 has been recorded daily during 14 days and at different temperatures. Nevertheless, no significant changes have been unravelled in none of the measured conditions, thus discarding a kinetic to thermodynamic transition (Figure 62). Probably, the high concentrations required for the formation of the gel impede any quick change, making necessary the application of a stronger stimulus in order to see which of the gels is the kinetically-trapped entity.

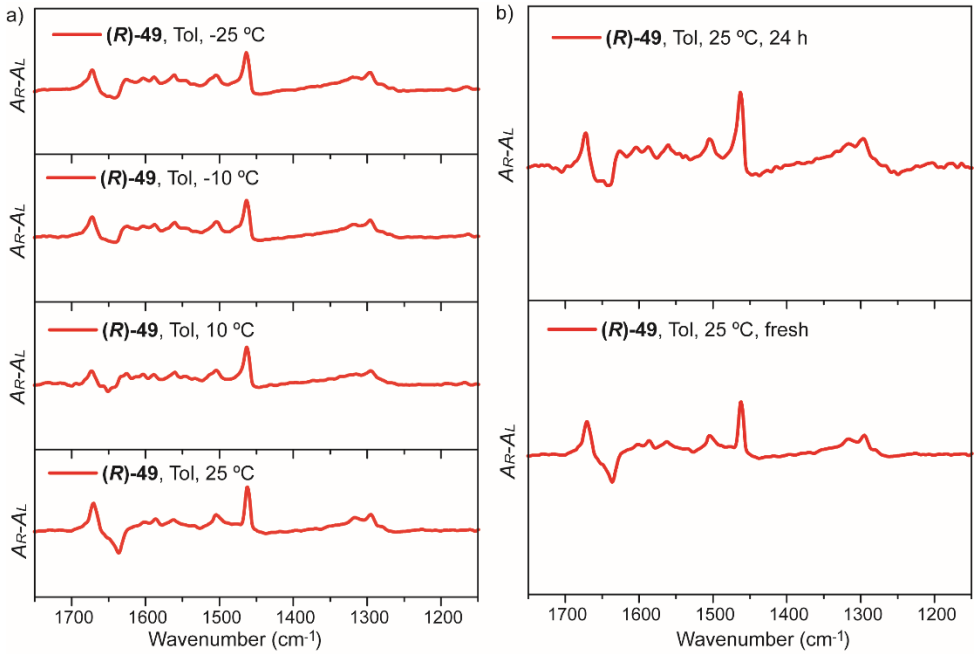

Figure 62. VCD spectra of the gel of **(*R*)-49** in Tol at different temperatures (a) and at different times (b).

To overcome this limitation, the gels have been prepared in the same solvents but applying ultrasounds during their generation, what constitutes a perfect force to disrupt the weak intermolecular interactions driving the gel formation. This tool provides a perfect scenario to heal the gel structure from conformational disorder. After treatment with ultrasounds, in the gel of **(*R*)-49** in Tol (Figure 63) the intensity of the $\tilde{\upsilon}$ (C=O) band roughly keeps constant while that of the amide I ($\tilde{\upsilon}$ = 1640 cm^{-1}) is shifted to lower wavenumber values affording a new negative band ($\tilde{\upsilon}$ = 1620 cm^{-1}). Furthermore, for the CH_2 deformation, the monosignated band at $\tilde{\upsilon}$ = 1464 cm^{-1} becomes a well-defined 1469/1461 cm^{-1} negative bisignated feature, with an overall up-shift of the δ (CH_2) wavenumber that might be related with a conformational reorientation of the alkyl conformations towards a more *pure* all-*trans* disposition (*i.e.*, the initial structure should have a portion of *gauche* conformational defects).[131] Therefore, the treatment of the gel in Tol with ultrasounds produces a better packed gel which seemingly evolves from a softer

[131] R. A. Vaia, R. K. Teukolsky, E. P. Giannelis, *Chem. Mater.* **1994**, *6*, 1017.

phase that however, does not involve an inversion in the helix handedness. While the Tol gels made with ultrasounds treatment remain without pattern inversion, the gels of **(*S*)-49** and **(*R*)-49** formed in CCl_4 with ultrasounds consists of an overall weaker spectrum with the ϑ (C=O) bands displaying a clear opposite +/- pattern compared with the -/+ for the gel generated in the absence of ultrasounds. In addition, the VCD pattern of the δ (CH_2) band is also reversed in the spectra before and after the ultrasonic treatment.

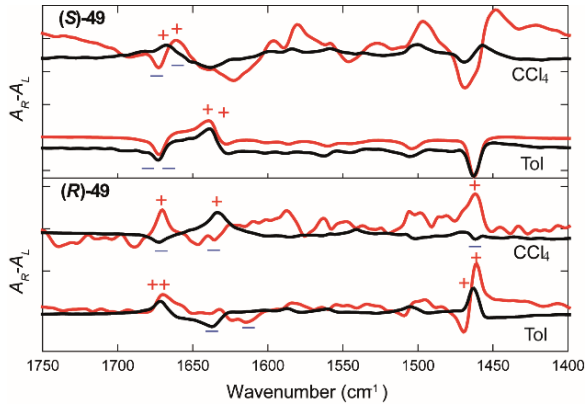

Figure 63. VCD spectra of the gels (20000 scans each) of **(*S*)-49** (top) and **(*R*)-49** (bottom) in CCl_4 and Tol at room temperature. The black and red lines depict the VCD spectra without and with ultrasound treatment, respectively. c_T = 20 mg mL^{-1} in Tol and c_T = 5 mg mL^{-1} in CCl_4.

These results imply that the initial chiroptical features of the gel in CCl_4 correspond to a kinetically trapped phase whilst the Tol gel corresponds to the thermodynamic gel state. The high concentration in the gel state could disfavour the transition from the kinetic to the thermodynamic phase with time, but the application of ultrasounds breaks the weak interacting forces among 1D fibres and permits the obtaining of the thermodynamic product. Therefore, VCD experiments provide firm evidences of the helicity inversion in compounds **(*S*)-49** and **(*R*)-49** as a consequence of the solvent interactions with the superhelices formed. The polarity and molecular size of CCl_4, might be at the origin of this complex behaviour.[132]

[132] V. A. Mallia, P. D. Butler, B. Sarkar, K. T. Holman, R. G. Weiss, *J. Am. Chem. Soc.* **2011**, *133*, 15045.

Thus, these results demonstrate the importance of H-bonding to complement the strong π-stacking in *N*-heterotriangulene tricarboxamides **48**, **(*S*)-49** and **(*R*)-49**, yielding H-type aggregates under a cooperative mechanism. The capability of these compounds to hierarchically organize is proved by the formation of gels in different organic solvents. Remarkably, the solvent directed helical stereomutation showed for **(*S*)-49** and **(*R*)-49** in the gel state seems a result of the initial interaction of the alkyl chains between 1D fibres in CCl_4, leading to a less ordered structure which evolve to the more stable one when a stimulus like ultrasounds enables the transition. These results reinforce the previously described tendency of *N*-heterotriangulenes to experience pathway complexity, unravel the importance of VCD to study pathway complexity in the gel state and, importantly, demonstrate the usefulness of the gel state to study uncommon chiroptical features, paving the way to a deeper understanding of the rules directing the transfer of chirality in the different hierarchical levels of organization.

4.4. Kinetically-controlled supramolecular polymerization of *N*-heterotriangulenes

4.4.1. Kinetically-controlled supramolecular polymerizations

As it has been pointed out in the Background section, the combination in cooperative self-assembling systems of strong non-covalent forces, like π-stacking between extended aromatic surfaces and H-bonding between amides, could arise pathway complexity phenomena, whose control permits the realization of living supramolecular polymerizations. The results obtained in the previous Section demonstrate the strong cooperative supramolecular polymerization followed by *N*-heterotriangulene ethynylene-extended tricarboxamides **48**, **(*S*)-49** and **(*R*)-49** and, importantly, the existence of a kinetic process in the gel state. These studies, and similar results obtained by Prof. Meijer´s group, in which the self-assembly of *N*-heterotriangulene derivatives yields kinetically trapped supramolecular polymers,[129] show the capability of this scaffold to yield complex supramolecular systems whose command can pave the way to the application of programmable supramolecular polymerizations.

Prompted by these results, CBTs **58**, **(*S*)-59** and **(*R*)-59**, have been synthesized (Figure 64). The introduction of an inner ester and an ethylene bridge between this group and the amide functionality should provide a perfect substitution pattern for the formation of an intramolecular H-bond stabilized by a 7-membered pseudocycle. This intramolecular interaction should slow down the polymerization and could generate metastable species in a similar way than referable kinetic traps.[64,133] The control over out-of-equilibrium entities could allow the attainment of seeded supramolecular polymerizations in *N*-heterotriangulene derivatives, thus furnishing aggregates with lower polydispersity. Additionally, the introduction of lineal and branched alkyl chains increases the solubility of the supramolecular polymers and, in the latter case, permits studying the influence of the chiral chain in kinetically controlled supramolecular polymerizations and in the seeded approach.

[133] S. Ogi, K. Matsumoto, S. Yamaguchi, *Angew. Chem. Int. Ed.* **2018**, *57*, 2339.

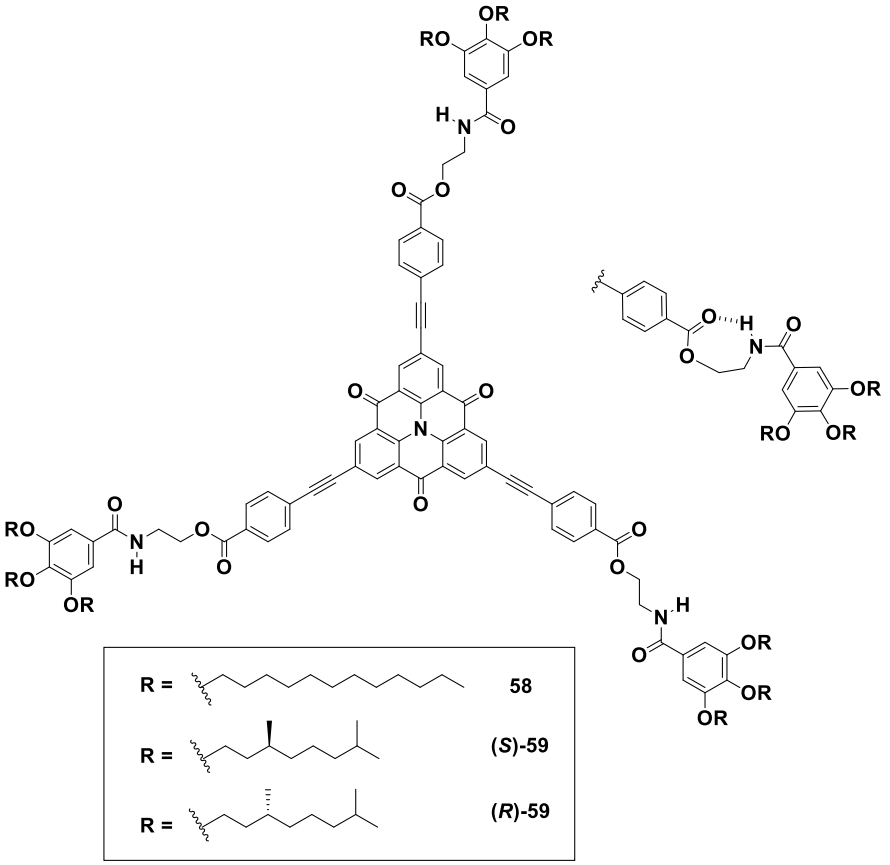

Figure 64. Chemical structure of *N*-heterotriangulenes **58**, **(*S*)-59** and **(*R*)-59**. The right part highlights the intramolecular H-bond between the ester and the amide groups.

4.4.2. Synthesis of N-heterotriangulenes 58, (S)-59 and (R)-59

The synthesis of the target CBTs **58** and **59** has been accomplished through a convergent route, which firstly involves the generation of the alkynes at the peripheral chain and finally the coupling of these outer moieties with the iodinated *N*-heterotriangulene core **57** in a triple Sonogashira reaction. The synthesis of the external unit is depicted in Scheme 6. Carboxylic acid **38** has been obtained as described in Section 2, by a triple Williamson etherification between methyl 3,4,5-trihydroxybenzoate and dodecyl bromide to afford **37** and a subsequent basic hydrolysis. To achieve the synthesis of its chiral counterparts **(*S*)-62** and **(*R*)-62**, a good leaving group attached to chiral chain is required. In this case, tosylates **(*S*)-60** and **(*R*)-60** have been selected as proper intermediates to attain these products.

The obtaining of these compounds implies the tosylation reaction of the previously synthesized alcohols **(*S*)-27** and **(*R*)-27**, employing tosyl chloride and trimethylamine.[134] After that, a Williamson etherification of these compounds with methyl 3,4,5-trihydroxybenzoate, yields **(*S*)-61** and **(*R*)-61**. Following basic hydrolysis of **(*S*)-61** and **(*R*)-61** affords the carboxylic acids **(*S*)-62** and **(*R*)-62** quantitatively.[127] These products are further subjected to an amidation reaction using ethanolamine, EDC as activating agent and DMAP as base, thus generating alcohols **63, (*S*)-64** and **(*R*)-64**.[135] **63** and its chiral analogues **64** should be coupled to acid **66** in order to generate the final peripheral chains. This reagent involves a previous two-step synthesis implying a Sonogashira coupling between commercial methyl 4-iodobenzoate and trimethylsilylacetylene, yielding **65**, and a subsequent reaction in which the simultaneous deprotection of the alkyne and the hydrolysis of the ester in a basic media is fulfilled.[136] **66** is then subjected to an esterification reaction with the corresponding alcohols **63** and **64**, using EDC as activating reagent and DMAP as base, allowing the generation of alkynes **67**, **(*S*)-68** and **(*R*)-68** in good yields.

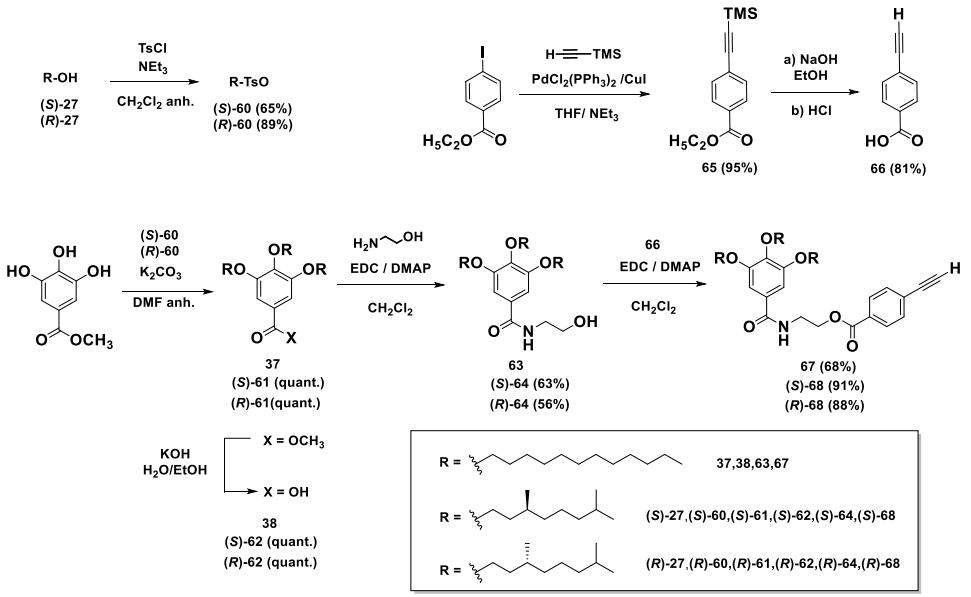

Scheme 6. Synthesis of the alkynes **67**, **(*S*)-68** and **(*R*)-68**.

[134] K. Mori, H. Harada, P. Zagatti, A. Cork , D. R. Hall, *Liebigs Ann. Chem.* **1991**, 259.
[135] F. Aparicio, L. Sánchez, *Chem. Eur. J.* **2013**, *19*, 10482.
[136] H. C. Bertrand, M. Schaap, L. Baird, N. D. Georgakopoulos, A. Fowkes, C. Thiollier, H. Kachi, A. T. Dinkova-Kostova, G. Wells, *J. Med. Chem.* **2015**, *58*, 7186.

Compounds **67**, **(*S*)-68** and **(*R*)-68** have been finally coupled with **57** (whose synthesis is described in Scheme 5 of Section 3) in a triple Sonogashira reaction, affording the *N*-heterotriangulenes **58**, **(*S*)-59** and **(*R*)-59** in moderate yields (Scheme 7).

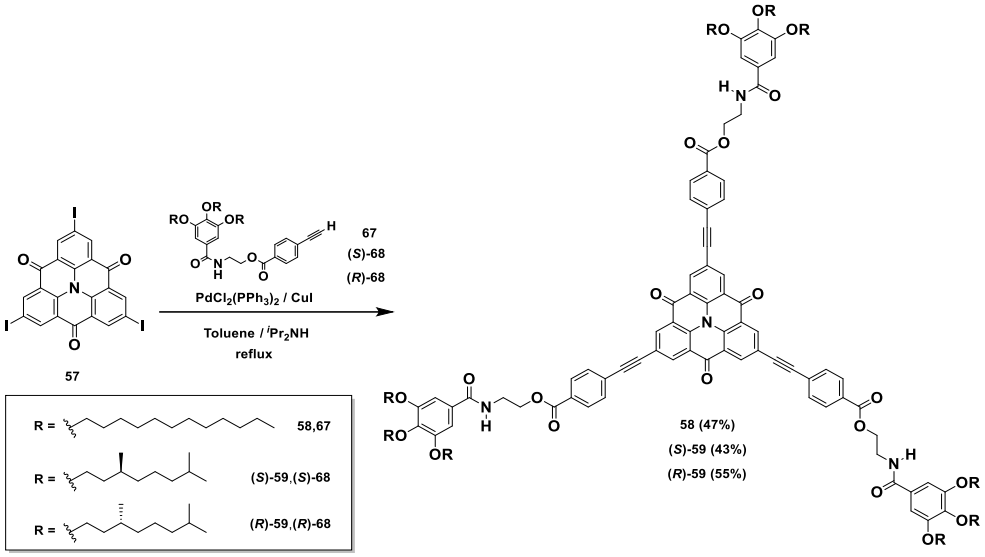

Scheme 7. Synthesis of the CBTs **58**, **(*S*)-59** and **(*R*)-59**.

The chemical structure of all the new synthesized compounds has been determined by means of the usual spectroscopic techniques (the complete characterization can be consulted in the Experimental Section Part).

4.4.3. Self-assembly of N-heterotriangulenes 58, (S)-59 and (R)-59 in solution

FTIR spectroscopy is the first tool unravelling the initial hint of the self-assembling capability of **58**. The N-H and Amide I (C=O) stretching bands and the Amide II (C-N) bending band appear at $\tilde{\upsilon}$ = 3300, 1638, and 1543 cm^{-1}, respectively (Figure 65). The comparison between these low wavenumbers and those reported for unbounded amides ($\tilde{\upsilon}$ = 3450, 1690, and 1550 cm^{-1} for the N-H, Amide I and Amide II bands, respectively) constitutes an indication of the strong tendency of **58**, **(*S*)-59** and **(*R*)-59** to self-assemble by the H-bonding interaction between the amide functional groups.[84,85,137]

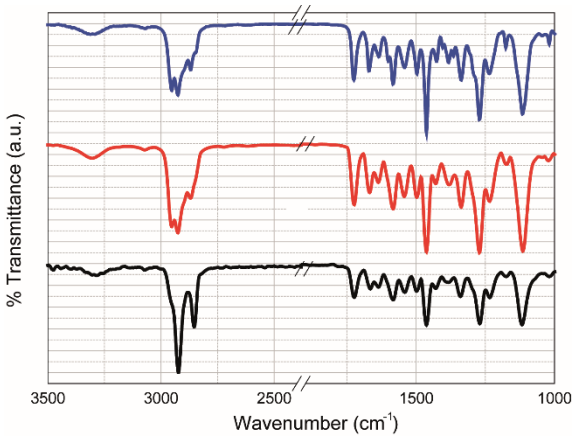

Figure 65. Partial FTIR spectra of *N*-heterotriangulenes **58** (black line), **(*S*)-59** (red line) and **(*R*)-59** (blue line) at room temperature.

Variable concentration ^{1}H NMR experiments provide another proof of the self-assembling capability of CBT **58** to form organized aggregates in solution (Figure 66). The downfield shift experienced by the N-H proton (δ ~ 7.0 ppm, purple dot) with increasing concentration is ascribable to the involvement of these protons in H-bonding. Notably, the shielding of the protons of the *N*-heterotriangulene core and the *para*-substituted benzoate unit (δ ~ 9.0 ppm, blue dot, and δ ~ 8.0 and 7.5 ppm, green and red dots, respectively) when the concentration is incremented are characteristic of their participation in π-stacking.

[137] M. M. J. Smulders, T. Buffeteau, D. Cavagnat, M. Wolffs, A. P. H. J. Schenning, E. W. Meijer, *Chirality* **2008**, *20*, 1016.

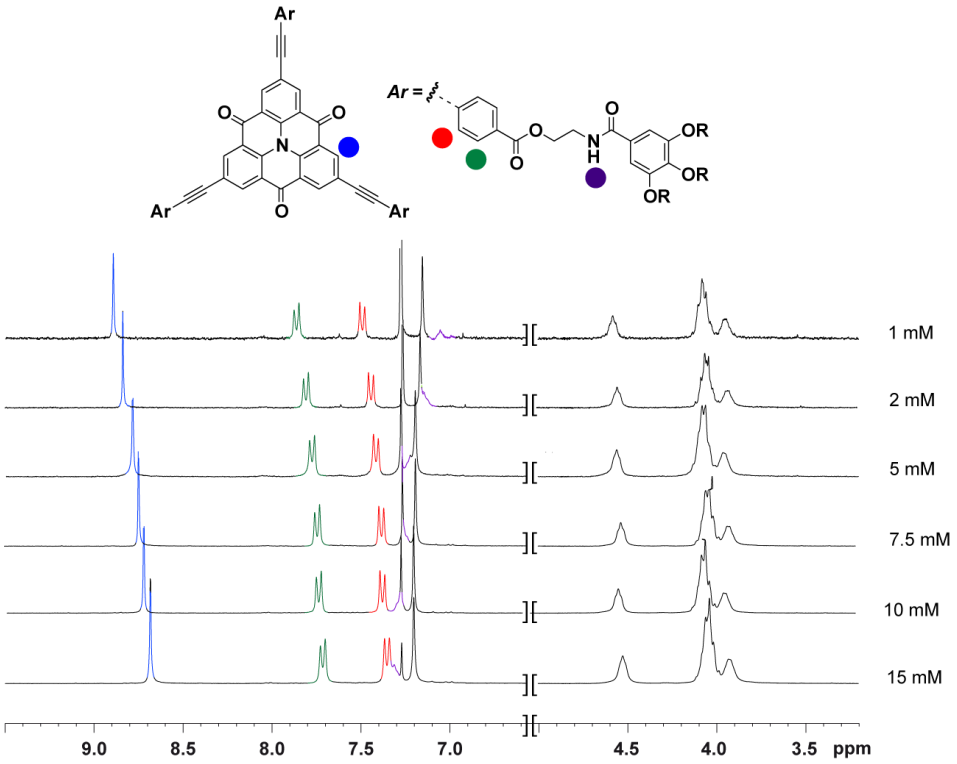

Figure 66. Partial ^{1}H NMR spectra of **58** at different concentrations ($CDCl_3$, 300 MHz, 298 K).

A detailed inspection of the supramolecular polymerization process of *N*-heterotriangulenes **58** has been carried out by VT-UV-Vis spectroscopy. The spectrum of **58** in MCH at 20 ºC exhibits a band centred at λ = 458 nm with a concomitant shoulder at λ = 434 nm. Remarkably, this pattern remains stable at 90 ºC, unveiling the high stability of the supramolecular polymers formed by these *N*-heterotriangulene derivatives. On the other hand, the spectra in a good solvent like toluene at 20 ºC and 90 ºC disclose a very similar, but hypsochromically shifted signature (λ = 441 nm and λ = 418 nm for the band and the shoulder, respectively). This bathochromic shift in the absorption maxima induced by the aggregation process is diagnostic of the formation of J-aggregates (Figure 67).[31]

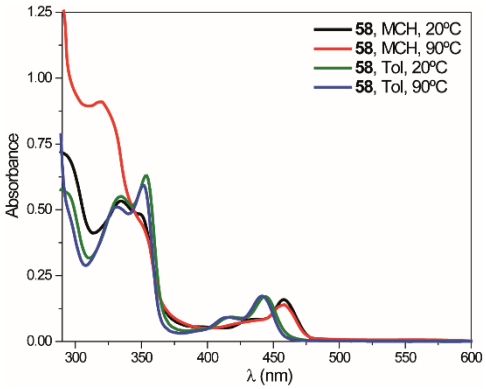

Figure 67. UV-Vis spectra of **58** in MCH and Tol at 20 and 90 ºC (c_T = 8 μM).

Therefore, in order to gain insight in the supramolecular polymerization mechanism, the use of MCH/Tol mixtures is required. Thus, in 2/1, 1/1 and 1/2 mixtures the pattern at 20 ºC is coincident with that observed in MCH whereas heating at 90 ºC permits obtaining a similar spectrum to that reflected in Tol, ascribable to the monomeric state (Figure 68 and Figure 69a).

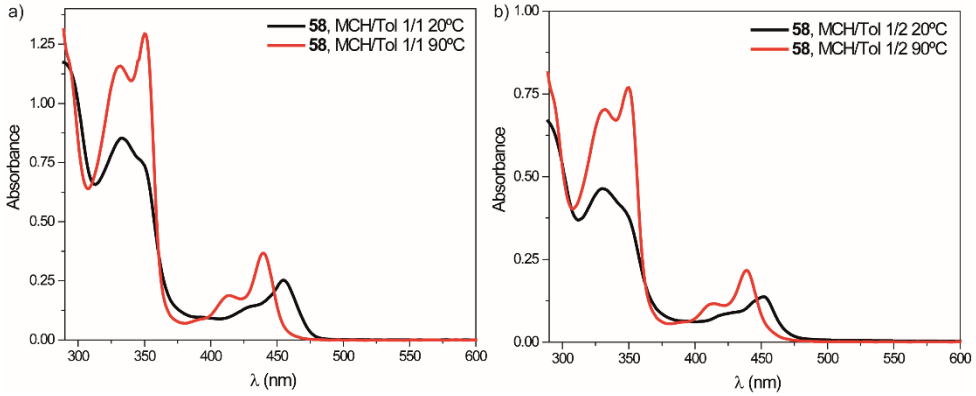

Figure 68. UV-Vis spectra of **58** (c_T = 8 μM) in a a) MCH/Tol (1/1) mixture and b) MCH/Tol (1/2) mixture at 20 ºC (black line) and 90 ºC (red line).

To derive the thermodynamic parameters of the supramolecular polymerization process, cooling curves at 1 K min^{-1} have been registered for all the mixtures, affording curves with a non-sigmoidal shape characteristic of a cooperative mechanism. As expected, the elongation temperature suffers a decrease upon increasing volumes of a good solvent like Tol. However, none of the resulting

curves can be accurately fitted to the EQ model (Figure 69), which can be symptomatic of a more complex supramolecular polymerization process.[138,139]

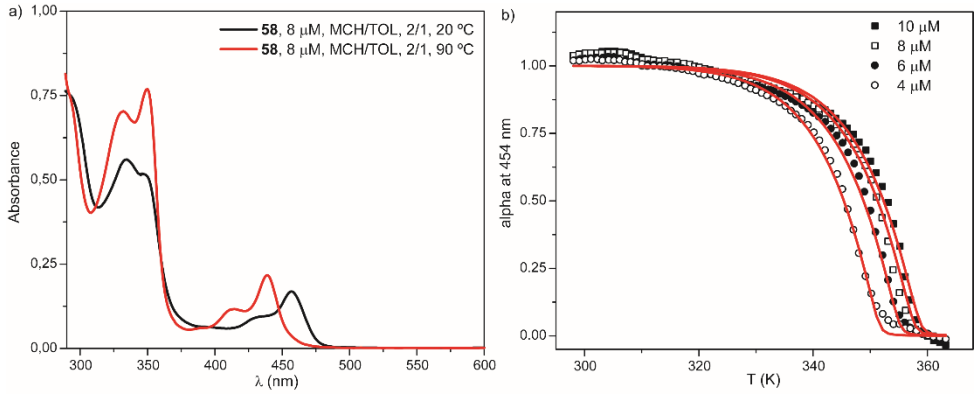

Figure 69. (a) UV-Vis spectra of **58** in a MCH/Tol (2/1) mixture (c_T = 8 μM). (b) Cooling curves obtained in a MCH/Tol (2/1) mixture (λ = 454 nm, 1 K min^{-1}). The fitting to the EQ model is depicted by the red line. The variation of absorbance has been previously normalized to obtain the degree of aggregation α, being this value 1 if the system is totally aggregated and 0 when it is in the monomeric state.

A conclusive proof of the existence of kinetic effects in the self-assembly of *N*-heterotriangulenes **58** and **59** is disclosed by the hysteresis shown after heating and cooling the solutions in all the conditions employed (Figure 70). In good correlation with referable systems, this inability to equilibrate opposite processes can be due to the formation of an intramolecular H-bond between the carbonyl group of the ester group and the N-H proton of the amide, generating an inactive monomer (*M**) through the formation of a stable 7-membered pseudocycle (Figure 64). This species provokes a delay in the supramolecular polymerization process.

[138] R. van der Weegen, A. J. P. Teunissen, E. W. Meijer, *Chem. Eur. J.* **2017**, *23*, 3773.
[139] B. Adelizzi, I. A. W. Filot, A. R. A. Palmans, E. W. Meijer, *Chem. Eur. J.* **2017**, *23*, 6103.

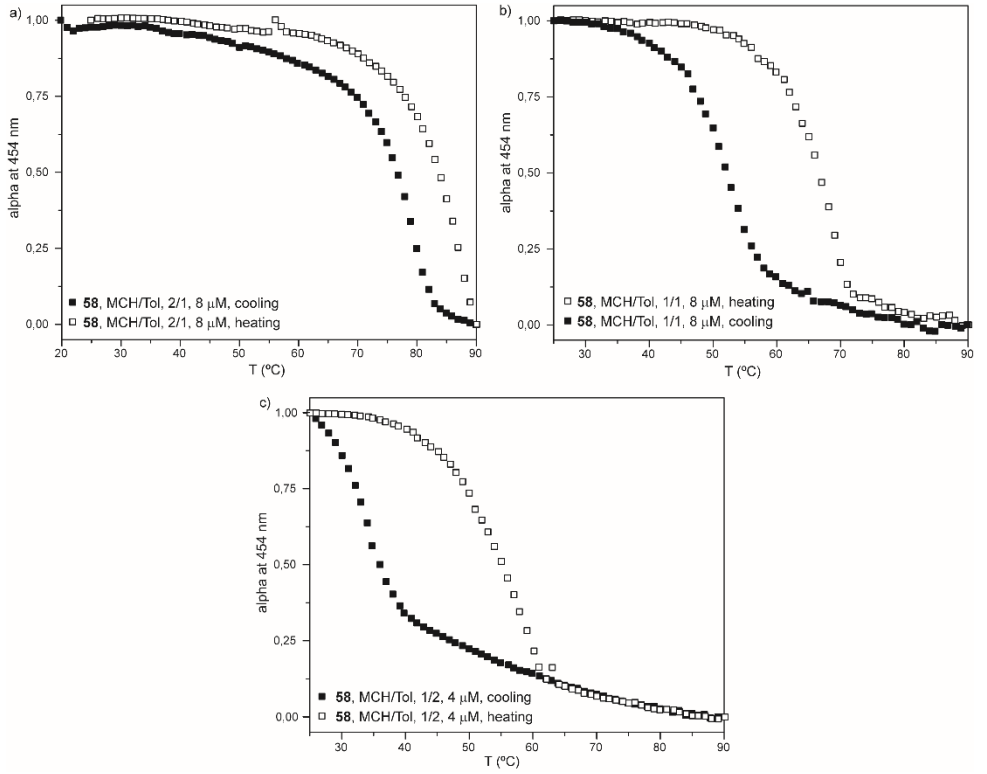

Figure 70. Heating (white dots) and cooling curves (black dots) of **58** in MCH/Tol mixtures (a) 2/1, c_T = 8 μM (b) 1/1, c_T = 8 μM and (c) 1/2, c_T = 4 μM (λ = 454 nm) obtained at a 1 K min^{-1} rate.

To check the presence of *M**, variable temperature ^{1}H NMR experiments in $CDCl_3$ have been performed at a concentration (1 mM) at which it has been previously proved by UV-Vis spectroscopy that *N*-heterotriangulene **58** is in the monomeric form (Figure 71a). The downfield shift of the amide proton with increasing temperatures in the ^{1}H NMR experiment can be justified by the operation of an intramolecular H-bond. At the same time, the lack of shifting in the aromatic resonances discards the π-stacking of the aromatic units and corroborates the formation of the metastable pseudocycle (Figure 71b).

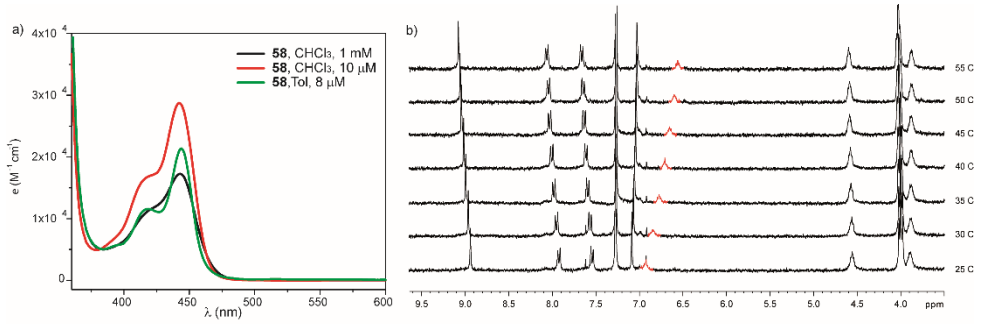

Figure 71. (a) UV-Vis spectra of **58** in $CHCl_3$ and Tol at different concentrations. (b) VT-partial ^1H NMR spectra of **58** ($CDCl_3$, 300 MHz, 0.5 mM). The red signal corresponds to the proton of the amide functional group.

In an attempt to unravel the supramolecular polymerization mechanism followed by *N*-heterotriangulene **58**, studies in an apolar solvent like CCl_4, which has also been demonstrated to be a good solvent to induce self-assembly,[140] have been carried out. Surprisingly, the freshly prepared solution of **58** in CCl_4 exhibits a hypsochromically shifted band centred at λ = 440 nm which disappears after heating at 70 ºC, rendering the monomer pattern as revealed in MCH/Tol mixtures at 90 ºC. These spectroscopic features are typical of H-type aggregates. Unexpectedly, this spectrum evolves after 24 h at room temperature to that assignable to the J-type aggregate previously observed in MCH and MCH/Tol mixtures (Figure 72a). This change implies a pathway complexity phenomena in CCl_4 in which an H-aggregate constitutes a kinetically-controlled (KC) entity whereas the J-type aggregate corresponds to the thermodynamically-controlled (TC) polymer. Notably, in this solvent, a clear hysteresis is also noticed when cooling and heating curves are registered (Figure 72b).

[140] J. Buendía, F. García, B. Yélamos, L. Sánchez, *Chem. Commun.* **2016**, *52*, 8830.

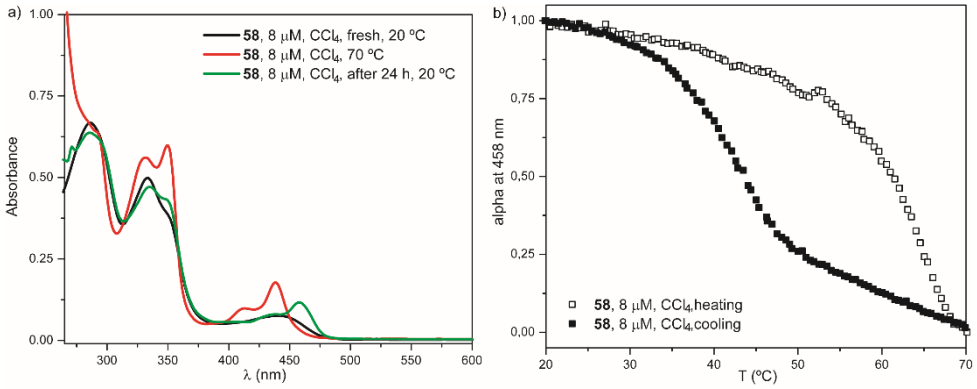

Figure 72. a) UV-Vis spectra of **58** in CCl_4 (black line, freshly prepared; red line, 70 ºC; green line, after 24 h at room temperature). b) Heating (white dots) and cooling curves (black dots) of **58** in CCl_4 (c_T = 8 μM, λ = 458 nm, 1 K min^{-1}).

To disclose the morphology of both competing aggregates, CD spectroscopy experiments of **(*S*)-59** and **(*R*)-59** in CCl_4 have been measured by taking advantage of the presence of stereogenic centres in their peripheral chains. These experiments also corroborate the existence of a pathway complexity as uncovered by the presence of two distinct chiroptical signatures for both aggregates (Figure 73). Thus, the mirror-like CD spectra of the H-type aggregates of **(*S*)-59** and **(*R*)-59** display three intense bands at λ = 354, 323 and 283 nm, whereas the J-type aggregate is characterized by three intense maxima at λ = 463, 383 and 333 nm. These spectra confirm the helical arrangement for both types of aggregates as unveiled by the presence of bisignated Cotton effects.

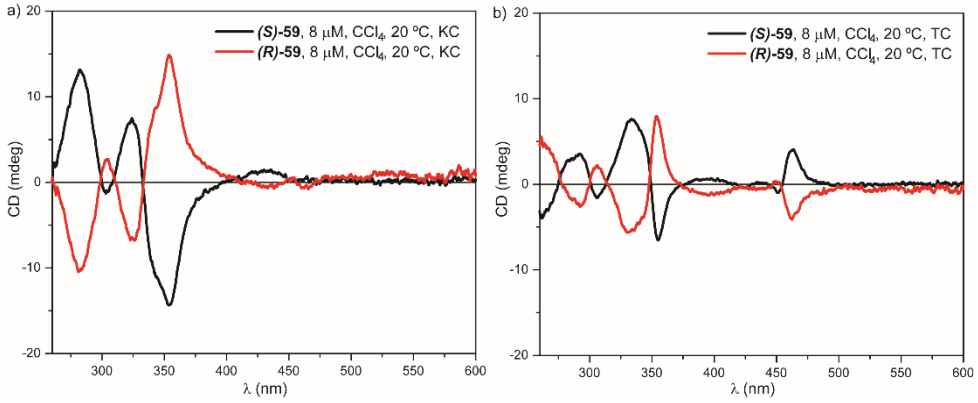

Figure 73. CD spectra of **(*S*)-59** (black line) and **(*R*)-59** (red line) of the freshly prepared solutions (a) and after a time evolution of 24 h (b) in CCl_4 (c_T = 8 μM, 20 ºC).

AFM has been utilized to closer inspect the morphology of both the kinetic and the thermodynamic aggregates in CCl_4. The freshly prepared 8 μM solution of **58** (presenting the H-type UV-Vis pattern) has been spin coated (2000 rpm) onto mica, furnishing disc-like micelles of 10 nm height and 200 nm width. This solution has been kept at room temperature during 24 hours to induce the transition to the thermodynamically favoured J-type aggregate. After that, a drop of this solution has also been spin coated onto mica, rendering rope-like fibrils that eventually bundle to form thicker aggregates. Considering that the diameter of the CBT central moiety is 0.9 nm,[117,119] and that the height of the single rope-like fibres is of 2 nm, the thermodynamic aggregates would be tilted regarding the plane of the mica surface in good correlation with the formation of slipped face-to-face J-type supramolecular structures (Figure 74).

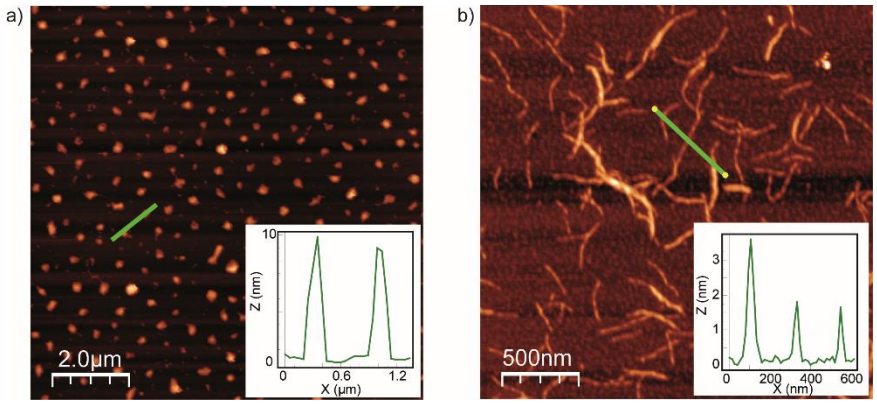

Figure 74. Height AFM images of the two competing aggregates of compound **58** in CCl_4. Left image shows the disk-like micelles observed for the H-type aggregates. Right images show the rope-like supramolecular structures observed for the J-type aggregates (c_T = 8 μM, mica as surface, z scale = 6.5 nm). The insets display the height profile along the green line in both images.

The synergy of spectroscopic evidences and AFM images reveal tunable energy landscapes in which the solvent plays a vital role. Thus, in MCH/Tol mixtures, the inactivated monomer *M** slows down the formation of the thermodynamically favoured J-aggregate but, however, is not able to drive the generation of the metastable H-aggregate. On the other hand, in a different media like CCl_4, the kinetically-trapped monomer leads to the formation of metastable H-aggregates that evolve with time to the more stable J-aggregates (Figure 75). The control over the metastable species can permit the fulfilment of seeded and living supramolecular

polymerizations.[56,61,66,68] These experiments require a complete understanding of the kinetic effects involved in the self-assembly of **58**.

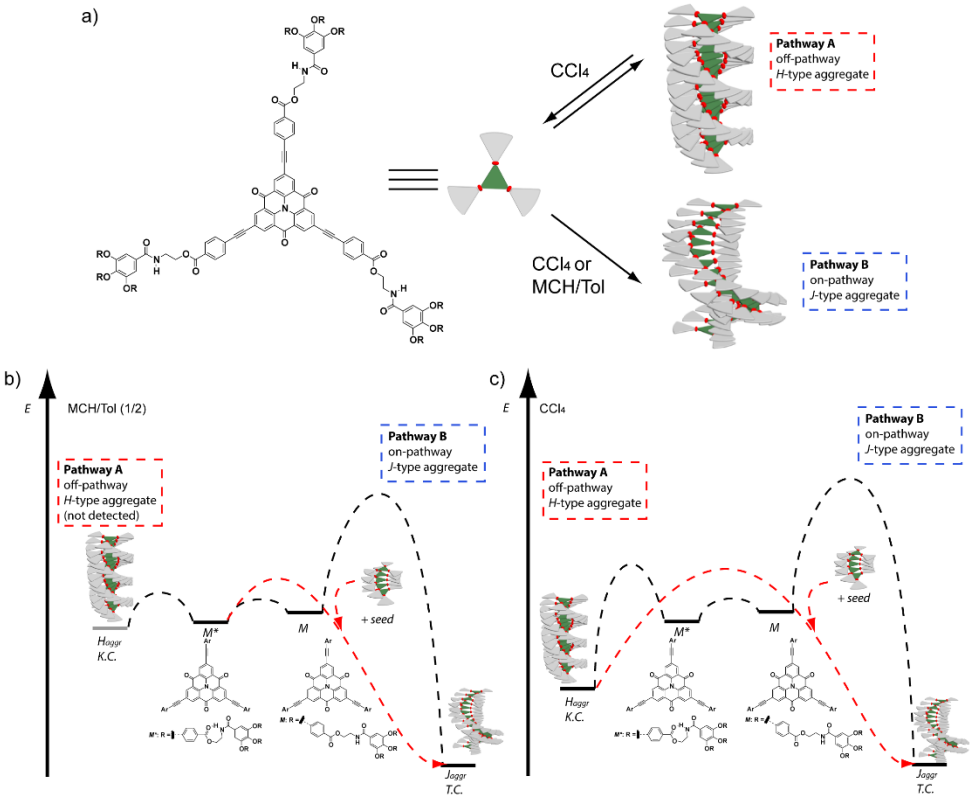

Figure 75. a) The investigated *N*-heterotriangulenes form thermodynamically favoured J-aggregates in MCH/Tol mixtures and CCl_4 (Pathway B). Notably, in CCl_4 this aggregation pattern is preceded by the generation of a metastable H-aggregate (Pathway A). Energy landscapes of the supramolecular polymerization coupled with a competing kinetic trap in b) a MCH/Tol (1/2) mixture and c) CCl_4. In MCH/Tol (1/2), the pathway complexity could not be detected, probably because the kinetic trap is too shallow in energy and only the J-type supramolecular polymer is spectroscopically detected (Pathway B). In pure CCl_4, the energy level of the kinetic trap should be lower, making possible the detection of both the metastable H-type aggregates (Pathway A) and the J-type aggregates (Pathway B). In both solvents, the addition of J-type seeds should accelerate the conversion.

4.4.4. Kinetic implications in the self-assembly of N-heterotriangulenes 58, (S)-59 and (R)-59

To gain insight in the kinetics of the self-assembly of **58** and **59**, a set of experiments has been realized in MCH/Tol and CCl_4 to evaluate the effect of concentration and temperature on the transition from the different metastable species to the thermodynamically favoured J-aggregate. Additionally, it is important to clarify what kind of metastable aggregate is the H-type aggregate (on- or off-pathway intermediate) present in CCl_4.

All the kinetic studies have been performed by a rapid heating (20 ºC min^{-1}) of the sample until the supramolecular polymer is disassembled, followed by a rapid cooling to the corresponding temperature. To equilibrate the solution, the time-dependent experiment is launched one minute after reaching this temperature.

The kinetics of **58** in the MCH/Tol mixtures has been studied in a 1/2 ratio and at $c_T = 4$ μM. These conditions have been found to be the optimal for the kinetic studies allowing the complete assembly and disassembly and being noticeable a hysteresis cycle. The transition curve from *M** to the J-aggregate exhibits a sigmoidal shape with a low lag phase which has been ascribed to an autocatalytic processes.[141,142] The shift from *M** to the J-aggregate is very rapid in these diluted conditions even at relatively high temperatures (37 and 39 ºC). Rising the temperature to 45 ºC slows down the process thus stabilizing the inactivated monomer, what can enable to perform seeded experiments in these conditions (Figure 76a). Additionally, increasing concentration unveils quicker transitions (Figure 76b). These trends are in agreement with previously reported inactivated monomers in the self-assembly of PBIs derivatives.[64] Singularly, in none of these experiments have been detected the H-aggregates which have been revealed in the CCl_4 solutions. Probably, in these conditions, the energy level of the inactivated monomer and the H-aggregate is very similar or the activation energy barrier is very low, therefore avoiding the formation of the metastable aggregates. Finally, it should be pointed out that agitation does not have any effect on the kinetic transition, which differs from other results obtained for referable systems.[56, 64]

[141] E. T. Powers, D. L. Powers, *Biophys. J.* **2006**, *91*, 122.
[142] E. T. Powers, D. L. Powers, *Biophys. J.* **2008**, *94*, 379.

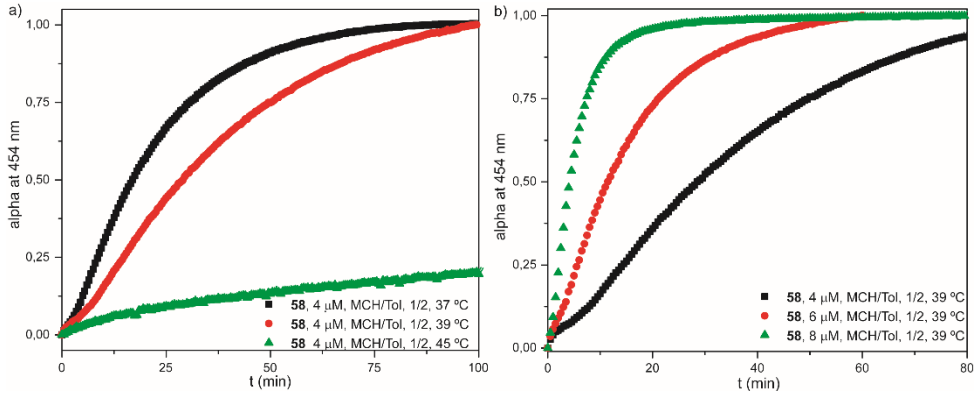

Figure 76. Time course evolution of the monomeric species of **58** into the thermodynamically-controlled J-aggregates in MCH/Tol 1/2 at different a) temperature and b) concentration (λ = 454 nm).

For the CCl_4 solutions of **58**, the presence of a competing aggregate can lead to two different scenarios, *i.e.*, sequential or parallel pathways. Thus, in a sequential pathway, the formation of a metastable conformationally disordered aggregate (on-pathway intermediate) can further reorganize or rearrange to afford the thermodynamic aggregate.[143] On the other hand, the parallel pathway is distinguished by the presence of a metastable aggregate (off-pathway intermediate) which can compete for the monomer with the more stable aggregate (on-pathway product) requiring the transition from one aggregate to the other through disassembly and further reassembly (Figure 77).

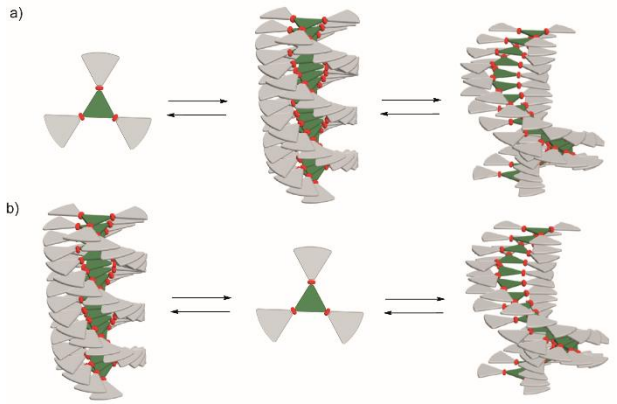

Figure 77. Schematic illustration of a (a) sequential and (b) parallel pathway.

[143] J. Baram, H. Weissman, B. Rybtchinski, *J. Phys. Chem. B* **2014**, *118*, 12068.

To check which the case is for **58** and its chiral counterparts in CCl_4, a set of experiments has also been carried out in this solvent by changing the concentration and the temperature. In analogy to the MCH/Tol mixture results, the transition from the H-aggregate to the J-aggregate also possesses a sigmoidal shape ascribable to an autocatalytic process. On the other hand, in a dissimilar way that in the MCH/Tol mixtures, increasing the temperature clearly speeds up the transition from the metastable H-aggregate to the energetically favoured J-aggregate. Unfortunately, the low boiling point of CCl_4 impedes to perform a detailed study of the influence of the concentration on the kinetics. Consequently, only a narrow range of concentrations could be utilized (5-15 μM) in which complete disassembly is achieved upon heating the sample at 70 °C. In this range of concentrations, the complete evolution of the metastable aggregate shows a weak dependence with concentration, revealing a slight quicker transition for lower concentrations. These results are also opposite to those acquired in MCH/Tol and, together with the temperature dependant experiments, can be justified by the existence of an off-pathway intermediate typical of parallel pathways in complex supramolecular processes.[52,56,66] This hypothesis is also confirmed by VT-UV-Vis experiments, in which the presence of the monomer is unveiled at intermediate temperatures (Figure 78a and 78b). Thus, increasing the temperature or decreasing the concentration facilitates that the H-aggregates, acting as a monomeric reservoir, overcome the activation energy barrier, thus depolymerizing and yielding the monomeric species. These monomeric species finally form the thermodynamically-favoured J-type aggregates.

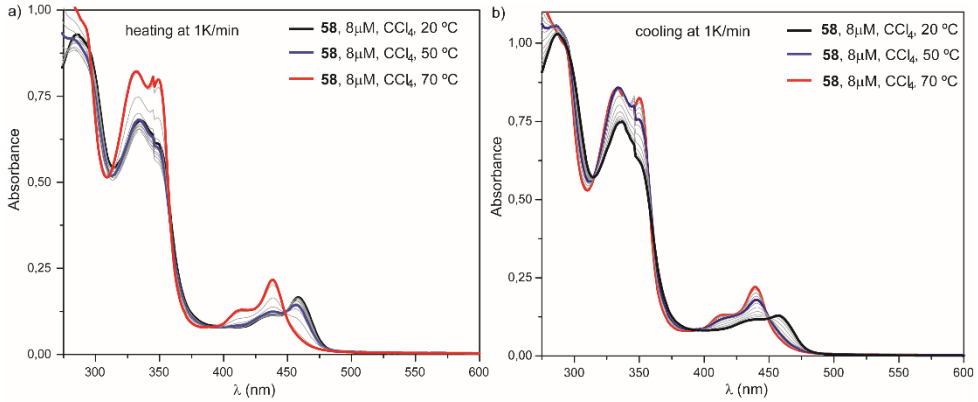

Figure 78. VT-UV-Vis spectra of **58** in CCl_4 by (a) heating or (b) cooling an 8 μM solution at 1 K min^{-1}. The black, blue and red spectra correspond to 20, 50 and 70 °C, respectively.

Interestingly, the presence of chiral side chains exerts a strong retardation on the kinetics of the conversion between the H- and J-aggregate. The kinetic profile of a solution of **(*S*)-59** in CCl_4, at c_T = 8 μM and 30 °C is markedly slower than that observed for **58** at the same experimental conditions. Nevertheless, and similarly to **58**, increasing the temperature results in the acceleration of the autocatalytic transformation between the kinetically and thermodynamically controlled aggregates. A likely explanation for the observed differences in the kinetics of the achiral and chiral CBTs could be the steric demand exerted by the more branched side chains in the chiral *N*-heterotriangulenes. The more difficult accommodation of these branched side chains in both the H- and J-aggregates for the chiral compounds could induce a delay in the conversion (Figure 79a and b).

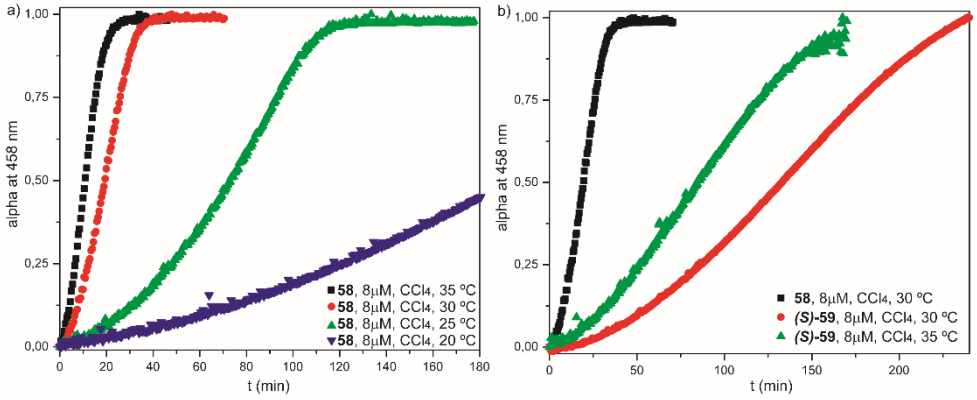

Figure 79. Time course transformation of the off-pathway H-aggregates of (a) **58** and (b) **(*S*)-59** in the J-aggregates at different temperatures (λ = 458 nm).

4.4.5. Seeded and living supramolecular polymerizations of N-hetero-triangulenes 58, (S)-59 and (R)-59

The detailed comprehension of the solvent-dependant energy landscape and kinetic evolution of the different metastable species in the self-assembly of **58**, **(*S*)-59** and **(*R*)-59** has paved the way to perform seeded and living supramolecular polymerizations experiments. In the case of the MCH/Tol mixtures, the addition of the seed to the monomeric stock solution can accelerate the formation of the J-aggregates. In CCl_4, this transition takes place from the H-aggregate reservoir solution and could be applied in several cycles in analogy to referable off-pathway intermediates.

The evolution of the self-assembly of the MCH/Tol 1/2 mixture has been primarily assessed. The seeding approach requires the preparation of short and active supramolecular polymers so-called seeds which act as reactive centres provoking the rapid growth of the polymer. The critical step is, hence, the optimization of these seeds. Thus, a stock solution of **58** in MCH/Tol at c_T = 4 μM has been sonicated during 10 minutes and the UV-Vis spectrum has been checked, exposing the J-aggregate pattern of the thermodynamically-favoured entity (Figure 80a). Therefore, the seeds maintain the spectroscopic features of the aggregate.

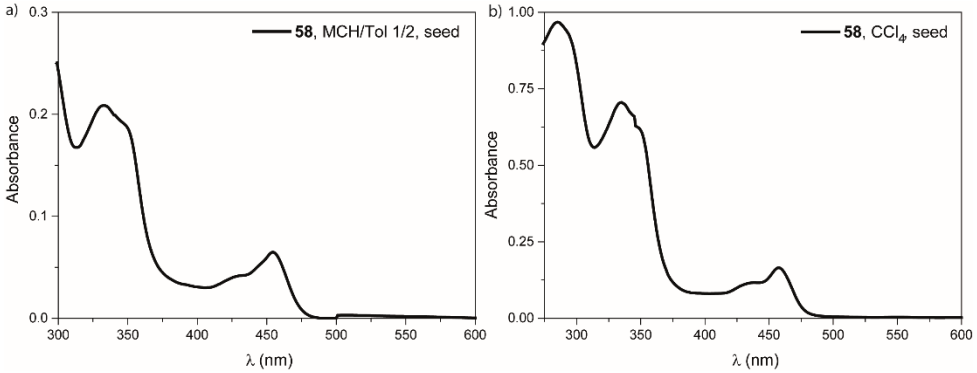

Figure 80. UV-Vis spectra of the seed of **58** (a) in MCH/Tol 1/2 (c_T = 4 μM, 20 ºC) and (b) in CCl_4 (c_T = 8 μM, 20 ºC).

To generate the monomeric reservoir, the stock solution has been heated to 90 ºC and subsequently cooled down to 45 ºC, conditions in which the inactivated monomer is the predominant species as demonstrated in the previous section, thus avoiding the spontaneous supramolecular polymerization. The addition of the seeds to the monomer reservoir triggers the supramolecular polymerization even at ratios monomer/seed as low as 700:1. Another proof of the capability of the seed to speed up the formation of the supramolecular polymer is unveiled after incrementing the amount of seed added. As depicted in Figure 81, the addition of higher amounts of seed (400:1 and 100:1) clearly accelerates the conversion from the inactivated monomer to the J-type aggregate.

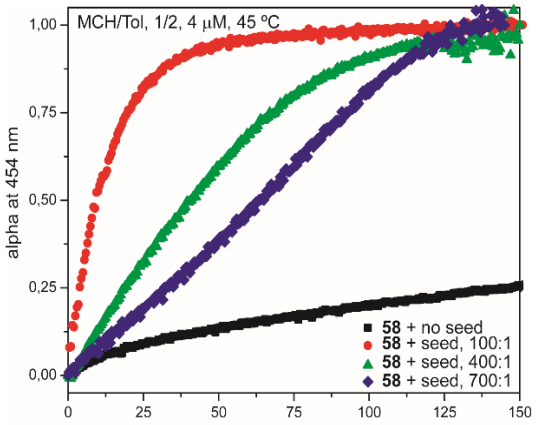

Figure 81. Kinetic profiles of the seeded supramolecular polymerization of **58** by adding different amounts of J-aggregate seeds in MCH/Tol 1/2 (c_T = 4 μM, 45 °C, λ = 454 nm).

In the CCl_4 solutions, the addition of J-aggregate seeds also enables the performance of seeded supramolecular polymerizations. In this case, the off-pathway H-aggregate acts as monomer reservoir. After different experiments, it has been found out that the better conditions to obtain the H-aggregate consists in utilizing an 8 μM solution which is kept at 25 ºC after heating at 70 ºC. To obtain the corresponding J-aggregate seed, an aliquot of an 8 μM CCl_4 solution of **58** has been sonicated during 15 minutes, maintaining the same spectroscopic features that the J-aggregate (Figure 80b). In analogy to the previous case, the addition of the seeds clearly accelerates the conversion from the H- to the J-aggregate, despite the fact that higher ratios are required when compared to the MCH/Tol mixture (Figure 82).

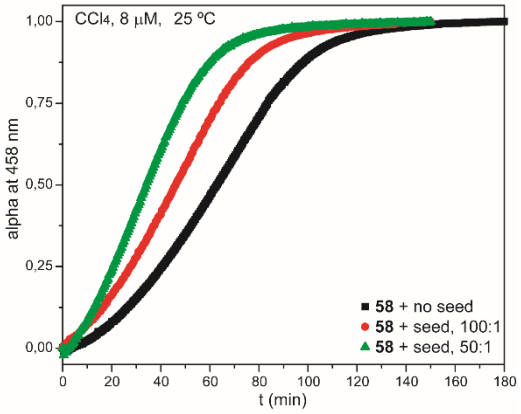

Figure 82. Kinetic profiles of the seeded supramolecular polymerization of **58** by adding different amounts of J-aggregate seeds in CCl_4 (c_T = 8 μM, 25 °C, λ=458 nm).

The influence of the sonication time for the seed generation on the kinetics of the conversion has also been studied in these conditions. As depicted in Figure 83, sonication during less (5 min) or more time (30 min) in 100:1 monomer/seed ratio affords less active seeds which do not accelerate the conversion from the H- to J-aggregate as effectively as the one generated upon sonication during 15 minutes.

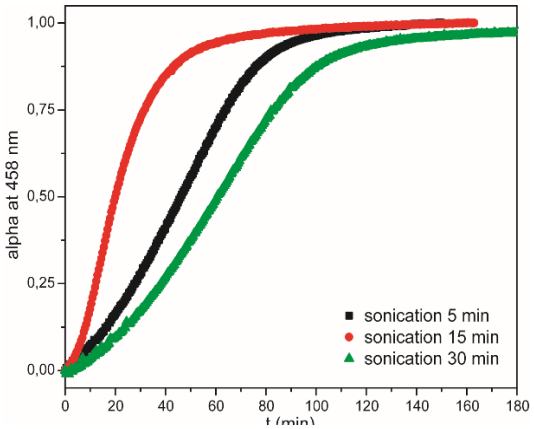

Figure 83. Time course evolution of the off-pathway H-type aggregates of **58** into the J-type aggregates by adding seeds in a 100:1 ratio obtained after different sonication times (CCl_4, c_T = 8 μM, 25 ºC, λ = 458 nm).

The seeded approach has also been applied to investigate the kinetic evolution of chiral **(*S*)-59**. As discussed in the previous section, the branched alkyl chains exert a restraint in the transition from the H- to the J-aggregate. The addition of the J-type seed to an H-aggregate reservoir of **(*S*)-59** in a 100:1 ratio (c_T = 8 μM, 30 ºC) results in a sigmoidal profile with nearly no changes when compared to the transition in the solution of pristine **(*S*)-59**. Only by using ratios of 10:1, the transition is speeded up considerably (Figure 84). These findings corroborate the differences imposed by the chiral side chains on the kinetics of the pathway complexity. The off-pathway formation of the H-type aggregates provokes a retardation of the spontaneous nucleation of the monomeric species, being the lag time longer for the chiral CBT congeners.

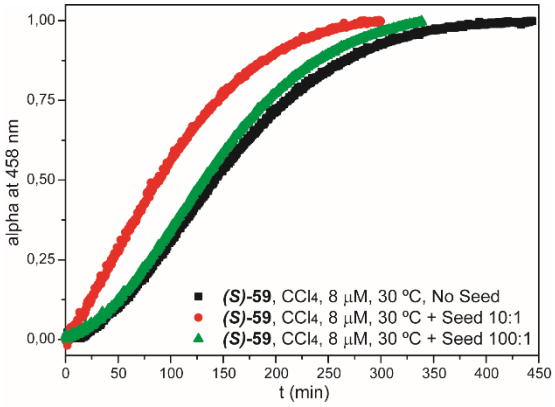

Figure 84. Kinetic profiles of the seeded supramolecular polymerization of **(*S*)-59** by adding different amounts of J-aggregate seeds (CCl_4, c_T= 8 μM, 30 ºC, λ = 458 nm).

The control over pathway complexity in the supramolecular polymerization of the CBTs **58**, **(*S*)-59** and **(*R*)-59** can be used to perform a multicycle seeded approach in a living way.[56,61,65] In this case, a solution of active J-type seeds is subjected to successive additions of H-aggregate solutions. To experimentally develop the living supramolecular polymerization of achiral **58** and chiral **(*S*)-59**, the methodology described by Takeuchi and co-workers has been followed,[56] evaluating the kinetic evolution of the transformation of the thermodynamically-favoured aggregate, in different cycles, upon successive additions of the off-pathway aggregates as depicted schematically in Figure 85.

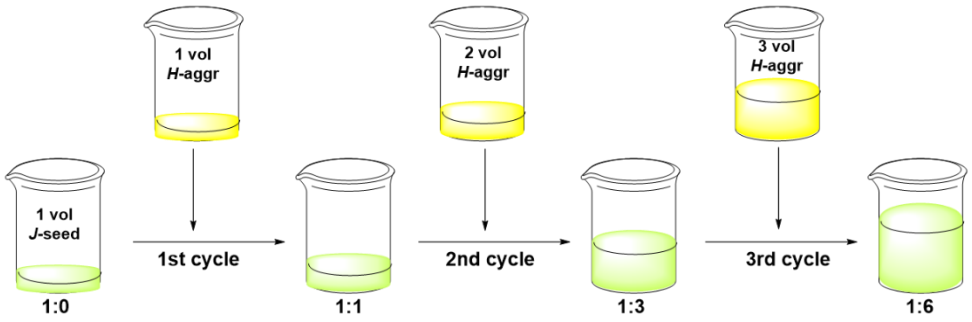

Figure 85. Schematic illustration of the living supramolecular polymerization experienced by CBTs **58** or **(*S*)-59**. The sonication of a solution of the J-aggregate for 15 min generates the active seeds. Successive aliquots with increasing volume of the off-pathway H-aggregate are added to this solution and the kinetic profile at λ = 458 nm (characteristic of the J-aggregate) is monitored. Experimental conditions: c_T = 8 μM for both the H- and J-aggregates; T = 25 ºC for **58** and T = 30 ºC for **(*S*)-59**.

In the first cycle, a solution of the H-aggregate at c_T = 8 μM has been added to the same amount of a seed of the J-aggregate solution at 25 ºC and the kinetic profile has been measured at λ = 458 nm. The supramolecular polymerization is finished after 30 and 60 min for **58** and **(*S*)-59**, respectively, laying bare again in the importance of the branched alkyl chain in the supramolecular polymerization process. Each addition of the H-aggregate solution reduces by half the speed of the process in analogy to the previous reported living supramolecular polymerizations,[56,66] as the seed/monomer ratio increases (Figure 86).

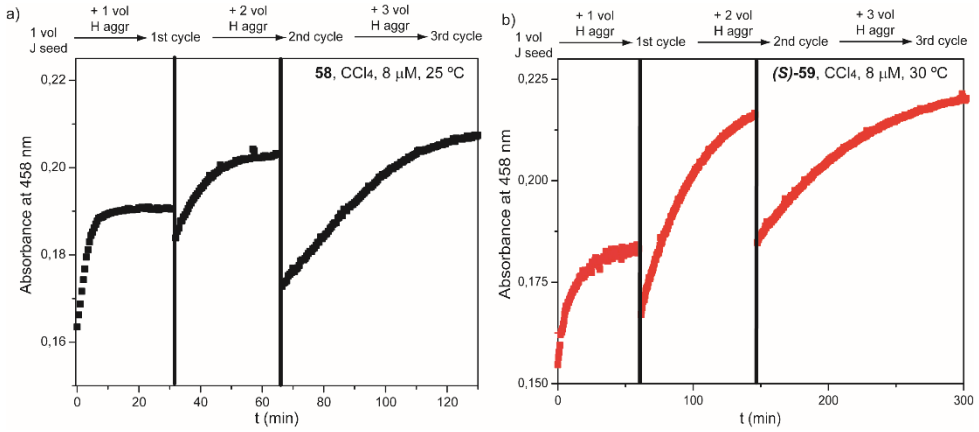

Figure 86. Time course of the change in absorption at λ = 458 nm while the J-aggregate seeds have been diluted with the off-pathway H-aggregates, showing repeated polymerization after each addition of off-pathway H-aggregate with increasingly slower rates.

The results presented in this part pinpoint the effect of the solvent in the stability of the different metastable entities in the supramolecular polymerization of *N*-heterotriangulenes **58**, **(*S*)-59** and **(*R*)-59** and confirm the strategy of the intramolecular H-bonding as a proper tool to generate kinetically-controlled supramolecular polymerizations. Notably, the change in the position of the amide respect to the aromatic core respect to the CBTs of Section 3 allows to obtain J-aggregates in this case. Furthermore, the evaluation of the concentration and the temperature effects enables the complete understanding of the kinetics of the process and the nature of the metastable entities present in each media, thus permitting the performance of seeded and living supramolecular polymerizations.

Finally, the presence of chiral chains in **(*S*)-59** has been demonstrated to slow down the transformation from the kinetic structures to the thermodynamic one, which can be attributed to the higher order required to accommodate in the nucleus its branched alkyl chains.

4.4.6. Out-of-equilibrium transfer and amplification of chirality

As it has been mentioned in Section 1, the transfer of chiral information from stereogenic centres or other sources of asymmetry to the supramolecular level, and the subsequent amplification of chirality experienced by the resulting entities, have been widely investigated in the field of supramolecular polymerization. Helical supramolecular polymers like those formed by BTAs, OPE-TAs or OPVs have been subjected to intensive studies regarding the amplification of chirality phenomena, especially by *SaS* and *MR* experiments.[144] The non-linear response in the expressed helicity of these supramolecular polymers when minute amounts of a chiral species are added is a remarkable process which has been linked to the origin of homochirality in Nature.[145] Despite the ubiquity of non-equilibrium processes in natural systems, the transfer and amplification of chirality have been barely tested in synthetic supramolecular polymers under kinetic conditions[146,147] or in the presence of metastable aggregates.[148]

Thus, the chiral centres in the peripheral chains of *N*-heterotriangulenes **(*S*)-59** and **(*R*)-59**, as well as their ability to generate kinetically-trapped monomers *M** and metastable aggregates as it has been tested in the previous section, has paved the way to investigate the chiroptical features of pristine solutions of these compounds and also their co-assembly characteristics by means of *MR* experiments. The tuning of temperature and time could disclose novel phenomena concerning kinetically-controlled amplification of chirality in dynamic systems. Importantly, the copolymerization of **(*S*)-59** or **(*R*)-59** with compound **58** in *SaS* experiments could yield interesting scenarios due to the retardation in the supramolecular polymerization of the chiral analogous in comparison with the achiral one (Figure 87).

---

[144] A. R. A. Palmans, E. W. Meijer, *Angew. Chem. Int. Ed.* **2007**, *46*, 8948.
[145] M. Liu, L. Zhang, T. Wang, *Chem. Rev.* **2015**, *115*, 7304.
[146] A. Lohr, M. Lysetska, F. Würthner, *Angew. Chem. Int. Ed.* **2005**, *44*, 5071.
[147] A. Lohr, F. Würthner, *Angew. Chem. Int. Ed.* **2008**, *47*, 1232.
[148] P. A. Korevaar, C. Grenier, A. J. Markvoort, A. P. H. J. Schenning, T. F. A. de Greef, E. W. Meijer, *Proc. Natl. Acad. Sci. U.S.A.* **2013**, *110*, 17205.

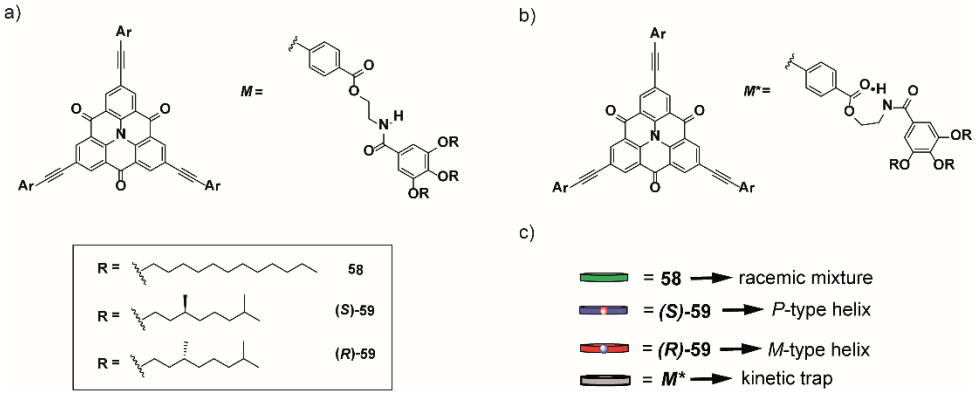

Figure 87. (a) Chemical structures of the extended monomer CBTs **58**, **(*S*)-59** and **(*R*)-59**. (b) Schematic representation of the metastable monomer *M** acting as kinetic trap and (c) of all the species involved in the chiral amplification studies.

4.4.7. Co-assembly of N-heterotriangulenes (S)-59 and (R)-59: Majority Rules experiments

The initial experiments to investigate the effect of the kinetic traps into the helical outcome of the self-assembling CBTs **58**, **(*S*)-59** and **(*R*)-59** have implied the measurement of the CD spectra of chiral ***(S)*-59** and ***(R)*-59** at a total concentration of 8 μM in a MCH/Tol mixture (2/1). In these conditions, as it has been unveiled in by UV-Vis spectroscopy, a hysteresis cycle, due to the formation of a metastable 7-membered pseudocycle by the establishment of an intramolecular H-bond, is present at temperatures ranging from 75 to 85 ºC. It should be pointed out that lower concentrations and higher volumes of toluene cause a drastic reduction of the dichroic signal and do not permit an accurate measurement of the amplification of chirality experiments.

Hence, ***(S)*-59** exhibits a weak dichroic Cotton effect with maxima at λ = 464, 346 and 309 nm (Figure 88, dashed lines). The positive sign Cotton effect is symptomatic of the formation of *P*-type helices. After heating the sample at 90 ºC to provoke disassembly and applying a quick cooling rate (20 K min^{-1}) until 20 ºC for further reassembly, the dichroic response experiences an initial rise (Figure 88, dotted lines) that is further incremented after keeping the solution at room temperature for 24 hours (Figure 88, solid lines). Mirror-image CD spectra are observed for ***(R)*-59** at the same conditions, involving the formation of *M*-type helices and thus demonstrating that the supramolecular polymerization of **(*S*)-59**

and **(*R*)-59** proceeds in a kinetically controlled way. Notably, these spectroscopic features are very similar to the CD signatures of the thermodynamically-favoured aggregates obtained in CCl_4 (see Figure 73b) except for the band centred at $\lambda = 346$ nm, which is inverted in sign by changing the solvent.

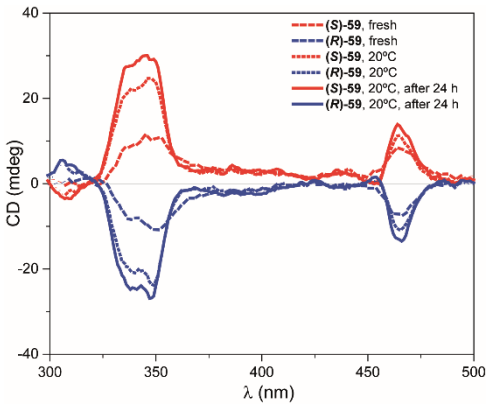

Figure 88. CD spectra of CBTs ***(S)*-59** (red traces) and ***(R)*-59** (blue traces) in MCH/Tol (2/1) as solvent (c_T = 8 μM). The dashed lines correspond to the freshly prepared solutions. The dotted lines represent the solution heated to 90 ºC and quickly cooled down (20 K min^{-1}) at 20 ºC. The solid lines belong to the solution aged for 24 h at 20 ºC.

After confirming the influence of the kinetic traps on the CD intensity of pure chiral CBTs ***(S)*-59** and ***(R)*-59**, chiral amplification experiments have been carried out to elucidate the influence of metastable monomers on the formation of homochiral aggregates from species with opposite chirality. Thus, *MR* experiments have been performed by mixing unequal percentages of both chiral ***(S)*-59** and ***(R)*-59** keeping constant a total concentration of 8 μM. Plotting the variation of the dichroic response upon increasing the enantiomeric excess (*ee*) of one of the two enantiomers ***(S)*-59** and ***(R)*-59** by direct mixing at room temperature discloses a linear tendency characteristic of a negligible chiral amplification (Figure 89a).[5] This trend is maintained after heating the mixtures at 90 ºC and cooling to 20 ºC at 20 K min^{-1} (Figure 90a and Figure 90b). The reduction of the dichroic signal can be due to the initial formation of the metastable monomers *M** of both ***(S)*-59** and ***(R)*-59** which decreases the effective concentration of the final chiral supramolecular polymers and, consequently, the dichroic response. The rupture of the intramolecular H-bonded pseudocycle, and the following incorporation of the monomer in the helical columnar aggregates by intermolecular H-bonding interactions between the amide functional groups, can cause an increase of the dichroic signal and the ability of

these species to amplify the chirality in the *MR* experiments (Figure 89b and Figure 90c). Another plausible explanation can be that the initial metastable monomers either are trapped in helices of opposite chirality or generate helices of opposite chirality that rearrange with time thus forming the supramolecular polymer with a preferred helicity dictated by the extended main chiral enantiomer.

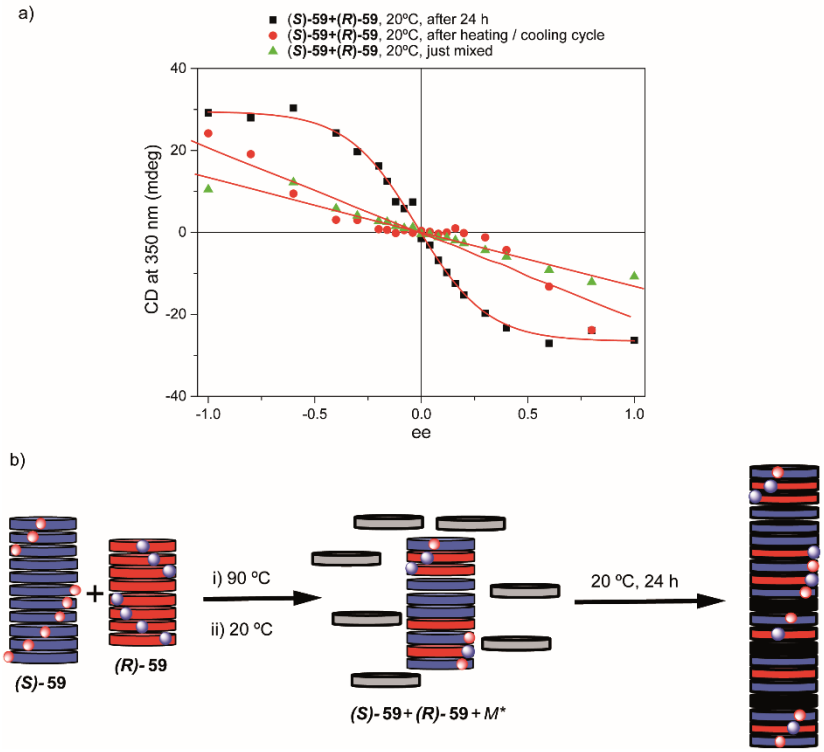

Figure 89. (a) Changes in CD intensity (λ = 350 nm) as a function of *ee* upon adding ***(S)*-59** to ***(R)*-59** (MCH/Tol 2/1; c_T = 8 μM, 20 ºC). *ee* = 1.0 corresponds to pure ***(S)*-59** and *ee* = -1.0 corresponds to pure ***(R)*-59**. The red lines depict the linear or sigmoidal fitting of the data to guide the eye. (b) Schematic illustration of the helical outcome obtained for the *MR* experiments.

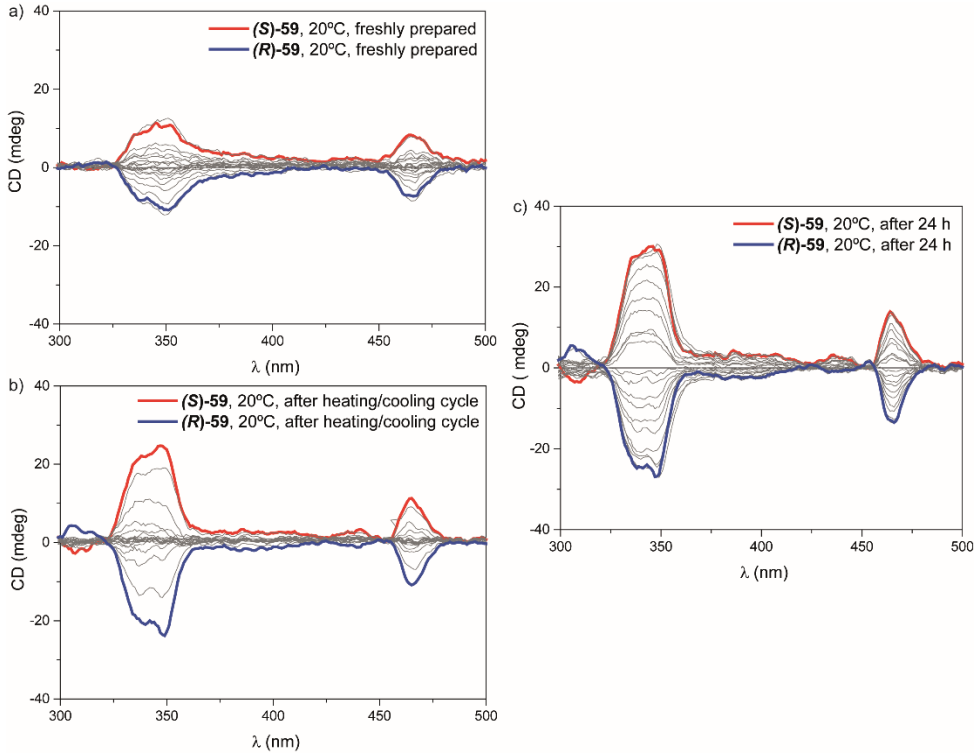

Figure 90. CD spectra obtained for the *MR* experiments performed by mixing unequal amounts of enantiomers ***(S)*-59** (red trace) and ***(R)*-59** (blue trace) keeping c_T = 8 µM in a MCH/Tol (2/1) mixture. Panel (a) corresponds to the experiments carried out by direct mixing of freshly prepared solutions at 20 ºC; panel (b) depicts the experiment developed by heating the mixtures to 90 ºC and quickly cooling down (20 K min^{-1}) to 20 ºC; panel (c) shows the CD spectra of the mixtures aged for 24 h at 20 ºC.

4.4.8. Co-assembly of N-heterotriangulenes (S)-59 and (R)-59 with 58: Sergeants and Soldiers experiments.

The co-assembly of structurally related self-assembling species is a prominent technique to achieve complex functionalities in supramolecular entities non-attainable in discrete supramolecular polymers.[149] In order to analyse the co-assembly of *N*-heterotriangulenes, the influence of kinetic traps in the supramolecular copolymerization of chiral CBTs ***(S)*-59** and ***(R)*-59** with achiral **58**

[149] B. Adelizzi, A. Aloi, A. J. Markvoort, H. M. M. Ten Eikelder, I. K. Voets, A. R. A. Palmans, E. W. Meijer, *J. Am. Chem. Soc.* **2018**, *140*, 7168.

on the resulting helical outcome has been studied. Similarly to the *MR* experiments, the direct mixture of unequal amounts of 8 μM solutions of chiral ***(S)*-59** or ***(R)*-59** and achiral **58** in MCH/Tol (2/1) mixtures maintaining constant c_T discloses a linear variation of the dichroic response with increasing *ee*, diagnostic of an insignificant chiral amplification (Figure 91, Figure 92a and Figure 92d). Unexpectedly, heating the mixtures with a lower percentage of chiral sergeant (up to 20 %) and cooling it at 20 K min^{-1} results in an inverse dichroic signal to that observed for the pristine sergeant which is incremented with time (Figure 91 and Figures 92b, 92c, 92e and 92f). At percentages of around 30% of the chiral sergeant, the heating/cooling cycle cancels the dichroic response that rises non-linearly at higher percentages of the chiral sergeant thus demonstrating the chiral amplification phenomenon (Figure 91 and Figures 92b, c, e and f).

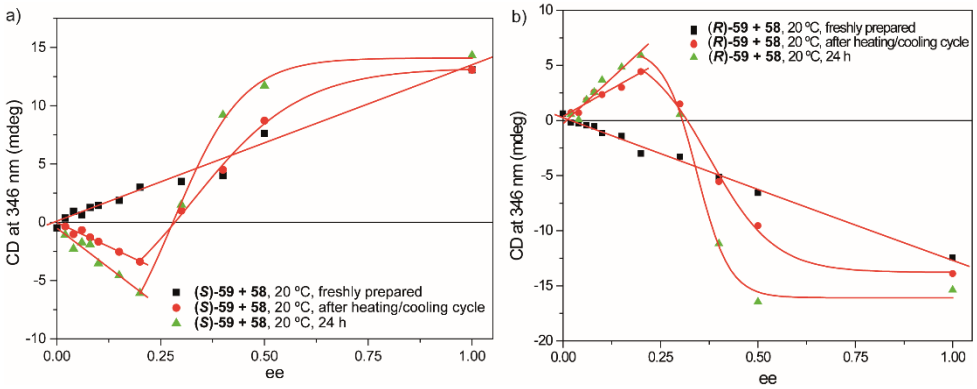

Figure 91. Changes in CD intensity as a function of *ee* upon adding **(*S*)-59** (a) or ***(R)*-59** (b) to **58** at 20 ºC. The red lines depict the linear or sigmoidal fitting of the data to guide the eye (c_T = 8 μM, λ = 346 nm).

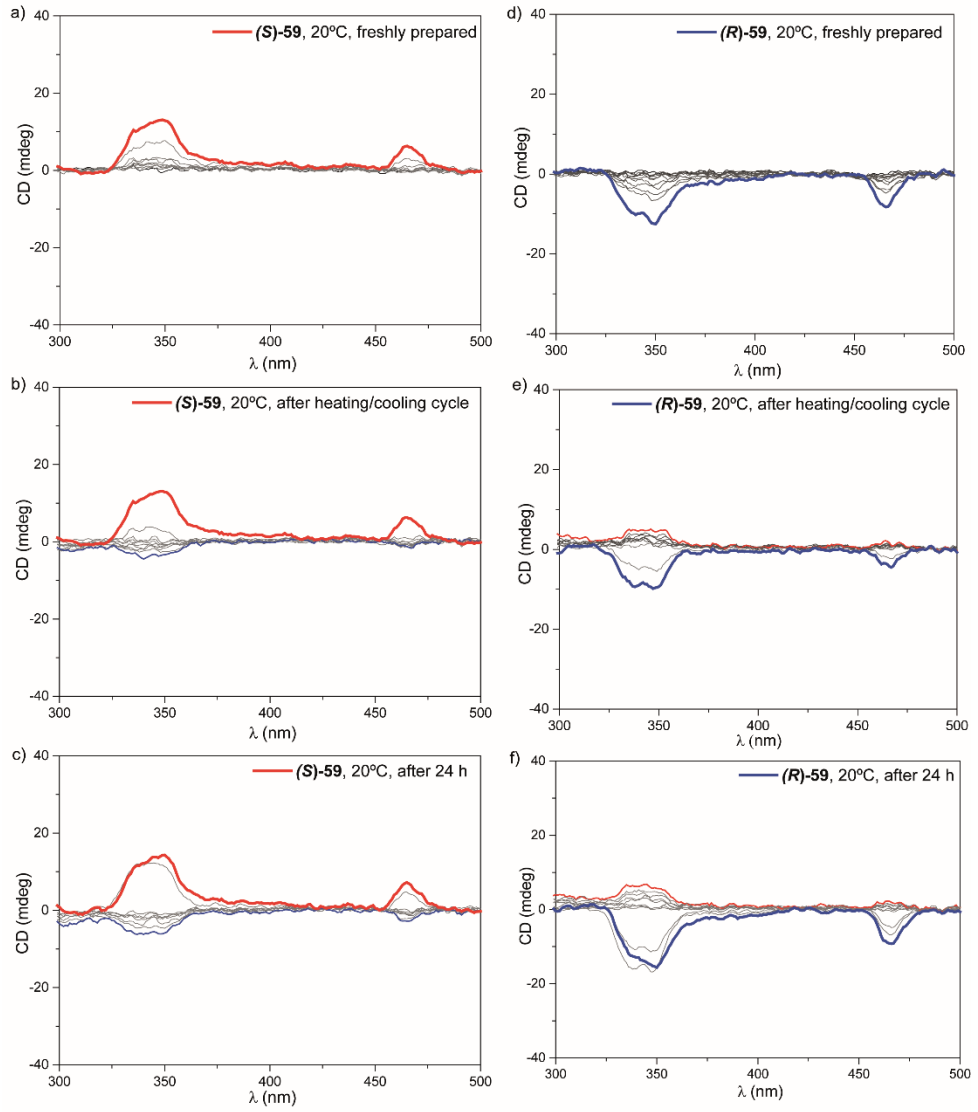

Figure 92. CD spectra obtained for the *SaS* experiments performed by mixing unequal amounts of enantiomers ***(S)*-59** (red trace) and **58** (a-c) and ***(R)*-59** (blue trace) and **58** (d-f) keeping c_T = 7 μM in a 2/1 mixture of MCH/Tol. Panels (a) and (d) correspond to the experiments performed by direct mixing of freshly prepared solutions; panels (b) and (e) depict the experiment developed by heating the mixtures to 90 ºC and cooling down (20 K min^{-1}) at 20 ºC; panels (c) and (f) shows the CD spectra of the mixtures aged for 48 h at 20 ºC.

This unforeseen stereomutation in *SaS* experiments has also been previously described by Prof. Ajayaghosh *et al.* for self-assembling OPVs.[150] However, these authors do not propose any feasible explanation for this intriguing phenomenon. Considering the tendency of self-assembling *N*-heterotriangulenes to experience pathway complexity, it can be conceived that the co-assembly of these CBTs generates off- and on-pathway aggregates of opposite chirality. To check these hypothesis in the *SaS* experiments, VT-UV-Vis mixture of pristine **58** and **(*S*)-59** as well as mixtures of both compounds at different percentages (20 and 50 %) has been registered. In all the cases, the monomeric pattern obtained at 90 ºC, with maxima at λ = 440, 356 and 330 nm, bathochromically shifts upon aggregation yielding a spectrum with maxima at λ = 460, 360 and 334 nm, ascribable to J-type aggregates (Figure 93).

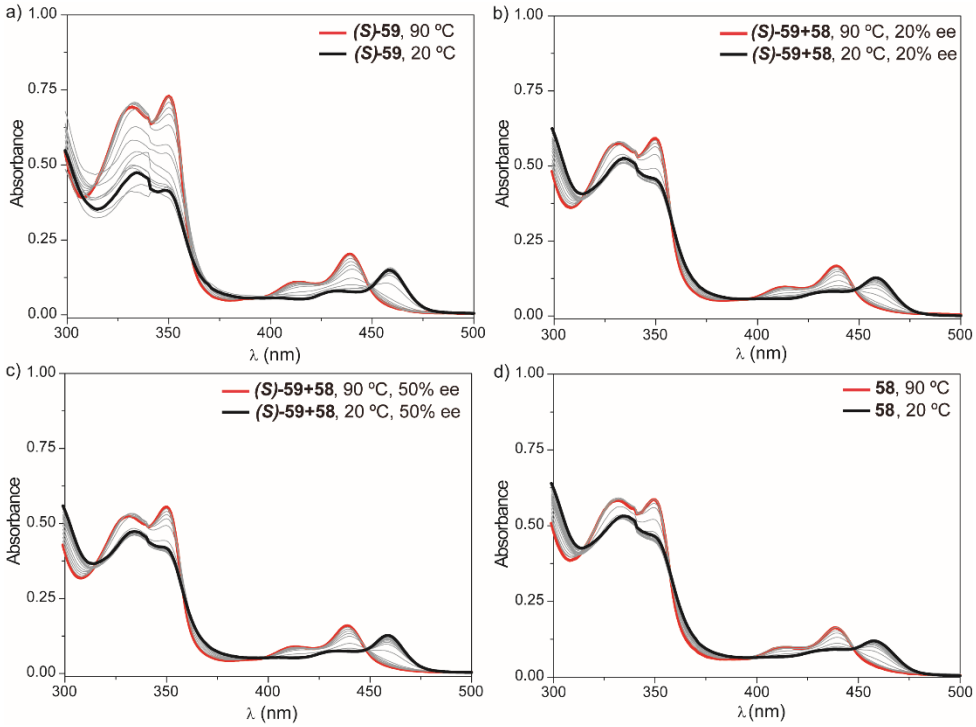

Figure 93. VT-UV-Vis spectra of (a) ***(S)*-59**, the mixture ***(S)*-59+58** with (b) 50% of *ee* and (c) 20% of *ee* and (d) **58** (MCH/Tol, 2/1; c_T = 7 µM, 1 K min^{-1})**.**

[150] A. Ajayaghosh, R. Varghese, S. J. George, C. Vijayakumar, *Angew. Chem. Int. Ed.* **2006**, *45*, 1141.

In accordance to the results obtained previously for the pristine solutions, the resulting cooling curves of these mixtures cannot be fitted with the EQ model, which is symptomatic of the existence of a kinetic process for all the samples. Importantly, the T_e lowers from 84 ºC to 73 ºC from pristine **58** to chiral **(*S*)-59** due to the higher order required to form the nucleus imposed by the chiral chain (Figure 94). The ***(S)*-59+58** mixture with 20% of *ee* and ***(S)*-59+58** with 50% of *ee* are in the half-way point of this trend. The higher stability of the kinetic trap in the chiral CBTs slows down the supramolecular polymerization.

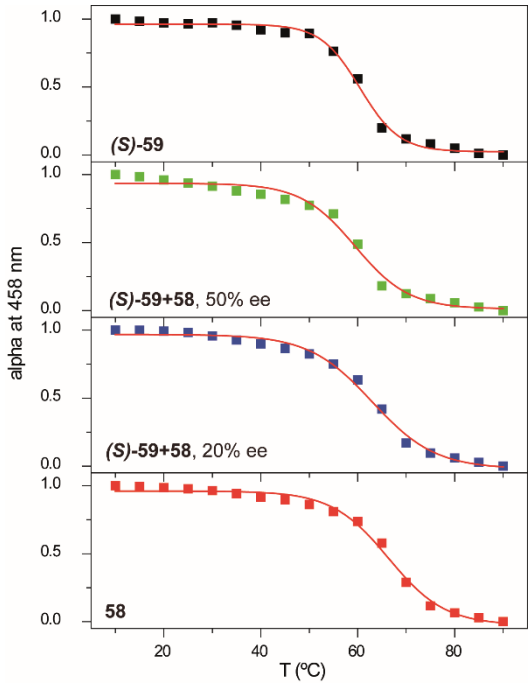

Figure 94. Cooling curves obtained from VT-UV-Vis experiments for pure CBTs ***(S)*-59** and **58** and for the mixtures ***(S)*-59+58** with *ee* of 20 and 50 % (MCH/Tol, 2/1, c_T = 7 µM, λ = 458 nm, 1 K min^{-1}).

The convergence of three different factors could explain the results obtained in the *SaS* experiments. First, the different stability of the different helical aggregates generated by the chiral and achiral species; second, the different collapse of the trapped monomer in **58** and in ***(S)*-59**/***(R)*-59**, which provokes different elongation temperatures for their corresponding polymers; and, finally, it should be considered that the *M* and *M** chiral species could afford different helical outcomes.

Thus, at around 80 ºC, the aggregates are depolymerized and, upon cooling, the kinetic traps of both the chiral and the achiral CBTs are the main species in the mixture. The chiral kinetic traps possess a large π-surface sufficient to generate initial nuclei whose helicity is inverse to that of the pure chiral CBTs. At low *ees*, the metastable chiral monomers are rapidly trapped by the achiral monomeric units expressing the initial helicity of the kinetic traps. On the other hand, at higher *ees*, even though these initial nuclei of reverse helicity are also formed, the lower number of achiral units enables the stereomutation to the more favored helical configuration that results in the chiral amplification of the whole mixture. To further corroborate this hypothesis, cooling and heating curves at 1 K min^{-1} in CD spectroscopy have been registered for the ***(R)*-59+58** mixtures with 20, 30 and 50 % of *ee*. For all the mixtures, a clear hysteresis assignable to a kinetically-controlled self-assembly process is evident (Figure 95).

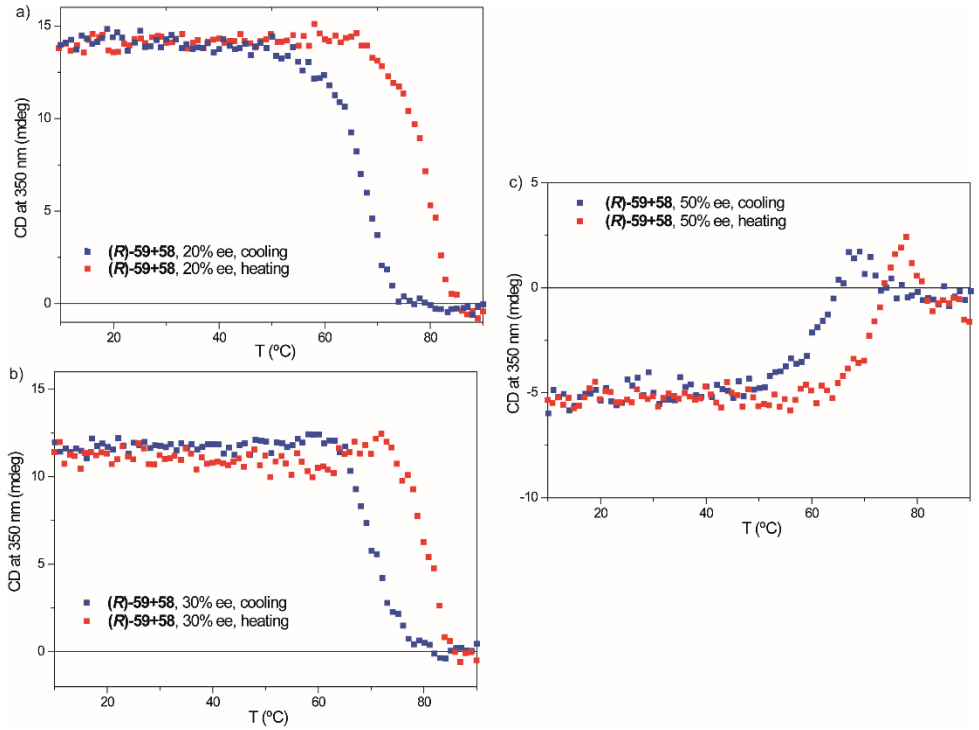

Figure 95. Cooling (blue squares) and heating (red squares) curves (1 K min^{-1}) of mixtures of ***(R)*-59+58** with *ee* = 20 % (a), *ee* = 30 % (b), and *ee* = 50 % (c) (MCH/Tol, 2/1, c_T = 7 μM, λ = 350 nm).

In the mixture of ***(R)*-59+58** at *ee* of 20%, the non-sigmoidal curve unveils the nucleation and elongation regimes. The former exhibits no CD response and the latter displays an increasing CD signal with decreasing temperatures which is opposite in sign to the CD signal of pure ***(R)*-59** (Figure 88 and 96a). At *ee* of 50 %, the cooling curve shows three regimes (Figure 96c). At very high temperatures (above 75 ºC), the absence of dichroic response due to the disassembly of the aggregates is observed. Interestingly, in the range from 75 to 65 ºC, the CD signal possesses a positive value. Between these two temperatures, the achiral monomers are already forming the columnar, racemic aggregates. However, the chiral units, which are mainly kinetically-trapped, could buffer the free achiral monomeric units to generate small aggregates of inverse helicity to that observed for the pure chiral CBT. Below 65 ºC, all the monomeric units that are not taking part of the small aggregates, interact by intermolecular H-bonds of the amide groups and the π-stacking of the aromatic moieties to yield homochiral aggregates.

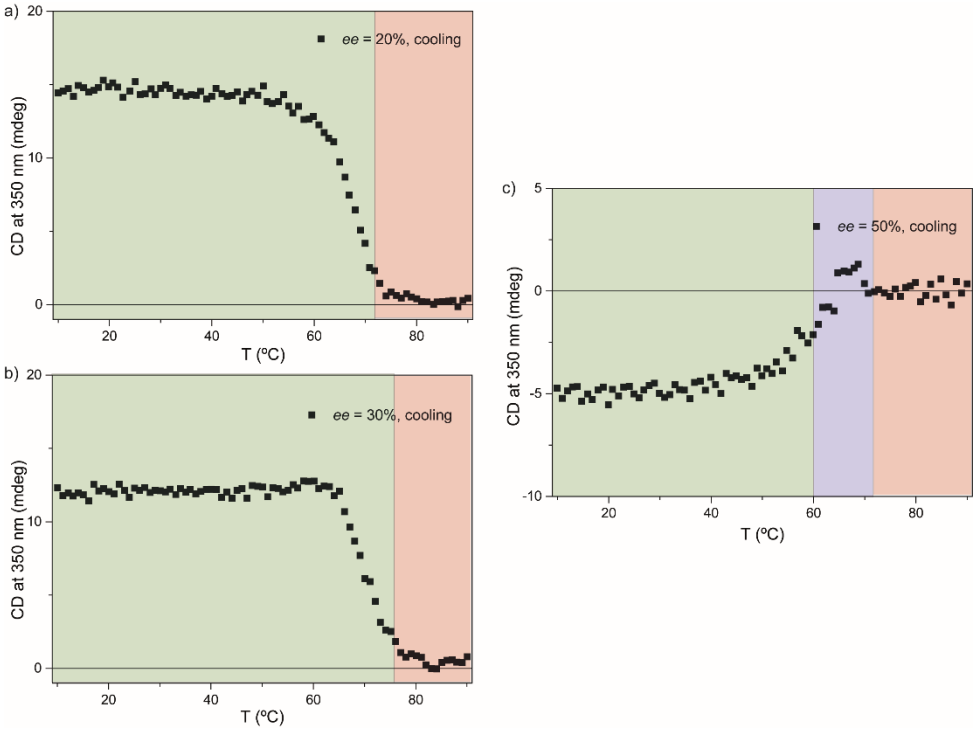

Figure 96. Cooling curves of mixtures of ***(R)*-59+58** at *ee* = 20 % (a), *ee* = 30 % (b), and *ee* = 50 % (c) (MCH/Tol, 2/1, c_T = 7 µM, λ = 350 nm). The green part of the curves depicts the elongation regime, the red part the nucleation regime and the blue part of (c) the regime in which the kinetic traps transfer their inherent chirality to the unbonded achiral monomers.

Very interestingly, the mixture of 30 % ***(R)*-59+58** at *ee* of 30% exhibits a strong dependence of the helical outcome on the cooling rate. This effect has been previously reported for *MR* experiments.[148] In this case, cooling this *SaS* mixture at 20 K min^{-1} results in a negligible dichroic response (Figure 91a). However, a sequential decrease of the cooling rate, results in a clear dichroic signal of contrary sign to that observed for the pure chiral CBT (Figure 96b). Applying a rapid cooling rate (20 K min^{-1}), the population of both the *M* and *M** species should be similar and, consequently, a racemic mixture of the two columnar J-aggregates of opposite handedness would form producing a null CD signal. At lower cooling rates (5 K min^{-1} and, especially, 1 K min^{-1}), the *M* ⇆ *M** equilibrium of the chiral molecules is shifted to the latter species, thus activating the stereomutation (Figure 97).

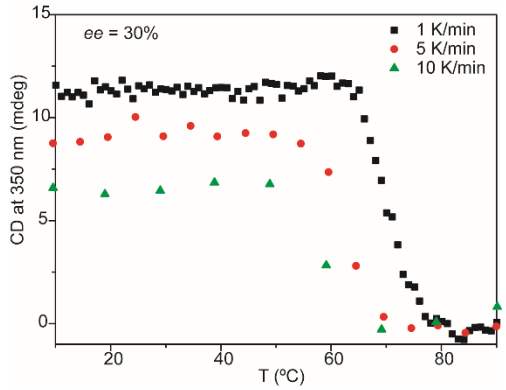

Figure 97. Cooling curves of the mixtures of ***(R)*-59+58** at *ee* = 30 % (MCH/Tol, 2/1, c_T = 7 μM).

In this way, by changing the amount of sergeant, and considering the different stability of the trapped monomer of the chiral and the achiral species, a stereomutative system is generated. Figure 98 schematizes the stereomutation generated in the *SaS* experiment of CBTs **(*S*)-59**, **(*R*)-59** and **58**.

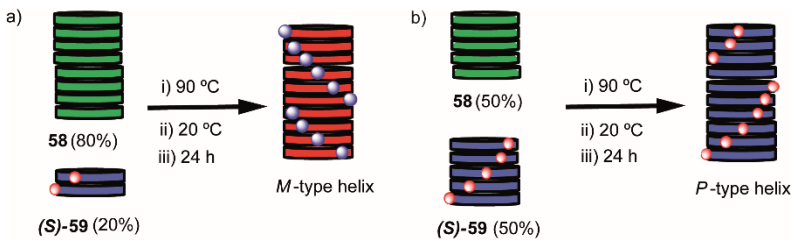

Figure 98. Schematic illustration of the helical outcome obtained for *SaS* experiments at different percentages of the chiral sergeant. Lower percentages of chiral sergeant (<20%) render aggregates of opposite helicity (a) to those generated when higher amounts of sergeant are added (b).

Thus, the kinetic effect clearly observed for the formation of helical aggregates from pristine chiral CBTs ***(S)*-59** and ***(R)*-59** and also for the copolymerization of these two chiral CBTs in *MR* experiments, is the responsible of the time-dependant amplification of chirality. Furthermore, the unexpected tunable helicity observed in the *SaS* experiments can only be explained by the differences in stability of the trapped monomers of the chiral and achiral species and the dissimilar inherent chirality of the *M* and *M** species, which results in an efficient and opposite chirality transfer that affords J-aggregates of inverse handedness. These results clearly demonstrate the importance of kinetic traps to generate new and dynamic functionalities in supramolecular polymerization processes.

5. EXPERIMENTAL SECTION

General Techniques

- *FTIR Spectroscopy*: the FTIR spectra have been registered in a Bruker Tensor 27 spectrophotometer equipped with an ATR dispositive. The signals are expressed in wavenumber units (cm^{-1}).

- *Nuclear Magnetic Resonance Spectroscopy (NMR)*: nuclear magnetic resonance spectra of ^{1}H y ^{13}C have been realized in Bruker Avance-300, 500 or 700 spectrometers at 298 K and using partly deuterated solvents as internal reference. The coupling constants (*J*) are expressed in Hertzs (Hz) and depending on its multiplicity, the signals are termed as follows: s = singlet, d = duplet, t = triplet, m = multiplet, dd = double duplet, ddd = double duplet of duplets, q = quadruplet, br = broad signal.

- *Mass Spectrometry*: the mass spectra have been obtained by electrospray ionization (ESI) in a mass spectrometer of ion trap Bruker (Esquirre-LC model) or in a mass spectrometer of flight time MALDI/TOF Bruker (ULTRAFLEX model). The high resolution mass obtained by ESI FTMS have been realized in a Bruker APEX Q IV, or by analysis of the time of flight MALDI-TOF/TOF, in a Bruker equipment (ULTRAFLEX model). The spectra obtained with the MALDI-TOF technique have been registered using dithranol as standard reference.

- *UV-Vis*: the UV-Vis measurements have been carried out in a Jasco-V630 spectrophotometer with a Peltier accessory and using a thermostatized bath for the variable temperature experiments.

- *Circular Dichroism:* the circular dichroism spectra have been taken in a Jasco J-1500 spectrophotometer and, for the measurements at different temperatures, a thermostatized bath NESLAB RTE-111 has been used.

- *Fluorescence*: fluorescence spectra have been recorded on a Jasco SP-6500. The quantum yields (ϕ_s) for compounds **25** and **(*S*)-26** have been calculated in $CHCl_3$ and MCH using a standard reference (anthracene in ethanol, $\phi_r = 0.27$)[151] and employing the equation: $\phi_s = \phi_r(A_rF_s/A_sF_r)(\eta_{s2}/\eta_{r2})$; where A_s and A_r make reference to the absorbance (OD = 0.1) of the sample and the standard reference respectively,

[151] D. F. Eaton, *J. Photochem. Photobiol. B* **1988**, *2*, 523.

at the same excitation wavelength (λ = 470 nm). F_s (8.7883 x 10^8) and F_r (1.30095 x 10^9) are the corresponding integrated fluorescence intensities of the sample and the reference and η the refractive index of the solvents employed [η_r = 1.3617 (ethanol), η_s = 1.490 (chloroform), η_s = 1.422 (MCH)].[152]

- *Theoretical Calculations:* theoretical calculations have been provided by Prof. Enrique Ortí´s group from the Universidad de Valencia. Theoretical calculations have been performed within the density functional theory (DFT) framework. **25** has been firstly modelled by replacing the aliphatic decyl chain by a hydrogen atom to reduce the computational cost. All the calculations have been performed by using the Gaussian 09 (revision D01) suite of programs.[153] The Grimme's B97D functional,[154] which includes dispersion corrections, has been employed in combination with the split-valence, double-zeta quality 6-31G** basis.[155, 156, 157] The molecular electrostatic potential (MEP) has been calculated for **25** using Becke's 3-parameter Lee-Yang-Parr hybrid functional (B3LYP)[158] together with the 6-31G** basis set. The geometry optimization of all the dimers has been performed by means of the Grimme's B97 functional including the most recent D3 dispersion correction using the Becke-Johnson damping function (B97D3).[159] The double-zeta 6-31G** basis set has been employed. No counterpoise correction has been applied to correct the basis set superposition error (BSSE). Note that the counterpoise method is believed to overestimate the BSSE, for which some authors propose to scale it down

[152] S. Fery-Forgues, D. Lavabre, *J. Chem. Ed.* **1999**, *76*, 1260.
[153] M. J. Frisch, G. W. Trucks, H. B. Schlegel, G. E. Scuseria, M. A. Robb, J. R. Cheeseman, G. Scalmani, V. Barone, B. Mennucci, G. A. Petersson, H. Nakatsuji, M. Caricato, X. Li, H. P. Hratchian, A. F. Izmaylov, J. Bloino, G. Zheng, J. L. Sonnenberg, M. Hada, M. Ehara, K. Toyota, R. Fukuda, J. Hasegawa, M. Ishida, T. Nakajima, Y. Honda, O. Kitao, H. Nakai, T. Vreven, J. A. Montgomery, J. E. Peralta, F. Ogliaro, M. Bearpark, J. J. Heyd, E. Brothers, K. N. Kudin, V. N. Staroverov, R. Kobayashi, J. Normand, K. Raghavachari, A. Rendell, J. C. Burant, S. S. Iyengar, J. Tomasi, M. Cossi, N. Rega, J. M. Millam, M. Klene, J. E. Knox, J. B. Cross, V. Bakken, C. Adamo, J. Jaramillo, R. Gomperts, R. E. Stratmann, O. Yazyev, A. J. Austin, R. Cammi, C. Pomelli, J. W. Ochterski, R. L. Martin, K. Morokuma, V. G. Zakrzewski, G. A. Voth, P. Salvador, J. J. Dannenberg, S. Dapprich, A. D. Daniels, Farkas, J. B. Foresman, J. V. Ortiz, J. Cioslowski and D. J. Fox, *Gaussian 09, Revision D.01*.
[154] S. Grimme, *J. Comput. Chem.* **2006**, *27*, 1787.
[155] V. A. Rassolov, M. A. Ratner, J. A. Pople, P. C. Redfern, L. A. Curtiss, *J. Comput. Chem.* **2001**, *22*, 976.
[156] R. Ditchfield, W. J. Hehre, J. A. Pople, *J. Chem. Phys.* **1971**, *54*, 724.
[157] M. M. Francl, W. J. Pietro, W. J. Hehre, J. S. Binkley, M. S. Gordon, D. J. D. Frees, J. A. Pople, *J. Chem. Phys.* **1982**, *77*, 3654.
[158] A. D. Becke, *J. Chem. Phys.* **1993**, *98*, 5648.
[159] S. Grimme, S. Ehrlich, L. Goerigk, *J. Comput. Chem.* **2011**, *32*, 1456.

by half of its value.[160] Non-covalent interaction (NCI) plots have been computed for the optimized geometries of dimers **A-F** at the B97D3/6-31G** level using the NCIPLOT program.[161,162] The method used for the NCI analysis is based on the relationship between the reduced density gradient (RDG) and the electron density (ρ). The molecular electron density computed from the sum of atomic contributions, the so-called promolecular density, has been employed as an approach to ρ. The density and RDG cut-offs have been kept at their default values. The tetramer modelled for the **F**-type aggregation mode has been fully optimized at the B97D3/6-31G** level of theory. The interaction energy between monomer pairs in the tetramer has been calculated at the same level of theory.

-*HPLC*: the separation of the atropisomers of compounds **35** and **36** has been carried out in an Agilent 1200 equipment using a chiral column (*R*,*R*)-Whelk 01 (5/100) (25 cm x 10 mm) using a mixture of toluene/2-propanol (97/3) in a 5 mL min^{-1} flow rate for compound **35** and hexane/2-propanol (80/20) with a 2.5 mL min^{-1} flow rate for compound **36** as eluents.

- *AFM*: AFM has been carried out in a SPM Nanoscope IIIa multimode working in tapping mode with TESPSS (Veeco) tips at working frequency of ~235 kHz.

-*Vibrational Circular Dichroism (VCD)*: VCD measurements have been carried out by the group of Prof. Juan Casado at the Universidad de Málaga. Infrared spectra have been recorded at room temperature using a Bruker Vertex 70 Fourier transform (FT) spectrometer purged with dry N_2 gas. VCD spectra have been measured with a Bruker PMA50 optical bench coupled to a Vertex 70 spectrometer. IR and VCD measurements have been registered simultaneously.

[160] H. Kruse, S. Grimme, *J. Chem. Phys.* **2012**, *136*, 154101.
[161] J. Contreras-García, E. R. Johnson, S. Keinan, R. Chaudret, J.-P. Piquemal, D. N. Beratan, W. Yang, *J. Chem. Theory Comput.* **2011**, *7*, 625.
[162] E. R. Johnson, S. Keinan, P. Mori-Sánchez, J. Contreras-García, A. J. Cohen, W. Yang, *J. Am. Chem. Soc.* **2010**, *132*, 6498.

Section 1

Synthetic Details and Characterization

Synthesis of formylbenzamides 31 and (*S*)-32. General Procedure.

1-Ethyl-3-(3-dimethylaminopropyl)carbodiimide hydrochloride (1.1 eq.) and 4-dimethylaminopyridine (1.1 eq.) are added to a solution of 4-formylbenzoic acid (1 eq.) in 20 mL of CH_2Cl_2 at 0 °C under argon atmosphere. After 15 minutes, the corresponding amine **30** and **(*S*)-29** (1.1 eq.) is added dropwise and the resulting mixture is stirred at room temperature overnight. After that, the reaction mixture is washed with HCl, NaOH and brine. The organic layer is dried over $MgSO_4$ and the solvent removed under vacuum. The afforded crude is subjected to silica column chromatography ($CHCl_3$/MeOH 10:0.3 as eluent) to give products **31** and **(*S*)-32** as white solids.

***N*-decyl-4-formylbenzamide (31).**

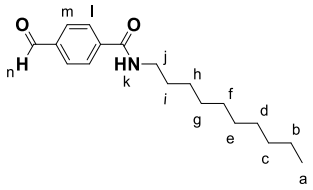

Yield: 52 %. ^{1}H NMR (300 MHz, $CDCl_3$) δ (ppm): 10.08 (s, $1H_n$), 7.95 (d, $2H_m$, ^3J = 8.9 Hz), 7.91 (d, $2H_l$, ^3J = 8.9 Hz), 6.22 (br, $1H_k$), 3.49 (br, $2H_j$), 1.70-1.27 (br, $16H_{b+c+d+e+f+g+h+i}$), 0.88 (t, $3H_a$, ^3J = 7.0 Hz). ^{13}C NMR (75 MHz, $CDCl_3$) δ (ppm): 191.6, 166.5, 140.2, 138.3, 130.0, 127.7, 40.5, 32.0, 29.7, 29.4, 27.1, 22.8, 14.2. FTIR ϑ̃ (cm^{-1}): 3331, 2955, 2922, 2850, 1707, 1696, 1629, 1610, 1536, 1500, 1474, 1322, 1308, 1206, 847, 819, 757, 637, 623. EI-MS: $C_{18}H_{27}NO_2$ $[M]^+$, 289.20.

(*S*)-*N*-(3,7-dimethyloctyl)-4-formylbenzamide ((*S*)-32).

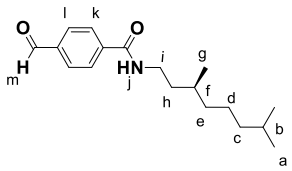

Yield: 40 %. ^{1}H NMR (300 MHz, $CDCl_3$) δ (ppm): 9.99 (s, $1H_m$), 7.89 (d, $2H_l$, ^{3}J = 8.8 Hz), 7.84 (d, $2H_k$, ^{3}J = 8.8 Hz), 6.76 (t, $1H_j$, ^{3}J = 4.9 Hz), 3.44 (m, $2H_i$), 1.72-1.04 (br, $10H_{b+c+d+e+f+h}$) 0.87 (d, $3H_g$, ^{3}J = 6.6 Hz), 0.80 (d, $6H_a$, ^{3}J = 6.6 Hz). ^{13}C NMR (75 MHz, $CDCl_3$) δ (ppm): 191.7, 166.5, 140.2, 138.2, 130.0, 127.7, 39.3, 38.6, 37.2, 36.8, 30.9, 28.1, 24.8, 22.8, 22.7, 19.7. FTIR ῡ (cm^{-1}): 3312, 3075, 2956, 2925, 2867, 1704, 1636, 1541, 1501, 1464, 1381, 1314, 1206, 1151, 1106, 1013, 849, 821, 758, 671, 628. EI-MS: $C_{18}H_{27}NO_2$ $[M]^+$, 289.20.

Synthesis of pyreneimidazole benzamides 25 and (*S*)-26. General Procedure.

The corresponding formylbenzamide **31** or **(*S*)-32** (1 eq.) and ammonium acetate (5 eq.) are added to a solution of 2,7-di-*tert*-butyl-4,5-pyrenedione (**34**) (1 eq.) in 5 mL of acetic acid. The resulting mixture is heated under reflux overnight. After that, the reaction mixture is quenched with 30 mL of water to afford a precipitate, which is subsequently dissolved in CH_2Cl_2. The resulting solution is dried over $MgSO_4$ and the solvent removed under vacuum. The residue is subjected to silica gel column chromatography (CH_2Cl_2 /MeOH 10:0.1 as eluent) to give products **25** and **(*S*)-26** as yellow solids.

4-(2,7-Di-*tert*-butyl-9H-pyrene[4,5-d]imidazole-10-yl)-*N*-decylbenzamide (25).

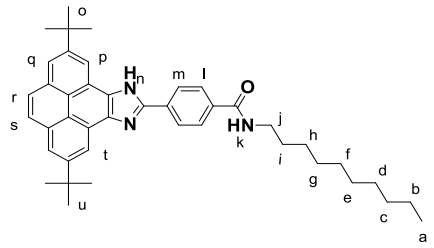

Yield: 56 %. ^{1}H NMR (700 MHz, DMSO-d_6) δ (ppm): 13.72 (s, $1H_n$) 8.91 (d, $1H_{t\ or\ p}$, ^{4}J = 1.2 Hz), 8.84 (d, $1H_{p\ or\ t}$, ^{4}J = 1.2 Hz), 8.62 (t, $1H_k$, ^{3}J = 5.8 Hz), 8.45

(d, 2H_m, ^3J = 8.2 Hz), 8.26 (d, 2H_q, ^4J = 1.2 Hz), 8.16 (d, 1$H_{s\ or\ r}$, ^3J = 8.9 Hz), 8.14 (d, 1$H_{r\ or\ s}$, ^3J = 8.9 Hz), 8.10 (d, 2H_l, ^3J = 8.2 Hz), 3.30 (br, 2H_j), 1.62 (s, 9$H_{u\ or\ o}$), 1.60 (s, 9$H_{o\ or\ u}$), 1.37-1.20 (br, 16$H_{b+c+d+e+f+g+h+i}$), 0.85 (t, 3H_a, ^3J = 7.0 Hz). ^{13}C NMR (175 MHz, DMSO-d_6) δ (ppm): 165.5, 148.7, 148.6, 148.2, 137.9, 134.9, 132.6, 131.3, 131.2, 128.8, 127.9, 127.6, 125.9, 125.7, 121.2, 121.1, 120.2, 120.1, 116.5, 115.9, 35.3, 35.1, 31.8, 31.3, 29.2, 29.1, 29.0, 28.8, 28.7, 26.6, 22.1, 14.0. FTIR ϑ̃ (cm^{-1}): 2965, 2925, 2854. 1633, 1613, 1556, 1531, 1467, 1386, 1362, 1306, 1276, 1220, 879, 858, 725. HRMS (ESI-FT) calcd. for $C_{42}H_{51}N_3O$ $[M]^+$, 613.4027; found, 613.4029.

(*S*)-4-(2,7-Di-*tert*-butyl-9H-pyrene[4,5-d]imidazole-10-yl)-*N*-(3,7-dimethyloctyl)-benzamide ((*S*)-26).

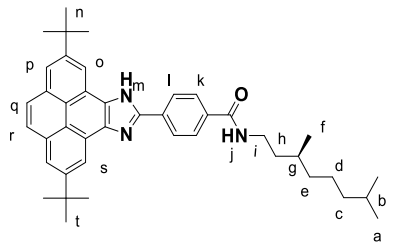

Yield: 62 %. ^{1}H NMR (700 MHz, DMSO-d_6) δ (ppm): 13.71 (s, 1H_m), 8.90 (d, 1$H_{s\ or\ o}$, ^4J = 2.0 Hz), 8.84 (d, 1$H_{o\ or\ s}$, ^4J = 2.0 Hz), 8.60 (t, 1H_j, ^3J = 5.5 Hz), 8.45 (d, 2H_l, ^3J = 8.6 Hz), 8.26 (d, 2H_p, ^4J = 1.8 Hz), 8.14 (d, 2H_{q+r}, ^4J = 1.0 Hz), 8.10 (d, 2H_k, ^3J = 8.6 Hz), 3.32 (br, 2H_i), 1.62 (s, 9$H_{t\ or\ n}$), 1.60 (s, 9$H_{n\ or\ t}$), 1.53-1.13 (br, 10$H_{b+c+d+e+g+h}$), 0.92 (d, 3H_f, ^3J = 7.4 Hz), 0.85 (t, 6H_a, ^3J = 7.4 Hz). ^{13}C NMR (175 MHz, DMSO-d_6) δ (ppm): 165.5, 148.7, 148.6, 148.2, 137.9, 134.9, 132.6, 131.3, 131.2, 128.8, 128.0, 127.9, 127.6, 125.9, 125.7, 121.3, 121.1, 120.2, 120.1, 116.6, 116.0, 38.8, 37.4, 36.7, 36.3, 35.3, 35.1, 31.8, 30.1, 27.4, 24.1, 22.6, 22.5, 19.6. FTIR ϑ̃ (cm^{-1}): 2954, 2928, 2869, 1635, 1613, 1559, 1529, 1470, 1385, 1363, 1318, 1276, 1220, 879, 857, 725. HRMS (ESI-FT) calcd. for $C_{42}H_{51}N_3O$ $[M]^+$, 613.4027; found, 613.4022.

Section 2

Racemization Experiments in solution

The values of the Gibbs activation energy of enantiomerization $\Delta G^{\ddagger}(T)$ for compounds ***P*-35** and ***M*-36** has been obtained by resolution of the corresponding enantiomers by HPLC and by following the decay of the enantioenriched sample dissolved in MCH, for ***P*-35**, and $CHCl_3$ for ***M*-36** at a determined temperature (328 K) over time (t) by monitoring the change in the maximum (λ = 332 nm for ***P*-35**, and λ = 349 nm for ***M*-36**) of the circular dichroism spectrum. The value ee_0 corresponds to the maximum at λ = 349 nm at 293 K, and it relates to the enantiopure sample as shown by HPLC. Considering that the racemization process follows a first-order kinetics, the representation of $ln\ (ee_t\ /ee_0)$ versus t (where ee_t corresponds to the CD signal at the maximum at different times) allows to obtain the k_{rac} as these parameters are related through the equation $ln(ee_t\ /ee_0) = -k_{rac}t$. The constant k_{rac} is also used to calculate the half-time of the process according to $t_{½} = \ln 2/k_{rac}$.

The free activation energy $\Delta G^{\ddagger}$(328K) for the racemization is calculated by using the Eyring equation $\Delta G^{\ddagger}(T) = -RT\ ln(k_e h/\kappa k_B T)$ where k_e is the constant of enantiomerization ($k_e = k_{rac}/2$), R is the gas constant (R = 8.31441 J K^{-1}), h is the Planck constant (h = 6.626176 x 10^{-34} J s), k_B is the Boltzmann constant (k_B = 1.380662 x 10^{-23} J K^{-1}), and κ is the transmission coefficient (κ = 0.5). The transmission coefficient κ = 0.5 in the Eyring equation has been used because the enantiomerization process is defined as a reversible first order reaction.[163,164] The data obtained for both compounds is summarized in Table 5.

[163] K. J. Laidler, *Chemical Kinetics*, 3rd ed.; Harper & Row: New York, **1987**.
[164] G. Schoetz, O. Trapp, V. Schurig, *Electrophoresis* **2001**, *22*, 3185.

Table 5. Kinetic data of the enantiomerization process of **(*P*)-35** and **(*M*)-36** in $CHCl_3$ and MCH, respectively.

	***(P)*-35**	**(*M*)-36**
k_{rac} [min^{-1}]	(4.3 ± 0.1) x 10^{-2}	(9.2 ± 0.7) x 10^{-2}
$t_{½}$ [min]	16.0 ± 0.4	7.5 ± 0.6
k_e [min^{-1}]	(2.2 ± 0.1) x 10^{-2}	(4.6 ± 0.4) x 10^{-2}
$\Delta G^{\ddagger}$*(328K)* [kcal mol^{-1}]	24.0 ± 0.6	23 ± 2

Synthetic Details and Characterization

(±)-7,8-Di(1-decynyl)[5]helicene (45).

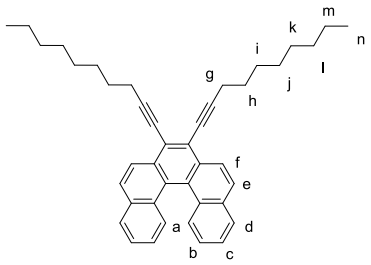

Compound **44** (290 mg, 0.67 mmol), $PdCl_2(PPh_3)_2$ (70 mg, 9.6 x 10^{-2} mmol), and CuI (10 mg, 4.8 x 10^{-2} mmol) are dissolved in anhydrous THF (18 mL) under argon atmosphere and subjected to three vacuum/argon cycles. Subsequently, 2 mL of a 1 M solution of tetrabutylammonium fluoride in THF (2 mmol) are added and the resulting mixture is subjected to vacuum/argon cycles. After that, 1-decyne (0.29 mL, 1.6 mmol) is charged and the solution is stirred under reflux overnight. After 24 hours, additional $PdCl_2(PPh_3)_2$ (70 mg), CuI (10 mg) and 1-decyne (0.15 mL) are added and the mixture is stirred and refluxed overnight. The solvent is evaporated and the residue is redissolved in $CHCl_3$ and washed with 1M aqueous HCl, sat. NH_4Cl and brine. The organic layer is dried with $MgSO_4$, and further filtration and removal of the solvent affords a residue which is subjected to a silica gel chromatography column (hexane as eluent) obtaining **45** as a pale yellow solid. Yield: 62%. ^{1}H NMR ($CDCl_3$, 300 MHz) δ (ppm): 8.49 (d, $2H_a$, ^3J = 8.8 Hz), 8.33 (d, $2H_{e\ or\ f}$, ^3J = 8.6 Hz), 7.97 (d, $2H_{f\ or\ e}$, ^3J = 8.6 Hz), 7,94 (d, $2H_d$, ^3J = 7.6 Hz), 7.51 (ddd, $2H_{b\ or\ c}$, ^3J = 7.6 Hz, ^3J = 7.4 Hz, ^4J = 1.1 Hz,), 7.25 (ddd, $2H_{c\ or\ b}$, ^3J = 8.8 Hz, ^3J = 7.4 Hz, ^4J = 1.3 Hz), 2.71 (t, $4H_g$, ^3J = 7.0 Hz), 1.86-1.75

(m, $4H_h$), 1.65-1.56 (m, $4H_i$), 1.41-1.33 (m, $16H_{j-m}$), 0.91 (t, $6H_n$, ^3J = 6.5 Hz). ^{13}C NMR ($CDCl_3$, 75 MHz) δ (ppm): 132.7, 131.8, 130.7, 129.5, 128.0, 127.8, 126.6, 126.5, 124.6, 124.6, 124.1, 100.4, 78.7, 32.1, 29.5, 29.5, 29.3, 29.2, 22.9, 20.3, 14.3. FTIR ϑ̃ (cm^{-1}): 2926, 2856, 2222, 1514, 1461, 1431, 1384, 1343, 1262, 817, 751, 664. HRMS m/z: $C_{42}H_{46}$ $[M]^+$ calculated 550.3600; found 550.3616.

(±)-7,8-Didecyl[5]helicene (46).

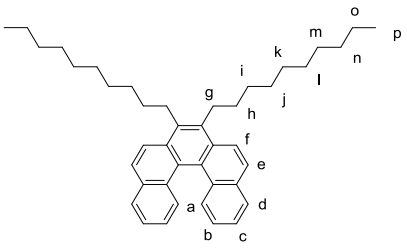

A solution of **45** (240 mg, 0.44 mmol) in CH_2Cl_2 (100 mL) is bubbled with argon for 10 minutes in absence of light. After that, 10% Pd/C (14 mg, 0.13 mmol) is added, and hydrogen is passed through the solution during 4 hours. After the removal of the catalyst by filtration through celite and subsequent elimination of the solvent, the residue is purified with a silica gel column chromatography (hexane as eluent), affording **46** as a light yellow solid. Yield: 60%.^1H NMR ($CDCl_3$, 300 MHz) δ (ppm): 8.28 (d, $2H_a$, ^3J = 8.4 Hz), 8.14 (d, $2H_{e\ or\ f}$, ^3J = 8.9 Hz), 7.96 (d, $2H_{f\ or\ e}$, ^3J = 8.9 Hz,), 7.93 (d, $2H_d$, ^3J = 7.4 Hz), 7.47 (ddd, $2H_c$, ^3J = 7.9 Hz, ^3J = 7.4 Hz, ^4J = 1.1 Hz,), 7.21 (ddd, $2H_b$, ^3J = 8.4 Hz, ^3J = 7.9 Hz, ^4J = 1.3 Hz,), 3.22 (t, $4H_g$, ^3J = 8.3 Hz), 1.77 (m, $4H_h$), 1.62 (m, $4H_i$), 1.51-1.25 (m, $24H_{j-o}$), 0.93 (t, $6H_p$, ^3J = 7.0 Hz). ^{13}C RMN ($CDCl_3$, 75 MHz) δ (ppm): 135.1, 131.6, 131.3, 130.9, 129.9, 127.4, 127.1, 126.2, 125.9, 124.4, 122.4, 32.1, 31.5, 30.6, 29.9, 29.8, 29.7, 29.6, 29.5, 22.9, 14.3. FTIR ϑ̃ (cm^{-1}): 2923, 2853, 1513, 1461, 1376, 1249, 1124, 808, 750. HRMS m/z: $C_{42}H_{54}$ $[M]^+$ calculated 558.4226; found 558.4240.

(±)-5,10-Dibromo-7,8-didecyl[5]helicene (47).

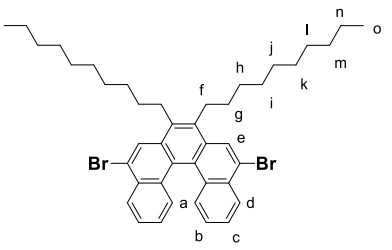

A solution of **46** (0.13 g, 0.31 mmol) in anhydrous CH_2Cl_2 (20 mL) is cooled down to -78 °C and a solution of bromine (36 μL, 0.69 mmol) in anhydrous CH_2Cl_2 (8 mL) is added dropwise. After 10 minutes, the mixture is allowed to reach room temperature and stirred overnight. The resulting organic phase is washed with sat. $Na_2S_2O_3$ and dried with $MgSO_4$. Further filtration and removal of the solvent affords a residue that is purified by silica gel column chromatography (hexane as eluent) giving **47** as a waxy pale yellow solid. Yield: 77%. ^{1}H NMR ($CDCl_3$, 300 MHz) δ (ppm): 8.34 (s, $2H_e$), 8.29 (dd, $2H_a$, ^3J = 8.5 Hz, ^4J = 1.6 Hz), 8.09 (d, $2H_d$, ^3J = 7.5 Hz), 7.49 (ddd, $2H_c$, ^3J = 7.9 Hz, ^3J = 7.5 Hz, ^4J = 1.2 Hz), 7.15 (ddd, $2H_b$, ^3J = 8.5 Hz, ^3J = 7.9 Hz, ^4J = 1.2 Hz), 3.07 (t, $4H_f$, ^3J = 7.8 Hz,), 1.65 (m, $4H_g$), 1.53 (m, $4H_h$), 1.50-1.24 (m, $24H_{i-n}$), 0.90 (t, $6H_o$, ^3J = 6.9 Hz). ^{13}C RMN ($CDCl_3$, 75 MHz) δ (ppm): 135.2, 132.2, 131.5, 130.0, 129.9, 127.2, 126.9, 126.3, 125.8, 125.5, 122.3, 32.1, 31.4, 30.4, 29.9, 29.8, 29.6, 29.5, 29.4, 22.9, 14.3. FTIR ϑ̃ (cm^{-1}): 2924, 2853, 1592, 1462, 1329, 1210, 865, 759. HRMS m/z: $C_{42}H_{52}Br_2$ $[M]^+$ calculated 716.2436; found 716.2466.

Synthesis of bisbenzamide and tetracarboxamide 35 and 36. General Procedure.

To a deoxygenated solution of **47** (1 eq.) and the corresponding boronic acid **40** or **41** (2.4 eq.) in tetrahydrofuran (24 mL), $Pd(PPh_3)_4$ (0.1 eq.), and an aqueous solution of K_2CO_3 (15 eq.) are added and the resulting mixture is deoxygenated again. The suspension is refluxed for 4 hours, and the crude is extracted with chloroform. The organic layer is washed with 1M aqueous HCl, NH_4Cl and brine. After drying and removal of the solvent, the crude is purified by silica gel column chromatography (gradient from $CHCl_3$ to 10:0.1 MeOH). The product obtained is further purified by precipitation in CH_2Cl_2/MeOH, affording **35** and **36** as yellow and dark yellow solids, respectively.

(±)-4,4´-(7,8-Didecyl[5]helicene-5,10-diyl)bis(*N*-decylbenzamide) (35).

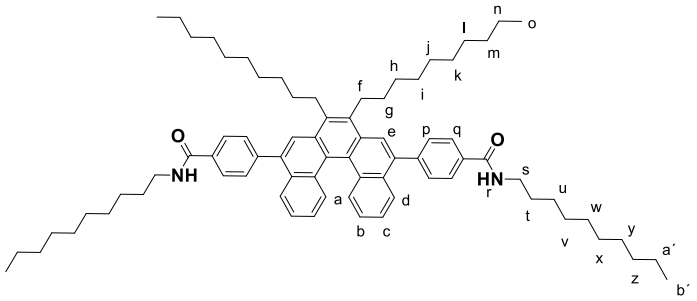

Yield: 34%. ^{1}H NMR ($CDCl_3$, 300 MHz) δ (ppm): 8.42 (d, $2H_a$, ^{3}J = 8.2 Hz), 8.07 (s, $2H_e$), 8.01 (d, $4H_q$, ^{3}J = 8.2 Hz,), 7.89 (d, $2H_d$, ^{3}J = 8.3 Hz,), 7.80 (d, $4H_p$, ^{3}J = 8.2 Hz), 7.40 (ddd, $2H_c$, ^{3}J = 8.3 Hz, ^{3}J = 7.7 Hz, ^{4}J = 1.0 Hz), 7.24 (ddd, $2H_b$, ^{3}J = 8.2 Hz, ^{3}J = 7.7 Hz, ^{4}J = 1.2 Hz), 6.30 (t, $2H_r$, ^{3}J = 5.8 Hz), 3.55 (m, $4H_s$), 3.18 (m, $4H_f$), 1.80-1.22 (m, $64H_{g\text{-}n\ +\ t\text{-}a'}$), 0.94-0.84 (m, $12H_{o+b'}$). ^{13}C NMR ($CDCl_3$, 75 MHz) δ (ppm): 167.5, 144.5, 137.9, 135.6, 134.0, 131.9, 130.5, 130.3, 130.0, 127.2, 126.2, 125.8, 125.7, 124.7, 123.2, 40.4, 32.0, 31.5, 30.4, 29.9, 29.8, 29.7, 29.6, 29.5, 29.5, 29.4, 27.2, 22.8, 14.3. FTIR ῡ (cm^{-1}): 3322, 2956, 2923, 2853, 1635, 1546, 1503, 1461, 1309, 1262, 1095, 1020, 856, 801, 765. HRMS m/z: $C_{76}H_{104}N_2O_2$ $[M]^+$ calculated 1076.8098; found 1076.8046.

(±)-*N*,*N*'-((((4,4'-(7,8-Didecyl[5]helicene-5,10-diyl)bis(benzoyl))bis-(azanediyl))bis(ethane-2,1-diyl))bis(3,4,5-tris(dodecyloxy)benzamide (36).

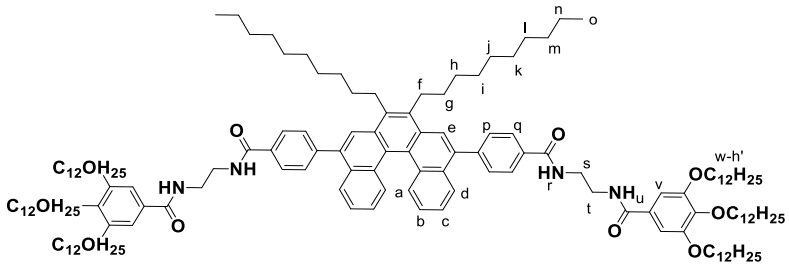

Yield: 44%. ^{1}H NMR ($CDCl_3$, 300 MHz) δ (ppm): 8.39 (d, $2H_a$, ^{3}J = 8.4 Hz), 8.09 (d, $4H_q$, ^{3}J = 7.9 Hz), 7.95 (s, $2H_e$), 7.86 (d, $2H_d$, ^{3}J = 8.4 Hz), 7.76 (d, $4H_p$, ^{3}J = 7.9 Hz), 7.81-7.70 (br, $2H_{r\ or\ u}$), 7.61-7.69 (br, $2H_{u\ or\ r}$), 7.36 (dd, $2H_c$, ^{3}J = 8.4 Hz, ^{3}J = 7.5 Hz), 7.20 (dd, $2H_b$, ^{3}J = 8.4 Hz, ^{3}J = 7.5 Hz), 7.14 (s, 4 H_v), 4.3 (m, $12H_w$), 3.81 (m, $8H_{s\text{-}t}$), 2.86 (br, $4H_f$), 1.81-1.13 (m, $152H_{g\text{-}n\ +\ x\text{-}i'}$), 0.94-0.79 (m,

$24H_{o+h'}$). ^{13}C NMR ($CDCl_3$, 75 MHz) δ (ppm): 168.9, 168.8, 153.2, 144.9, 141.2, 137.7, 135.5, 132.9, 131.9, 130.5, 130.4, 130.4, 129.9, 128.8, 127.6, 126.2, 126.2, 125.8, 125.5, 124.7, 123.2, 105.7, 73.6, 69.3, 43.6, 41.4, 41.1, 32.1, 32.0, 31.3, 30.5, 30.4, 29.9, 29.9, 29.8, 29.8, 29.7, 29.6, 29.5, 29.5, 26.3, 26.2, 22.8, 22.8, 14.3, 14.2. FTIR ϑ (cm^{-1}): 3307, 3020, 2923, 2853, 1631, 1581, 1544, 1498, 1467, 1344, 1304, 1265, 1215, 1115, 858, 752, 668. HRMS m/z: $C_{146}H_{226}N_4O_{10}$ $[M + Na]^+$ calculated 2218.7197; found 2218.7236.

Section 3

Synthetic details and characterization

General synthetic procedure for compounds 48, (*S*)-49 and (*R*)-49

Iodinated *N*-heterotriangulene **57** (1 eq.), the corresponding benzamide **54**, **(*S*)-55** or **(*R*)-55** (3.3 eq.), $PdCl_2(PPh_3)_2$ (0.05 eq.) and CuI (0.1 eq.) are dissolved in anhydrous toluene (4.5 mL) and are subjected to argon/vacuum cycles. Anhydrous diisopropylamine (1.5 mL) is then added and the mixture is subjected to additional argon/vacuum cycles. The reaction mixture is heated at 75 ºC overnight, the solvent is evaporated and the crude is dissolved in chloroform, washed with brine and dried over $MgSO_4$. Further filtration and removal of the solvent under vacuum gives a residue that is purified by silica gel column chromatography ($CHCl_3$/MeOH 10:0.1 as eluent). Subsequent precipitation from CH_2Cl_2/MeOH, affords compounds **48**, **(*S*)-49** and **(*R*)-49** as dark yellow solids.

4,4',4''-((4,8,12-Trioxo-8,12-dihydro-4H-benzo[1,9]quinolizino[3,4,5,6,7-d,e,f,g]acridine-2,6,10-triyl)tris(ethyne-2,1-diyl))tris(*N*-decylbenzamide) (48).

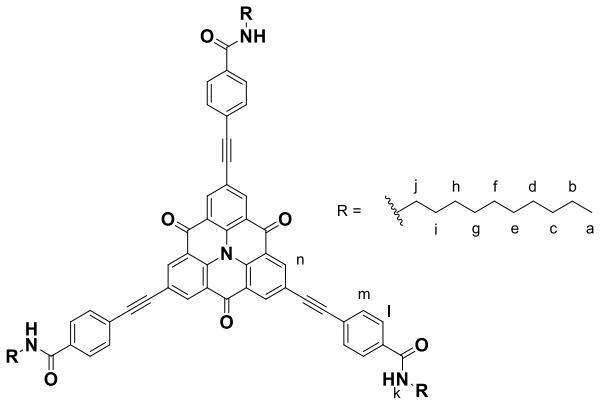

Yield: 48%. ^{1}H NMR (500 MHz, THF-d_8) δ (ppm): 8.02 (br, 3H$_k$). 7.96 (s, 6H$_n$), 7.24 (d, 6H$_l$, ^{3}J = 6.0 Hz), 7.02 (d, 6H$_m$, ^{3}J = 6.0 Hz), 3.41 (m, 6H$_j$), 1.33-1.47 (br, 48H$_{b+c+d+e+f+g+h+i}$), 0.92 (d, 9H$_a$, ^{3}J = 7.0 Hz). ^{13}C NMR (125 MHz, THF-d_8) δ (ppm): 172.8, 168.0, 136.7, 136.1, 134.8, 132.0, 127.8, 124.7, 122.8, 122.0, 93.4, 88.0, 40.8, 32.7, 30.5, 30.4, 30.3, 30.1, 28.0, 25.5, 23.3, 14.2. FTIR ῦ (cm^{-1}): 3283, 3069, 2923, 2853, 2221, 1668, 1635, 1586, 1544, 1504, 1462, 1294, 877, 849, 766. HRMS (MALDI-TOF) m/z calcd. for $C_{78}H_{84}N_4O_6$ [M+H]$^+$, 1173,6391; found, 1173.6418.

4,4',4''-((4,8,12-trioxo-8,12-dihydro-4H-benzo[1,9]quinolizino[3,4,5,6,7-d,e,f,g]acridine-2,6,10-triyl)tris(ethyne-2,1-diyl))tris(*N*-((*S*)-3,7-dimethyloctyl)benzamide) ((*S*)-49).

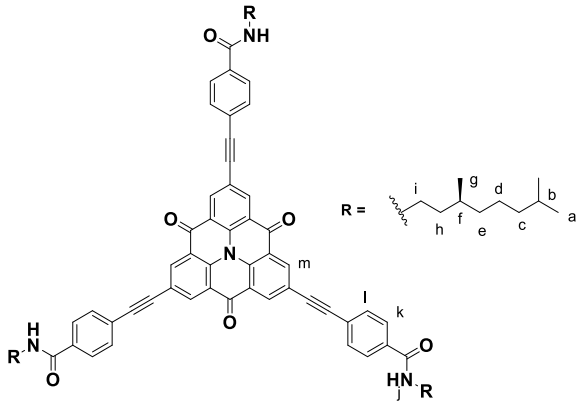

Yield: 49 %. ^{1}H NMR (500 MHz, THF-d_8) δ (ppm): 8.33 (br, 3H$_j$), 7.67 (s, 6H$_m$), 7.05 (d, 6H$_k$, ^{3}J = 6.0 Hz), 6.82 (d, 6H$_l$, ^{3}J = 6.0 Hz), 3.45 (m, 6H$_i$) 1.20-1.80 (br, 30H$_{b+c+d+e+f+h}$), 1.02 (d, 9H$_g$, ^{3}J = 6.7 Hz), 0.91 (d, 18H$_a$, ^{3}J = 6.7 Hz). ^{13}C NMR (125 MHz, THF-d_8) δ (ppm): 172.2, 168.5, 136.5, 135.9, 134.0, 131.9, 127.7, 124.6, 122.2, 121.9, 93.5, 87.7, 40.1, 38.9, 38.2, 37.5, 31.7, 28.8, 23.0, 22.9, 20.0. FTIR ϑ̃ (cm^{-1}): 3279, 3075, 2924, 2861, 2219, 1668, 1636, 1594, 1548, 1504, 1463, 1296, 1157, 925, 849, 801. HRMS (MALDI-TOF) m/z calcd. for $C_{78}H_{84}N_4O_6$ $[M+H]^+$, 1173.6391; found, 1173.6418.

4,4',4''-((4,8,12-trioxo-8,12-dihydro-4H-benzo[1,9]quinolizino[3,4,5,6,7-d,e,f,g]acridine-2,6,10-triyl)tris(ethyne-2,1-diyl))tris(N-((*R*)-3,7-dimethyloctyl)benzamide) ((*R*)-49).

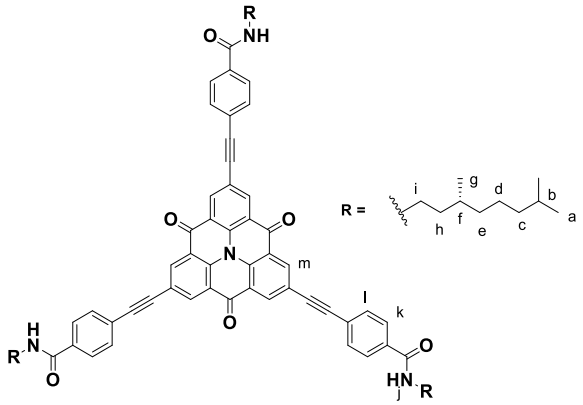

Yield: 44%. ^{1}H NMR (700 MHz, THF-d_8) (δ / ppm): 8.04 (br, 3H$_j$) 7.97 (s, 6H$_m$), 7.24 (d, 6H$_k$, ^{3}J = 6.0 Hz), 7.03 (d, 6H$_l$, ^{3}J= 6.0 Hz), 3.46 (m, 6H$_i$), 1.19-1.82 (br, 30H$_{b+c+d+e+f+h}$), 1.03 (d, 9H$_g$, ^{3}J = 6.7 Hz), 0.92 (d, 18H$_a$, ^{3}J = 6.7 Hz). ^{13}C NMR (175 MHz, THF-d_8) δ (ppm): 172.9, 168.0, 136.8, 136.2, 134.9, 132.1, 127.8, 124.9, 122.9, 122.0, 93.4, 88.0, 40.1, 39.0, 38.2, 37.6, 31.8, 28.8, 22.9, 22.8, 20.0. FTIR ϑ̃ (cm^{-1}): 3275, 3073, 2924, 2862, 2220, 1669, 1636, 1594, 1548, 1504, 1462, 1296, 1159, 923, 849, 800. HRMS (MALDI-TOF) m/z calcd. for $C_{78}H_{84}N_4O_6$ $[M+H]^+$, 1173.6391; found, 1173.6411.

Section 4

Synthetic details and characterization

3,4,5-Tris((*R*)-3,7-dimethyloctyloxy)-*N*-(2-hydroxyethyl)benzamide ((*R*)-64)

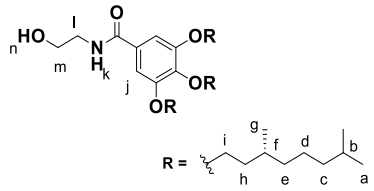

To a stirred suspension of **(*R*)-61** (597 mg, 1.01 mmol) in 4 mL of anhydrous CH_2Cl_2, 1-ethyl-3-(3-dimethylaminopropyl)carbodiimide hydrochloride (213 mg, 1.13 mmol) and 4imethylaminopyridine (136 mg, 1.13 mmol) are added portionwise at 0 ºC and under argon atmosphere. After 15 minutes, 2-aminoethanol (70 μL, 1.13 mmol) is added and the reaction is stirred overnight at room temperature. The resulting organic mixture is washed with HCl, aqueous NaCl solution and dried over $MgSO_4$. After filtration and removal of the solvent, the residue is subjected to a silica gel chromatography column (Hex 7:3 EtOAc as eluent), affording **(*R*)-64** as a white sticky solid (356 mg, 0.56 mmol). Yield: 56%. ^{1}H NMR (300 MHz, $CDCl_3$) δ (ppm): 6.99 (s, $2H_j$), 6.56 (t, $1H_k$, ^3J = 5.4 Hz), 4.04 (m, $6H_i$), 3.84 (t, $2H_l$, ^3J = 5.0 Hz), 3.62 (m, $2H_m$), 1.84 (m, $6H_h$), 1.11-1.65 (br, $24H_{b+c+d+e+f}$), 0.93 (m, $9H_g$), 0.86 (d, $18H_a$, ^3J = 6.6 Hz). ^{13}C NMR (75 MHz, $CDCl_3$) δ (ppm): 168.8, 153.3, 141.4, 129.2, 105.8, 71.9, 67.8, 62.8, 43.2, 39.5, 39.4, 37.6, 37.5, 36.5, 29.9, 29.8, 28.1, 24.9, 22.9, 22.8, 19.7. FTIR ϑ̃ (cm^{-1}): 3288, 2954, 2924, 1630, 1580, 1542, 1499, 1464, 1426, 1378, 1337, 1234, 1116, 1056, 849, 755, 666, 603. MALDI-MS: $C_{39}H_{71}NO_5$ $[M]^+$ 634.33.

General procedure for the synthesis of 67, (*S*)-68 and (*R*)-68

To a stirred suspensión of 4-ethynylbenzoic acid (1 eq.) in 3 mL of anhydrous dicloromethane, 1-ethyl-3-(3-dimethylaminopropyl)carbodiimide hydrochloride (1.1 eq.) and 4-dimethylaminopyridine (1.1 eq.) are added portionwise at 0ºC under argon atmosphere. After fifteen minutes, the corresponding alcohol **63, (*S*)-64** or **(*R*)-64** (1.1 eq.) is added and the reaction mixture is stirred overnight at room temperature. The resulting crude is washed with an aqueous NaCl solution and dried over $MgSO_4$. After filtration and removal of the solvent, the residue is subjected to

a silica gel chromatography column ($CHCl_3$ 10:0.1 MeOH as eluent), affording **67, (*S*)-68** and **(*R*)-68** as pale orange flakes.

2-(3,4,5-Tris(dodecyloxy)benzamido)ethyl-4-ethynylbenzoate (67)

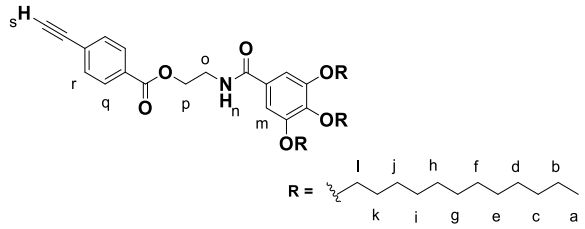

Yield: 68%. ^{1}H NMR (300 MHz, $CDCl_3$) δ (ppm): 8.01 (d, $2H_r$, ^3J = 8.4 Hz), 7.55 (d, $2H_q$, ^3J = 8.4 Hz), 6.95 (s, $2H_m$), 6.55 (t, $1H_n$, ^3J = 5.0 Hz), 4.57 (t, $2H_p$, ^3J = 5.2 Hz), 3.99 (m, $6H_l$), 3.85 (m, $2H_o$), 3.25 (s, $1H_s$), 1.31-1.85 (br, $60H_{b+c+d+e+f+h+i+j+k}$), 0.89 (m, $9H_a$). ^{13}C NMR (75 MHz, $CDCl_3$) δ (ppm):167.8, 166.5, 153.2, 132.3, 129.8, 129.7, 129.2, 129.2, 127.3, 105.7, 82.7, 80.5, 73.6, 69.4, 64.1, 32.0, 30.4, 29.9, 29.8, 29.8, 29.7, 29.5, 29.5, 26.2, 22.8, 14.3. FTIR ϑ̃ (cm^{-1}): 3277, 2919, 2852, 1724, 1636, 1581, 1543, 1499, 1464, 1428, 1384, 1342, 1269, 1235, 1119, 1025, 853, 767, 723, 655, 615. MALDI-MS: $C_{54}H_{87}NO_6$ $[M]^+$ 846.61.

2-(3,4,5-Tris((*S*)-3,7-dimethyloctyloxy)benzamido)ethyl-4-ethynylbenzoate ((*S*)-68)

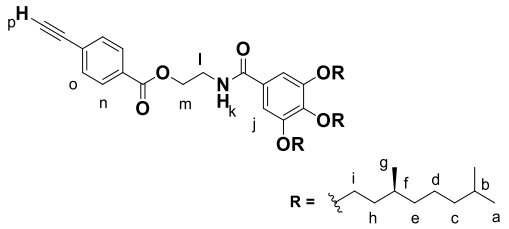

Yield: 91%. ^{1}H NMR (300 MHz, $CDCl_3$) δ (ppm): 8.01 (d, $2H_n$, ^3J = 8.2 Hz). 7.56 (d, $2H_o$, ^3J = 8.2 Hz), 6.97 (s, $2H_i$), 6.52 (t, $1H_k$, ^3J = 5.2 Hz), 4.58 (t, $2H_m$, ^3J = 5.2 Hz), 4.04 (m, $6H_i$), 3.85 (m, $2H_l$), 3.26 (s, $1H_p$), 1.84 (m, $6H_h$), 1.15-1.69 (br, $24H_{b+c+d+e+f}$), 0.93 (m, $9H_g$), 0.87 (d, $18H_a$, ^3J = 6.6 Hz). ^{13}C NMR (75 MHz, $CDCl_3$) δ (ppm): 167.8, 166.6, 153.3, 141.3, 132.3, 129.8, 129.7, 129.3, 127.4, 105.7, 82.8, 80.6, 71.9, 67.7, 64.1, 40.0, 39.5, 39.4, 37.5, 37.5, 36.5, 30.0, 29.8, 28.1, 24.9, 24.9, 22.8, 22.7, 19.7. FTIR ϑ̃ (cm^{-1}): 3307, 2956, 2927, 1721, 1636, 1582,

1544, 1499, 1464, 1427, 1384, 1341, 1274, 1239, 1116, 856, 765, 695, 653, 620. MALDI-MS: $C_{48}H_{75}NO_6$ $[M]^+$ 762.47.

2-(3,4,5-tris((*R*)-3,7-dimethyloctyloxy)benzamido)ethyl-4-ethynylbenzoate ((*R*)-68)

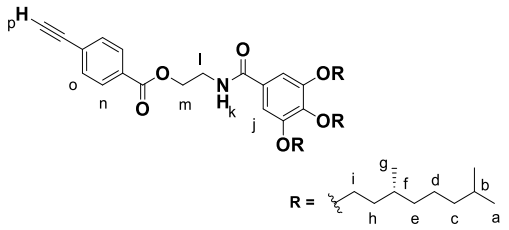

Yield: 88%. ^{1}H NMR (300 MHz, $CDCl_3$) δ (ppm): 8.01 (d, $2H_n$, ^3J = 8.3 Hz), 7.55 (d, $2H_o$, ^3J = 8.3 Hz), 6.97 (s, $2H_i$), 6.55 (t, $1H_k$, ^3J = 5.2 Hz), 4.58 (t, $2H_m$, ^3J = 5.5 Hz), 4.04 (m, $6H_i$), 3.85 (m, $2H_l$), 3.26 (s, $1H_p$), 1.84 (m, $6H_h$), 1.14-1.70 (br, $24H_{b+c+d+e+f}$), 0.93 (m, $9H_g$), 0.86 (d, $18H_a$, ^3J = 6.6 Hz). ^{13}C NMR (75 MHz, $CDCl_3$) δ (ppm): 167.8, 166.6, 153.3, 141.3, 132.3, 129.8, 129.7, 129.2, 127.4, 105.6, 82.8, 80.6, 71.9, 67.7, 64.1, 40.0, 39.5, 39.4, 37.6, 37.5, 36.5, 30.0, 29.8, 28.1, 24.9, 24.9, 22.9, 22.8, 19.7. FTIR ϑ̃ (cm^{-1}): 3307, 2955, 2926, 1723, 1636, 1581, 1542, 1497, 1464, 1428, 1380, 1338, 1271, 1236, 1115, 857, 766, 696, 654, 618. MALDI-MS: $C_{48}H_{75}NO_6$ $[M]^+$ 762.45.

General Procedure for the synthesis of compounds 58, (*S*)-59 and (*R*)-59

Iodinated *N*-heterotriangulene **57** (1 eq.), the corresponding alkyne **67, (*S*)-68** or **(*R*)-68** (3.3 eq.), $PdCl_2(PPh_3)_2$ (0.05 eq.) and CuI (0.1 eq.) are dissolved in anhydrous toluene (1.5 mL) and subjected to argon/vacuum cycles. Anhydrous diisopropylamine (0.5 mL) is then added and the mixture is subjected to additional argon/vacuum cycles. The reaction mixture is heated at 75 ºC overnight, the solvent is evaporated and the crude is dissolved in chloroform, washed with brine and dried over $MgSO_4$. Further filtration and removal of the solvent in vacuum gives a residue that is purified by silica gel column chromatography ($CHCl_3$/MeOH 10:0.1 as eluent). Subsequent precipitation from CH_2Cl_2/MeOH, affords compounds **58, (*S*)-59** and **(*R*)-59** as tan yellow solids.

Tris(2-(3,4,5-tris(dodecyloxy)benzamido)ethyl)-4,4',4''-((4,8,12-trioxo-8,12-dihydro-4H-benzo[1,9]quinolizino[3,4,5,6,7-d,e,f,g]acridine-2,6,10-triyl)tris (ethyne-2,1-diyl))tribenzoate (58)

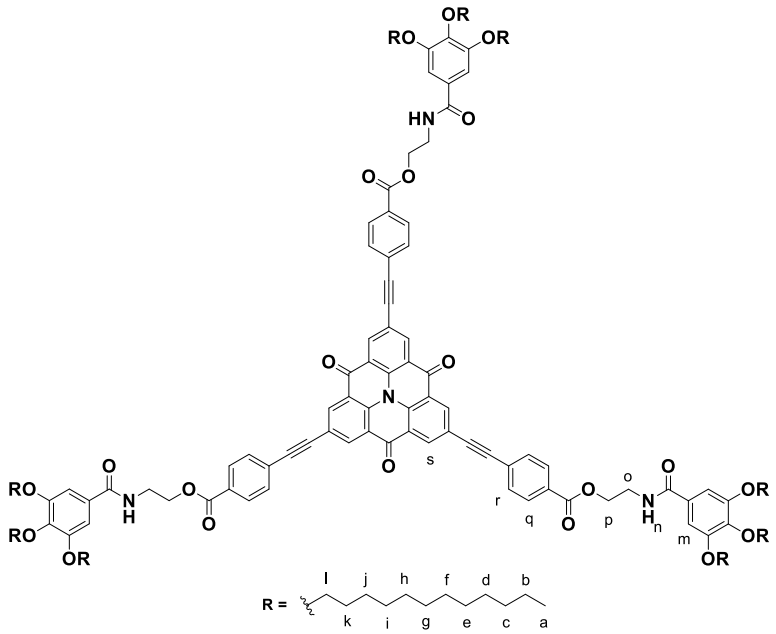

Yield: 47%. ^{1}H NMR (700 MHz, $CDCl_3$) δ (ppm): 8.75 (s, $6H_s$), 7.76 (d, $6H_q$, ^{3}J = 8.6 Hz), 7.40 (d, $6H_r$, ^{3}J = 8.6 Hz), 7.23 (br, $3H_n$), 7.15 (s, $6H_m$), 4.51 (t, $6H_p$, ^{3}J = 5.9 Hz), 3.98 (m, $18H_l$) 3.89 (m, $6H_o$), 1.76 (br, $18H_k$), 1.24-1.49 (br, $162H_{b+c+d+e+f+h+i+j}$), 0.86 (m, $27H_a$). ^{13}C NMR (175 MHz, $CDCl_3$) δ (ppm): 173.8, 167.9, 166.3, 153.2, 141.3, 137.0, 135.5, 131.9, 129.7, 129.5, 129.1, 126.9, 122.9, 121.7, 105.9, 92.6, 89.1, 73.7, 69.4, 64.2, 32.0, 30.5, 29.9, 29.9, 29.9, 29.8, 29.8, 29.6, 29.6, 29.5, 26.2, 22.9, 14.3. FTIR ῡ (cm^{-1}): 3286, 2923, 2853, 1724, 1666, 1636, 1583, 1541, 1498, 1463, 1429, 1340, 1270, 1234, 1117, 855, 803,764. HRMS (MALDI-TOF) m/z for $C_{183}H_{264}N_4O_{21}Na$ $[M+Na]^+$ calcd. 2876.9611; found, 2876.9595.

Tris(2-(3,4,5-Tris((*S*)-3,7-dimethyloctyloxy)benzamido)ethyl)-4,4',4''-((4,8,12-trioxo-8,12-dihydro-4H-benzo[1,9]quinolizino[3,4,5,6,7-d,e,f,g]acridine-2,6,10-triyl)tris(ethyne-2,1-diyl))tribenzoate ((*S*)-59)

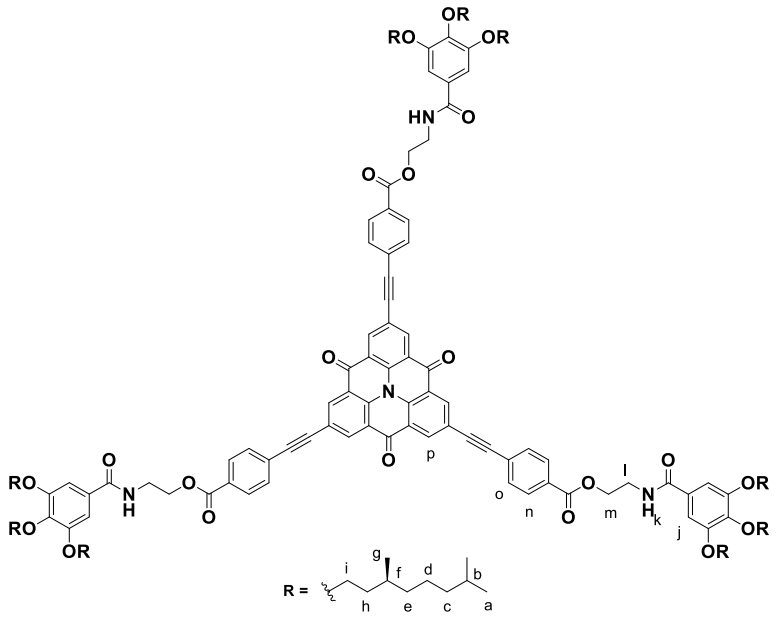

Yield: 43%. ^{1}H NMR (700 MHz, $CDCl_3$) δ (ppm): 8.82 (s, $6H_p$), 7.71 (d, $6H_n$, ^{3}J = 8.7 Hz), 7.44 (d, $6H_o$, ^{3}J = 8.7 Hz), 7.16 (s, $6H_j$), 7.15 (br, $3H_k$), 4.53 (t, $6H_m$, ^{3}J = 5.5 Hz), 4.03 (m, $18H_i$), 3.91 (m, $6H_l$), 1.84 (br, $18H_h$), 1.13-1.71 (br, $72H_{b+c+d+e+f}$), 0.91 (m, $27H_g$), 0.86 (d, $54H_a$, ^{3}J = 6.6 Hz). ^{13}C NMR (175 MHz, $CDCl_3$) δ (ppm): 174.0, 167.9, 166.5, 153.3, 141.3, 137.1, 135.8, 131.9, 129.7, 129.5, 129.1, 127.0, 123.0, 121.6, 105.8, 92.6, 89.2, 71.9, 67.7, 64.3, 39.7, 39.5, 39.4, 37.7, 37.5, 36.5, 30.0, 29.9, 29.8, 28.1, 24.9, 24.9, 22.9, 22.8, 19.7, 19.6. FTIR ῡ (cm^{-1}): 3304, 2953, 2916, 2870, 1724, 1668, 1637, 1583, 1543, 1498, 1463, 1429, 1338, 1271, 1235, 1114, 856, 801, 764, 692. HRMS (MALDI-TOF) m/z for $C_{165}H_{228}N_4O_{21}Na$ $[M+Na]^+$ calcd. 2624.6794; found, 2624.6875.

Tris(2-(3,4,5-Tris((*R*)-3,7-dimethyloctyloxy)benzamido)ethyl)-4,4',4''-((4,8,12-trioxo-8,12-dihydro-4H-benzo[1,9]quinolizino[3,4,5,6,7-d,e,f,g]acridine-2,6,10-triyl)tris(ethyne-2,1-diyl))tribenzoate ((*R*)- 59)

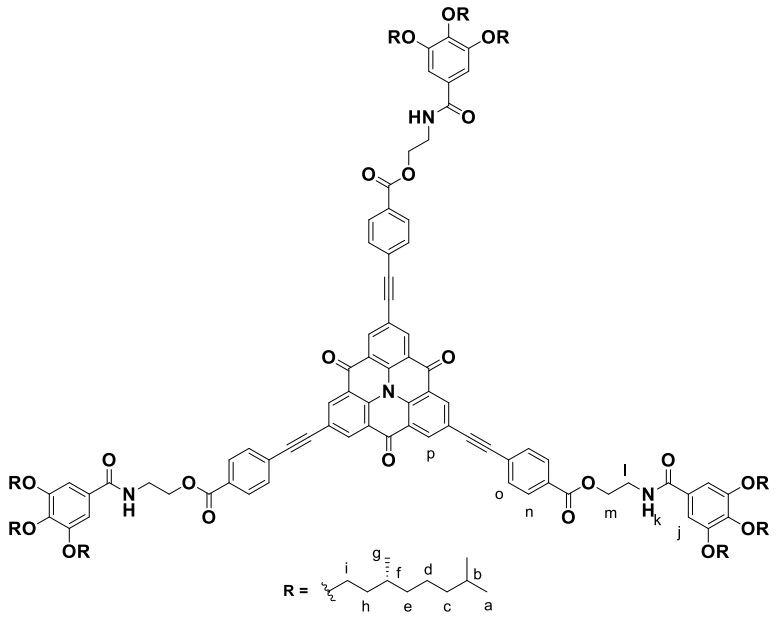

Yield: 55%. ^{1}H NMR (700 MHz, $CDCl_3$) δ (ppm): 8.80 (s, $6H_p$), 7.79 (d, $6H_n$, ^{3}J = 8.6 Hz), 7.42 (d, $6H_o$, ^{3}J = 8.6 Hz), 7.20 (br, $3H_k$), 7.18 (s, $6H_j$), 4.52 (t, $6H_m$, ^{3}J = 5.0 Hz), 4.03 (m, $18H_i$), 3.91 (m, $6H_l$), 1.83 (br, $18H_h$), 1.71-1.14 (br, $72H_{b+c+d+e+f}$), 0.91 (m, $27H_g$), 0.86 (d, $54H_a$, ^{3}J = 6.6 Hz). ^{13}C NMR (175 MHz, $CDCl_3$) δ (ppm): 173.9, 167.9, 166.5, 153.3, 141.3, 137.0, 135.7, 131.9, 129.7, 129.4, 129.1, 127.0, 123.0, 121.7, 105.8, 92.6, 89.2, 71.9, 67.7, 64.3, 39.7, 39.5, 39.4, 37.7, 37.5, 36.5, 30.0, 29.9, 29.8, 28.1, 24.9, 24.9, 22.9, 22.8, 19.7, 19.6. FTIR ῡ (cm^{-1}): 3312, 2953, 2926, 2869, 1725, 1670, 1637, 1584, 1542, 1497, 1463, 1426, 1338, 1271, 1236, 1115, 855, 802, 765, 692. HRMS (MALDI-TOF) m/z for $C_{165}H_{228}N_4O_{21}Na$ $[M+Na]^+$ calcd. 2624.6794; found, 2624.6845.

6. CONCLUDING REMARKS

Some general conclusions can be inferred by the results obtained in this Thesis. Thus, supramolecular polymerization has been demonstrated to be an adequate tool to organize π-scaffolds through the appropriate molecular design. Importantly, the inclusion of amide groups, able to establish H-bonds, in combination with other non-covalent forces like π-stacking, usually renders supramolecular polymers based on π-scaffolds through a cooperative mechanism, especially in C_3-symmetric molecules like *N*-heterotriangulenes. However, as it has been demonstrated in the self-assembly of the pyrene and helicene derivatives, the presence of bulky substituents in the π-core or a curved aromatic geometry could prevent an efficient π-stacking, resulting in an isodesmic or weakly cooperative mechanisms. Even though this fact can be seen as a drawback regarding the self-assembly viewpoint, the reduction of π-stacking permits, in some cases, to attain notable molecular properties within the supramolecular aggregate. Interestingly, the obtaining of H- and J-aggregates in C_3-symmetric systems like *N*-heterotriangulenes seems to be related to the position of the amide group in regard to the aromatic core, as well as to the presence of more alkyl chains in the periphery. Remarkably, the incorporation of the proper functionalities at the periphery of the π-scaffold can lead to kinetic phenomena and, therefore, to kinetically-controlled supramolecular polymerizations and copolymerizations. It should be pointed out that referable outer chains (like in the case of the helicene moiety) do not always generate kinetically-controlled supramolecular polymerizations, suggesting the necessity of a fine balance of all the intermolecular forces. Notably, the incorporation of long alkyl chains has been corroborated as a proper strategy to generate π-gels since it favours the interactions among fibres and with the solvent.

The particular remarks in each Section are the following:

In Section 1, the supramolecular polymerization of the pyreneimidazole derivatives **25** and **(*S*)-26**, decorated with amides on their periphery, have been demonstrated to proceed through a weakly cooperative mechanism. The thermodynamic data extracted for the self-assembly process of both molecules are slightly dissimilar, which is a cause of their different alkyl substituents. The inclusion of bulky groups at the pyrene core, as well as the presence of the imidazole ring, have a huge impact on the capability of **25** and **(*S*)-26** to experience efficient π-stacking. This affects to the mechanism of the supramolecular polymerization and, notably, has an unexpected consequence, since this weak π-stacking avoids the formation of

excimers typical of pyrene-based aggregates, yielding highly emissive blue-emitting pyrene-based aggregates.

The presence of different groups capable of establishing H-bonding and the lack of directionality of the π-forces, which favours the existence of other interactions like C-H···π, C-H···C-H or π-π interactions, opens many possibilities for the molecular arrangement to generate supramolecular polymers. Thus, the explanation for the self-assembling features of the systems presented in this Section requires of the synergy between experimental and theoretical studies. These studies reveal that the formation of the aggregate proceeds through an alternating array of H-bonds among the amide and imidazole rings and the stabilization by means of C-H···π interactions. Therefore, even though the absence of π-stacking yields supramolecular polymers through a weakly cooperative mechanism, this strategy permits that the resulting aggregates maintain the pyrene monomeric emissive pattern, demonstrating that the appropriate molecular arrangement within the supramolecular polymer can yield organized structures keeping the properties of the isolated molecular building blocks.

In Section 2, the study of the self-assembly in organic solvents of the racemic and enantioenriched 1,14-unsubstituted [5]-helicenes **35** and **36** has proved the importance of amide functionalities to generate helicene-based supramolecular polymers. The lack of π-stacking, justified by the curved geometry of the helicene core, makes bisamide **35** incapable of aggregating in solution, whereas **36** is able to form supramolecular polymers in solution due to the establishment of a quadruple intermolecular array of H-bonding between its four amide groups. Thus, the curved geometry of the helicene skeleton diminishes the ability to interact by π-stacking and other non-covalent forces are required to attain supramolecular polymers based on these helicenes. The resolution of the atropisomers in **35** and **36** demonstrates the enormous importance of the enantiopurity of the sample in the supramolecular polymerization mechanism, being the mechanism isodesmic for the racemic mixture and cooperative for the enantioenriched sample ***M*-36**. Finally, the precluding of the racemization process in the enantioenriched aggregates disclosed in this Section unveils a new strategy to avoid the racemization in 1,14-unsubstituted [5]-helicenes and shows the importance of self-assembly as a new tool to stabilize the configuration of unstable enantiopure helicenes.

In Section 3, the supramolecular polymerization of *N*-heterotriangulene tricarboxamides **48, (*S*)-49** and **(*R*)-49** has been disclosed as an enthalpically driven process which proceeds upon a cooperative mechanism. Even though the strong tendency to self-assemble is evident, the lack of solubility of these compounds in pristine MCH makes the comparison with self-assembling related compounds inaccurate. The inclusion of the amide group close to the aromatic core directs the formation of H-type aggregates in a helical arrangement whose helicity is dictated by the stereogenic centre. These findings are in agreement with other C_3-symmetric molecules able to form supramolecular polymers. After discarding any type of kinetic effects in the supramolecular polymerization, the strong ability of these compounds to self-assemble has also been proved by the tendency to form organogels in apolar solvents like Tol and CCl_4 at high concentrations. Interestingly, a further inspection of the chiroptical features of these organogels by CD and VCD reveals a chiroresponsive system in which the helicity of the fibres constituting the gels is dictated by the achiral solvent utilized and not by the stereogenic centre at the peripheral side chains, thus affording solvent-directed helical stereomutation. A closer study of the gels formed in CCl_4 reveals that this stereomutation is a consequence of a pathway complexity in the gel state that can be triggered by the application of ultrasounds. Probably, the high concentration required to form the gels makes a time dependant evolution without stimuli a very slow process. However, other experiments evaluating longer times and the effect of concentration and temperature could disclose new phenomena. These results show the relevance of the hierarchical organization in supramolecular polymers and the importance of the gel state as a benchmark to study uncommon chiroptical phenomena as well as the necessity of a better understanding of the mechanistic rules dictating the chirality transmission in higher levels of organization.

In Section 4, the capability of forming intramolecular H-bonding in self-assembling *N*-heterotriangulenes **58**, **(*S*)-59** and **(*R*)-59** discloses a series of kinetic implications in which the nature of the solvent plays a vital role. Thus, in MCH/Tol mixtures, whether the formation of the inactivated monomer *M** retards the formation of the J-aggregate, in CCl_4 solutions, a pathway complexity is evident due to the presence of an off-pathway H-type aggregate which evolves with time to the thermodynamically-controlled J-aggregate. Furthermore, these aggregates have a helical disposition and different morphology. Probably, *M**, which possesses an extended π-surface, can lead to the off-pathway H-aggregate in conditions in which the π-stacking is not diminished. However, the presence of Tol in the solvent

mixture employed avoids the formation of this aggregate in these experimental conditions. Importantly, it should be pointed out that the presence of amides in the periphery as well as the existence of long alkyl chains seems to favour the obtaining of a J-type aggregate in this scaffold. Notably, the evaluation of concentration and temperature effects unveils opposite trends in the kinetic transitions in MCH/Tol and in CCl_4, consequence of the different nature of the intermediate species in both systems (on- or off-pathway). The complete understanding of the kinetic processes in both conditions has been demonstrated to be key in the attainment of seeded and living supramolecular polymerization in these systems. Interestingly, the presence of branched chains in **(*S*)-59** and **(*R*)-59** slows down the transformation of the metastable species to the energetically-favoured polymers. This can be a result of the higher order required in the formation of the nucleus in these entities, as a consequence of the steric hindrance imparted by the branched and chiral chain. These results indicate the importance of the solvent as a tool to bias pathway complexity and the importance of molecular design to generate programmable supramolecular polymerizations.

Finally, the kinetically controlled co-assembly of **(*S*)-59**, **(*R*)-59** and **58** has been investigated by *MR* and *SaS* experiments. The kinetic effect is clearly observed for the formation of helical aggregates from pristine chiral CBTs ***(S)*-59** and ***(R)*-59** and also for the copolymerization of these two chiral CBTs in *MR* experiments. In these cases, the helical outcome increases upon 24 h rendering a time-dependent amplification of chirality due to the delay exerted by the formation of *M**. Significantly, the co-assembly of one of these chiral CBTs with achiral **58** in *SaS* experiments results in a tunable helicity conditioned by the percentage of the chiral sergeant and by the cooling rate in the co-assembly. UV-Vis and CD spectroscopy firstly exclude the existence of another metastable aggregate and, therefore, a pathway complexity phenomena cannot be invoked. The results seem to be due to the differences in stability of *M** of the chiral and achiral species and the dissimilar inherent chirality of the *M* and *M** species, which results in the efficient transfer of opposite chirality that affords J-aggregates of inverse handedness. The resulting stereomutative system demonstrates the enormous influence of kinetic traps on self-assembly and, especially, to bias the helicity of the final aggregates, and paves the way to the study of another interesting phenomena derived from programmable supramolecular polymerizations.

7. SUMMARY

The properties of π-conjugated compounds, including luminescence, charge transport and electronic conductivity, have made them strong candidates for applications in organic electronics. To attain efficient materials based on aromatic scaffolds, the control over the different hierarchical levels of organization has been demonstrated to be mandatory. Supramolecular polymerization, *i.e.*, the formation of macromolecules through the establishment of reversible non-covalent interactions among monomers, has been envisioned as a proper tool to adequately organize π-extended scaffolds, yielding well-defined mono dimensional structures. Notably, the electronic coupling between π-conjugated molecules gives rise to functionalities and properties non-exhibited by single building blocks, widening the scope of organic semiconductors. The thermodynamic aspects of supramolecular polymerization processes have been accurately described through isodesmic and cooperative mechanisms, producing macromolecules with different features depending on the mechanism. However, significant aspects such as the relation between molecular design and the final morphology of the aggregate as well as the control over the different kinetic implications of the process, like pathway complexity, are not totally comprehended, especially in the polymerization of π-conjugated compounds. Therefore, further understanding of the structural and mechanistic rules, which control the formation of different supramolecular aggregates based on π-scaffolds, results imperative.

The main aim of the present thesis consists in the study of the supramolecular polymerization process of different π-conjugated compounds to yield highly organized nanostructures in organic solvents. The general strategy involves the decoration of these moieties with amide groups capable of forming H-bonds, and, together with the π-stacking among the aromatic units, should render supramolecular polymers through a cooperative mechanism. Additionally, long alkyl chains are also included at the periphery of the π-scaffolds to enhance the solubility of these compounds in apolar media and direct the formation of organogels. The synergy between spectroscopic and microscopic techniques permits the obtaining of the thermodynamic parameters governing the process and the visualization of the morphology of the resulting aggregates. Other objectives comprise the study of kinetically-controlled supramolecular polymerizations through an adequate molecular design and the study of interesting phenomena like transfer and amplification of chirality in equilibrium and out-of-equilibrium conditions by means of the inclusion of asymmetry centres.

In Section 1, the self-assembling abilities of the achiral **25** and chiral **(*S*)-26** pyrene imidazole derivatives, endowed with an amide group, are investigated. VT-UV-Vis spectroscopy allows to disclose that the supramolecular polymerization process proceeds through a weak cooperative mechanism. Fluorescence spectroscopy reveals an unexpected blue emission in the supramolecular polymer characteristic of the pyrene monomer, which cannot be invoked to a helical arrangement as demonstrated by CD spectroscopy. The combination of ROESY ^{1}H NMR experiments and DFT calculations finally permits to elucidate the disposition of the pyreneimidazole moieties within the aggregates. The establishment of an alternate array of H-bonds between the amides and the imidazole rings and additional C-H$\cdots\pi$ interactions direct the organization of the monomers and prevents π-stacking, thus avoiding the formation of excimers and generating the characteristic blue emission of pyrene monomers.

The supramolecular polymerization of [5]-helicenes **35** and **36**, decorated with two and four amides, respectively, and unsubstituted at the inner part of the helicene skeleton, is carried out in Section 2. NMR and UV-Vis studies demonstrate the influence of the number of amides in the supramolecular polymerization of [5]-helicenes. Thus, **35** is not able to aggregate in solution whereas racemic **36** polymerizes through an isodesmic mechanism. The inherent chirality of the helicene moiety permits to obtain, after resolution with HPLC, the enantioenriched mixtures of **36**, which polymerize through a cooperative mechanism and, as shown by AFM, possess a different morphology than the racemic mixture. Finally, CD spectroscopy unveils that the self-assembling ability of the enantioenriched mixtures of **36** gives them an enhanced stability against racemization, despite the absence of substituents in the inner position of the helicene ring.

Section 3 comprises the study of the self-assembly process of the achiral *N*-heterotriangulene tricarboxamide **48** and its chiral counterparts **(*S*)-49** and **(*R*)-49**. UV-Vis and CD studies demonstrate that the supramolecular polymerization renders H-type aggregates through a cooperative mechanism in different solvents, affording helices of preferred handedness determined by the chiral centre. Remarkably, VCD spectroscopy discloses, for the same enantiomer, a solvent directed helical stereomutation in the gel state in CCl_4 and Tol. Further experiments unveil that this phenomenon is due to the initial formation in CCl_4 of a metastable state that evolves after sonication to the thermodynamic gel, thus disclosing a pathway complexity in these conditions.

Prompted by these results, the kinetically-controlled supramolecular polymerization of *N*-heterotriangulene **58** and its chiral analogues **(*S*)-59** and **(*R*)-59**, capable of forming a metastable monomer *M** through an intramolecular H-bond between an ester and amide group, is studied in Section 4. VT- ^{1}H NMR and UV-Vis spectroscopy prove the formation of *M**, which retards the formation of the J-type aggregates in MCH/Tol mixtures. In CCl_4, *M** yields a metastable H-aggregate that evolves with time to the thermodynamically favoured J-aggregate. CD spectroscopy demonstrates that both aggregates form helices, and AFM microscopy discloses that these aggregates possess different morphology. The evaluation of the concentration and temperature in the kinetics of the process permits the command of the different kinetic scenarios and allows to realize seeded and living supramolecular polymerizations.

The presence of chiral centres in **(*S*)-59** and **(*R*)-59** makes possible the study of transfer and amplification of chirality phenomena in out-of-equilibrium conditions. The majority rules experiments in MCH/Tol mixtures depict a time-controlled amplification of chirality which is consequence of the formation of *M**. Remarkably, the sergeants and soldiers experiments between **58** and **(*S*)-59** / **(*R*)-59** furnish a system with a tunable helicity conditioned by the percentage of sergeant and by the cooling rate applied. UV-Vis and CD experiments suggest that this process is the result of the dissimilar inherent chirality of the extended and inactivated monomers in **(*S*)-59** and **(*R*)-59** as well as of the different stability of the *M** in **58** and **(*S*)-59** / **(*R*)-59**.

8. RESUMEN

La luminiscencia, la capacidad para el transporte de cargas y la conductividad electrónica son algunas de las propiedades de los compuestos π-conjugados que los convierte en buenos candidatos para su aplicación en electrónica orgánica. Para obtener materiales eficientes basados en moléculas aromáticas, el control de los distintos niveles jerárquicos de organización es un requisito indispensable. La polimerización supramolecular, *i.e.*, la formación de macromoléculas a través de interacciones no covalentes entre monómeros, es una buena herramienta para lograr la organización de los compuestos π-conjugados, ya que permite producir estructuras con características bien definidas. Además, el acoplamiento electrónico entre moléculas aromáticas genera nuevas propiedades inaccesibles en la molécula discreta, ampliando de esta manera los límites de las aplicaciones de los semiconductores orgánicos. Los aspectos termodinámicos de la polimerización supramolecular se han estudiado en profundidad, siendo descritos mediante mecanismos isodésmicos o cooperativos. Aunque algunas de las propiedades de los agregados supramoleculares vienen determinadas por el mecanismo de formación, otros aspectos importantes como la relación entre el diseño molecular y la morfología resultante, así como los aspectos cinéticos del proceso, no están del todo controlados. Por lo tanto, la potencial aplicación de estos compuestos requiere de una mayor comprensión de las reglas estructurales y mecanísticas que gobiernan la formación de agregados supramoleculares.

El objetivo principal de la presente tesis doctoral consiste en el estudio de la polimerización supramolecular de distintos compuestos π-conjugados para obtener estructuras altamente organizadas. La estrategia general implica la introducción en estas estructuras de grupos amida capaces de formar enlaces de hidrógeno que, combinados con las interacciones π entre unidades aromáticas, generan polímeros supramoleculares mediante un mecanismo cooperativo. Adicionalmente, la inclusión de cadenas alquílicas en la periferia mejora la solubilidad de estos sistemas en medios apolares. La sinergia entre las distintas técnicas espectroscópicas y microscópicas permite obtener los parámetros termodinámicos que dominan el proceso, así como la visualización de la morfología de los agregados resultantes. Otros objetivos son el estudio de las polimerizaciones supramoleculares controladas cinéticamente mediante un diseño molecular adecuado, y el estudio de la transferencia y amplificación de quiralidad en condiciones de equilibrio y no equilibrio mediante la incorporación de distintos centros de asimetría en la molécula.

En la Sección 1 se investiga la capacidad de autoensamblaje de los derivados de pirenoimidazol aquiral **25** y quiral **(*S*)-26**, dotados de un grupo amida. Mediante espectroscopía UV-Vis se muestra que el proceso de polimerización supramolecular es débilmente cooperativo. La espectroscopía de fluorescencia revela un patrón de emisión en el polímero supramolecular típico de pireno monomérico que, como demuestra la espectroscopía CD, no se debe a la formación de hélices. La combinación de experimentos ROESY y cálculos DFT permite dilucidar la disposición de los monómeros de pirenoimidazol en los agregados supramoleculares. La formación de una red alternada de enlaces de hidrógeno entre las amidas y los anillos de imidazol junto con las interacciones C-H$\cdots\pi$ dirige la formación del agregado, evitando la formación de excímeros y generando el patrón de emisión observado.

En la Sección 2 se estudia la polimerización supramolecular de los [5]-helicenos **35** y **36**, dotados de dos y cuatro grupos amida, respectivamente, y sin sustituyentes en las posiciones internas. Las estudios de RMN y UV-Vis demuestran la influencia del número de grupos amida en la polimerización supramolecular de los [5]-helicenos. Así, el heliceno **35** no agrega en disolución mientras que la mezcla racémica de **36** polimeriza mediante un mecanismo isodésmico. La quiralidad intrínseca de los helicenos permite separar, mediante HPLC, las fracciones enantioenriquecidas de **36**, que en este caso polimerizan mediante un mecanismo cooperativo y, como muestran las imágenes de AFM, presentan una morfología diferente a la mezcla racémica. Finalmente, los estudios de CD revelan que la capacidad para autoensamblar confiere a **36** una mayor estabilidad frente a la racemización a pesar de la ausencia de sustituyentes en las posiciones internas.

En la Sección 3, se evalúa el proceso de autoensamblaje del *N*-heterotrianguleno aquiral **48** y sus análogos quirales **(*S*)-49** y **(*R*)-49**. Las estudios de UV-Vis, CD y AFM demuestran que se forman agregados tipo H mediante un mecanismo cooperativo, generando hélices cuya helicidad está dictada por el centro estereogénico. Los espectros de VCD en estado gel muestran que para cada enantiómero se produce una estereomutación helicoidal dirigida por el disolvente en CCl_4 y Tol. Experimentos adicionales explican que este fenómeno se debe a la formación inicial de un estado metaestable en CCl_4 que evoluciona con el tiempo al gel termodinámico.

En la Sección 4 se estudia la polimerización supramolecular controlada cinéticamente del *N*-heterotrianguleno aquiral **58** y de sus congéneres quirales **(*S*)-59** y **(*R*)-59**. Estos sistemas forman un monómero metaestable *M** mediante un enlace de hidrógeno intramolecular entre un grupo éster y un grupo amida. Los experimentos de ^{1}H RMN y UV-Vis confirman la existencia de *M**, cuya formación retrasa la obtención del agregado tipo J en mezclas MCH/Tol. En CCl_4, *M** origina un agregado tipo H metaestable que evoluciona con el tiempo al agregado tipo J termodinámicamente favorecido. Los estudios de CD y AFM revelan que ambos agregados son helicoidales y poseen morfologías diferentes. La evaluación de los efectos producidos por cambios de concentración y temperatura en la cinética del proceso permite controlar los distintos escenarios y la realización de polimerizaciones supramoleculares vivas.

Asimismo, la presencia de centros estereogénicos en **(*S*)-59** y **(*R*)-59** hace posible el estudio de fenómenos de transferencia y amplificación de quiralidad en condiciones fuera del equilibrio. Los experimentos de reglas de mayoría en mezclas MCH/Tol muestran una amplificación de quiralidad controlada por el tiempo debida a la formación de *M**. Sorprendentemente, los experimentos de sargentos y soldados entre **58** y **(*S*)-59** / **(*R*)-59** generan un sistema con helicidad modulable que está condicionada por el porcentaje de sargento y por la velocidad de enfriamiento aplicada. Los experimentos de UV-Vis y CD sugieren que este proceso es el resultado de la diferente quiralidad del monómero en sus estados extendido e inactivado en **(*S*)-59** y **(*R*)-59** así como de la diferente estabilidad de *M** en **58** y **(*S*)-59** / **(*R*)-59**.

9. REFERENCES

[1] G. M. Whitesides, J. P. Mathias, C. T. Seto, *Science* **1991**, *254*, 1312.
[2] G. M. Whitesides, B. Grzybowski, *Science* **2002**, *295*, 2418.
[3] J. M. Lehn, *Proc. Natl. Acad. Sci. U.S.A.* **2002**, *99*, 4763.
[4] J. M. Lehn, *Angew. Chem. Int. Ed.* **1990**, *29*, 1304.
[5] J. M. Lehn, *Science* **1993**, *260*, 1762.
[6] F. Biedermann, H.-J. Schneider, *Chem. Rev.* **2016**, *116*, 5216.
[7] M. D. Shoulders, R. T. Raines, *Annu. Rev. Biochem.* **2009**, *78*, 929.
[8] B. J. G. E. Pieters, M. B. van Eldijk, R. J. M. Nolte, J. Mecinovic, *Chem. Soc. Rev.* **2016**, *45*, 24.
[9] F. Aparicio, F. García, L. Sánchez, in *Encyclopedia of Polymer Science and Technology*, John Wiley & Sons, Inc., **2012**.
[10] L. Brunsveld, B. J. B. Folmer, E. W. Meijer, R. P. Sijbesma, *Chem. Rev.* **2001**, *101*, 4071.
[11] D. A. Fletcher, R. D. Mullins, *Nature* **2010**, *463*, 485.
[12] C. Fouquey, J. M. Lehn, A. M. Levelut, *Adv. Mater.* **1990**, *2*, 254.
[13] L. Yang, X. Tan, Z. Wang, X. Zhang, *Chem. Rev.* **2015**, *115*, 7196.
[14] T. Aida, E. W. Meijer, S. I. Stupp, *Science* **2012**, *335*, 813.
[15] T. F. A. de Greef, M. M. J. Smulders, M. Wolffs, A. P. H. J. Schenning, R. P. Sijbesma, E. W. Meijer, *Chem. Rev.* **2009**, *109*, 5687.
[16] Z. Chen, A. Lohr, C. R. Saha-Möller, F. Würthner, *Chem. Soc. Rev.* **2009**, *38*, 564.
[17] S. Ghosh, V. K. Praveen, A. Ajayaghosh, *Annu. Rev. Mater. Res.* **2016**, *46*, 235.
[18] A. T. Haedler, K. Kreger, A. Issac, B. Wittmann, M. Kivala, N. Hammer, J. Köhler, H.-W. Schmidt, R. Hildner, *Nature* **2015**, *523*, 196.
[19] A. Vidyasagar, K. Handore, K. M. Sureshan, *Angew. Chem. Int. Ed.* **2011**, *50*, 8021.
[20] F. Aparicio, E. Matesanz, L. Sánchez, *Chem. Commun.* **2012**, *48*, 5757.
[21] E. Mattia, S. Otto, *Nat. Nanotech.* **2015**, *10*, 111.
[22] S. Dhiman, A. Sarkar, S. J. George, *RSC Advances* **2018**, *8*, 18913.
[23] M. Pope, C. E. Swenberg, in *Electronic Processes in Organic Crystals and Polymers*, 2nd ed.; Oxford University Press, **1999**.
[24] M. Muccini, *Nat. Mater.* **2006**, *5*, 605.
[25] A. W. Hains, Z. Liang, M. A. Woodhouse, B. A. Gregg, *Chem. Rev.* **2010**, *110*, 6689.
[26] K. Müllen, U. Scherf, *Organic Light Emitting Devices*, VCH: Weinheim, Germany **2006**.
[27] M. Gsänger, D. Bialas, L. Huang, M. Stolte, F. Würthner, *Adv. Mater.* **2016**, *28*, 3615.
[28] M. Mas-Torrent, C. Rovira, *Chem. Rev.* **2011**, *111*, 4833.
[29] O. Ostroverkhova, *Chem. Rev.* **2016**, *116*, 13279.

[30] X. Hu, A. Damjanović, T. Ritz, K. Schulten, *Proc. Natl. Acad. Sci. U.S.A.* **1998**, *95*, 5935.
[31] F. Würthner, T. E. Kaiser, C. R. Saha-Möller, *Angew. Chem. Int. Ed.* **2011**, *50*, 3376.
[32] M. Kastler, W. Pisula, D. Wasserfallen, T. Pakula, K. Müllen, *J. Am. Chem. Soc.* **2005**, *127*, 4286.
[33] X. Feng, W. Pisula, M. Takase, X. Dou, V. Enkelmann, M. Wagner, N. Ding, K. Müllen, *Chem. Mater.* **2008**, *20*, 2872.
[34] Z. Chen, V. Stepanenko, V. Dehm, P. Prins, L. D. A. Siebbeles, J. Seibt, P. Marquetand, V. Engel, F. Würthner, *Chem. Eur. J.* **2007**, *13*, 436.
[35] C. R. Martinez, B. L. Iverson, *Chem. Sci.* **2012**, *3*, 2191.
[36] D. González-Rodríguez, A. P. H. J. Schenning, *Chem. Mater.* **2011**, *23*, 310.
[37] E. D. Glowacki, M. Irimia-Vladu, S. Bauer, N. S. Sariciftci, *J. Mat. Chem. B* **2013**, *1*, 3742.
[38] C. Rest, R. Kandanelli, G. Fernández, *Chem. Soc. Rev.* **2015**, *44*, 2543.
[39] P. Jonkheijm, P. van der Schoot, A. P. H. J. Schenning, E. W. Meijer, *Science* **2006**, *313*, 80.
[40] M. Kasha, H. R. Rawls, M. A. E. Bayoumi, *Pure Appl. Chem.* **1965**, *11*, 371.
[41] F. Würthner, C. R. Saha-Möller, B. Fimmel, S. Ogi, P. Leowanawat, D. Schmidt, *Chem. Rev.* **2016**, *116*, 962.
[42] T. E. Kaiser, V. Stepanenko, F. Würthner, *J. Am. Chem. Soc.* **2009**, *131*, 6719.
[43] S. Ghosh, X.-Q. Li, V. Stepanenko, F. Würthner, *Chem. Eur. J.* **2008**, *14*, 11343.
[44] V. Stepanenko, X.-Q. Li, J. Gershberg, F. Würthner, *Chem. Eur. J.* **2013**, *19*, 4176.
[45] A. Ajayaghosh, V. K. Praveen, *Acc. Chem. Res.* **2007**, *40*, 644.
[46] S. S. Babu, V. K. Praveen, A. Ajayaghosh, *Chem. Rev.* **2014**, *114*, 1973.
[47] F. García, J. Buendía, S. Ghosh, A. Ajayaghosh, L. Sánchez, *Chem. Commun.* **2013**, *49*, 9278.
[48] P. A. Korevaar, T. F. A. de Greef, E. W. Meijer, *Chem. Mater.* **2014**, *26*, 576.
[49] F. Würthner, *Nat. Chem.* **2014**, *6*, 171.
[50] R. D. Mukhopadhyay, A. Ajayaghosh, *Science* **2015**, *349*, 241.
[51] D. van der Zwaag, T. F. A. de Greef, E. W. Meijer, *Angew. Chem. Int. Ed.* **2015**, *54*, 8334.
[52] P. A. Korevaar, S. J. George, A. J. Markvoort, M. M. J. Smulders, P. A. J. Hilbers, A. P. H. J. Schenning, T. F. A. de Greef, E. W. Meijer, *Nature* **2012**, *481*, 492.
[53] M. Szwarc, *Nature* **1956**, *178*, 1168.

[54] D. Zhao, J. S. Moore, *Org. Biomol. Chem.* **2003**, *1*, 3471.
[55] S. Dhiman, S. J. George, *Bull. Chem. Soc. Jap.* **2018**, *91*, 687.
[56] S. Ogi, K. Sugiyasu, S. Manna, S. Samitsu, M. Takeuchi, *Nat. Chem.* **2014**, *6*, 188.
[57] X. Wang, G. Guerin, H. Wang, Y. Wang, I. Manners, M. A. Winnik, *Science* **2007**, *317*, 644.
[58] P. A. Rupar, L. Chabanne, M. A. Winnik, I. Manners, *Science* **2012**, *337*, 559.
[59] W. Zhang, W. Jin, T. Fukushima, A. Saeki, S. Seki, T. Aida, *Science* **2011**, *334*, 340.
[60] S. Ogi, T. Fukui, M. L. Jue, M. Takeuchi, K. Sugiyasu, *Angew. Chem. Int. Ed.* **2014**, *53*, 14363.
[61] T. Fukui, S. Kawai, S. Fujinuma, Y. Matsushita, T. Yasuda, T. Sakurai, S. Seki, M. Takeuchi, K. Sugiyasu, *Nat. Chem.* **2017**, *9*, 493.
[62] J. Kang, D. Miyajima, T. Mori, Y. Inoue, Y. Itoh, T. Aida, *Science* **2015**, *347*, 646.
[63] J. Kang, D. Miyajima, Y. Itoh, T. Mori, H. Tanaka, M. Yamauchi, Y. Inoue, S. Harada, T. Aida, *J. Am. Chem. Soc.* **2014**, *136*, 10640.
[64] S. Ogi, V. Stepanenko, K. Sugiyasu, M. Takeuchi, F. Würthner, *J. Am. Chem. Soc.* **2015**, *137*, 3300.
[65] S. Ogi, V. Stepanenko, J. Thein, F. Würthner, *J. Am. Chem. Soc.* **2016**, *138*, 670.
[66] W. Wagner, M. Wehner, V. Stepanenko, S. Ogi, F. Würthner, *Angew. Chem. Int. Ed.* **2017**, *56*, 16008.
[67] E. E. Greciano, L. Sánchez, *Chem. Eur. J.* **2016**, *22*, 13724.
[68] E. E. Greciano, B. Matarranz, L. Sánchez, *Angew. Chem. Int. Ed.* **2018**, *57*, 4697.
[69] A. Sorrenti, J. Leira-Iglesias, A. J. Markvoort, T. F. A. de Greef, T. M. Hermans, *Chem. Soc. Rev.* **2017**, *46*, 5476.
[70] S. H. Jung, D. Bochicchio, G. M. Pavan, M. Takeuchi, K. Sugiyasu, *J. Am. Chem. Soc.* **2018**, *140*, 10570.
[71] H. Frisch, E.-C. Fritz, F. Stricker, L. Schmüser, D. Spitzer, T. Weidner, B. J. Ravoo, P. Besenius, *Angew. Chem. Int. Ed.* **2016**, *55*, 7242.
[72] G. Ashkenasy, T. M. Hermans, S. Otto, A. F. Taylor, *Chem. Soc. Rev.* **2017**, *46*, 2543.
[73] T. M. Figueira-Duarte, K. Müllen, *Chem. Rev.* **2011**, *111*, 7260.
[74] C. Wang, H. Dong, W. Hu, Y. Liu, D. Zhu, *Chem. Rev.* **2012**, *112*, 2208.
[75] M. Stępień, E. Gońka, M. Żyła, N. Sprutta, *Chem. Rev.* **2017**, *117*, 3479.
[76] F. Liu, C. Tang, Q.-Q. Chen, F.-F. Shi, H.-B. Wu, L.-H. Xie, B. Peng, W. Wei, Y. Cao, W. Huang, *J. Phys. Chem. C* **2009**, *113*, 4641.

[77] M. Nieuwenhuizen, M. L, T. F. A. de Greef, R. L. J. van der Bruggen, J. M. J. Paulusse, W. P. J. Appel, M. M. J. Smulders, R. P. Sijbesma, E. W. Meijer, *Chem. Eur. J.* **2010**, *16*, 1601.
[78] T. Terashima, T. Mes, T. F. A. de Greef, M. A. J. Gillissen, P. Besenius, A. R. A. Palmans, E. W. Meijer, *J. Am. Chem. Soc.* **2011**, *133*, 4742.
[79] G. Koeckelberghs, L. De Cremer, W. Vanormelingen, W. Dehaen, T. Verbiest, A. Persoons, C. Samyn, *Tetrahedron* **2005**, *61*, 687.
[80] T. Yamato, A. Miyazawa, M. Tashiro, *Chem. Ber.* **1993**, *126*, 2505.
[81] J. Hu, D. Zhang, F. W. Harris, *J. Org. Chem.* **2005**, *70*, 707.
[82] D. Kumar, K. R. J. Thomas, C.-C. Lin, J.-H. Jou, *Chem. Asian J.* **2013**, *8*, 2111.
[83] E. Pretsch, P. Bülhman, M. Badertscher, *IR Spectroscopy in Structure Determination of Organic Compounds*, Springer, **2009**.
[84] F. García, L. Sánchez, *J. Am. Chem. Soc.* **2012**, *134*, 734.
[85] A. J. Markvoort, H. M. M. ten Eikelder, P. A. J. Hilbers, T. F. A. de Greef, E. W. Meijer, *Nat. Comm.* **2011**, *2*, 509.
[86] H. M. M. ten Eikelder, A. J. Markvoort, T. F. A. de Greef, P. A. J. Hilbers, *J. Phys. Chem. B* **2012**, *116*, 5291.
[87] C. Kulkarni, E. W. Meijer, A. R. A. Palmans, *Acc. Chem. Res.* **2017**, *50*, 1928.
[88] F. M. Winnik, *Chem. Rev.* **1993**, *93*, 587.
[89] Y. Kamikawa, T. Kato, *Langmuir* **2007**, *23*, 274.
[90] M. M. Green, J.-W. Park, T. Sato, A. Teramoto, S. Lifson, R. L. B. Selinger, J. V. Selinger, *Angew. Chem. Int. Ed.* **1999**, *38*, 3138.
[91] M. M. J. Smulders, I. A. W. Filot, J. M. A. Leenders, P. van der Schoot, A. R. A. Palmans, A. P. H. J. Schenning, E. W. Meijer, *J. Am. Chem. Soc.* **2010**, *132*, 611.
[92] M. M. J. Smulders, P. J. M. Stals, T. Mes, T. F. E. Paffen, A. P. H. J. Schenning, A. R. A. Palmans, E. W. Meijer, *J. Am. Chem. Soc.* **2010**, *132*, 620.
[93] A. Wong, R. Ida, L. Spindler, G. Wu, *J. Am. Chem. Soc.* **2005**, *127*, 6990.
[94] C. Kulkarni, S. Balasubramanian, S. J. George, *ChemPhysChem* **2013**, *14*, 661.
[95] Y. Shen, C.-F. Chen, *Chem. Rev.* **2012**, *112*, 1463.
[96] M. Gingras, *Chem. Soc. Rev.* **2013**, *42*, 1051.
[97] M. Shigeno, Y. Kushida, M. Yamaguchi, *Chem. Commun.* **2016**, *52*, 4955.
[98] R. H. Janke, G. Haufe, E.-U. Würthwein, J. H. Borkent, *J. Am. Chem. Soc.* **1996**, *118*, 6031.
[99] P. Ravat, R. Hinkelmann, D. Steinebrunner, A. Prescimone, I. Bodoky, M. Juríček, *Org. Lett.* **2017**, *19*, 3707.
[100] K.-H. Ernst, *Acc. Chem. Res.* **2016**, *49*, 1182.
[101] C. Nuckolls, T. J. Katz, L. Castellanos, *J. Am. Chem. Soc.* **1996**, *118*, 3767.

[102] F. Aparicio, B. Nieto-Ortega, F. Nájera, F. J. Ramírez, J. T. López Navarrete, J. Casado, L. Sánchez, *Angew. Chem. Int. Ed.* **2014**, *53*, 1373.
[103] J. Buendía, E. E. Greciano, L. Sánchez, *J. Org. Chem.* **2015**, *80*, 12444.
[104] A. Dawn, N. Fujita, S. Haraguchi, K. Sada, S. Shinkai, *Chem. Commun.* **2009**, 2100.
[105] M. Gingras, *Chem. Soc. Rev.* **2013**, *42*, 968.
[106] N. Ito, T. Hirose, K. Matsuda, *Org. Lett.* **2014**, *16*, 2502.
[107] S. K. Collins, A. Grandbois, M. P. Vachon, J. Côté, *Angew. Chem. Int. Ed.* **2006**, *45*, 2923.
[108] D. C. Harrowven, I. L. Guy, L. Nanson, *Angew. Chem. Int. Ed.* **2006**, *45*, 2242.
[109] T. Ooi, M. Kameda, K. Maruoka, *J. Am. Chem. Soc.* **2003**, *125*, 5139.
[110] S. Goretta, C. Tasciotti, S. Mathieu, M. Smet, W. Maes, Y. M. Chabre, W. Dehaen, R. Giasson, J.-M. Raimundo, C. R. Henry, C. Barth, M. Gingras, *Org. Lett.* **2009**, *11*, 3846.
[111] P. Ravat, T. Šolomek, M. Rickhaus, D. Häussinger, M. Neuburger, M. Baumgarten, M. Juríček, *Angew. Chem. Int. Ed.* **2016**, *55*, 1183.
[112] P. A. Korevaar, C. Schaefer, T. F. A. de Greef, E. W. Meijer, *J. Am. Chem. Soc.* **2012**, *134*, 13482.
[113] N. Harada, K. Nakanishi, *J. Am. Chem. Soc.* **1969**, *91*, 3989.
[114] T. Taniguchi, T. Usuki, *Circular Dichroism Spectroscopy*, John Wiley & Sons, Inc., **2012**.
[115] Z. Xie, V. Stepanenko, K. Radacki, F. Würthner, *Chem. Eur. J.* **2012**, *18*, 7060.
[116] N. Pavliček, A. Mistry, Z. Majzik, N. Moll, G. Meyer, D. J. Fox, L. Gross, *Nat. Nanotech.* **2017**, *12*, 308.
[117] J. E. Field, D. Venkataraman, *Chem. Mater.* **2002**, *14*, 962.
[118] N. Hammer, T. A. Schaub, U. Meinhardt, M. Kivala, *Chem. Rec.* **2015**, *15*, 1119.
[119] M. Kivala, W. Pisula, S. Wang, A. Mavrinskiy, J.-P. Gisselbrecht, X. Feng, K. Müllen, *Chem. Eur. J.* **2013**, *19*, 8117.
[120] C.-M. Chou, S. Saito, S. Yamaguchi, *Org. Lett.* **2014**, *16*, 2868.
[121] N. Hammer, T. E. Shubina, J.-P. Gisselbrecht, F. Hampel, M. Kivala, *J. Org. Chem.* **2015**, *80*, 2418.
[122] T. Kim, T. Mori, T. Aida, D. Miyajima, *Chem. Sci.* **2016**, *7*, 6689.
[123] F. García, P. M. Viruela, E. Matesanz, E. Ortí, L. Sánchez, *Chem. Eur. J.* **2011**, *17*, 7755.
[124] H. Zhang, S. Wang, Y. Li, B. Zhang, C. Du, X. Wan, Y. Chen, *Tetrahedron* **2009**, *65*, 4455.
[125] J. Puigmartí-Luis, V. Laukhin, Á. Pérez del Pino, J. Vidal-Gancedo, C. Rovira, E. Laukhina, D. B. Amabilino, *Angew. Chem. Int. Ed.* **2007**, *46*, 238.

[126] A. Rödle, B. Ritschel, C. Mück-Lichtenfeld, V. Stepanenko, G. Fernández, *Chem. Eur. J.* **2016**, *22*, 15772.
[127] X.-Q. Li, V. Stepanenko, Z. Chen, P. Prins, L. D. A. Siebbeles, F. Würthner, *Chem. Commun.* **2006**, 3871.
[128] F. García, P. A. Korevaar, A. Verlee, E. W. Meijer, A. R. A. Palmans, L. Sánchez, *Chem. Commun.* **2013**, *49*, 8674.
[129] A. T. Haedler, S. C. J. Meskers, R. H. Zha, M. Kivala, H.-W. Schmidt, E. W. Meijer, *J. Am. Chem. Soc.* **2016**, *138*, 10539.
[130] J. Buendía, J. Calbo, E. Ortí, L. Sánchez, *Small* **2017**, *13*, 1603880.
[131] R. A. Vaia, R. K. Teukolsky, E. P. Giannelis, *Chem. Mater.* **1994**, *6*, 1017.
[132] V. A. Mallia, P. D. Butler, B. Sarkar, K. T. Holman, R. G. Weiss, *J. Am. Chem. Soc.* **2011**, *133*, 15045.
[133] S. Ogi, K. Matsumoto, S. Yamaguchi, *Angew. Chem. Int. Ed.* **2018**, *57*, 2339.
[134] K. Mori, H. Harada, P. Zagatti, A. Cork , D. R. Hall, *Liebigs Ann. Chem.* **1991**, 259.
[135] F. Aparicio, L. Sánchez, *Chem. Eur. J.* **2013**, *19*, 10482.
[136] H. C. Bertrand, M. Schaap, L. Baird, N. D. Georgakopoulos, A. Fowkes, C. Thiollier, H. Kachi, A. T. Dinkova-Kostova, G. Wells, *J. Med. Chem.* **2015**, *58*, 7186.
[137] M. M. J. Smulders, T. Buffeteau, D. Cavagnat, M. Wolffs, A. P. H. J. Schenning, E. W. Meijer, *Chirality* **2008**, *20*, 1016.
[138] R. van der Weegen, A. J. P. Teunissen, E. W. Meijer, *Chem. Eur. J.* **2017**, *23*, 3773.
[139] B. Adelizzi, I. A. W. Filot, A. R. A. Palmans, E. W. Meijer, *Chem. Eur. J.* **2017**, *23*, 6103.
[140] J. Buendía, F. García, B. Yélamos, L. Sánchez, *Chem. Commun.* **2016**, *52*, 8830.
[141] E. T. Powers, D. L. Powers, *Biophys. J.* **2006**, *91*, 122.
[142] E. T. Powers, D. L. Powers, *Biophys. J.* **2008**, *94*, 379.
[143] J. Baram, H. Weissman, B. Rybtchinski, *J. Phys. Chem. B* **2014**, *118*, 12068.
[144] A. R. A. Palmans, E. W. Meijer, *Angew. Chem. Int. Ed.* **2007**, *46*, 8948.
[145] M. Liu, L. Zhang, T. Wang, *Chem. Rev.* **2015**, *115*, 7304.
[146] A. Lohr, M. Lysetska, F. Würthner, *Angew. Chem. Int. Ed.* **2005**, *44*, 5071.
[147] A. Lohr, F. Würthner, *Angew. Chem. Int. Ed.* **2008**, *47*, 1232.
[148] P. A. Korevaar, C. Grenier, A. J. Markvoort, A. P. H. J. Schenning, T. F. A. de Greef, E. W. Meijer, *Proc. Natl. Acad. Sci. U.S.A.* **2013**, *110*, 17205.
[149] B. Adelizzi, A. Aloi, A. J. Markvoort, H. M. M. Ten Eikelder, I. K. Voets, A. R. A. Palmans, E. W. Meijer, *J. Am. Chem. Soc.* **2018**, *140*, 7168.
[150] A. Ajayaghosh, R. Varghese, S. J. George, C. Vijayakumar, *Angew. Chem. Int. Ed.* **2006**, *45*, 1141.

[151] D. F. Eaton, *J. Photochem. Photobiol. B* **1988**, *2*, 523.
[152] S. Fery-Forgues, D. Lavabre, *J. Chem. Ed.* **1999**, *76*, 1260.
[153] M. J. Frisch, G. W. Trucks, H. B. Schlegel, G. E. Scuseria, M. A. Robb, J. R. Cheeseman, G. Scalmani, V. Barone, B. Mennucci, G. A. Petersson, H. Nakatsuji, M. Caricato, X. Li, H. P. Hratchian, A. F. Izmaylov, J. Bloino, G. Zheng, J. L. Sonnenberg, M. Hada, M. Ehara, K. Toyota, R. Fukuda, J. Hasegawa, M. Ishida, T. Nakajima, Y. Honda, O. Kitao, H. Nakai, T. Vreven, J. A. Montgomery, J. E. Peralta, F. Ogliaro, M. Bearpark, J. J. Heyd, E. Brothers, K. N. Kudin, V. N. Staroverov, R. Kobayashi, J. Normand, K. Raghavachari, A. Rendell, J. C. Burant, S. S. Iyengar, J. Tomasi, M. Cossi, N. Rega, J. M. Millam, M. Klene, J. E. Knox, J. B. Cross, V. Bakken, C. Adamo, J. Jaramillo, R. Gomperts, R. E. Stratmann, O. Yazyev, A. J. Austin, R. Cammi, C. Pomelli, J. W. Ochterski, R. L. Martin, K. Morokuma, V. G. Zakrzewski, G. A. Voth, P. Salvador, J. J. Dannenberg, S. Dapprich, A. D. Daniels, Farkas, J. B. Foresman, J. V. Ortiz, J. Cioslowski and D. J. Fox, *Gaussian 09, Revision D.01*.
[154] S. Grimme, *J. Comput. Chem.* **2006**, *27*, 1787.
[155] V. A. Rassolov, M. A. Ratner, J. A. Pople, P. C. Redfern, L. A. Curtiss, *J. Comput. Chem.* **2001**, *22*, 976.
[156] R. Ditchfield, W. J. Hehre, J. A. Pople, *J. Chem. Phys.* **1971**, *54*, 724.
[157] M. M. Francl, W. J. Pietro, W. J. Hehre, J. S. Binkley, M. S. Gordon, D. J. D. Frees, J. A. Pople, *J. Chem. Phys.* **1982**, *77*, 3654.
[158] A. D. Becke, *J. Chem. Phys.* **1993**, *98*, 5648.
[159] S. Grimme, S. Ehrlich, L. Goerigk, *J. Comput. Chem.* **2011**, *32*, 1456.
[160] H. Kruse, S. Grimme, *J. Chem. Phys.* **2012**, *136*, 154101.
[161] J. Contreras-García, E. R. Johnson, S. Keinan, R. Chaudret, J.-P. Piquemal, D. N. Beratan, W. Yang, *J. Chem. Theory Comput.* **2011**, *7*, 625.
[162] E. R. Johnson, S. Keinan, P. Mori-Sánchez, J. Contreras-García, A. J. Cohen, W. Yang, *J. Am. Chem. Soc.* **2010**, *132*, 6498.
[163] K. J. Laidler, *Chemical Kinetics*, 3rd ed.; Harper & Row: New York, **1987**.
[164] G. Schoetz, O. Trapp, V. Schurig, *Electrophoresis* **2001**, *22*, 3185.